The 13th International Conference on Multi-Functional Materials and Applications (ICMMA 2019)

Conference Chairman:

Prof. Ming Ding (President, Bengbu University, China)

Conference Vice Chairman:

Prof. Jin Liu (Anhui Jianzhu University, China)

Prof. Won-Chun Oh (Hanseo University, Korea)

Advisory Chairman:

Prof. Mingxu Zhang (Anhui University of Science & Technology, China)

Prof. Zhigang Chen (Suzhou University of Science and Technology, China)

Prof. Saksit Chanthai (Khon Kaen University, Thailand)

Conference Local Chairman:

Prof. Won-Chun Oh (Hanseo University, Korea)

Prof. Jin Liu (Anhui Jianzhu University, China)

Prof. Ding Ming (Bengbu University, China)

Prof. Chuyang Xu (Anhui University of Science & Technology, China)

Prof. Shin Mukai (Hokkaido University, Japan)

Dr. Chong-Hun Jung (Korea Atomic Energy Research Institute, Korea)

Dr. Cheol Gyu Kim (AM Nano Tech., Korea)

Prof. Heon-Chang Kim (Hoseo University, Korea)

Prof. Masahiro Toyoda (Oita University, Japan)

Prof. Chan-Kyung Kim (Inha University, Korea)

Prof. Daosung Sun (Hefei Normal University, China)

Prof. Zhaoqi Sun (Anhui University, China)

Prof. Chen-Hao Wang (National Taiwan University of Science and Technology, Taiwan)

Prof. Ram Agarwal (AJC Editor Chief, India)

Prof. Bao-Lin Wang (Nanjing Normal University, China)

Prof. Prawit Nuengmatcha (Nakhon Si Thammarat Rajabhat University, Thailand)

Prof. Benhong Yang (Hefei University, China)

Prof. Jingbiao Cui (University of North Texas, USA)

Prof. Minh-Vien Le (Ho Chi Minh City University of Technology , Vietnam)

Committee Board Members:

Prof. Shao-Jie Feng (Anhui Jianzhu University, China)

Dr. Hui-Jun Won (Korea Atomic Energy Research Institute, Korea)

Prof. Won-Kweon Jang (Hanseo University, Korea)

Prof. Ke Wu (Hefei University, China)

Prof. Chang-Sung Lim (Hanseo University, Korea)

Prof. Qinfang Zhang (Yancheng Institue of Technology, China)

Prof. Seung-Kyu Park (Hoseo University, Korea)

Prof. Dongtian Wang (Suzhou University of Science and Technology, China)

Dr. Hangkyo Jin (Korea Research Institute of Chemical Technology, Korea)

Dr. Kwang Yeon Cho (Korea institute of Ceramic Eng. and Tech., Korea)

Prof. Jong-Sung Yu (Daegu Gyeungbuk Institute of Science & Technology, Korea)

Prof. Feng-Jun Zhang (Anhui Jianzhu University, China)

Prof. Kunhong Hu (Hefei University, China)

Prof. Young Chul Kim (Eulji University, Korea)

Prof. Chengbao Liu (Suzhou University of Science and Technology, China)

Prof. Ze-Da Meng (Suzhou University of Science and Technology, China)

Prof. Jae-Won Lee (Dankook University, Korea)

Prof. Yin Liu (Anhui University of Science and Technology, China)

Prof. Cheol-Kyu Jun (Hoseo University, Korea)

Dr. Lei Zhu (Yancheng Institute of Technology, China)

Prof. Goutam Mukhopadhyay (B.C.D.A College of Pharmacy &Technology, India)

Prof. Suresh Sagadevan (University of Malaya, Malaysia)

Prof. Wei Chang Hao (BeiHang University, China)

Dr. Jyothi Rajesh Kumar (Korea Institute of Geoscience and Mineral Resources, Korea)

Dr. Yu-Jin Han (Korea Institute of Energy Research, Korea)

Prof. Chunhu Wang (Bengbu University, China)

Prof. Sirinuch Loita (Khon Kaen University, Thailand)

Prof. Rachadaporn Benchawattananon (Khon Kaen University, Thailand)

Prof. Gang He (Anhui University, China)

Conference Academic Chairman:

Prof. Ming Ding (President, Bengbu University, China)

Prof. Won-Chun Oh (Hanseo University, Korea)

Prof. Jin Liu (Anhui Jianzhu University, China)

Hotel:

Ming Culture Palace Hotel (Damingwenhua Hotel)

Email：1069058472@qq.com

Address: Tanghuananlu, Bengbu city, Anhui, China (汤和南路大明文化园内)

Phone: 0552-3258777

Internet link: http://www.dmwhy.cn/wap

Single bed :350 RMB/night*

Double bed :420 RMB/night*

*Special rate (including breakfast) only for this conference, and has to book via the local organizing committee.

Venue: Labray Building, Bengbub University, China

Room A: Lecture Room A
Room B: Lecture Room B
Room C: Lecture Room C

Agenda of ICMMA2019-Opening Ceremony

(Host by Prof. Dr. **Ming Ding**)

Library Building (Room Main)

<table>
<tr><td>08:50~09:00</td><td colspan="2">Report address by Prof. Ming Ding (President, Bengbu University, China)
–Conference Chairman -</td></tr>
<tr><td rowspan="3">09:00~09:30</td><td>09:00~09:10</td><td>Opening Address by
Prof. Dr. Zegong Liu (Secretary of Party Committee, Bengbu University, China)
-Secretary of Party Committee-</td></tr>
<tr><td>09:10~09:20</td><td>ICMMA News by
Prof. Dr. Won-Chun Oh
(Hanseo University, Korea) – Conference Vice Chairman
Introduction of Potential Scientists</td></tr>
<tr><td>09:20~09:30</td><td>Address byProf. Dr. Ho Seob Kim
(Sunmoon University, Korea)
Introduction of ICMMA2020</td></tr>
<tr><td>09:30~09:40</td><td colspan="2">"Award of Appreciation Plaque"
Plaque to Prof. Dr. Chan Kyung Kim
(Inha University, Korea)
“Award of Appreciation Plaque to Retired Scientists”
Prof. Mingxu Zhang (Anhui University of Science and Technolgy, China)
Prof. Zhigang Chen (Suzhou University of Science and Technolgy, China)
Prof. Saksit Chantai (Khon Kaen University, Thailand)</td></tr>
<tr><td>09:40</td><td colspan="2">The conference chairman announces ICMMA 2019 begins</td></tr>
<tr><td>09:50</td><td colspan="2">Group Photo</td></tr>
</table>

Conference Program

November 21 (Thursday), 2019

12:00-18:00	Onsite Registration
18:00-20:00	Welcome Reception
20:00~	Conference Committee Board Meeting (for ICMMA2019)

November 22 (Friday), 2019

08:30~	Onsite Registration
08:50-10:00	Opening Ceremony(Bengbu University, China)
Session I (RoomA: 107) (10:00-11:00) (Session Chairman : Prof. Dr. Won-Chun Oh)	
10:00-10:30	**PlenaryLecture 1** Prof. **Kyo-Seon Kim** (Department of Chemical Engineering, Kangwon National University, Chuncheon, Kangwon-Do, South Korea) ***Fast Preparation of Nanostructured Photocatalyst Thin Film by Combustion and Its Application***
10:30-11:00	**PlenaryLecture 2** Prof.**Masahiro Toyoda** (Department of Applied Chemistry, Oita University, 700 Dannoharu, Oita 870-1124, Japan) ***EDLC characteristics of carbon materials derived from COAL EXTRACT***
11:00-11:10 Coffee Break	
Session II-1(RoomA: 107) (11:10-12:30) (Session Chairman : Prof. Dr.Shin-ichi Kondo)	
11:10-11:30	**Invited Lecture 1** Prof. **Minh-Vien Le** (Faculty of Chemical Engineering, Ho Chi Minh city University of Technology, 268 Ly Thuong Kiet, 14 Ward, District 10, Ho Chi Minh City, Vietnam) ***Investigation on the Photoactivity of La-doped $SrTiO_3$ Nanocubes for Degradation of 2-naphthol under the Visible Light Irradiation***
11:30-11:50	**Invited Lecture 2** Prof. **Gaofeng Wang (**Key Laboratory of Integrated Exploitation of Bayan Obo Multi-Metal Resources, Inner Mongolia University of Science and Technology, Baotou, China) ***Magnetocaloric Properties of MnFePSiGeB Compounds Prepared by Spark Plasma Sintering***

11:50-12:10	**Invited Lecture 3** Dr. **Jyothi Rajesh Kumar** (Convergence Research Center for Development of Mineral Resources (DMR), Korea Institute of Geoscience and Mineral Resources (KIGAM), Daejeon 34132, South Korea) ***Critical Rare Earths Recovery for Clean Energy Technology Applications***
12:10-12:30	**Invited Lecture 4** Prof.**Feng Liu** (College of Chemistry, Nanchang University Xuefu Avenue 999, Honggutan New District, Nanchang 330031, PR China) ***Bio-based polymers derivated from several aromatic or alicyclic biomass small molecules***
Session II-2(RoomB: 106) (11:10-12:30) (Session Chairman : Dr.Estelle Leonard)	
11:10-11:30	**Invited Lecture 5** Prof.**Hongzhi Liu** (School of Chemistry and Chemical Engineering, Shandong University, Jinan, China) ***Hybrid Silsesquioxanes-Based Luminescent Porous Materials***
11:30-11:50	**Invited Lecture 6** Prof. **Suresh Sagadevan** (Nanotechnology & Catalysis Research Centre, University of Malaya, Kuala Lumpur, Malaysia) ***Synthesis, Growth, and Characterization of Thiourea and Thiocyanate Family Non-Linear Optical Single Crystals for Optoelectronic Device Applications***
11:50-12:10	**Invited Lecture 7** Prof. **Chinnawut Pipatpanukul** (Faculty of Engineering, Burapha University) ***Photoactive Polymer Network Approaches for DNA Microarray Biosensor***
12:10-12:30	**Invited Lecture 8** Prof.**Nunticha Limchoowong**(Materials Chemistry Research Center, Department of Chemistry and Center of Excellence for Innovation in Chemistry, Faculty of Science, Khon Kaen University, Khon Kaen 40002, Thailand) ***Preconcentration and trace determination of copper(II) in Thai food recipes using Fe_3O_4@Chi–GQDs nanocomposites as a new magnetic adsorbent***
12:30-13:30 Lunch Time	
Session III (RoomA: 107) (13:30-15:00) (Session Chairman : Prof. Dr.Masahiro Toyoda)	
13:30-14:00	**Plenary Lecture 3** Prof.**Shin-ichi Kondo** (Faculty of Science, Yamagata University) ***Anion Recognition and Chiral Anion-induced CD by Cyclic Bisurea Derivatives***

	with 2,2'-Binaphthalene as Spacers
14:00-14:30	**PlenaryLecture 4** Prof. **Estelle Leonard (**T.I.M.R. EA 4297 ESCOM/UTC, 1allée du réseau Jean-MarieBuckmaster, F-60200 COMPIEGNE) ***The use of azobenzene in sustainable development context***
14:30-15.00	**PlenaryLecture 5** Prof. **Xiangke Wang (**North China Electric Power University, Beijing, 102206, P.R. China) ***Efficient removal of metal ions from aqueous solutions using carbon nanomaterials***
Poster Session (15:00-15:30) (Session Chairman: Prof. Dr. Chuyang Xu) with Coffee and Beverage **(Attachment time : Before 11:00)**	
Session IV-1 (RoomA: 107) (15:30-16:40) (Session Chairman : Prof. Dr.ChanKyung Kim)	
15:30-15:50	**Invited Lecture 9** Dr. **Himanshu Agarwal** (Executive Editor, Asian Journal of Chemistry (ISSN: ISSN 0970-7077) & Director, Asian Publishing Corporation, India) ***Ranking of Journals using Bibliometrics: A Controversial Metrics***
15:50-16:10	**Invited Lecture 10** Prof. **Hu Kunhong** (School of Energy, Materials and Chemical Engineering, Hefei University, Hefei, 230601, China) ***Multi-functional nano-MoS2: Preparation, tribological properties, and functional conversion from lubrication to photocatalysis***
16:10-16:25	**Oral Lecture 1** Prof. **Chengbao Liu** (Jiangsu Key Laboratory for Environment Functional Materials, Suzhou University of Science and Technology, Suzhou 215009, China) ***Acarbon quantum dots/gold nanoparticles modified carbon pasteelectrode as a sensor for selective and sensitive detection of glucose***
16:25-16:40	**Oral Lecture 2** Prof. **Bo Zhong** (School of Materials Science and Engineering, Harbin Institute of Technology at Weihai *, Weihai 264209, People's Republic of China) ***Lightweight hexagonal boron nitride and carbon nanomaterial composites with excellent microwave absorption: Design and massive fabrication***
Session IV-2 (RoomB: 106) (15:20-16:40) (Session Chairman : Prof. Dr.Hongzhi Liu)	
15:30-15:50	**Invited Lecture 11**

	Prof.**Zhi-Jun Zhang** (School of Materials Science and Engineering, Shanghai University, Shanghai, 200444, P. R. China) ***Intense Red Emitting Photoluminescence and Mechanoluminescence from MZnSO:TM for stress sensor***
15:50-16:10	**Invited Lecture 12** Prof **Jingbiao Cui** (Department of Physics, University of North Texas, TX 76203, USA) ***Emerging 2D Material Si_2Te_3 for Next Generation Memory Application***
16:10-16:25	**Oral Lecture 3** **Yonrapach Areerob** (Department of Advanced Materials Science & Engineering, Hanseo University, Chungnam 356-706, South Korea) ***Three-dimensional of graphene oxide Ba_2VPbSe_6 frameworkcomposite attach on cellulose based counter electrode for dye-sensitized Solar cell***
16:25-16:40	**Oral Lecture 4** Prof. **Prawit Nuengmatcha** (Nanomaterials Chemistry Research Unit, Department of Chemistry, Faculty of Science and Technology, Nakhon Si Thammarat Rajabhat University, 80280, Thailand) ***Preparation of highly efficient and magnetically recyclable Fe_2O_3/graphene/CuO nanocomposite for the photocatalytic degradation of methylene blue under visible light***
16:40-16:50 Coffee Break	
Session V-1 (**Room A: 107) (16:50-18:05) (Session Chairman: Prof.Dr. Xiangke Wang)**	
16:50-17:05	**Invited Lecture 13** Prof. **Jong-Sung Yu** (Department of Energy Science and Engineering, Daegu Gyeongbuk Institute of Science and Technology (DGIST), Daegu, 42988, Republic of Korea) ***Novel scalable production of single-layer graphene coated-metal nanoparticles for water splitting***
17:05-17:20	**Oral Lecture 5** Prof.**Guang Li,** (College of Materials Science and Engineering, Donghua University, Shanghai, China) ***Fabrication of porous carbon nanofiber andits promising application as catalyst support to enhance performance of H_2/O_2 fuel cell***

17:20-17:35	**Oral Lecture 6** Prof. **Saksit Chanthai,** (Materials Chemistry Research Center, Department of Chemistry and Center of Excellence for Innovation in Chemistry, Faculty of Science, Khon Kaen University, Khon Kaen 40002, Thailand) ***Ultrasound-assisted magnetic solid-phase microextraction and enrichment of heavy metals in water samples using thiol-functionalized graphene oxide composited with iron oxide***
17:35-17:50	**Oral Lecture 7** Prof. **JingWang,** (College of materials science and engineering, Anhui University of Science and Technology, Huainan, Anhui 232001) ***New Carbon Nanomaterials and Their Composites***
17:50-18:05	**Oral Lecture 8** Prof. **Rachadaporn Benchawattananon,** (Integrated Science Faculty of Science Khon Kaen University Khon Kaen Thailand 40000) ***Health risks of hidden heavy metal in lipstick in Khon Kaen Thailand***
Session V-2 (RoomB: 106) (16:35-18:05)(Session Chairman : Prof. Dr. Saksit Chanthai)	
16:50-17:05	**Oral Lecture 9** Prof. **Paweena Porrawatkul** (Nanomaterials Chemistry Research Unit, Department of Chemistry) ***Effect of aluminium ion doping on the deactivation of photocatalytic activity of green synthesized ZnO nanopowder for application in sunscreens***
17:05-17:20	**Oral Lecture 10** Prof. **Saiqa Ikram** (Department of Chemistry, Faculty of Natural Sciences, Jamia Millia Islamia (Central University) New Delhi-110025 INDIA ***Natural Gums Derived Materials as Superabsorbent (SAPs) for Hygiene & Agriculture Applications***
17:20-17:35	**Oral Lecture 11** Prof. **Yucheng Hao,** (Department of Chemical and Material Engineering, Hefei University, Hefei 230000, China) ***Two Dimensional Uranyl Borates: From Conventional to Extreme Conditions***
17:35-17:50	**Oral Lecture 12** Prof. **Nong Xu,** (School of Energy, Materials & Chemical Engineering, Hefei University, Hefei, P. R. China 230601) ***Novel Sequential Electroless Plating for Fabrication of Palladium-Ruthenium***

	Composite Membrane and its Characterization of Hydrogen Separation/Purification
17:50-18:05	**Oral Lecture 13** Prof.**Yanfen Wang,** (School of Physics & Materials Science, Anhui University, Hefei 230601, PR China) ***A novel Ag/rGO/TiO2 nanorod array as powerful substrate for photocatalytic degradation and SERS detection***
Session V-3 (RoomC: 107) (16:35-18:05)(Session Chairman : Prof. Dr. Feng Liu)	
16:50-17:05	**Oral Lecture 14** Prof.**Gang He,** (School of Physics and Materials Science, Anhui University, Hefei 230039, P.R. China) ***Low-Voltage-Operating ZnSnO Transistors and Logic Circuits Based on Water-Driven ZrGdOx Dielectric***
17:05-17:20	**Oral Lecture 15** Prof.**Qin-fang Zhang,** (School of Materials Science and Engineering, Yancheng Institute of Technology, Yancheng 224051, P. R. China) ***Electronic and adsorption properties of two-dimensional quantum dots for gas sensing and wastewater treatment***
17:20-17:35	**Oral Lecture 16** Prof.**Xian-Yang Sun,** (Key Laboratory of Functional Molecule Design and Interface Process, Anhui Jianzhu University, Hefei Anhui, P. R. China, 230601) ***WO_3•0.33H_2O induced synthesis of porous g-C_3N_4/WO_3 photocatalyst for efficient hydrogen generation under visible light***
17:35-17:50	**Oral Lecture 17** Prof. **Siree Saengthong,** (Integrated Science Faculty of Science Khon Kaen University Khon Kaen Thailand 40000) ***Use of Scanning Electron Microscope for Investigation Artificial Jewelry***
17:50-18:05	**Oral Lecture 18** Prof. **Atiwat Yaowakul,** (Integrated Science Faculty of Science Khon Kaen University Khon Kaen Thailand 40000) ***Teeth Cleaning Technique for Forensic Dentistry***

Banquet (18:30 ~20:30)	**Ming Culture Palace Hotel, Poster Awards**
20:20-20:30	Closing Remark**(Prof. Dr. Zhaoqi Sun)**

November 23(Saturday), 2019

9:30 ~ ~12:00	Conference Tour
13:00~	Free tour

November 24(Sunday), 2019

Depature

Presentation Guide

Plenary Lectures

Invited Lectures

Oral Lectures

Posters

Plenary Lecture

Fast Preparation of Nanostructured Photocatalyst Thin Film by Combustion and Its Application

Kyo-Seon Kim*

Department of Chemical Engineering, Kangwon National University, Chuncheon, Kangwon-Do, South Korea

E-mail: kkyoseon@kangwon.ac.kr

Abstract

For practical application of photocatalyst materials, it is quite important to prepare the photocatalyst thin film with large surface area rapidly. We have demonstrated that the vertically aligned NW-structured WOx can be grown fast in a combustion system incorporated with wire feeders.[1-2]The nanostructured WO_3 photocatalyst thin film was prepared by combustion process, was modified to prepare the hybrid photocatalyst system and was applied to water splitting reaction with high efficiency.[3]

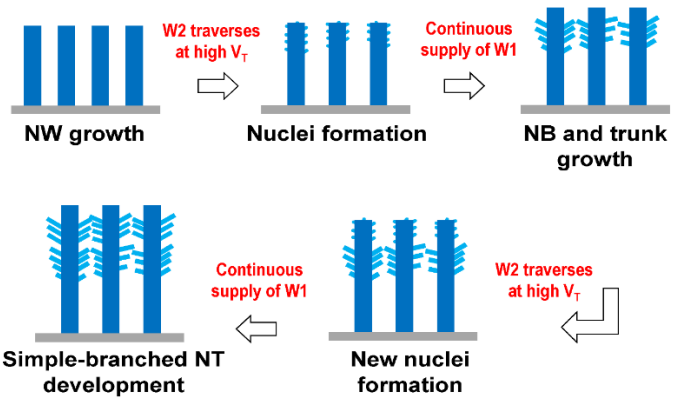

Keywords: WO_3 photocatalyst, nanostructured thin film, combustion process

References

(1) Ding J.-R.; Kim K.-S. Facile growth of 1-D nanowire-based WO_3 thin films with enhanced photoelectrochemical performance. *AlChE J*. 2016, 62, 421-428.http://dx.doi.org/10.1002/aic.15105.

(2) Ding J.-R.; Kim K.-S. Rapid growth of vertically aligned tungsten oxide nanostructures by flame vapor deposition process. *Chem. Eng. J*. 2016, 300, 47-53. http://dx.doi.org/10.1016/j.cej.2016.04.106.

(3) Ding J.-R.; Kim K.-S. 1-D WO_3@$BiVO_4$ heterojunctions with highly enhanced photoelectrochemical performance. *Chem. Eng. J*. 2018, 334, 1650-1656.https://doi.org/10.1016/j.cej.2017.11.130.

EDLC characteristics of carbon materials derived from COAL EXTRACT

Masahiro Toyoda[1], Tomoki Tsumura

Department of Applied Chemistry, Oita University,

700 Dannoharu, Oita 870-1124, Japan

1. Introduction

Hyper coal (HPC) is the thermally extracted ash-free component of coal, which dissolves in pyridine to yield a highly conductive viscous solution. This solution prepares carbon fiber precursors via an electrospinning equipment; subsequently, these precursors are heat treated. Carbon fibers obtained are dominated by micropores containing an approximately specific surface area of 1000 m2/g. Moreover, because the carbon fibers are obtained in the form of a nonwoven fabric, they are directly available as electrodes without a binder. A previous study reports that the specific capacitance of the electric double layer capacitor (EDLC) is 300 F/g at a current density of 50 mA/g. When water is used for HPC as poor solvent, the HPC is precipitated from the solution, resulting in a powdered carbon precursor that is converted into a powdered carbon material through heat treatment. This study examines the EDLC characteristics of the microporous carbon powder using HPC as the raw material. Results indicate that the EDLC of the powdered carbon material without activation exceeded 50 F/cm2 in aqueous sulfuric acid (H2SO4).

2. Materials and methods

HPC was derived from bituminous coal and its powder was prepared via precipitation method, in which it was dissolved in pyridine and subsequently precipitated by pouring the prepared HPC solution in water. The precipitated HPC powder was stabilized by heating it at 300 °C for 1 h in atmosphere and carbonized by heating it at 900 °C for 30 min under N2 atmosphere. The surface characteristics of the prepared carbon powder were evaluated through N2 adsorption–desorption measurement, and its specific surface area was calculated through the αS analysis of the adsorption isotherm. The EDLC electrode was prepared by mixing the carbon material, acetylene black, and polytetrafluoroethylene in the molar-weight ratio of 8: 1: 1. The EDLC characteristics were evaluated on a tripolar-type cell comprising a 40 % H2SO4 electrolyte and an Ag/AgCl reference electrode. Galvanostatic constant-current

charge–discharge measurements were taken within 50 – 5000 mA/g, whereas the electrostatic capacitance was calculated in the range of 0.2 – 0.8 V of the discharge curves.

3. Result and discussion

For the N2 adsorption–desorption isotherms of the powdered carbon material obtained through the precipitation method, the adsorbed amount of the powdered carbon material increased sharply to 100 cc/g under zero relative pressure, indicating the formation of micropores. The specific surface area was around 400 m2/g. The EDLC characteristics were evaluated using the charge– discharge measurement (in the range of 0 – 1 V) of an electrode prepared using the powdered carbon material. On charge–discharge curve at 50 μA/g, electrostatic capacitance calculated within 0.2–0.8 V of the discharge curve was approximately 220 F/g (capacitance per unit area = 255 μF/cm2), which is far higher than that of activated carbon (22 μF/cm2). On the currentdensity dependence of the electrostatic capacitance, the capacitance slightly decreased with an increase in current density; at the highest current density (5000 mA/g), the capacitance per unit area of the powdered carbon material prepared using the precipitation method was 46 μF/cm2, confirming that 90% of capacitance at 50 mA/g was retained at 5000 mA/g. In summary, the capacitance of the powered-carbon-material electrode prepared using HPC as raw material was 50 μF/cm2 , sufficiently robust to an increase in current density.

Anion Recognition and Chiral Anion-induced CD by Cyclic Bisurea Derivatives with 2,2'-Binaphthalene as Spacers

Shin-ichi Kondo

Faculty of Science, Yamagata University

We have reported that 2,2'-binaphthalene derivatives bearing urea groups at 8- and 8'-poisitions including receptor **2** showed potent anion recognition ability, in particular chloride selective ability in polar organic solvents.[1,2]Suitable separation of two urea groups perform four N-H hydrogen bonding to an anion to achieve such selective binding of anions. A cyclic bisurea derivative **1b**, which has an additional 2,2'-binaphthyl unit, showed larger association constants for anions than those of acyclic **2** in one or two orders of magnitude due to the rigid macrocyclic effect.[3] From the X-ray crystal structure and the DFT calculations of **1b**· Cl^-, the complex showed distorted D_2 symmetry (Fig. 2), indicating equilibration of two enantiomers of **1b**· Cl^- in solution.

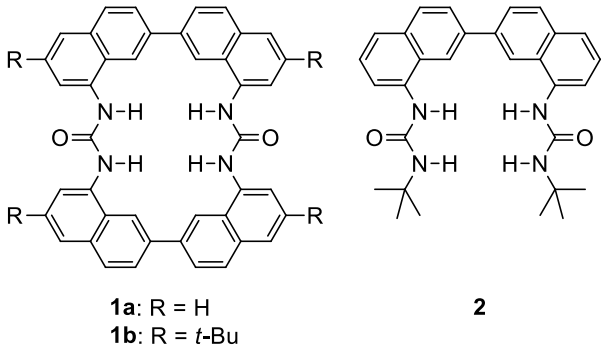

Figure 1. Molecular structures of acyclic and cyclic bisurea derivatives

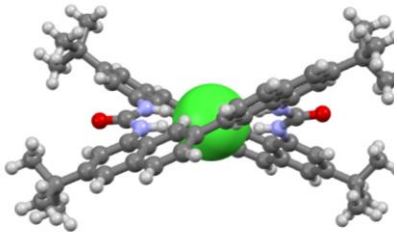

Figure 2. The X-ray structure of **1b**· Cl^-

Addition of chiral guest anions into a solution of receptor **1b**, two diastereomeric mixture should be formed. If the energy difference between two diastereomeric complexes is sufficient, one of the diastereomer should be excess and the corresponding circular dichroic (CD) spectrum should be measured from the spatial arrangement of two binaphthyl units. Therefore, we observed the association properties and CD of the receptor **1b** upon the addition of tetrabutylammonium salts of *N*-acetyl-α-amino acids. UV-vis spectral titrations of **1b** for *N*-Ac-AlaO$^-$, *N*-Ac-ValO$^-$, *N*-Ac-LeuO$^-$, and *N*-Ac-PheO$^-$, as guest anions, suggest 1:1 complexation and the association constants were one or two order smaller than that for AcO$^-$, which may due to the steric repulsion of amino acid side chains with the receptor. In the

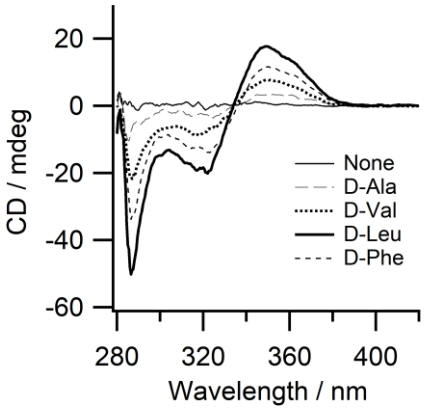

Figure 3. TheCD spectra of **1b** in the absence and presence of 2 equiv of chiral carboxylates in MeCN at 298 K.

absence of guest, CD of **1b** was silent, however, the addition of D-amino acid derivatives induced positive Cotton effect at around 350 nm (Fig. 3) and the mirror images were obtained upon the addition of the enantiomers (L-form). The CD intensities were saturated upon the addition of ca. 1 equiv of the guests. Addition of chiral amino acid derivatives into a solution of receptor **2** also induced CD signal, however the intensities were extremely smaller comparing with those of **1b**. These results suggest that receptor **1b** forms 1:1 complex with chiral amino acid derivatives and one of the diastereomers was predominantly formed during the titrations[4]. The stable conformation and CD spectrum of the diastereomers by DFT calculations showed good agreement of the observed spectrum.

References

1. S. Kondo, M. Nagamine, S. Karasawa, M. Ishihara, M. Unno, and Y. Yano, *Tetrahedron*, **2011**, *67*, 943.

2. S. Kondo, H. Sonoda, T. Katsu, and M. Unno, *Sens. Actuators B*, **2011**, *160*, 684.

3. A. Satake, Y. Ishizawa, H. Katagiri, and S. Kondo, *J. Org. Chem.*, **2016**, 81, 9848.

4. K. Osawa, H. Tagaya, and S. Kondo, *J. Org. Chem*, **2019**, *84*, 6623.

The use of azobenzene in sustainable development context

Estelle Leonard*

T.I.M.R. EA 4297 ESCOM/UTC, 1 allée du réseau Jean-Marie Buckmaster, F-60200 COMPIEGNE

E-mail: e.leonard@escom.fr

Abstract

Photochromic molecules such as azobenzenes can involve a huge amount of applications, such as forensics, food coloring or textile dyes… Here we will see how they can integrate a sustainable concept, especially for photochromic micellar catalysis.[1]

Indeed, their capability of isomerization can lead to a better on-off catalysis, with a better products recovery and thus a better recyclability of the media.[2,3]

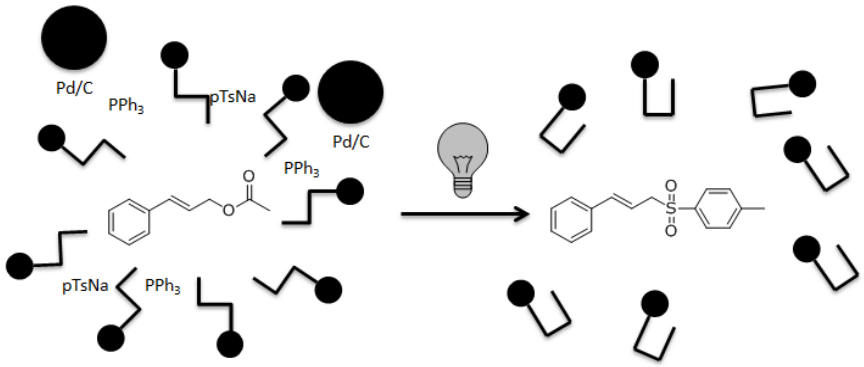

Keywords: Azobenzenes, micellar catalysis

References

(1) Léonard, E.; Mangin, F.; Villette, C.; Billamboz, M.; Len, C. Azobenzenes and Catalysis. *Catal. Sci. Technol.***2016**, *6* (2), 379–398. https://doi.org/10.1039/C4CY01597E.

(2) Billamboz, M.; Mangin, F.; Drillaud, N.; Chevrin-Villette, C.; Banaszak-Léonard, E.; Len, C. Micellar Catalysis Using a Photochromic Surfactant: Application to the Pd-Catalyzed Tsuji–Trost Reaction in Water. *J. Org. Chem.***2014**, *79* (2), 493–500. https://doi.org/10.1021/jo401737t.

(3) Drillaud, N.; Banaszak-Léonard, E.; Pezron, I.; Len, C. Synthesis and Evaluation of a Photochromic Surfactant for Organic Reactions in Aqueous Media. *J. Org. Chem.***2012**, *77* (21), 9553–9561. https://doi.org/10.1021/jo301466w.

Efficient removal of metal ions from aqueous solutions using carbon nanomaterials

Xiangke Wang

North China Electric Power University, Beijing, 102206, P.R. China

* Corresponding author: xkwang@ncepu.edu.cn.

This paper presents the surface modification of carbon nanomaterials (carbon nanotubes, graphene oxides) using different functional groups and their application for the efficient and selective elimination of heavy metal ions from aqueous solutions. The interaction mechanism between heavy metal ions and carbon nanomaterials was studied by batch sorption experiments, surface complexation modeling, spectroscopy analysis (XPS and EXAFS) and theoretical calculations. The results showed that the carbon nanomaterials have high sorption capacity in the preconcentration of heavy metal ions from large volume of aqueous solutions, and the surface grafting functional groups could enhance the selectivity of target metal ions from solutions. The interaction of Eu(III), Am(III) and U(VI) with graphene oxides and carbon nanotubes were studied under different experimental conditions, and the difference in the interaction of trivalent lanthanides and actinides were found quite different under same experimental conditions, which were quite different from the physicochemical behaviors of lanthanides and actinides on clay minerals and oxides. The difference was attributed to the surface properties of nanomaterials and the heavy metal ions.

The following Figures show the interaction of Eu(III) and Am(III)-243 with carbon nanotubes and the interaction of U(VI) with graphene oxides with different functional groups. From the DFT calculations, the bind energy of metal ions with different functional groups are quite different.

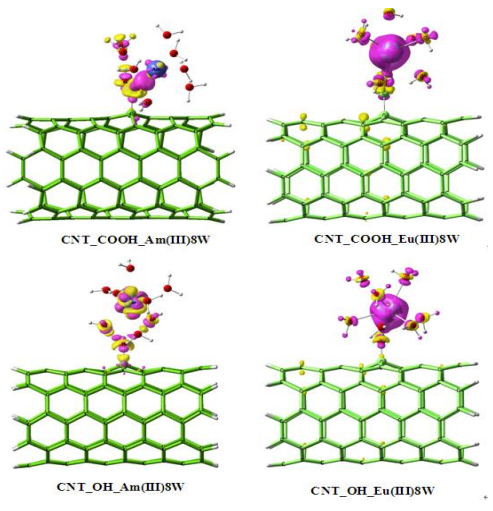

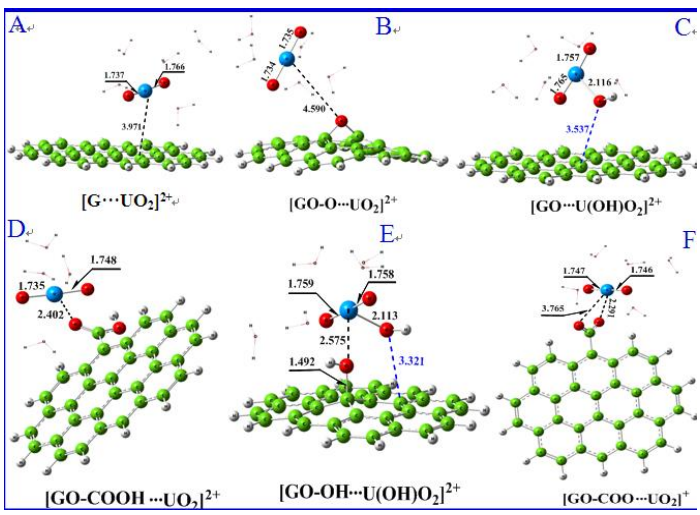

Invited Lectures

Investigation on the Photoactivity of La-doped $SrTiO_3$ Nanocubes for Degradation of 2-naphthol under the Visible Light Irradiation

Quoc Cuong Le, Xuan-Duy-Thao Nguyen, Ngoc-Quoc-Duy Vo and Minh-Vien Le

Faculty of Chemical Engineering, Ho Chi Minh city University of Technology, 268 Ly Thuong Kiet, 14 Ward, District 10, Ho Chi Minh City, Vietnam

** E-mail: lmvien@hcmut.edu.vn*

Abstract

In the present study, $SrTiO_3$ nanocubes were synthesized via hydrothermal method with $SrCl_2.6H_2O$ and TiO_2 as the precursor agents. The hydrothermal synthetic process was conducted under the alkaline media at various hydrothermal temperatures (and various durations. The influences of hydrothermal temperature and time on the physicochemical properties of synthesized $SrTiO_3$ were characterized in terms of structure, surface area, morphology, and band-gap energy through X-ray diffraction (XRD), Brunauer-Emmett-Teller (BET), scanning electron microscopy (SEM) and UV-Vis Diffuse Reflectance spectra (DRS) methods. The XRD results revealed that single phase of $SrTiO_3$ was obtained in all samples. The sample which was synthesized at 130 °C for 48h (STO 130-48) shows the regular nanocube shape with estimated to be 40 nm. The surface area and band gap energy were measured to be 28.93 m^2/g and 3.14 eV, respectively. Their photocatalytic activity was tested through the degradation of 10 ppm 2-naphthol in water solution under the simulatedsolar light irradiation. The decomposition of 2-naphthol was described by Langmuir-Hinshelwood [1] using the following formula:

$$\ln\left(\frac{C}{C_0}\right) = -kt \qquad ------(1)$$

Where, *k* is the reaction rate constant and *t* (min) is the reaction time. The fitted results showed that the reaction rate constant of $SrTiO_3$ nanocubes synthesized at 130 °C for 48 h show the highest rate constance of 1.83×10^{-2} min^{-1}, which was higher than that of 12 h, 24 h, and 72 h (1.69×10^{-2} min^{-1}, 1.79×10^{-2} min^{-1} and 1.73×10^{-2} min^{-1}, respectively)

Moreover, the calculated band gap energies of La-doped $SrTiO_3$ ($Sr_{1-x}La_xTiO_3$) which x=0, 0.03, 0.05, 0.1 were corresponding to 3.15 eV, 3.06 eV, 2.98 eV and 3.17 eV respectively. The reduction in band gap energy may lead to raises the photocatalytic activity. Reaction rate constant increased from $SrTiO_3$ (1.83×10^{-2} min^{-1}) < $Sr_{0.9}La_{0.1}TiO_3$ (1.86×10^{-2} min^{-1}) < $Sr_{0.97}La_{0.03}TiO_3$ (1.88×10^{-2} min^{-1}) < $Sr_{0.95}La_{0.05}TiO_3$ (1.96×10^{-2} min^{-1}). In the La-doped $SrTiO_3$, Ti^{4+} cations were successfully replaced by La^{3+}, thus the bandgap energy is narrowed resulting

in enhanced photocatalytic activity in the visible light region.

Keyword: $SrTiO_3$, Photocatalyst, perovskite, 2-naphthol

References:

[1]. Xekoukoulotakis NP, Drosou C, Brebou C, Chatzisymeon E, Hapeshi E, Kassinos DF, Mantzavinos D. Kinetics of UV-A/TiO_2 photocatalytic degradation and mineralization of the antibiotic sulfamethoxazole in aqueous matrices. Catal. Today. 2011;161: 163-168

Magnetocaloric Properties of MnFePSiGeB Compounds Prepared by Spark Plasma Sintering

Gaofeng Wang and Tao Jing

Key Laboratory of Integrated Exploitation of Bayan Obo Multi-Metal Resources, Inner Mongolia University of Science and Technology, Baotou, China

Email:gaofengwang1982@163.com

Magnetic refrigeration based on the magnetocaloric effect (MCE) is a new application for replacing vapor-compression-cycle refrigeration around room temperature due to its high energy efficiency and low environmental impacts. Therefore, obtaining magnetic materials with large MCE is crucial to the successful application of magnetic refrigeration. In recent years, a number of magnetic compounds with large magnetocaloric effect (MCE) have been paid much attention due to the potential utilization in magnetic cooling application [1]. The Fe_2P-type compounds, such as $(Mn, Fe)_2(P, X)$, where X stands for one or two elements of as, Si, Ge [2,3], and $(Mn, Fe)_2(P, Si, Y)$, where Y represents an element of B, N or C [4], have been considered as one of the most promising refrigerants for magnetic refrigeration near room temperature. Traditionally, the Fe_2P-type compounds are prepared using ball milling followed by a long annealing process at high temperatures (at 1273 K - 1423 K for several hours up to several days). The obtained samples are normally in the form of powder or bulk but with low density and hardness, which is disadvantageous to the succeeding fabrication for practical application. Spark plasma sintering (SPS) is a new technique which takes short time to finish a sintering process, when comparing to the traditional sintering. In this work, we report on the crystal structure and magnetocaloric properties of MnFePSiGeB compounds prepared by SPS.

Tow series of compounds with nominal compositions of $Mn_{1.15}Fe_{0.85}Si_{0.16}Ge_{0.2}P_{0.64-x}B_x$ and $Mn_{1.15}Fe_{0.85}Si_{0.16}Ge_{0.2}P_{0.64}B_y$have been prepared by SPS at a sintering temperature of 1123 K and under a sintering pressure of 50 MPa. Analyses of the X-ray diffraction patterns indicate that the compounds crystallize mainly in the Fe_2P-type hexagonal structure (space group$P\bar{6}2m$). The compounds show good compactness. The Curie temperature increases and subsequently decreases with increasing content of B. All the studied compounds exhibit

first-order phase transitions due to the observation of thermal hysteresis. For the same quantity of B addition, the magnitudes of the Curie temperature variations are different in the two series of compounds. Isothermal entropy changes (ΔS_T) for the studied compounds have been determined from isofield magnetization curves using Maxwell relation. In general, the ΔS_T decreases with increasing B content. For a field change from 0 to 3 T, the maximum values of ΔS_T are found to be 13.9 J/kgK for x = 0.01 and 12.5 J/kgK for y = 0.02 near 300 K. The results reveal that the studied MnFePSiGeB compounds are potential candidates for magnetic refrigeration near room temperature.

References

[1]A. M. Tishin and Y. I. Spichkin, *The Magnetocaloric Effect and Its Applications*, Bristol, MA: IoP, 2003.

[2]O. Tegus, E. Brück, K. H. J. Buschow, et al., *Nature*, vol. 415, no. 6868, pp. 150-152, 2002.

[3]N. H. Dung, Z. Q. Ou, L. Caron, et al., *Adv. Mater.*, vol. 1, no. 6, pp. 1215-1219, 2011.

[4]X.F. Miao, N.V. Thang, L. Caron, et al., *Scripta Mater.*, vol. 124, 129-132, 2016.

Acknowledgments

The present work was supported by the National Natural Science Foundation of China (11564030), the Research Program of Science and Technology at Universities of Inner Mongolia Autonomous Region (NJYT-18-B07), the Natural Science Foundation of Inner Mongolia (2017MS0110), the Innovation Fund of Inner Mongolia University of Science and Technology (2016YQL02).

Critical Rare Earths Recovery for Clean Energy Technology Applications

Jyothi Rajesh Kumar

Convergence Research Center for Development of Mineral Resources (DMR), Korea Institute of Geoscience and Mineral Resources (KIGAM), Daejeon 34132, South Korea

E-mail: rkumarphd@kigam.re.kr, Tel: 82-42-868-3313

Abstract

In new millennium (21stcentury) Geologists, Chemists and Engineers focused much on research and development on rare earths processing; due to widespread high-tech applications of rare earths in many fields as well as daily lives. The supply and demand of the rare earths also one of main reason to focus scientist allover world. Predominantly rare earths natural resources are located in China; from year 2010, China controlled the export policy. In periodic table atomic number 57 to 71 (lanthanum to lutetium) are commonly called as rare earths or lanthanides. Yttrium (AN 39) and scandium (AN 21) also chemically having similar properties like lanthanides, due to this reason these two elements also belong to rare earths group. Based recent survey by DoE, USA some of the rare earths are in critical situation for future demands. Those are yttrium, europium, terbium, neodymium and dysprosium. At the same time these rare earths are widely used in clean energy technologies. The present study focused on how to recover the critical rare earths from used materials and how it will full will the future demands in clean energy technology applications. Hydrometallurgy deals the aqueous processing of the metals ions, up to industrial materials preparation. This lecture contains rare earths importance and motivation to present work followed by to recover hydrometallurgical techniques utilizationfinally the critical rare earths claim in clean energy technology applications.

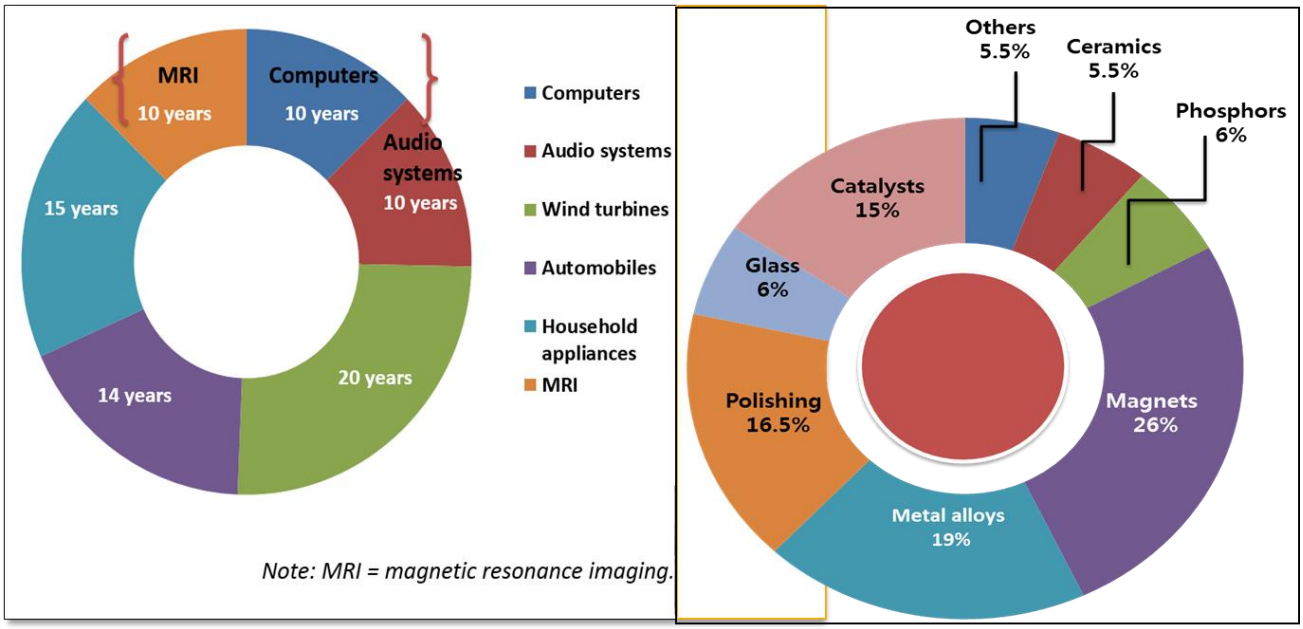

Life span of the electrical and electronic goods and demand of the rare earths in various sectors (Data adopted from *J. Ind. Ecol. 2011, 15, 836)*

Bio-based polymers derivated from several aromatic or alicyclic biomass small molecules

Haixia Qi, Juan Li, Hengsheng zhang, Zhongkai Wang, Feng Liu*

College of Chemistry, Nanchang University

Xuefu Avenue 999, Honggutan New District, Nanchang 330031, PR China

Correspondence to Feng Liu, email: liuf@ncu.edu.cn, Tel: 086-791 83969984

Abstract

The development of bio-renewable polymers is an important solution to release human dependence on the dwindling fossil resources. Of the vast amount of biomass varieties, small molecule derivatives have recently gained considerible attention due to the presence of abundant functional groups, which are capable of structural functionalization into the monomers tailored to different polymeriztion approachesincluding ADMET, ATRP and RAFT, etc. Compared with the long-chain alkyl biomass small molecules as represented by the fully studied α, ω-diol or diacid derivated from plant oil, the aromatic, especially alicylic biomass small molecules have been less investigated.

This talk deals with our recent work on converting the aromatic vanillin and alicyclic natural camphor into bio-based polymers. The only discrete industrialized aromatic lignin-derivative vanillin has been transformed into asymmetric diamine with phenoxyl-benzyloxyl linkage and pendent methoxyl group, which impart the resulting polyimides with balanced processing performance and thermal stabilities. A series of degradable polyimides under both acidic and basic environments have been devoloped by introducing acetal functionality and pyridine ring. Natural camphor has the molecular scaffold of alicyclic bicyclo [2.2.1] ketone that could readily be oxidatively clevaged into monocyclo difunctional compounds, such as cyclopentyl primary diol. Starting from this primary diol, we prepared a series of alicyclic-functionalied polyimides which exhibit low dielectric constant (ε') and high optical transparency, desired for microelectronic and optoelectronic applications. Polyacetal, polyacrbonate and polyoxalate have also been obtained from the alicylic diol by functional group metathesis polymerization (FGMP). It is revealed that the camphor-derivated alicyclic diol demonstrates adequate polymerization reactivity and imparts the resulting

polymers with higher thermal stabilty than the alkyl analogues. Our work indicates that several aromatic and alicyclic biomass small molecules including vanillin and camphor are promisng candidates for preparing bio-based polymers with high performance or via novel polymerization approaches.

Key words: bio-based polymer; biomass small molecules; polyimides; functional group metathesis polymerization.

Hybrid Silsesquioxanes-Based Luminescent Porous Materials

Hongzhi Liu

School of Chemistry and Chemical Engineering, Shandong University, Jinan, China

Recently, more attention has been devoted to hybrid porous materials considering their exhibiting some unique properties by combination with the advantages of inorganic and organic components. Cage silsesquioxaneshave proven to be an ideal building block to prepare hybrid nanoporous materials with enhanced thermal and mechanical properties in view of their rigidity and multifunctionality. [1, 2]

Very recently, octavinylsilsesquioxane (OVS) has been successfully used to preparesilsesquioxanes-basedporous materials *via*Friedel-crafts reaction and Heck reaction, cationic polymerization by us. [3-5] Moreover, the bulky cage could prevent the aggregation of chromophores and enhanceluminescent quantum yields in these hybrid materials. These silssesquioxanes-based luminescence porous polymers exhibited high surface area and thermal stability, which make them multifunctional and potentially apply in gas storage, water treatment, energy storage and sensors *etc.*

References:

1. Furgal, J. C.; Jae Hwan, J.; Theodore, G.; Laine, R. M. Analyzing Structure-Photophysical Property Relationships for Isolated T_8, T_{10}, and T_{12} Stilbenevinylsilsesquioxanes. *J. Am. Chem. Soc.* **2013,***135*, 12259-12269.
2. Watcharop, C.; Masaru, K.; Takahiko, M.; Ayae, S. N.; Atsushi, S.; Tatsuya, O. Porous Siloxane-Organic Hybrid with Ultrahigh Surface Area Through Simultaneous Polymerization-Destruction of Functionalized Cubic Siloxane Cages. *J. Am. Chem. Soc.* **2011,***133*, 13832-13835.
3. Yang, X.; Liu, H. Ferrocene-Functionalized Silsesquioxane-Based Porous Polymer for Efficient Removal of Dyes and Heavy Metal Ions. Chem. Eur. J. **2018,***24*, 13504-13511.
4. Ge, M.; Liu, H. A Silsesquioxane-Based Thiophene-Bridged Hybrid Nanoporous Network as A Highly Efficient Adsorbent for Wastewater Treatment. *J. Mater. Chem. A.* **2016,***4*, 16714-16722.
5. Y. Du, M. Ge, H. Liu, Porous Polymers Derived from Octavinylsilsesquioxaneby Cationic Polymerization. *Macromol. Chem. Phys.***2019**, *220*, 1800536-1800543.

Synthesis, Growth, and Characterization of Thiourea and Thiocyanate Family Non-Linear Optical Single Crystals for Optoelectronic Device Applications

Suresh Sagadevan

Nanotechnology & Catalysis Research Centre, University of Malaya, Kuala Lumpur, Malaysia

E-mail: sureshsagadevan@gmail.com

Abstract

Recently, the nonlinear optical properties (NLO) of some products of thiourea have attracted great interest because these metal-organic crystalline materials have the potential for combining high optical nonlinearity and the chemical flexibility of organics with the physical ruggedness of inorganics. The thiourea molecule is an interesting inorganic matrix modifier due to its large dipole moment and its ability to form an extensive network of hydrogen bonds. The centrosymmetric thiourea molecule, when combined with inorganic salts yields noncentrosymmetric complexes, which has nonlinear optical properties. Metal complexes of thiourea, commonly called semi-organic, include the advantage of both organic and inorganic part of the complex. In addition to retaining the high optical nonlinearities of the organic molecules, they also possess favourable physical properties. An added advantage is that large single crystals can be grown from slow evaporation solution growth technique. However, for practical applications, organic materials have certain setbacks such as inadequate transparency, poor optical quality, and low laser damage threshold. Hence, the recent search is concentrated on semi-organic materials due to their large nonlinearity, high resistance to laser-induced damage, low angular sensitivity and good mechanical hardness. Hence, keeping this in view, attempts have been made in this study to grow and characterize the single crystals of tetra thiourea potassium iodide (TTPI) and tetra thiourea potassium bromide (TTPB). During the last two decades, the investigation on the crystal growth and properties of organometallic and coordination complex crystal materials exhibiting excellent second-order nonlinear optical (SONLO) properties has attracted the researchers. As a novel kind of SONLO crystal materials, such materials have the potential in a class by themselves for combining the high optical nonolinearity and chemical flexibility of organics with excellent mechanical properties and short wavelength transmittance of inorganics. Like organics, organometallic compounds can

offer the advantages of architectural flexibility and ease of fabrication and tailoring. Like inorganics, organometallic compounds have excellent mechanical and thermal stability. Hence, keeping this in view, attempts are made to combine the thiocyanate ligand with the transition metal ions such as Cd^{2+} and Hg^{2+}. Thiocyanate (SCN) ion is a good chromophore for second-order NLO properties and it forms coordination compounds with metal ions.

Therefore, my talk will be an overview of various technological important artificial inorganic single crystals ranging in size from very small to large is given appreciable attention. Further, the growth mechanism, nucleation kinetics, origin of nonlinearities and the effect of impurities on the habit modification of some NLO crystals viz. Besides, fundamentals of the crystal growth and the problems involved will be briefly discussed during my presentation.

Keywords: Nonlinear optical material, crystal growth, Thiourea and Thiocyanate, and Optoelectronic Device Applications

Photoactive Polymer Network Approaches forDNA Microarray Biosensor

Chinnawut Pipatpanukul

Faculty of Engineering, Burapha University

For the small detection of biomedical assays such DNA or protein microarray. The immobilized biomolecules on the surface of biochips is the major factor. A variety of immobilizing technique have been published over the year. Almost of them need rather complicated production processes and difficultly surface modification. We report a simple fabrication method, which is based on photoactive polymer networks. DNA microarray biochip on the surface-attached polymer network is preformed onto unmodified polymer surface using photoactive benzophenone group. Both surface modification and immobilization is achieved in a few step process. Biomolecules are mixed with the photoactive copolymer in buffer solution and spotted onto the surface of substrate. Then, the substrate was cross-linked as well as bound to the surface during short expose to UV light at 254 nm. DNA immobilized surface quality was studied. Fluorescence and microscope imaging techniques were used to determine the DNA probe distribution that related to their hybridization signal. In identical spot DNA microarray containing varied chemical component in the printing solution such co-solvents, surfactants, salt buffers and fabrication parameter such humidity and temperature are involved. Two fluorescence emission imaging data for individual microarrays were correlated with the same fabrication condition. Fluorescence image analysis confirmed both printed DNA distributions and copolymer dispersion by tracking bound Cy5 dye conjugated DNA

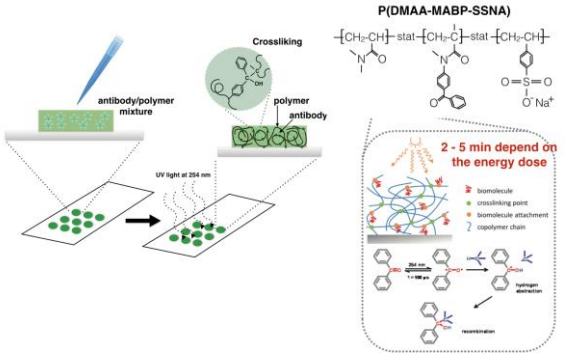

Figure 1. Fabrication of microarray by photoactive surface-attached polymer networks

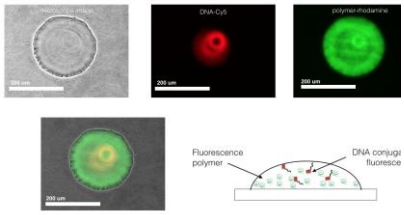

Figure 2. The optical and fluorescent image of DNA probe distribution on a spot of photoactive polymer network microarray.

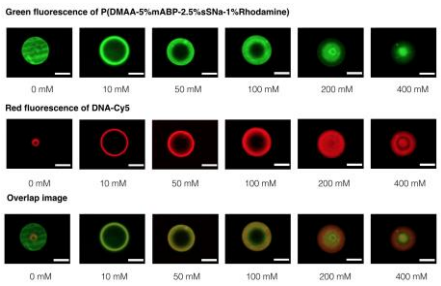

Figure 3. Images of DNA distribution and polymer morphology by the effect of spot condition with salt

probe and Rhodamine B side-chain in copolymer correlating to fluorescence patterns within identical spots. Both polymer and DNA fluorescence image support the phase separation effect on dried spot microarrays, with high-density DNA-Cy5 located in spot centers and was covered by polymer. Fluorescence image analysis results for DNA droplet drying show DNA distribution pattern depends upon salt crystalline structure. The phase separation was soared where humidity and temperature increasing during fabrication. The study directly supports different printing chemical component and environment within spots that yield microarray signal variations known to affect DNA target hybridization efficiencies and kinetics. These variations critically affect probe-target duplex formation and DNA microarray signal generation.

References

1. M. Rendl, A. Bonisch, A. Mader, K. Schuh, O. Prucker, T. Brandstetter, and J. Ruhe, *Langmuir* **2011**, 27, 6116-6123.

2. C. Pipatpanukul, R. Amarit, A. Somboonkaew, B. Sutapun, A. Vongsakulyanon, P. Kitpoka, T. Srikhirin, and M. Kunakorn, M., *Vox Sang.* **2016**,110(1), 60-69.

3. C. Pipatpanukul, C. Kataphiniharn, T. Wangkam, B. Sutapun, P. Kitpoka, M. Kunakorn, T. Srikhirin, Sens. and Actua. B, **2018**, 273, 703-709.

4. M. Moschallski, J. Baader, O. Prucker, J. Rühe, *Anal Chim Acta.* **2010**, 25, 671(1-2), 92-98

Preconcentration and trace determination of copper(II) in Thai food recipes using Fe_3O_4@Chi–GQDs nanocomposites as a new magnetic adsorbent

Nuntricha Limchoowong,[1,2] Phitchan Sricharoen,[1]Prawit Nuengmatcha,[1,3]Thitiya Sripakdee,[1,4]Suchila Techawongstien,[5]Saksit Chanthai,[1,*]

[1] *Materials Chemistry Research Center, Department of Chemistry and Center of Excellence for Innovation in Chemistry, Faculty of Science, Khon Kaen University, Khon Kaen 40002, Thailand*

[2] *Department of Chemistry, Faculty of Science, Srinakharinwirot University, Bangkok 10110, Thailand*

[3] *Department of Chemistry, Faculty of Science and Technology, Nakhon Si Thammarat Rajabhat University, Nakhon Si Thammarat 80280, Thailand*

[4] *Chemistry Program, Faculty of Science and Technology, Sakon Nakhon Rajabhat University, Sakon Nakhon 47000, Thailand*

[5] *Department of Plant Science and Agricultural Resources, Faculty of Agriculture, Khon Kaen University, Khon Kaen 40002, Thailand*

**E-mail: sakcha2@kku.ac.th*

Abstract:

This study describes the preparation, characterization, and application of a new magnetic chitosan–graphene quantum dots (Fe_3O_4@Chi–GQDs) nanocomposite as an adsorbent for the preconcentration of Cu(II) in Thai food recipes or the so-called “Som Tam” (green papaya salad) prior to determination by inductively coupled plasma–optical emission spectrometry. The spectroscopic and magnetic properties along with the morphology and thermal property were analyzed using FTIR, EDX, XRD, TGA, VSM, and TEM. Preconcentration optimizations including pH, dosage of adsorbent, adsorption–desorption time, concentration and volume of elution solvent, sample volume and enrichment factor, and reusing time were investigated. Good linearity was obtained ranging from 0.05 to 1500 μg L^{-1} with correlation coefficient of 0.999. Limit of detection was 0.015 μg L^{-1}. Relative recoveries of

85.4–107.5% were satisfactorily obtained. This Fe_3O_4@Chi–GQDs has high potential to be used as preconcentration method and can be reused 7 times with high extraction efficiency.

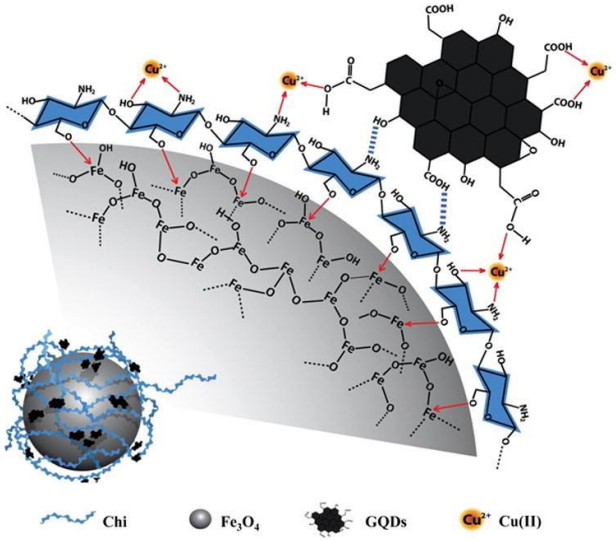

Ranking of Journals using Bibliometrics: A Controversial Metrics

Himanshu Agarwal

Executive Editor, Asian Journal of Chemistry (ISSN: ISSN 0970-7077)

&

Director, Asian Publishing Corporation, India

E-mail: asianpubco@gmail.com

Abstract

As everybody knows **THE IMPACT FACTOR** of a journal reflects the number of times the average article is cited in the two years following publication. Normally, Researchers/Scientists would view a high initial impact factor as a **BLESSING**. Whereas I think that having high impact factor means that the journal is **HIGHLY RATED** and **CITED** and that the texts published probably have scientific importance. Moreover, Overuse of impact factors suppresses controversial ideas means that had been **SELECTED FOR PUBLICATION** not because of their scientific merit but because of their **PUBLICITY VALUE**, which resulted in the system of peer review had failed to detect **SUBSTANTIAL FLAWS** in several articles [1]. Using bibliometrics like impact factor, Eigen-factor score, CiteScore, SCImago Journal Rank, Source-Normalised Impact per Paper, H-index, *etc*. *etc. etc*…. may not assess the influence and importance of an acceptable research articles [2]. So, just the impact factor alone, might not represent the fairest and most legitimate approach to assess the influence and importance of an acceptable journal, and/or not only a sound journal in their respective disciplines.

References

1. T.A. Branch, Citation Patterns of a Controversial and High-Impact Paper: Worm et al. (2006) ‘‘Impacts of Biodiversity Loss on Ocean Ecosystem Services’’. ***PLoS ONE*** 8(2): e56723 (2013). doi: 10.1371/journal.pone.0056723
2. Ernesto Roldan-Valadez, Shirley Yoselin Salazar-Ruiz, Rafael Ibarra-Contreras and Camilo Rios, ***Irish Journal of Medical Science*** (2018); https://doi.org/10.1007/s11845-018-1936-5

Multi-functional nano-MoS_2: Preparation, tribological properties, and functional conversion from lubrication to photocatalysis

Hu Enzhu, Chen min, Shi yongjie, Hu Kunhongi

School of Energy, Materials and Chemical Engineering, Hefei University, Hefei, 230601, China

Abstract: Molybdenum disulfide (MoS_2) is widely applied as lubricating additives and catalysts. The morphology of MoS_2 particles affects their properties. Spherical MoS_2 nanoparticles present excellent lubrication performances but very bad catalytic activity. The lubrication of spherical MoS_2 can be attributed to the deformation and exfoliation of nano-spheres in the friction process. The exfoliation of nano-sphere can produce platelet-like MoS_2 with a good photocatalytic performance in the degradation of organic pollutants. The exfoliation of nano-sphere and tribochemical reaction may change the chemical activity of MoS_2, which may possibly induce a functional conversion from lubrication to photocatalysis for the degradation of waste organic lubricants. The research item investigated the formation mechanism of MoS_2 nano-sphere on natural layered minerals, the tribological properties of the obtained MoS_2 composites, the relative morphological wear mechanism (nano-spheres→nano-platelets), the synergetic lubrication and the tribochemical behaviors. The mechanism of functional transformation (lubrication → photocatalysis) of nano-spheres/minerals composites after worn into nano-platelets composites will also be studied. The continued work will try to provide an idea to design green lubricants with potential photocatalytic properties. The item is to establish a "from lubricant to catalyst" designing method. This work tries to resolve the pollution of lubricants via a new approach. The research results reveal significances in lubricating materials, tribology, and pollution control chemistry.

Keywords: lubricant; tribology; molybdenum disulfide; tribochemistry; photocatalysis

*Corresponding author, Email: hukunhong@163.com

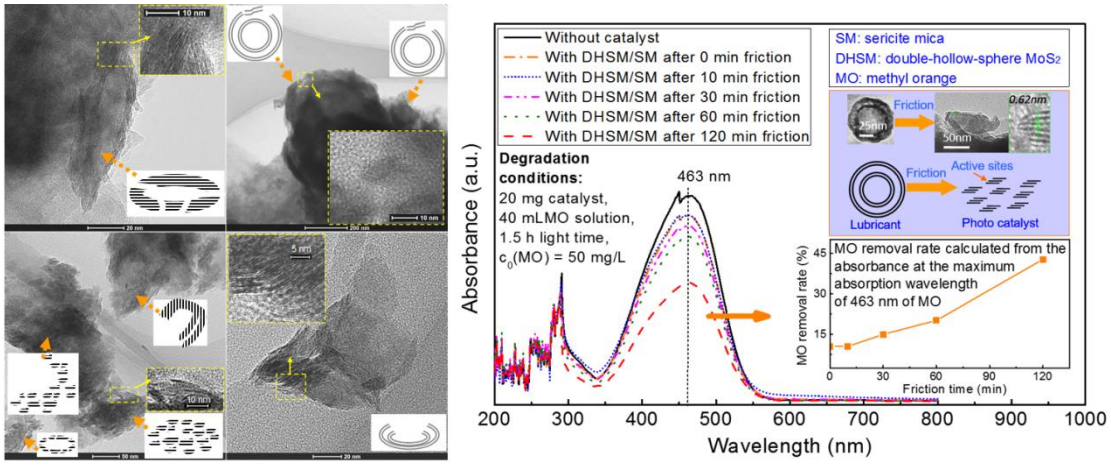

Acknowledgments: This project was supported by Anhui Province Universities and Colleges Natural Science Foundations (Grant Nos. KJ2018ZD053) and National Natural Science Foundation of China (Grant No. 51375139).

Intense Red Emitting Photoluminescence and Mechanoluminescence from *M*ZnSO:TM for stress sensor

Zhi-Jun Zhang, [a,] *Yu Zhou, [a] Yun-Ling Yang, [b] Jing-Tai Zhao*

[a]*School of Materials Science and Engineering, Shanghai University, Shanghai, 200444, P. R. China*

**E-mail Address: zhangzhijun@shu.edu.cn, jtzhao@shu.edu.cn*

Novel red emitting mechanoluminescent phosphors *TM*-activated *M*ZnSO (*TM*= transition metal, *M*=Ca, Sr) were successfully synthesized by solid-state reaction at high temperature. Photoluminescence (PL) and mechanoluminescence (ML) properties of *TM*-activated *M*ZnSO phosphors were investigated for the first time. The high PL/ML efficiency and tunable emission color of these phosphors make them to show potential applications in self-diagnosis systems, human-machine interfacing, information encryption, and smart-skin.

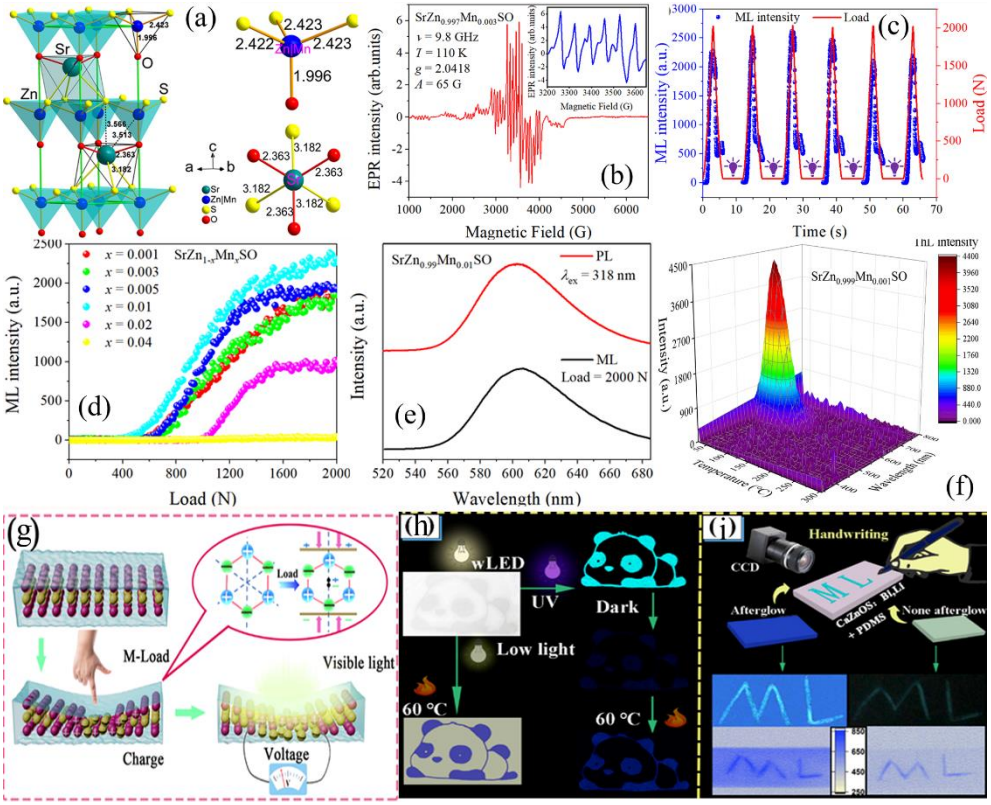

Figure 1. Crystal structure and coordination environment of $SrZn_{0.99}Mn_{0.01}SO$ on the basis of Rietveld refinement (a), EPR spectrum of $SrZn_{0.997}Mn_{0.003}SO$ at 110 K (b), ML recoverable performance of $SrZn_{0.99}Mn_{0.01}SO$ during six load cycles after UV irradiation in each cycle (c), ML responses of $SrZn_{1-x}Mn_xSO$ induced by compressive load up to 2000 N (d), comparison of

ML spectrum and PL spectrum in $SrZn_{0.99}Mn_{0.01}SO$ (e), ThL emission spectrum of $SrZn_{0.999}Mn_{0.001}SO$ (f), Schematic of the internal electric fieldgenerated in the CaZnOS (g), Photograph printed a “panda” with self-made ink using CaZnOS: Bi^{3+}, Li^{+} powder dispersed in glycerin and eth ylene glycol (h),Demonstration of recording the signing habits (i).

References

[1] D. Tu, C.-N. Xu, Y. Fujio and A. Yoshida, *Light: Science & Applications*, 2015, **4**, e356.

[2] Yu Zhou, Yun-Ling Yang, Yu-Ting Fan, Jing-Tai Zhao and Zhi-Jun Zhang, Journal of Materials Chemistry, 2019, 7 8070-8078.

Emerging 2D Material Si_2Te_3 for Next Generation Memory Application

Jingbiao Cui

Department of Physics, University of North Texas, TX 76203, USA

As a silicon-based chalcogenide, semiconducting Si_2Te_3 has recently attracted attention as an emerging layered 2D material. $Si_2Te_3$with various morphologies including nanowires and nanoplates are synthesized by chemical vapor deposition. Optical studies indicate that the Si_2Te_3 nanomaterials have a band gap of 2.2 eV. Both the nanowires and nanoplates exhibit a unique reversible resistance switching behavior driven by an applied electrical potential, which leads to switching of the NWs from a high-resistance state to a low-resistance state. The induced low-resistance state is stable unless a reverse potential is applied to switch back to high resistance. This novel resistance switching property is not only interesting for fundamental exploration but also holds promises for applications in memory devices. The mechanism behind the resistance switching behavior is studied and explained by an internal structural change resulting from the applied potential.

Novel scalable production of single-layer graphene coated-metal nanoparticles for water splitting

Chunfei Zhang, Cheol-hwan Shin, Gisang Park, and Jong-Sung Yu*

1Department of Energy Science and Engineering, Daegu Gyeongbuk Institute of Science and Technology (DGIST), Daegu, 42988, Republic of Korea

Graphene-coated metal nanoparticles (NPs) have attracted great attention owing to their unique structural, photochemical and electrochemical properties based on electron communication between graphene and metal NPs. The development of highly efficient and non-precious metal-based electrocatalysts for water splitting comprising hydrogen evolution reaction (HER) and oxygen evolution reaction (OER) is still a big challenge. The hybridization of nitrogen (N)-doped carbon and cost-effective transition metals is a promising approach to produce highly active catalysts for HER and OER. Herein, a highly controllable chemical vapor deposition method is designed for large-scale synthesis of nickel nanoparticle wrapped by single-layer N-doped graphene (Ni@SNG), where silica work as molecule sieve to tactfully assist single-layer graphene growth by depressing diffusion of carbon radicals. The Ni@SNG sample synthesized at 800 oC shows excellent activity for HER in alkaline solution with a low overpotential of 100 mV at 10 mA cm-2, which is close to state-of-the-art Pt/C catalyst. Furthermore, the Ni@SNG catalyst supported on nickel foil is developed as a magnetic adsorption binder-free electrode, which exhibits much improved performance on catalytic activity and stability than common Nafion binder-based electrode. Therefore, magnetism adsorption technique, taking full advantages of magnetic catalysts, will be a greatly promising approach to overcome high electron resistance and poor adhesive stability of polymer binder-based electrode sinactual applications.

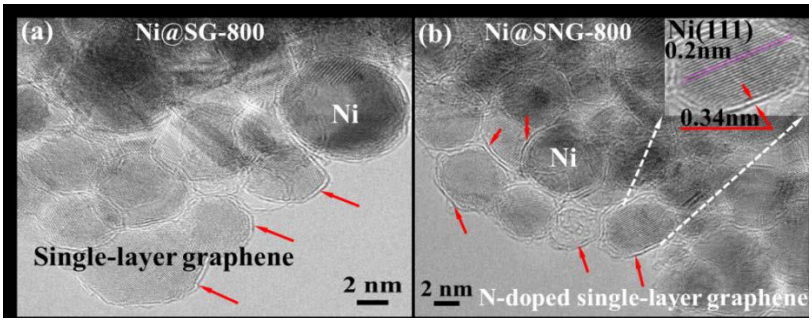

Oral Lectures

Acarbon quantum dots/gold nanoparticles modified carbon pasteelectrode as a sensor for selective and sensitive detection of glucose

Chengbao Liu[a, *], Jian Pan[a], Junchao Qian[a], Zhigang Chen[a]

a. Jiangsu Key Laboratory for Environment Functional Materials, Suzhou University of Science and Technology, Suzhou 215009, China;

Electrochemical sensing technology is very important in the field of biological and environmental measurement and analysis. In electrochemical analysis technology, quantum dots have very high surface defects, which can quickly adsorb target analytes in electrochemical analysis and improve target measure. Emerging as a potent alternative to classical metal-based semiconductor quantum dots (QDs), carbon quantum dots (CQDs) possess the distinctive advantages of convenient synthesis, prominent biocompatibility, colorful photoluminescence, and low cost.

We prepare hybrid nanomaterials of carbon quantum dots (CQDs)/gold nanoparticles (AuNPs) by simple hydrothermal method, such that the cheapness and versatility on the CQDs is directly combined with the inertness and electrochemical activity of the AuNPs to create a new electrochemical biosensor. Glucose oxidase enzyme was chosen as analyte. Pass detection, this new biosensor showed a high level of reproducibility and was also shown to be very selective towards glucose in the presence of the possible interference species ascorbic acid, uric acid and acetaminophen. Finally, it is demonstrated that the sensor is capable of reliably detecting glucose levels in human serum. The results show that the proposed sensor has high detection sensitivity, wide dynamic range, and as well acceptable reproducibility, selectivity and stability. We believe that this novel highly-sensitive sensor will have potential applications in various areas such as clinical diagnosis, food analysis and environmental monitoring.

Lightweight hexagonal boron nitride and carbon nanomaterial composites with excellent microwave absorption: Design and massive fabrication

Meng Wang and Bo Zhong *

*School of Materials Science and Engineering, Harbin Institute of Technology at Weihai *, Weihai 264209, People's Republic of China.*

Corresponding author (zhongbo@hit.edu.cn).

Abstract:

Our previous research has demonstrated that the introduction of BN into carbon based materials can effectively improve their MA performance [1-5]. However, the uncontrollable morphology and insufficient characterization of the pores during the preparation may bring randomness to the composites and reducing MA performance. Therefore, it is necessary to find simple and controllable way to fabricate h-BN/carbon nanomaterial composites. The adjustment of the structure and amount of pores of porous h-BN carbon nanomaterial (CNTs and multilayer grapheme (MG)) composites is also beneficial to reduce the density and improve the MA performance of them. Herein, a controllable way to fabricate porous h-BN and carbon nanomaterial composites (BN@CNTs and BN/MG) has been developed. This fabrication process involves two steps of synthesis of CNTs or MG melamine diborate precursors [6] and subsequent thermal treatment of these as-obtained precursors process. This design is based on the previous study of the controlled synthesis of the morphology of porous h-BN we reported [7]. The as-obtained composites are porous BN microrods with carbon nanotubes (CNTs) or multilayer graphen (MG) randomly distributed on their surfaces, marked as BN@CNTs and BN@MG. The specific surface area and density of the products can be tuned by adjusting the relative amounts of CNTs or MG in the composites. The highest specific surface areas are 583.63 and 795.06 m^2/g while the lowest densities are 0.072 ± 0.0046 and 0.212 ± 0.011 g/cm^3 respectively for BN@CNTs and BN/MG. These composites exhibit excellent MA properties with effective absorbing reflection loss (RL) bandwidth less than -10 dB from 2.8 to 18 GHz for BN@CNTs and from 3.52 to 18 GHz for BN/MG with absorber thickness of 1.0-6.0 mm. Moreover, the minimum RL values can reach up to -48.45

dB for BN@CNTs with absorber thickness of 1.4 mm and -40.15 dB for BN/MG with absorber thickness of 5.3 mm. More importantly, this facile and controllable fabrication process offers a new strategy for designing and fabricating porous BN and other material composites.

Keywords: Hexagonal boron nitride, Carbon nanomaterials, Structure design, Specific surface area and density, Excellent microwave absorption.

References:

[1] B. Zhong, Y. Cheng, M. Wang, Y. Bai, X. Huang, Y. Yu, H. Wang, G. Wen, three dimensional hexagonal boron nitride nanosheet/carbon nanotube composites with light weight and enhanced microwave absorption performance, Composites Part A: Applied Science and Manufacturing 112 (2018) 515-524.

[2] B. Zhong, W. Liu, Y. Yu, L. Xia, J. Zhang, Z. Chai, G. Wen, Enhanced microwave absorption properties of graphite nanoflakes by coating hexagonal boron nitride nanocrystals, Applied Surface Science 420 (2017) 858-867.

[3] B. Zhong, C. Wang, G. Wen, Y. Yu, L. Xia, Facile fabrication of boron and nitrogen co-doped carbon@Fe2O3/Fe3C/Fe nanoparticle decorated carbon nanotubes three-dimensional structure with excellent microwave absorption properties, Composites Part B: Engineering 132 (2018) 141-150.

[4] B. Zhong, C. Wang, Y. Yu, L. Xia, G. Wen, Facile fabrication of carbon microspheres decorated with B(OH)3 and α-Fe2O3 nanoparticles: Superior microwave absorption, Journal of Colloid and Interface Science 505 (2017) 402-409.

[5] B. Zhong, X. Zhang, L. Xia, Y. Yu, G. Wen, Large-scale fabrication and utilization of novel hexagonal/turbostratic composite boron nitride nanosheets, Materials & Design 120 (2017) 266-272.

[6] A. Roy, A. Choudhury, C.N.R. Rao, Supramolecular hydrogen-bonded structure of a 1:2 adduct of melamine with boric acid, Journal of Molecular Structure 613 (2002) 61-66.

[7] M. Wang, Y. Bai, B. Zhang, B. Zhong, Y. Yu, J. Zhang, X. Huang, G. Wen, Large scale fabrication of porous boron nitride microrods with tunable pore size for superior copper (II) ion adsorption, Ceramics International 45 (2019) 6684-6692.

Three-dimensional of graphene oxide Ba_2VPbSe_6 frameworkcomposite attach on cellulose based counter electrode for dye-sensitized Solar cell

Yonrapach Areerob, Won-Chun Oh*

Department of Advanced Materials Science & Engineering, Hanseo University, Chungnam 356-706, South Korea.

E-mail: wc_oh@hanseo.ac.kr

Abstract

Increasing energy demand pushes human beings to find more and more renewable energy devices. To achieve this goal, the three-dimensional of graphene oxide/Ba_2VPbSe_6 composites with cellulose (GB@C) have been successfully synthesized via a simple hydrothermal method and used as the counter electrodes (CEs) in dye-sensitized solar cells (DSSCs). The three-dimensional GB@C framework showed multiple benefits, such as high surface area, electrocatalytic ability, stability, and high-speed electron conduction, which can improve the conversion efficiency of DSSCs. For this reason, this material is particularly suitable to be the alternative material to solve the energy problem in the future.

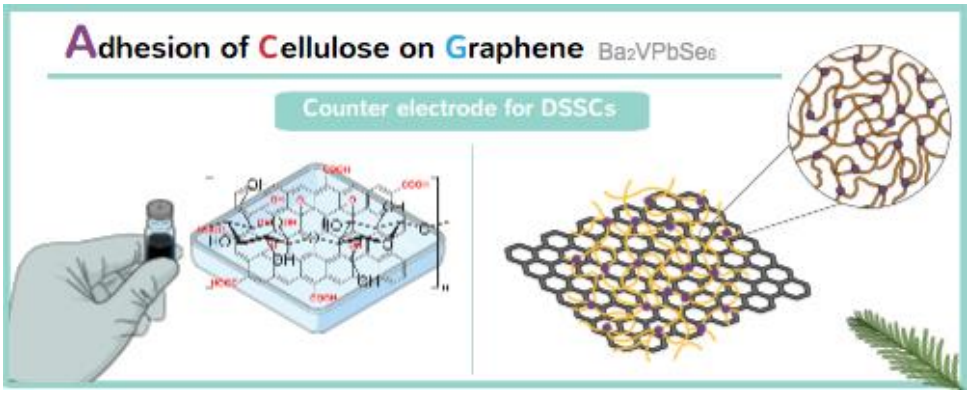

Keywords: Graphene, Perovskite material, Cellulose, Dye-Sensitized Solar Cells

References

Won-Chun Oh, K.Y. Cho, C.-H. Jung, Y. Areerob*J. Photochem. Photobiol., A*, 372 (2019) 11–20.

Preparation of highly efficient and magnetically recyclable Fe_2O_3/graphene/CuO nanocomposite for the photocatalytic degradation of methylene blue under visible light

Prawit Nuengmatcha,* Tuangrat Senmard, Alisa Pipak and Nichapa Rattanakomon

[1]*Nanomaterials Chemistry Research Unit, Department of Chemistry, Faculty of Science and Technology, Nakhon Si Thammarat Rajabhat University, 80280, Thailand.*

**Corresponding author. e-mail: pnuengmatcha@gmail.com; Tel. +66-7537-7443, Fax +66-7537-7443*

Abstract

Visible light responsive photocatalyst of Fe_2O_3/graphene/CuO (FGC) nanocomposite was successfully synthesized via simple solvothermal method and characterized by XRD, SEM, TEM and HR-TEM, UV-Visible DRS and VSM. From the results, it was confirmed that CuO, Fe_2O_3, and graphene have been successfully loaded together onto the FGC composite material. The UV-Visible DRS spectra reveal that the FGC catalyst absorbs light in the visible region and shows an excellent photocatalytic degradation performance of MB solution without any additional oxidant or reductant. The photocatalytic performance of the as-synthesized FGC exhibited better than that of bare CuO, Fe_2O_3, and graphene. Remarkably, the developed hybrid nanocomposite with magnetized Fe_2O_3 could be easily separated and recycled by applying an external magnetic field, and their catalytic activity did not decrease significantly with the increase of cycles which retaining its catalytic performance (> 90%) even after 5 cycles used. Overall, the outcome of this studies suggests that the FGC catalyst could be not only an excellent photocatalyst for the photocatalytic degradation and a great potential in the practical treatment of dye wastewater but also a suitable candidate for eco-friendly environmental applications.

Keywords: Fe_2O_3/graphene/CuO; Photocatalytic degradation; Hybrid composite material

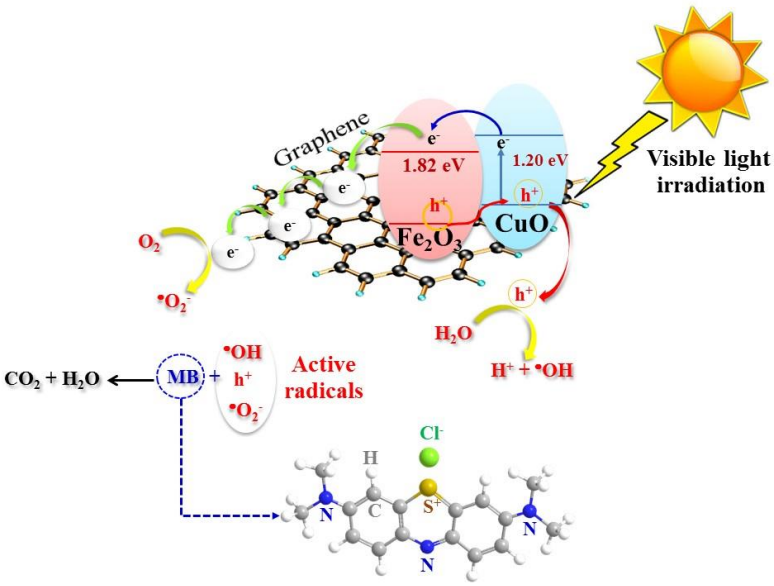

Postulated mechanism for the photocatalytic activity of FGC composite

Acknowledgements

This work was supported by Research and Development Institute and Nanomaterials Chemistry Research Unit, Department of Chemistry, Faculty of Science and Technology, Nakhon Si Thammarat Rajabhat University.

Fabrication of porous carbon nanofiber andits promising application as catalyst support to enhance performance of H_2/O_2 fuel cell

Zunhong Chen, Yukun Zhang, Junhong Jin, Shenglin Yang, Guang Li*

College of Materials Science and Engineering, Donghua University, Shanghai, China

*lig@dhu.edu.cn

As a specific form of carbon materials, porous carbon nanofiber (PCNF) shows some unique features which may elevate its applications. Thus the facile production of PCNF is worthy investigating and processing. It was found that the polymer blend spinning and following carbonization is a facile way to fabricate PCNF. When the resultant PCNF was used as support to prepare Pt catalyst (Pt/PCNF), the higher electrocatalytic activity and stability towards oxygen reduction reaction (ORR) was found compared to Pt/C catalyst (JM20), as show in Figure 1. The special morphology of PCNF support may lead to Pt nanoparticles uniform deposition and distribution on support, provide more exposure of active sites. Moreover, the loose 3D-channels of the catalyst layer composed of PCNF support could reduce mass transfer resistance significantly, thus increase local Pt catalyst utilization, and the catalyst layer consisting of Pt/PCNF could act as microporous layer so that water drainage can be improved to prevent the electrode from flooding. Thus porous carbon nanofiber shows promising support for platinum catalyst to enhance ORR in H_2/O_2 fuel cells.

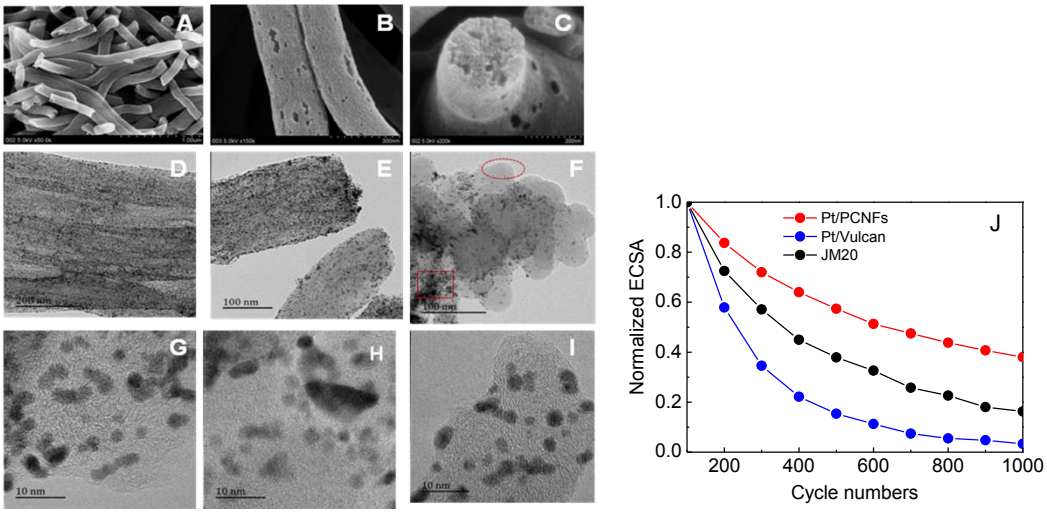

Figure 1(A), (B), (C) FE-SEM images of PCNF support; (D), (E), (G) HR-TEM images of Pt/PCNF; (F), (H) HR-TEM images of Pt/Vulcan; (I) HR-TEM image of JM20. (J) the normalized ECSA curves

Ultrasound-assisted magnetic solid-phase microextraction and enrichment of heavy metals in water samples using thiol-functionalized graphene oxide composited with iron oxide

Natthida Lamaiphan[1], Chinawooth Sakaew[1], Phitchan Sricharoen[1], Nunticha Limchoowong[2] and Saksit Chanthai[1]*

[1]*Materials Chemistry Research Center, Department of Chemistry and Center of Excellence forInnovation in Chemistry, Faculty of Science, Khon Kaen University, Khon Kaen 40002, Thailand*

[2]*Department of Chemistry, Faculty of Science, Srinakharinwirot University, Bangkok 10110, Thailand*

**Corresponding author, e-mail address*: sakcha2@kku.ac.th

Abstract

Preparation and characterization of thiol-functionalized graphene oxide/iron oxide) Fe_3O_4-GO-SH(nanocomposite as a novel magnetic adsorbent for simultaneous pre-concentration of heavy metal ions including Ag(I), Pb(II), Cd(II)and Cr(III)from water samples using an ultrasound-assisted magnetic solid-phase microextraction (UA-MSPME)prior to determination by atomic absorption spectrometry was carried out.The magnetic nanosorbent was synthesized by co-precipitation method associated with an ultrasound irradiation using 3-mercaptopropyl trimethoxysilanefor specific functionalization. Characterization of the obtained nanocomposite was performed by SEM, TEM, EDX, XRD, FTIR and VSM. Pre-concentration optimizations via UA-MSPME method including pH solution, amount of adsorbent, ultrasound power for both adsorption and desorption process, adsorption time, and type and concentration of eluting solvent were studied. Under the optimum conditions, their linear ranges were found to be 0.02–1.0 ppm for Ag(I)and Cd(II), and 0.2-10.0 ppm for Pb(II)and Cr(III)with R^2> 0.99. Limits of detection (ppb) were1.7 (Ag), 14.1 (Pb),0.9 (Cd)and 48.9 (Cr) and limits of quantification (ppb) were 5.9 (Ag), 47.3 (Pb), 3.2 (Cd), and 157.1 (Cr). The method precisioncalculated from the slope of their calibration curve (%RSD, n = 3x3) for both intra-day and inter-day analyses were 1.3 & 2.8(Ag), 5.0 & 3.9(Pb), 0.8 & 6.3(Cd), and 6.7 & 1.6(Cr), respectively. The recoveries of these metal ions,

Ag(I), Pb(II) and Cd(II),for water samples (drinking water, tap water, swamp water and wastewater from plating plant) was ranged between 80% and 115%.The enrichment factors of this procedure were about 20-fold for Ag(I), Pb(II) and Cd(II)and 10-fold for Cr(III), ensuring trace determination of the metal residues.Therefore, this magnetic nanocomposite adsorbent can potentiallybe used for simultaneouspre-concentration and determination of such heavy metal ions from real water samples. Also its reusability can be easily done via deionized water treatment, preferably lined with green analytical chemistry.

Keywords: Ultrasound, Magnetic solid-phase microextraction, Silver, Cadmium, Lead, Chromium, Graphene oxide, Thiol-functionalization, Nanocomposite, Pre-concentration

New Carbon Nanomaterials and Their Composites

JingWang *, Xiachun Zhu, Youyang Chen, Jiaqi Liu, Jingwei Mao

College of materials science and engineering, Anhui University of Science and Technology, Huainan, Anhui 232001

*Corresponding author (Phone and WeChat: + 0086 (13855418833); jingwang@aust.edu.cn)

Abstract: In recent years, low dimensional carbon materials caused the research upsurge around the world, especially in Graphene and Carbon nanotubes which preparation and properties of composite materials research is developing rapidly, moreover, a new type of optoelectronic carbon nanomaterials is in the ascendant, Carbon quantum dots with quantum size effect of nanomaterials, low toxicity and biocompatibility of carbon materials, and excellent optical properties. With these advantages, the discovery of new carbon nanomaterials and their composites triggered a research boom, and showed broad application prospects in optoelectronic devices, bioimaging, photocatalysis and so on. We use low-cost green technology such as physical stripping method, solvent stripping method and microwave auxiliary method to get the single layer graphene and carbon dots. Surface modification of these new carbon nanomaterials surface improves their dispersion in aqueous solution. Composite powder is prepared with In-situ composite technology in precursor in the aqueous solution and with washing, low temperature treatment or calcination. Dense Graphene/ceramic, Carbon nanotubes /ceramic and Carbon dots/Graphene/polymer composites structure are obtained through controlling the interface and process parameters. The conductive, opto, electrochemical, dielectric and magnetic absorbing properties of the composites were tested and analyzed, expecting to further promote the low dimensional carbon nanomaterials in composites in the practical application.

Key words: Carbon nanomaterials, Graphene, Carbon quantum dots, Carbon nanotubes, Surface treatment, In-situ composite, Properties

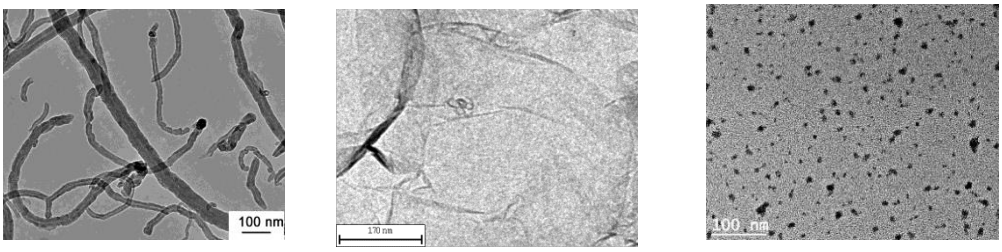

(a) (b) (c)

Fig.1 TEM of modified Carbon Nanomaterials (a) Carbon nanotubes (b) Graphene and (c) Carbon quantum dots

Reference

[1] Si Yongchao, Samulski E.T. Synthesis of water soluble graphene. Nano Lett. [J], 2008, 8(6): 1679—1682.

[2] Lerf Anton., He Heyong., Riedl Thomas, et al.^{13}C and ^{l}H MAS NMR studies of graphite Oxideandits chemically modidied derivatives[J]. Solid State Ionics, 1997, 101(1): 857.

[3] Hu Shengliang, Tian Ruixue, Dong Yingge, et al. Modulation and effects of surface groups on photoluminescence and photocatalytic activity of carbon dots[J]. Nanoscale, 2013, 5(23): 11665-11671.

[4] Gong Qiaojuan, Li Hejun, Wang Xiang et al. Effects of Annealing on the purity and structure of disordered carbon nanotubes [J]. Rare metal materials and Engineering, 2007, 36: 269 ~ 272.

[5] Wei Huang, Yao Wang, Guohua Luo et al. 99.9% purity multi-walled carbon nanotubes by vacuum high-temperature annealing[J]. Carbon.2003,41: 2585 ~ 2590.

[6] Shen Jianfeng, Huang Weishi, Wu Liping et al. Purification and modification of multi-walled carbon nanotubes [J]. Materials Review 2006,20: 117 ~ 119.

[7] Zhang Lixia, Qilu. Dispersion of multi-walled carbon nanotubes[J]. SFC,2008,6:32 ~ 35.

[8] Stankovich S, Dikin D A, Dommett GHB, et al. Graphene based composite materials[J]. Nature, 2006,442（7100:282-286.

[9] Li Sufang, Chen Zongzhang, Nano graphene based composite wave absorbing material and preparation method thereof[P].2009, CN101550003A.

[10] Liang Jiajie, Wang Yan, Huang Yi, et al, ElectromagneticInterference shielding of graphene/epoxy composites [J]. Carbon.2009,47(3):922-925.

Health risks of hidden heavy metal in lipstick in Khon Kaen Thailand

Rachadaporn Benchawattananon

Integrated Science Faculty of Science Khon Kaen University Khon Kaen Thailand 40000

Email : rachadaporn@kku.ac.th

Abstract

This research study to find quality of lead, cadmium and mercury contaminate in lipstick with ICP-OES technique by randomly orange and red shade lipsticks. The lipsticks which popular sale at department store for 5 brands 30 samples. The wavelength used for analysis equal to 220.353,228.802 and 184.950 NM respectively. The finding cadmium and mercury was not detected but leads can detect in 2.11- 22.85 ppm. With lipstick sample 1 sample had exceeded the standard value of industrial products, Ministry of industry defined not more than 20 ppm. The ICP-OES technique is accuracy and precision for finding the lead, cadmium and mercury quantity which standard deviation of relative quantities value in allowable range. Recommendation for customer should screening all of ingredients of lipstick and doing the best to reach non-detectable heavy metal limits when possible for health – protective company standards.

Effect of aluminium ion doping on the deactivation of photocatalytic activity of green synthesized ZnO nanopowder for application in sunscreens

Paweena Porrawatkul[*1], Prawit Nuengmatcha[1], Rungnapa Pimsen[1] and Montakarn Thongsom[2]

[1]Nanomaterials Chemistry Research Unit, Department of Chemistry, [2]Department of Biology Science,

Faculty of Science and Technology, Nakhon Si Thammarat Rajabhat University, 80280, Thailand.

[*]Corresponding author e-mail: paweena.n@gmail.com; Tel. +66-7537-7443, Fax +66-7537-7443

Abstract

The green synthesis of ZnO nanoparticles using aqueous *Musa acuminata Colla* peel extract doped with aluminium (Al) metal was applied for sunscreen. The Al doped ZnO materials was prepared by a simple co-precipitation method from corresponding metal precursors. The effect of Al ion doping on the crystal structure, morphology and optical properties of ZnO was respectively characterized by XRD, SEM, EDX and UV–visible diffuse reflectance. The photocatalytic activity was evaluated via the bleaching of methylene blue under UV irradiation. According to the results, the Al ion doping modified the cell volume, reduced the crystallinity and decreased the particle size of ZnO, which induces the increase of structural defects and then the suppression of its photocatalytic activity. The metal doped ZnO materials exhibited the UV absorption capacity comparable to the undoped ZnO. However, the optical properties in the visible region of ZnO were influenced by the nature of metal dopant. The Al ion doped ZnO sample showed the visible light transparency, which make this material a promising constituent of sunscreen.

Keywords: ZnO nanoparticles, Sunscreen, Photocatalytic activity, Metal doping

Natural Gums Derived Materials as Superabsorbent (SAPs) forHygiene & Agriculture Applications

Saiqa Ikram*,

*Department of Chemistry, Faculty of Natural Sciences,

Jamia Millia Islamia (Central University)

New Delhi-110025 INDIA

sikram@jmi.ac.in

Abstract:

Life is polymeric in its essence. The most important components of living cell (proteins, carbohydrates and nucleic acids) are all polymers. Nature uses polymers both for construction and as part of the complicated cell machinery. Among natural polymers; gums represent one of the bountiful raw materials derived from the vegetation. They are mainly studied because of their sustainable, biocompatible and biodegradable characteristics. Their common properties are characterized by their property of forming viscose dispersion and/or gels in water. Hence, gel formation i.e. these hydrogels as a subsequent product of gums or of hydrocolloids intended to a phenomenon involving the association or crosslinking of polysaccharide units that traps or immobilize water within to take shape of a rigid structure that is resistant to flow. Because of this property, great interest had been developed is devoted to these systems by varying their physicochemical properties which can be tuned, in designing the innovative devices for a modulated system. One of the most environmentally significant applications of natural gums is in their uses for reducing industrial contamination of natural water sources. Besides, the brilliant properties of these polysaccharides macromolecules, their potential in hydrogel chemistry and new generation formulation technology still lay less exploited as compared to other backbones such as cellulose, starch, chitosan etc. However, their modifications, in terms of their practical applications is rather far more challenging not only in terms of understanding hydrogel chemistry, but also for visualization polymer network, which is one of biggest dream of material scientist. In the similar direction, a simple and facile macromolecular architecture towards obtaining the hydrogels via modifying the carboxymethyl tamarind gum and polyvinyl alcohol crosslinked with borax is designed. FTIR, XRD, and SEM are employed to characterize the structure, crystallinity, and morphologies of as-synthesized hydrogels. The

effect of some composition variables on the swelling performance of synthesized hydrogel was thoroughly studied. The swelling ratio, re/de-swelling and water retention properties of hydrogel are also investigated. Furthermore, swelling behaviour was monitored as a function of various salts. The salt sensitivity, good water absorbency, and excellent water retention capability of the hydrogels is line with to groom these hydrogels as superabsorbent demonstrating their wide potential in sanitary hygienic applications.

Keywords: Natural Gums, Polysaccharides, Hydrogels, Superabsorbents, & Tamarind Gum

Two Dimensional Uranyl Borates: From Conventional to Extreme Conditions

Yucheng Hao[§†*], Linbo He[§], Guangjie Ge[§], Yu Ruan[§], Evgeny V. Alekseev[†]

[§]*Department of Chemical and Material Engineering, Hefei University, Hefei 230000, China*

[†]*Institute of Energy and Climate Research (IEK-6), Forschungszentrum Jülich GmbH, 52428 Jülich, Germany*

Abstract

A systematic investigation of uranyl borates system under different synthetic conditions resulted in five new 2D compounds, namely, (H_3O) $[(UO_2)$ $(BO_3)]$, $Li[(UO_2)$ $(BO_3)] \cdot (H_2O)$, α-$K_4[(UO_2)_5(BO_3)_2O_4]$, β-$K_4[(UO_2)_5(BO_3)_2O_4]$ and $K_{2.5}[(UO_2)_5(BO_3)_2O_{2.5}(OH)_{1.5}] \cdot (H_2O)_{2.5}$. $(H_3O)[(UO_2)(BO_3)]$and$Li[(UO_2)(BO_3)]\cdot(H_2O)$ were obtained from hydrothermal reactions at 220°C using same mineralizer. Both materials demonstrate uranophane sheet topology with different symmetry of unit cells. In the structure of (H_3O) $[(UO_2)$ $(BO_3)]$ and$Li[(UO_2)$ $(BO_3)] \cdot (H_2O)$, UO_7 pentagonal bipyramids are sharing edges and vertexes with four BO_3 planar triangles. α-$K_4[(UO_2)_5(BO_3)_2O_4]$ andβ-$K_4[(UO_2)_5(BO_3)_2O_4]$ are the polytypes, where, α-$K_4[(UO_2)_5(BO_3)_2O_4]$ was synthesized from high-temperature solid-state reaction under ambient pressure and β-$K_4[(UO_2)_5(BO_3)_2O_4]$ was obtained from high-temperature/high-pressure (HT/HP) reaction. Both structures have identical anion topology, but β-$K_4[(UO_2)_5(BO_3)_2O_4]$ crystallizes in a higher symmetry. In $K_{2.5}[(UO_2)_5(BO_3)_2O_{2.5}(OH)_{1.5}]\cdot(H_2O)_{2.5}$, whichwas obtained from hydrothermal reaction, UO_7 polyhedra share vertexes and edges with two independent BO_3triangles, forming themost complex uranyl borate layers among all five novel compounds. The different synthetic routes, novel topologies, thermal behavior as well as Raman spectra are discussed in this work.

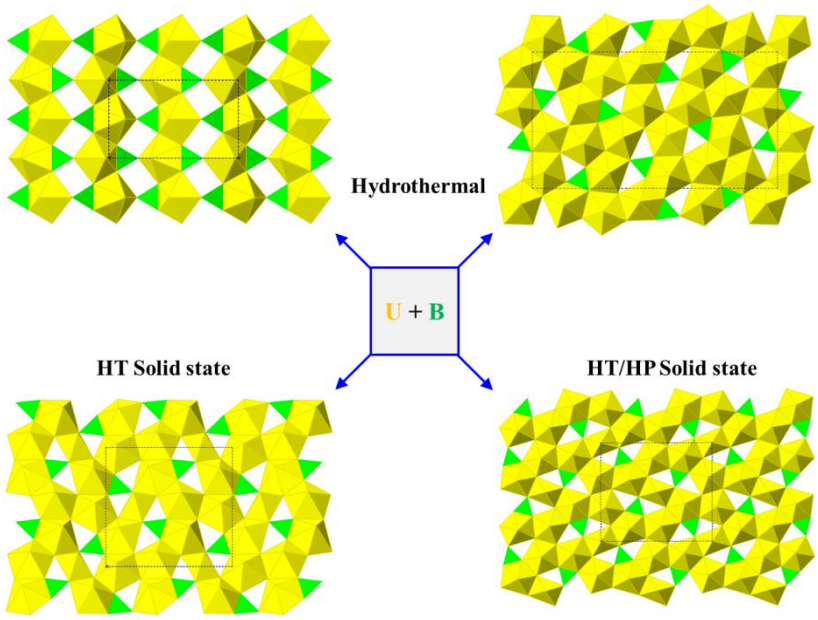

TOC Figure and Synopsis. Five novel uranyl borates with monovalent countercations have been synthesized using three different synthetic methods, namely, hydrothermal, high temperature solid state and high-temperature/high-pressure solid state reactions. The structures of these materials, their spectroscopic and thermal propertieshave been investigated. The relationship between U/B ratio and structural complexity has been discussed.

Novel Sequential Electroless Plating for Fabrication of Palladium-Ruthenium Composite Membrane and its Characterization of Hydrogen Separation/Purification

Nong Xu, Qiao Liu, Qiang Dong*, Long Fan, Aiqing Ding

School of Energy, Materials & Chemical Engineering, Hefei University, Hefei, P. R. China 230601

Abstract:

Usually, Pd composite membranes are prepared by various coating methods, such as sputtering, CVD (Chemical Vapor Deposition), PVD (Physical Vapor Deposition), electroplating or electroless plating. Pd-Ag, Pd-Cu and Pd-Cu-Ni are the commonly used Pd based composite membranes by above methods. The stability of these membranes is not stable at elevated temperatures. On one hand, hydrogen permeability of pure Pd membrane and Pd alloy composite membranes decreases with temperature at 400°C or higher due to its metallurgical structure change. On the other hand, hydrogen selectivity decreases because of surface cracks of composite membranes occurring at higher temperature. Former researchers found that small amounts of ruthenium (ca. 5 wt. %) can highly improve the performance of Pd based composite membrane. They used Pd and Ru co-deposition by electroless plating. But the deposition rates of Pd and Ru varied during the course of plating. Pd and Ru were not evenly distributed and their compositions were not settled along the cross-section of membrane. Also ruthenium chloride was not completely dissolved in the solution of co-deposition plating bath, causing Ru aggregates to deposit and increasing the possibility of surface cracks at high temperature. Pd and Ru can be deposited as two separate layers by electroless plating. We successively developed this method. This paper relates to fabrication of novel, thin-film Pd-Ru composite membrane for hydrogen separation. Porous metal substrate is used as the substrate for the composite membrane in this study to support thin Pd-Ru membrane. The surface of the substrate is pretreated by washing, polishing, etching, alumina coating and calcinations steps which was achieved in our former research. Thin Pd and Ru layers are deposited on the surface of the pretreated substrate separately. The thicknesses of both layers are controlled by adjusting the bath conditions and plating time. Leak-tight membranes with a Ru composition about 5% have been obtained. The thickness of the membranes varies from 2 to 7 μm, much thinner than dense foil membranes. The membrane has been tested for a long time at 450 and 550°C. Measured permeate purity has been very high and "pure" hydrogen has been produced (>99.99% H_2 given the detector accuracy). Hydrogen permeation flux of the Pd-Ru membrane suggests that hydrogen permeability is up to ~50% higher than pure Pd membranes. Testing with low levels of H_2S (up to 25 ppm) indicates that the Pd-Ru membrane has higher sulphur tolerance than Pd-Ag (silver) membranes. The EDX (Energy Dispersive X-ray spectrometer) profiles of the front and back sides of the membrane and cross-sectional EDX line scanning confirmed the $Ru/Pd/Al_2O_3$/PSS (Porous Stainless Steel) structure of the novel composite membrane.

Key Words:

Palladium, Ruthenium, Sequential electroless plating, Membrane, Hydrogen separation/purification

A novel Ag/rGO/TiO2 nanorod array as powerful substrate for photocatalytic degradation and SERS detection

Yanfen Wang

[1]*School of Physics & Materials Science, Anhui University, Hefei 230601, PR China*

[2]*School of Materials Science & Engineering, Anhui University of Science and Technology, Huainan 232001, PR China*

A novel graphene oxide/TiO_2 nanorod array (GO/TNR) decorated with Ag nanoparticles (NPs) is successfully prepared as a photocatalyst and a surface-enhanced Raman scattering (SERS) substrate for organic molecule detection. The as-obtained Ag/GO/TNR sample exhibited a large specific surface area and high adsorption capacity toward Rhodamine 6G (R6G) molecules. Moreover, the GO interlayer with suitable content had a significant effect on the absorption intensity of lightand Raman signals for the Ag/GO/TNR substrate. For R6G as probe molecules, the Ag/GO/TNR substrate with 5 min of GO-deposition achieved a lower detection limit of 1.0×10^{-12} M and an improved enhancement factor (EF) of 5.86×10^{5} as compared to other films. Furthermore, the relative standard deviation (RSD) value of the Raman vibration at 1650 cm^{-1} cm was approximately 8.71%, and the good uniformity remained. Using Xenon lamp irradiation, the outstanding photocatalytic ability endowed the substrate with good self-cleaning and reusable properties. Based on the above results, a synergistic effect of three components (Ag NPs, GO interlayer, and TNR) is proposed to produce an excellent SERS performance, namely, a large adhesion area, the interaction of excited photons, and high-density hotspots in the active substrate.

Low-Voltage-Operating ZnSnO Transistors and Logic Circuits Based on Water-Driven ZrGdOx Dielectric

Gang He

School of Physics and Materials Science, Anhui University, Hefei 230039, P.R. China

In current work, the nontoxic eco-friendly water-induced (WI) gadolinium doped zirconium oxide ($ZrGdO_x$) gate dielectrics have been integrated with low cost spin-coating-driven ZnSnO films for thin film transistors (TFTs) and logic circuits with superior performance for the first time. High transmittance over 90% and the formation of the metastable cubic phase of Zr_2O have qualified its potential application in transparent electronics. 430^oC-annealed ZnSnO films integrated with $ZrGdO_x$ films demonstrate remarkable electrical properties and low voltage operation (2 V), including high current on/off ratio of ~1.1×10^6, large saturation carrier mobilityof ~3.1$cm^2V^{-1}S^{-1}$, extreme low leakage current density of 6×10^{-10} A cm^{-2} and a slight shift inthreshold voltage of 0.26 V for bias stability, respectively. To verify the practicability in logic circuits, the resistor-loaded inverters are built by using $ZrGdO_x$/ZnSnO TFTs. This work firstly put forward and verify the WI gate dielectrics can be well favorable to heterogeneous clean interface with solution-derived ZnSnO channel layer, which takes an important step towards low operating voltage and eco-friendly flexible integrated circuit.

Electronic and adsorption properties of two-dimensional quantum dots for gas sensing and wastewater treatment

Qin-fang Zhang[1], Hazem Abdelsalam[1,2], Nahed Teleb[3], Vasil Saroka[4], Medhat Ibrahim[5], Mikhail Portnoi[6], Igor Lukyanchuk[7]

[1]*School of Materials Science and Engineering, Yancheng Institute of Technology, Yancheng 224051, P. R. China.*

[2]*Theoretical Physics Department, National Research Centre, Dokki, Giza, 12622, Egypt.*

[3]*Electron Microscope and Thin Films Department, National Research Centre, Dokki, Giza, 12622, Egypt.*

[4]*Institute for Nuclear Problems, Belarusian State University, Bobruiskaya 11, 220030 Minsk, Belarus.*

[5]*Spectroscopy Department, National Research Centre, El-Buhouth Str., Dokki, Giza,12622, Egypt.*

[6]*School of Physics, University of Exeter, Stocker Road, Exeter EX4 4QL, United Kingdom*

[7]*University of Picardie, Laboratory of Condensed Matter Physics, Amiens 80039, France.*

The discovery of novel two dimentional materials opens the unprecedented roots for the engineering of efficient nanodevices for various applications including gas sensing and wastewater treatment due to their high surface area and tunable surface chemistry. The present review focuses on studying different types of two dimensional quantum dots (QDs) such as graphene, silicene, phosphorene, and boron nitride QDs using the tight binding model (TB) and density functional theory (DFT). The TB calculations show that, depending on the shape and edge termination of the dot, the band structure is divided into two bands, the bulk band from electrons in the bulk atoms and edge band from edge electrons. The edge states can be precisely controlled by applying an electric field where the quantum dot can be transformed from semiconductor to conductor and vise versa which in turn permits to design the field-effect scalable QDs devices. The DFT investigations are then performed to study the effect of chemical functionalization on the electronic and adsorption properties. It confirms

the stability of all the studied two-dimensional QDs before and after functionalization with different elements and groups. The electronic and magnetic properties can be efficiently tuned. For instance, the band gap of square born nitride flake may have a wide range of values starting from 6 to 0.2 eV. Additional, doping graphene flakes with odd number of alkali metal transforms the structure from the antiferromagnetic to the ferromagnetic state. The adsorption of CH4, H2S, CO, NH3 gas molecules is successfully achieved on the surface and edge of phosphorene QDs. The adsorption strength can be enhanced by applying in-plane electric field. Chemical modification also provides additional enhancement to the adsorption properties. Functionalized graphene QDs have shown a strong capability to adsorb hydrated heavy metals from wastewater.

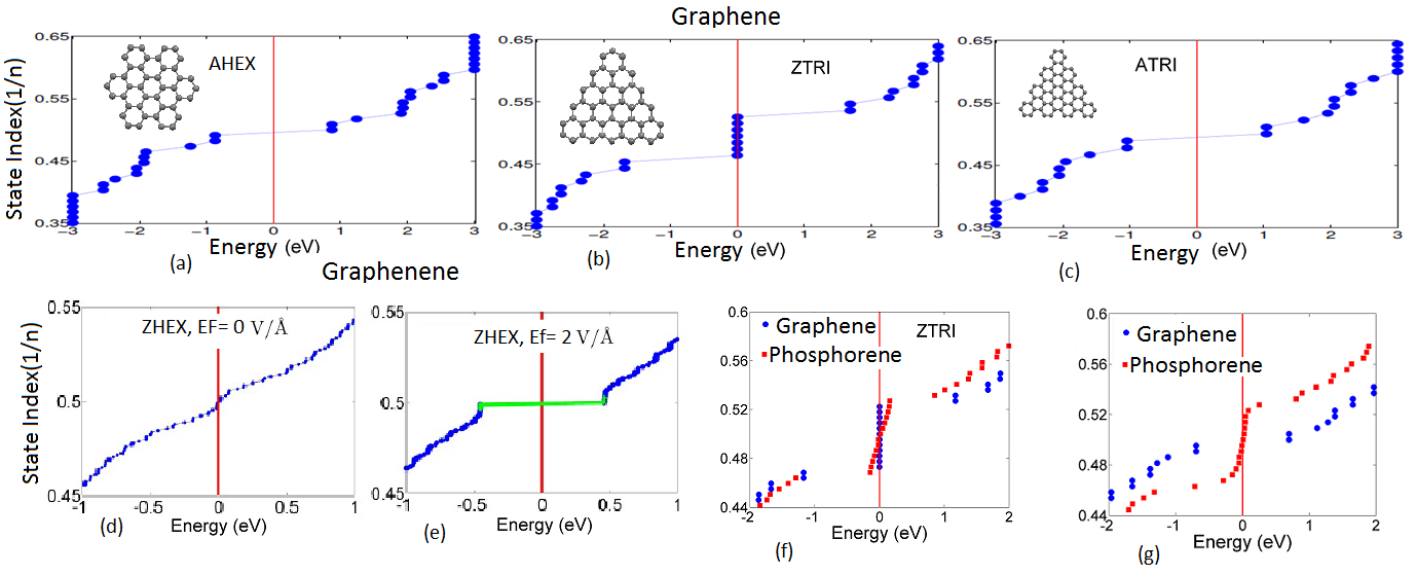

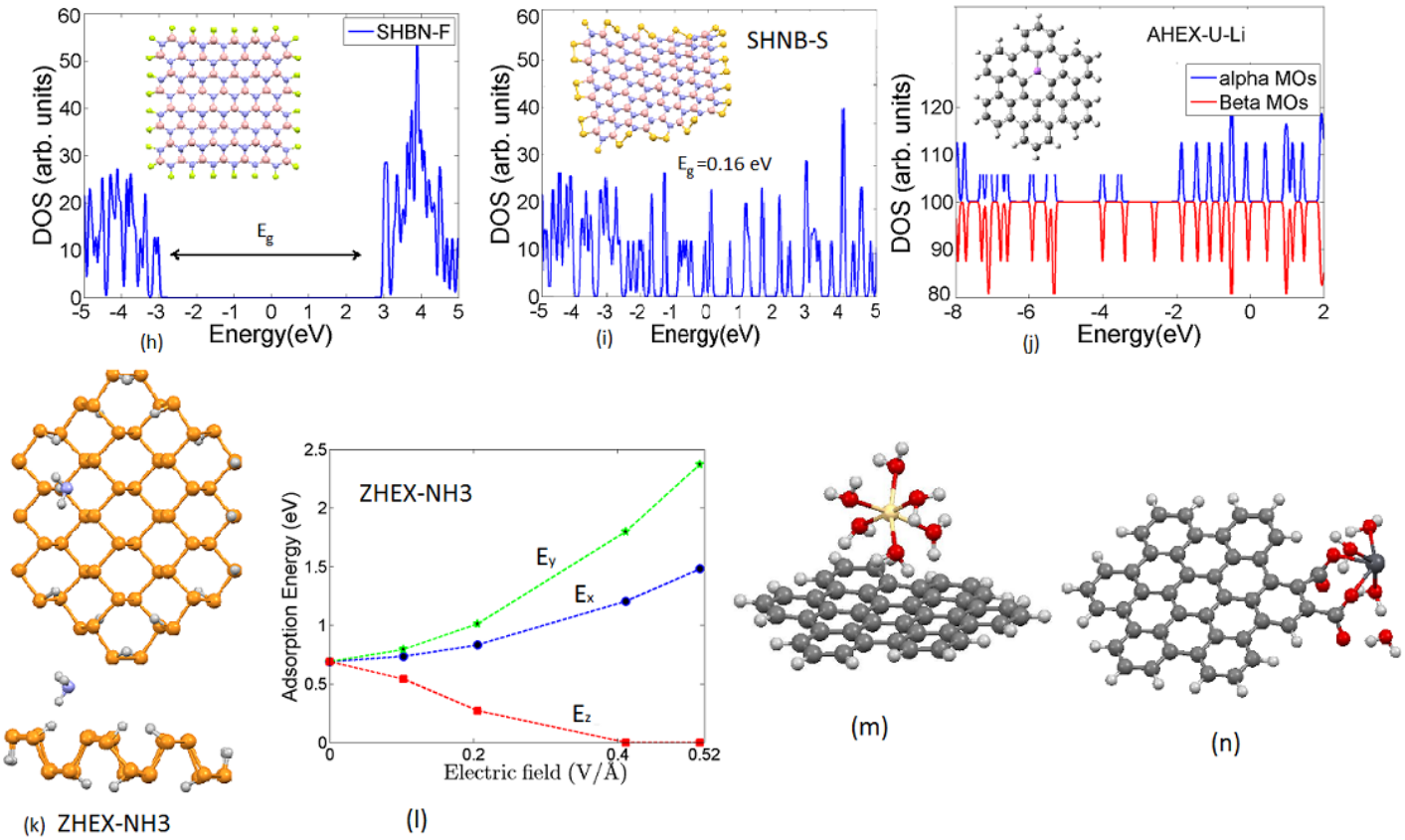

Fig. 1. Band structure and density of states of selected 2D quantum dots under the effect of shape (a-c), electric field (d, e), puckering (f, g), and chemical modification (h-j). The optimized structures of phosphorene QDs after adsorption of NH3 on the surface (k) and the effect of electric field on the adsorption strength (l). Adsorption of hexahydrated Cd (m) and pentahydrated Pb (n) by graphene QDs.

WO_3•0.33H_2O induced synthesis of porous g-C_3N_4/WO_3 photocatalyst for efficient hydrogen generation under visible light

Xian-YangSun[1],Feng-Jun Zhang[1,2*], Cui Kong[1], Chun-Mei Kai[1],Wei- Qin Jiang[1], Shan-Shan Cheng[1]

[1]*Key Laboratory of Functional Molecule Design and Interface Process, Anhui Jianzhu University, Hefei Anhui, P. R. China, 230601*

[2]*Anhui Key Laboratory of Advanced Building Materials, Anhui Jianzhu University, Hefei Anhui, P. R. China, 230022*

Corresponding author:Feng-Jun Zhang, E-mail: fjzhang@ahjzu.edu.cn

Tel: +86-0551-63828262 Fax: +86-0551-63828106

Abstract

A novel porous g-C_3N_4/WO_3 photocatalyst was successfully obtained by adopting urea and WO_3•0.33H_2O as precursor. The structural characteristics, photoelectric properties, and hydrogen generation efficiency of g-C_3N_4/WO_3 were studied. The relationship between the amount of precursor and the change of nano-pore size was also researched. The best photocatalytic hydrogen generation efficiency of the g-C3N_4/WO_3 was 963 μmol^{-1} h^{-1}, it was about 3 times than pure g-C_3N_4. The formation of nano-pore increases the reaction activity site, which contribute to increase the efficiency of hydrogen generation. The mechanism of photocatalytic hydrogen generation was proposed.

Key words

WO_3•0.33H_2O, g-C_3N_4/WO_3, nano-pores, photocatalytic hydrogen production

Acknowledgments

This work was financially supported by the Natural Science Foundation of Anhui province (1808085ME129), Outstanding Young Talents Support Program in Colleges and Universities (gxyqZD2018056) and the College Students' Science and Technology Innovation Foundation (2019-177).

Use of Scanning Electron Microscope for Investigation Artificial Jewelry

Siree Saengthong and Rachadaporn Benchawattananon

Integrated Science Faculty of Science Khon Kaen University Khon Kaen Thailand 40000

E-mail: auu_siree@hotmail.com

Abstract

Currently, counterfeiting of jewelry by people who want the large profits by simulating gems from various materials or adulterating the properties of gems i.e. using chemicals such as paints, oils and resins as an additional substance. Moreover, advanced technology produces the production of artificial jewelry or gems more similar to the genuine causing the problem of counterfeiting of jewelry for sale consumers. The purpose of this research is to investigate the differences between artificial and genuine jewelry. In the trial 20 samples of genuine and artificial jewelry; Sapphire, Garnet, Black Spinal, Turquoise, and Emerald were analyzed by Scanning Electron Microscope (SEM) to study the external structure of samples with Energy Dispersive X-ray Spectrometer to identify the elements of samples. The refractive index was also considered include Sapphire (1.762-1.778), Garnet (1.72-1.95), Black Spinal (1.77-1.78), Turquoise (1.610-1.650), and Emerald (1.569-1.602) to compare between the artificial and genuine samples. The result shows that the surface and compound elements of the genuine gems differentiates from the artificial gems. Besides, this technique can be use to distinguish between the artificial and genuine jewelry and this research can be help in forensic field.

Keywords: Artificial jewelry, Genuine jewelry, Scanning Electron Microscope**,** Energy Dispersive X-ray Spectrometer

Teeth Cleaning Technique for Forensic Dentistry

Atiwat YaowakulandRachadaporn Benchawattananon

Integrated Science Faculty of Science Khon Kaen University Khon Kaen Thailand 40000

E-mail*: *tatiya.phu@gmail.com

Abstract

Teeth are an accurate sample for the age estimation in forensic dentistry field. Due to the durability, teeth can be resistant to high temperature and not be incorruptible over time. There are several techniques of samples acquisitions for dental studies in forensic dentistry. The aim of this research is to present the techniques used to collect the teeth samples used in dental histology studies with the primary aim of using teeth to estimate the age of a person. The method is to collect 132 samples (1st and 2nd premolar) from two sources. The first source is examples of Freshly extracted teeth from The Oral and Jawbone Surgery Clinic, faculty of Dentistry maintained in 10% Formalin and cleaning with DI water. The second source is the Cadaver teeth from the Department of Anatomy Faculty of Medicine Khon Kaen University collecting by using an electric saw to cut the jaw and soak in 10% potassium hydroxide for 7 days, then, extracting teeth from the jaw and cleaning with DI water. From the longitudinal buccolingual section, which look through the stereo microscope, shows that Freshly extracted teeth have enamel broken or loose, which may result from the section, but does not affect the age estimation. On the other hand, Cadaver teeth have found the same enamel as Freshly extracted and found to be missing or loose of cementum which may be the result of erosion of 10% potassium hydroxide, which can affect age estimation. In conclusion, 10% Formalin can make to be more accurate in estimating age.

Keywords: forensic dentistry, teeth cleaning technique, dental histology, estimate age

Posters

Statistical Analysis in Enrichment of Total Whey Protein by RSM Technique

Goutam Mukhopadhyay

Associate Professor

BCDA College of pharmacy and Technology, Barasat, Kolkata-700127.

Abstract

The objective of the present study was to optimize the operating conditions in the separation of the total whey proteins from whey by continuous foam fractionation method using response surface methodology (RSM). The effects of the different process variables such as pH (X1) of proteins in feed, Gas flow rate, GFR (X2) of initial feed solution, protein: surfactant ratio, PSR (X3) and volumetric flow rate, VFR (X4) were investigated on the performance criteria of fractionation of raw processed whey. Four factors, three levels Box-Behnken design was used for the optimization procedure. Quadratic model regression equations and response surface plots correlate independent variables (X_1, X_2, X_3 and X_4) and dependent variables (response) such as concentration of Foamate (C_f), Enrichment ratio (E_r), and percentage Recovery ($\%R_p$) of total whey proteins can be achieved easily. All the four factors had significant effects on the response variables. The model predicted that the optimized values of the factors (X_1, X_2, X_3, X_4) were 5, 290, 1.5, 14 respectively. The predicted responses were (concentration of Foamate, Enrichment ratio, and percentage Recovery) such as 6647.32, 13.27, and 78.02 respectively. Experiments were performed with the predicted values of factors.

New Design ofMesoporous SiO_2CombinedIn$_2O_3$-Graphene Semiconductor Nanocomposite for Highly Effective and Selective Gas Detection

Kamrun Nahar Fatema, Chang Sung Lim & Won-Chun Oh*

Department of Advanced Materials Science & Engineering, Hanseo University, Seosan-si, Chungnam, Korea, 356-706

Abstract:

We successfully prepared various gas-sensing devices consisting of a thin-film sensor made with mesoporous silica combined In_2O_3-graphene semiconductor nanocomposite for detecting gases such as CO_2, O_2, and NH_3. We demonstrated that the sensor had high selectivity for CO_2 by recognizing O_2 and NH_3 in the vapor stage brilliantly with exact change into electrical signals in devices. These mesoporous semiconducting IGS10 sensors showed quick response/recovery times for detecting a wide scope of gases, including CO_2, O_2, and NH_3. The superior gas-sensing capacity of mesoporous IGS10 compared to In_2O_3, IG, and IGS20 was predominantly due to the inferred ideal measure of the synthesized sample. Thus, we demonstrated a simple way to obtain various gas-sensing devices with the potential for immense applications.[ii]

[ii] Lin, C.Y., Fang, Y.Y., Lin, C.W., Tunney, J.J. and Ho, K.C., 2010. *Sensors and Actuators B: Chemical*, *146*(1), pp.28-34.

Photocatalytic performance of iron doped zinc oxide (Fe/ZnO) composite under simulated sunlight

Kongsak Pattarith

Department of Chemistry, Faculty of Science, Buriram Rajabhat University, Buriram 31000, Thailand

Corresponding author: e-mail pkongsak@hotmail.com; Fax :+66 44612858

Abstract

Iron doped zinc oxide (Fe/ZnO) were successfully synthesized via hydrothermal process. The samples were characterized by X-ray diffraction (XRD), ultraviolet–visible (UV–vis) diffuse spectroscopy, fourier transform infrared (FTIR) and scanning electron microscopy (SEM). The photocatalytic activities were also evaluated for the degradation of methylene blue under simulated sunlight illumination. The effects of various parameters includingcontract time, light intensity, dopant concentrations and photocatalytic dosage, were studied. The suitable condition for degradation of methylene blue were 120 min, 200 W/m^{2,}250 mg/L and 0.05 g, respectively. The purposed mechanism of methylene blue degradation was discussed.

Keywords: Fe doped ZnO; Hydrothermal method; Zinc oxide; Photocatalyst

Adsorption Behaviors of Perfluorocarbon Surfactant

Chong-Hun Jung*, Hui-Jun Won, Seon-Byeong Kim, and Byum-Kyung Seo

Decommissioning Research Division, Korea Atomic Energy Research Institute,

P.O. Box 105, Yuseong, Daejeon, Korea, 305-600

**Corresponding author:E-mail:nchjung@kaeri.re.kr*

Perfluorocarbon (PFC-5070, 3M Co.) decontamination process using a solution of fluorinated surfactant (Krytox 157, Dupont Co.) in a perfluorocarbon liquid is effective for the removal of micron sized hot particulate in a hot cell. Spent fluorinated surfactant solutions can be recovered by an adsorption process to remove the PFC surfactant. In this study, we conducted experiments on the adsorption of a PFC surfactant from a solution of a high molecular weight fluorinated surfactant with an activated carbon fiber (ACF) adsorbent. The adsorption behaviors such as the adsorption capacity were investigated and compared with that by the active carbon (AC) adsorbents.

The ACF-15 shows the best adsorption performance and its adsorption capacity is about 0.6g-surfactant/g-adsorbent, but the ACF-7 shows the lowest adsorption capacity of 0.15g surfactant/g adsorbent after a 24-hour contact. While the adsorption capacities of AC-45x100 and AC-20x45 are 0.2 g-surfactant/g-adsorbent and 0.3 g-surfactant/g-adsorbent, respectively. This results might be due to the high surface area of ACF-15 when compared with activated carbon adsorbents (AC-45x100 and AC-20x45).

The adsorption capacity increased with an increase of packing density of ACF adsorbents. The adsorption rate is shown to increase with an increase of the solution flow rate. Especially at the initial stage of an adsorption, the uptake rates are strongly dependent on the flow rates, which is obviously due to the film mass-transfer resistance. The adsorption capacity of an ACF-15 was about 0.6g-surfactant/g-carbon, which is higher than that of a granular AC by a factor of two.

Key words: Perfluorocarbon, Fluorinated Surfactant, Adsorption, Activated Carbon Fiber

Anion Recognition by Phosphorus Triamide-based Receptors

Chenyi Lei, Honoka Kumagai, Yuka Yoshida, and Shin-ichi Kondo*

Department of Chemistry, Faculty of Science, Yamagata University, Yamagata 990-8560, Japan

Anion recognition is an emerging area in host-guest chemistry because of its wide range of applications in medicinal and environmental chemistry. It is well known that urea-based receptors (**1**) have been widely used due to the cooperative hydrogen bonds by two N-H groups. Phosphorus triamide (**2**) has three N-H groups on one phosphorus atom, so it can be expected to recognize anions by these N-H groups in three-dimensional manner, resulting in stronger and more selective anion recognition ability than amide and urea-based ones. Therefore, we have studied the recognition ability of simple phosphorus triamide-based receptors **2** (R = alkyl or phenyl) by UV-vis and NMR titration techniques. We have also designed 2,2'-binaphthalene having two phosphorus triamide groups for more selective and strong recognition of anions due to six hydrogen bonds. Synthesis and anion recognition ability of receptor **3** will be discussed in this symposium.

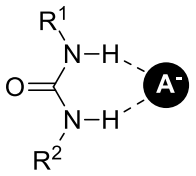

1•A^-

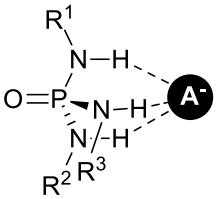

2•A^-

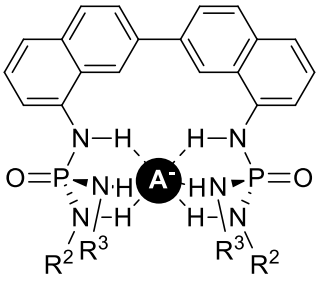

3•A^-

Recent studies on semiconducting material for photoelectrochemical hydrogen evolution under visible light irradiation

Md Nazmodduha Rafat and Won-Chun Oh *,

[1]*Department of Advanced Materials Science & Engineering, Hanseo University, Seosan-si, Chungnam, Korea, 356-706*

Abstract

Photoelectrochemical hydrogen evolution, a method which is driven photo, has been drawing enormous attention in recent years for its low cost and environmental friendship in solving the energy shortage through facile solar to chemical conversion. To be an ideal photocatalyst, its must need to meet the requirements that include wide range optical utilization, effective separation of photo-generated carriers and high-efficient surface redox reaction. The photocatalytic efficiency of semiconductors is mainly determined by the coordination and balance of thermodynamics and kinetics. Titanium dioxide (TiO_2) as a popular and first reported photocatalyst used in hydrogen evolution, CO_2 reduction and environmental applications has been extensively investigated. Hydrogen energy has received significant research effort due to the high energy density, eco-friendly, and robustness. One particular focus has been to produce hydrogen effectively, and splitting water using the hydrogen evolution reaction (HER) is considered to be a promising and key route. In our lab, we are trying to design combined semiconducting material to get efficient photocatalysts. In our work, we find out that as a photocatalyst LaCdSe-GO-TiO_2 (LCS) has shown a good potential in photoelectrochemical water splitting for hydrogen evolution. In this work, LCS nanoparticles were synthesized by ultrasonic process under ambient pressure. The small particle size plays a key role in suppressing the recombination of photo-induced carriers, and thus promoting the photocatalytic activity. In the presence and absence of 20% methanol as a sacrificial agent, its show good photocatalytic activity. This work provides a good example on size control, low-cost synthesis and photocatalysts' design. Small size particles or low-dimension materials enable shorter diffusion distance of electrons and holes which could facilitate the surface redox reaction as compared to their bulk counterparts. Various synthetic techniques have been applied in controlling particle size, including solvothermal, sonochemical and wave-assisted

hydrothermal methods in recent years. It is well-known that most of these methods demand harsh reaction conditions such as good quality equipment, high temperature or high pressure. Therefore, for the purpose of meeting the requirements of industrial application, it is highly competitive to make use of ultrasonic process under ambient pressure conditions. Our group has demonstrated that LaCdSe-GO-TiO_2 (LCS) can be prepared by ultrasonic method. We reckon, in the future it will be applicable for synthesizing novel materials.

Keyword: Water splitting, photocatalyst, Semiconductor, hydrogen, ultrasonic.

Antibacterial activity of GQDs from various fresh fruits as precursors

Nongyao Teppaya[1,2] and Prawit Nuengmatcha*[1,2]

[1]Creative Innovation in Science and Technology, [2]Nanomaterials Chemistry Research Unit, Department of Chemistry, Faculty of Science and Technology, Nakhon Si Thammarat Rajabhat University, 80280, Thailand.

[*]Corresponding author. e-mail: pnuengmatcha@gmail.com; Tel. +66-7537-7443, Fax +66-7537-7443

Abstract

Graphene quantum dots)GQDs(was successfully synthesized by pyrolysis method. Various fresh fruits including pineapple watermelon lemonade and tangerine were used as precursors. All samples were characterized by using ultraviolet visible spectrophotometer (UV-vis), scanning electron microscopy (SEM) and energy-dispersive X-ray spectroscopy (EDX). Antibacterial activity was determined by disc diffusion method against strains of *Escherchia coli* (*E. coli*) and *Staphylococcus aureus* (*S. aureus*). The synthesized lemonade GQDs demonstrated excellent antibacterial activity for *S. aureus* and *E. coli* with inhibition zone was 2.30 ± 0.6 cm and 1.65 ± 0.4 cm, respectively. While the other synthesized GQDs materials: pineapple juice GQDs, watermelon juice GQDs and tangerine juice GQDs have no activity for both grams positive bacterialand gram negative bacterial.

Keywords: Antibacterial activity, Graphene quantum dots, Escherchia *coli*, *Staphylococcus Aureus*

Formation of iron active species on HZSM-5 catalysts by varying iron precursors for phenol hydroxylation

Siriphorn Butthaa, Sujittra Youngmea, Jatuporn Wittayakunb, Sirinuch Loihaa, *

aMaterials Chemistry Research Center, Department of Chemistry and Center of Excellence for Innovation in Chemistry, Faculty of Science, Khon Kaen University, Khon Kaen 40002, Thailand

bSchool of Chemistry, Institute of Science, Suranaree University of Technology, Nakhon Ratchasima, 30000, Thailand

Email: Sirilo@kku.ac.th

Abstract

Iron-containing HZSM-5 zeolite (Fen+-HZSM-5) are performed by ion exchange with varying iron precursors of Fe2+, Fe3+ and equivalent molar of Fe2+/Fe3+. Variation of the iron species on the HZSM-5 surface is expected. All Fen+-HZSM-5 catalysts are applied for phenol hydroxylation in reflux condition at 70 °C in the presence of H2O2. Discrimination in the iron structures on the catalysts is determined using UV-Vis DRS and EXAFS techniques. The iron species found in the Fe2+-HZSM-5 and Fe3+-HZSM-5 catalysts is an isolated Fe3+ species in tetrahedral geometry indicating the presence of iron in zeolite framework (Fe-OF). While a mixture of isolated Fe3+ and iron-dioxo species (FO-Fe-OF) in octahedral geometry existing in small particles on the HZSM-5 is determined in the Fe2+/Fe3+-HZSM-5 catalyst. The presence of iron mixture in the Fe2+/Fe3+-HZSM-5 catalyst showed the highest turnover number (TON) for phenol hydroxylation comparing with bulk α-Fe2O3 and α-FeOOH catalysts. Moreover, an improvement of catechol selectivity by the existence iron-dioxo species on HZSM-5 catalyst is proposed.

Keywords: HZSM-5; α-Fe2O3; α-FeOOH; EXAFS; phenol hydroxylation

Preparation and Photocatalytic Activity of CdS/$BiVO_4$ Composite Semiconductor

CHEN Yihua[1]，HU Junjun[1]，DING Tongyue[iii]，YANG Benhong[2*]

1. Department of Biological and Environmental Engineering，Hefei University，Hefei，230601, China；

2. Department of Chemistry and Materials Engineering，Hefei University，Hefei，230601, China

Abstract: CdS/$BiVO_4$ composite photocatalyst was prepared via in situ growth of CdS crystals on $BiVO_4$ template by hydrothermal method, and was characterized by XRD, SEM and other means. The photocatalytic degradation of methylene blue by CdS/$BiVO_4$ showed a degradation rate of 94.79% after 60 min visible light irradiation, significantly higher than that of pure $BiVO_4$ and pure CdS.

Key words: $BiVO_4$; CdS; Semiconductor; Photocatalytic activity

Bismuth vanadate ($BiVO_4$) has a narrow band gap and shows good photocatalytic activity under visible light irradiation. However, the photogenerated electron-hole pairs of pure $BiVO_4$ tend to recombine fast, and the quantum efficiency is low. In order to solve this problem, predecessors have made many attempts, such as precious metal deposition [1], element doping [2], semiconductor recombination [3] and so on. Semiconductor recombination is an effective method for photocatalytic modification. When two semiconductor materials with different compositions contact and combine together, the exchange of electrons and holes will occur at the two-phase interface, forming a space charge area, enabling the rapid separation of photogenerated electrons and holes, therefore improving the photocatalytic activity [4]. The band gap width of semiconductor CdS is about 2.4 eV, and the photoelectric effect is relatively strong in visible light [5]. The CdS/$BiVO_4$ composite semiconductor prepared via in situ combining $BiVO_4$ with CdS, would effectively promote the electron-hole separation, and improve the photocatalytic activity. In this paper, CdS/$BiVO_4$ composite semiconductor

[*]**Corresponding author, Email: yangbh@hfuu.edu.cn.**

This project was supported by National Natural Science Foundation of China (51403048).

photocatalyst was prepared by hydrothermal method, and was used to investigate the degradation performance of methylene blue (MB).

1 Experimental Section

1.1 Preparation of catalysts

1.1.1 Preparation of $BiVO_4$

2.43 g $Bi(NO_3)_3 \cdot 5H_2O$ was dissolved in 10 mL HNO_3 solution (2 mol/L). 0.58 g of NH_4VO_3 was dissolved in 10 mL of NaOH solution (2 mol/L). The two solutions were slowly mixed and stirred for 2 h, diluted to 80 mL with water, adjusted to pH 2, and heated at 180 ºC for 6 h in a 100 mL autoclave. The products were centrifuged, washed, dried for later use.

1.1.2 Preparation of $CdS/BiVO_4$ composite photocatalyst

0.62g $Cd(NO_3)_2 \cdot 4H_2O$ and 0.15g C_2H_5NS were respectively dissolved in 30 mL deionized water. The two solutions were mixed slowly, and stirred for 30 minutes. 0.32g of self-made $BiVO_4$ powder was added to the above solution, ultrasonically shocked for 30 min, diluted to 80 mL with water, adjusted to pH 5, and heated at 125 ºC for 10 h in a 100 mL autoclave. The products were centrifuged, washed, dried for later use.

1.2 Degradation of Methylene Blue

1.41 g of catalyst and 100 mL of MB solution (5 mg/L) were mixed together in room temperature and kept in dark for 30 min. Then the light source (xenon lamp, 700 W) was turned on. 5 mL of MB solution was taken out for light absorbance measurement every 15 min. the concentration of MB solution was obtained by using standard curve. The catalytic degradation rate was calculated according to the formula $(C_0-C_t)/C_0\times$ 100%, where C_0 is the original concentration of MB, and C_t is the MB concentration after catalytic degradation for t min.

2 Results and discussion

2.1 SEM analysis

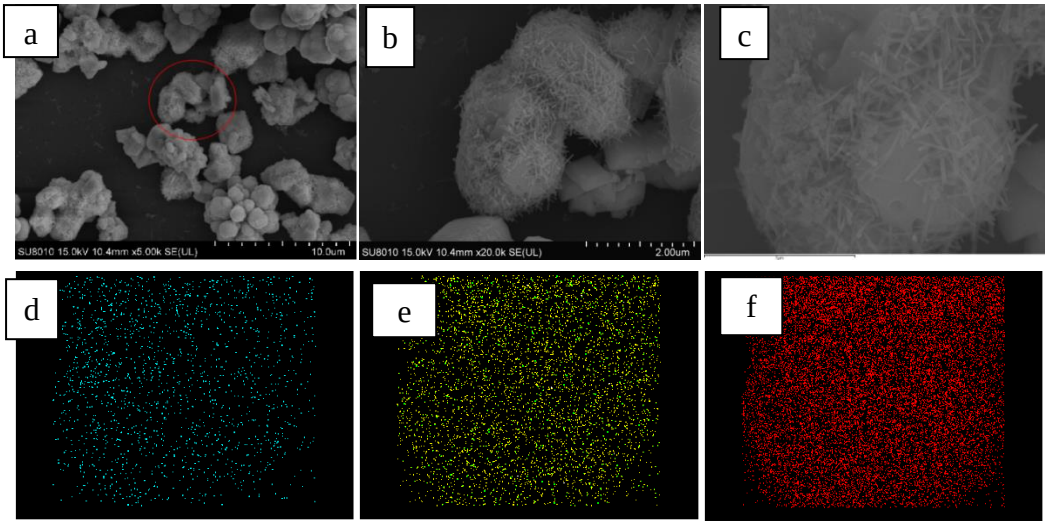

Fig. 1 SEM images and EDS Mapping photos of CdS/$BiVO_4$

Figure 1 shows the SEM images and EDS Mapping photos of CdS/$BiVO_4$. As can be seen from figure 1(a, b, c), $BiVO_4$ shows square flake particles with side length between 1-2 μm and thickness of 0.2-0.3 μm. A large number of rod-like CdS nanoparticles attached to the surface of $BiVO_4$ flakes, forming a very rough surface, which is obviously beneficial to improving the adsorption capacity and catalytic activity of photocatalyst. The CdS/$BiVO_4$ surface was analyzed by EDS mapping as shown in figure 1(d, e, f). It can be seen that three main elements, Cd, Bi and V, were evenly distributed in the scanning area, indicating that CdS was evenly distributed on the surface of $BiVO_4$, and CdS nanoparticles successfully combined with $BiVO_4$ flakes.

2.2 XRD analysis

Figure 2 shows the XRD spectra of $BiVO_4$, CdS and CdS/$BiVO_4$. From the XRD spectrum of $BiVO_4$, it can be seen that there are obvious diffraction peaks at the diffraction angles as 28.7°, 30.54° and 53.31°, corresponding to the crystal faces of (121), (040) and (161) of $BiVO_4$ standard card (JCPDS 14-0688) with monocline schescheite structure. The XRD spectrum of CdS shows that diffraction peaks appear at 26.4°, 43.9° and 51.9° respectively, corresponding to the crystal faces of (111), (220) and (311) of the standard CdS card (JCPDS 89-0440). The diffraction peak of CdS/$BiVO_4$ is almost the superposition of the diffraction peaks of both $BiVO_4$ and CdS, indicating the successful preparation of CdS/$BiVO_4$ composite photocatalyst.

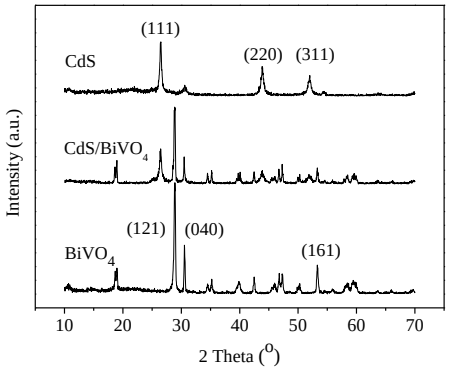

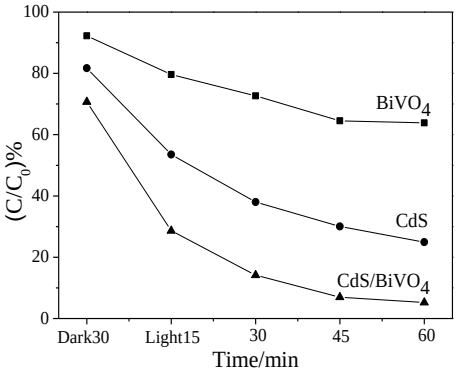

Fig.2 XRD spectraof $BiVO_4$, CdS and $CdS/BiVO_4$

Fig.3 Photodegradation curves of MB solution

2.3 Photocatalytic performance

Figure 3 shows the photodegradation curves of MB solution by different catalysts. As can be seen from the figure, the degradation rate of MB solution increased with the extension of illumination time. After 60 min of illumination, the degradation rates of MB solutions photocatalyzed by $BiVO_4$, CdS and $CdS/BiVO_4$ were 36.15%, 75.09% and 94.79%, respectively. The photocatalytic activity of $CdS/BiVO_4$ composite photocatalyst is significantly higher than that of pure $BiVO_4$ and pure CdS.

3 Conclusions

$CdS/BiVO_4$ composite photocatalyst was prepared by hydrothermal method. SEM characterization showed that a large number of rod-like CdS nanoparticles attached to the surface of $BiVO_4$, increasing the specific surface area. The photocatalytic activity test showed that the degradation rate of MB photocatalyzed by $CdS/BiVO_4$ could reach 94.79%.

References：

[1] Yaw C S, Ruan Q S, Tang J W, et.al. *Chem. Eng. J.*, 2019, **364**: 177-185.

[2] Zhang J, Zhang Q N, Yue Y W, et.al. *Catal. Commun.*, 2019, **123**: 100-104.

[3] Abega A V, Ngomo H M, Nongwe I, et.al. *Synt. Met.*, 2019, **251**: 1-14.

[4] Liu Y, Huang B, Dai Y, et.al. *Catal. Commun.*,2009, **11**: 210-213.

[5] Chang Y S, Choi M, Baek M, et.al. *Appl.Catal., B,*2018,**225**: 379-385.

Preparation and characterization of $Ce_{0.8}Sm_{0.2-x}Cu_xO_{1.9-\delta}$as electrolyte for intermediate temperature Solid Oxide Fuel Cells

SHAO Linbo[1], WANG Yajun[2], CHEN Jie[2], LIANG Sheng[2]， TIAN Changan[2*]

1.Department of Biological and Environmental Engineering，Hefei University，Hefei，230601, China；

2. Department of Chemistry and Materials Engineering，Hefei University，Hefei，230601, China

Abstract: In this study, ultrafine $Ce_{0.8}Sm_{0.2-x}Cu_xO_{1.9-\delta}$ (x = 0 ~ 0.20) powders have been successfully prepared by sol-gel auto-combustion method. The samples were characterized by FTIR, TG-DSC, XRD, Raman spectroscopy, BET, SEM, AC impedance, and thermal expansion measurements. The results indicated that $Ce_{0.8}Sm_{0.2-x}Cu_xO_{1.9-\delta}$ powders with highly phase-pure cubic fluorite-type structure were obtained after calcining at 600 ºC for 2 h. The as-synthesized powders exhibited high sintering activity, $Ce_{0.8}Sm_{0.2-x}Cu_xO_{1.9-\delta}$ series electrolytes which have higher relatively dense over 96% can obtain after sintering at 1500 ºC for 3 h. $Ce_{0.8}Sm_{0.18}Cu_{0.02}O_{1.89}$ electrolyte sintered at 1500 ºC for 3 h exhibits the highest oxide ionic conductivity ($\sigma_{800\,^{\circ}C}$ = 0.058 S cm^{-1}), lowest electrical activation energy (E_a = 0.33 eV) . Therefore, it was concluded that co-doping with appropriate ratio of Sm/Cu can further improve the properties of ceria electrolytes.

Key words: Solid Oxide Fuel Cells, Electrolyte, Sol-gel auto-combustion method, conductivity

Controllable Synthesis of Magnetite with Various Shapes and Applications

Chengliang Han, Li Yao, Lixin Wan, Kunhong Hu,

College of Energy Materials and Chemical Engineering, Hefei University, Hefei 230601, China

Abstract

Magnetite(Fe_3O_4) is an important materialwidely used in magnetic components, magnetic separation and catalysts. Synthesis of Fe_3O_4 nanomaterials are mainly focused on the control of their morphology, size and pore structure. However, researches on Fe_3O_4 compositesare also very common. For example, Fe_3O_4 nanocrystals combined with various catalysts to formcomposite magnetic catalysts could be used as effective photocatalysts or adsorbents for wastewater treatment. Recently, Novel Fe_3O_4 porous fibers were successfully obtained by conventional hydrothermal route using protein as templates, sodium citrate as a reducing agent and $FeCl_3.6H_2O$ as single iron raw material. This magnetic fiberwith high specific surface area could be applied to remove heavy metal ions and dyes in waster water. Then, Fe_3O_4 nanoparticlesfor oil and water separation were obtained from the above reaction systems using mannitol instead of sodium citrate. In the end, quasi-spherical Fe_3O_4 particles with excellent optical properties were prepared by replacing the above protein templates with polyacrylamide. In summary, we developed a facile and effective method to synthesize various morphological Fe_3O_4 by changing templates and reducing agents in the reaction system. The as-obtained Fe_3O_4could be used in the field of environmental pollutantstreatment.

Research on GO/Pal nanocomposite powder and its antibacterial activity

Difang Zhao, lixing Zhang

Department of Chemical and Materials Engineering, Hefei University, Anhui, China,230601

Abstract: This study reports the graphene oxide/palygorskite (GO/Pal) nanocomposite materials prepared by liquid phase method. Experiments were carried out to evaluate their potential applications. The results of scanning electron microscopy (SEM), infrared spectroscopy (IR) and differential scanning calorimetry (DSC) show that palygorskite nanorods are firmly attached to the lamellar surface of two-dimensional graphene oxide particle and and the original agglomeration of both graphene oxide and palygorskite particles was not observed. The thermal stability of GO/Pal composite powders is between the thermal decomposition temperature of graphene oxide and palygorskite. The antibacterial test showed that the antibacteril ratio of GO/Pal composite powder on Escherichia coli reached 98.3%.

Keywords: Nanocomposite, Antibacterial, Graphene Oxide, Palygorskite

1.Introduction

Antimicrobial nanocarbons such as single-walled carbon nanotubes, multiwalled carbon nanotubes, and graphene materials seemingly function through the damaging of cellular envelopes via the combinational effect of multiple “physicochemical” routes. [1] However, GO often fails to perform its surface physicochemical effects well due to its agglomeration. Therefore, it is an urgent problem to disperse graphene oxide sheets when they were applied. Palygorksite (attapulgite) is a kind of mineral clay which classed as a 2:1 layer inverted structure along with the elongate habit and the fine particle size, give a high surface area (porous structure).[2] The charge on the particles, the channels through the structure, and the high surface area give palygorskite a capacity to absorb and adsorb various materials.[3] The objectives here are to focus on the preparation of graphene oxide and palygorskite nanocomposite materials with good antibacterial properties.

2.Experimental

Palygorskite (Pal) was obtained from Haiyang Powder Technology (China), Nanometer Graphene oxide (GO) aqueous dispersion was puchased from Suzhou Hengqiu nanometer

reagent Co., LTD. Commercial m550-7 polyquaternary ammonium salt cationic surfactant was puchased from Guangzhou Crane international trade Co., LTD. Escherichia Coli (E. Coli) was obtained from the Hefei Health and Epidemic Prevention Station. Other chemical were purchased from Sinopharm (China). Palygorskite powder was dispersed into water suspension. After ultrasonic treatment, quaternary ammonium salt solution was added and mixed with GO water dispersion in a certain proportion, after centrifugation, the products were washed and dried at 40 ◦C for 12 h. The suface morphology of GO, Pal and GO/Pal nanocomposites (NCs) was evaluated by scanning electron microscopy (SEM, Hitachi SU8010). The infrared spectra (IR) of the samples mixed with KBr were recorded with a Series 100 PerkinElmer IR 1650 spectrophotometer, operating in the range 200 - 4000 cm-1. The differential scanning calorimetric (DSC) measurements were realized by using a DSC-kind SETARAM 121 apparatus, operating under an argon flow and at a heating rate of 10 ◦C min-1. The antibacterial experiment was carried out to investigate the antibacterial performance of the NCs powder according to a plate count method [4].

3. Results and discussion

In order to observe the microstructure of composite powder, the samples of GO, Pal and GO/Pal was observed by SEM. Shown in Fig.1 are SEM images of the GO, Pal and GO/Pal. As shown in Fig. 1 (a), the GO sheets are stacked together, and Fig. 1 (b) shows that Pal particles are also clustered together. Fig. 1 (c) is the GO/Pal composite powder. In this figure, palygorskite nanorods adhere tightly to the graphene oxide lamella surface, making the graphene lamella no longer stack and palygorskite nanorods no longer reunite. The reason for this is that the surface energy of GO and Pal is reduced when Pal particles adheres to the surface of GO.

The spectra shown in Fig. 2 reflect the changes in the absorption bands of the composion product of GO/Pal powders. Thus, the spectra of GO/Pal powder are the same as the GO for the vibrations at 982, 1508, 2364 and 3629 cm-1 of GO/Pal are virtually no remove. But the large and sharp band at 1508 cm-1 becomes small and shallow. On the contrary, the little and dissymetric band at 2364 cm-1 becomes sharp and symmetrical about a maximum at 2362 cm -1 (Fig. 2 GO and GO/Pal). The absorption band at 1640 cm-1 of Pal is not seen in GO/Pal perhaps because the content of palygorskite in the composite powder is small, and the other

absorption bands of Pal are overlap with GO's absorption bands.

The thermal stability of inorganic antibacterial agent is a very important index and the presence of the oxygen functional groups makes GO thermally unstable, as it undergoes pyrolysis at elevated temperatures. The thermal behavior of the GO/Pal nanocomposite powder was investigated by DSC. As shown in Fig. 3, Pal, GO and GO/Pal all have largeendothermic peak at 100-200 ℃, However, GO/Pal has an endothermic peak temperature between GO and Pal.This is mainly because palygorskite improves the thermal stability of composite powders. GO/Pal and GO both have a large exothermic peak at 200 - 250℃. GO/Pal nanocomposite powder still has heat absorption after 300℃, mainly due to the crystalline water absorbs heat inside palygorskite of the composite powder.

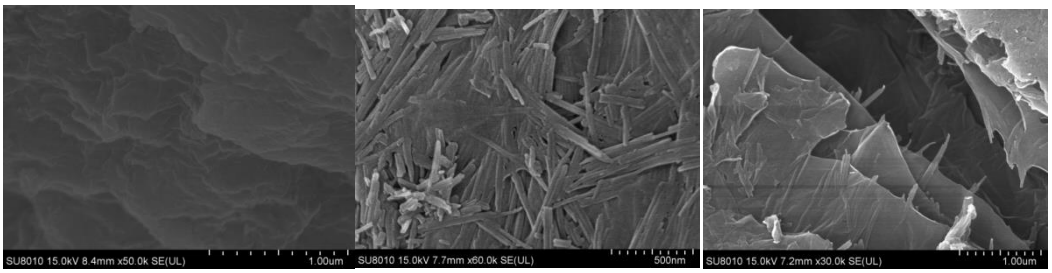

(a) (b) (c)

Fig.1 SEM images of the samples. (a): GO (b): Pal particles (c): GO/Pal composite powder

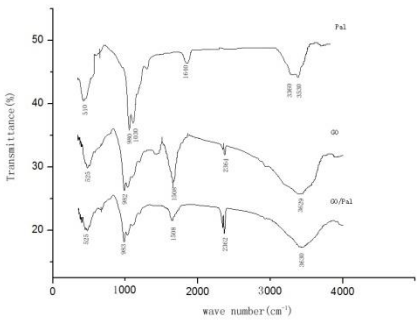

Fig.2 I.R. spectra of Pal, GO and GO/Pal powders at room temperature.

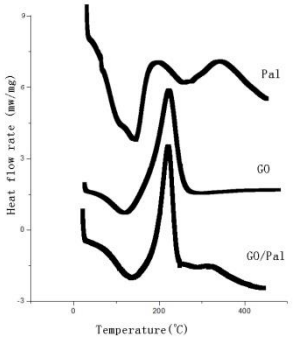

Fig.3 The DSC curves of GO, Pal and GO/Pal.

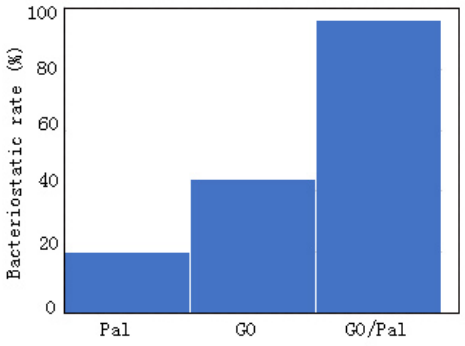

Fig.4 The antibacteial rate of the Pal, GO and GO/Pal.

Antibacterial experiments were carried out by measuring the inhibition rate of the nanocomposite powder against E. coli through a plate counting method. Fig. 4 displays the bacteriostatic rates of the samples. The Pal powder had a weak antibacterial property, which could be attributed to there is no antibacterial antivity factors in silicoalumonate mineral

substance. Graphene showed weak antibacterial properties because of its internal electrical conductivity, but because of its overlapping layers, its antibacterial properties were weak. GO/Pal composite powder showed significant antibacterial properties than the Pal and GO, which may be mainly due to the separation of phazelite between graphene sheets, improving its antibacterial activity. At the same time, the dispersion of palygorskite particles also improves the adsorption of bacteria.

4. Conclusions

Nanocomposite powder of Pal nanorod particles loaded on the surface of GO were prepared by a facile method. The characteriazation results by SEM, IR and DSC confirmed the Pal particles on the GO. It was noticed that the agglomeration of GO and Pal powders due to their higher surface energy when they existed seperately is no longer present. Meanwhile, the thermal stability of Go/Pal composite powders was higher than that of GO but lower than that of Pal. Furthermore, the prepared GO/Pal NCs demonstrated high antibacterial activity against the tested E. coli bacteria with the amount of Pal content is 10%.

Acknowledgement

The authors would like to acknowledge the support of the chemical and materials engineering department, Hefei University, Anhui, China (230601).

References

[1] I. Barbolina, C. R. Woods, N. Lozano, et al., Purity of graphene oxide determines its antibacterial activity 2D Mater., 2016, 3(2), 25025.

[2] Frost, R.L., Locos, O.B., Ruan, H., et al., Near-infrared and mid-infraredspectroscopic study of sepiolites and palygorskites. J. Theo. Kloprogge. 2001,27 (1), 1–13.

[3] Zheng, M.S., Wang, A.Q., Zan, G.S., The Application Research of Attapulgite Clay.Chemical Industry Press, Beijing. 2007.

[4] H. E. Karahan, L. Wei, K. Goh, et al. Synergism of Water Shock and a Biocompatible Block Copolymer Potentiates the Antibacterial Activity of Graphene Oxide," Small, 2016,12(7), 951–962.

Preparation and Photocatalytic Activity of BiOBr/g-C_3N_4 Heterojunction

DING Tongyue[iv],CHEN Yihua[1], HU Junjun[1],YANG Benhong[2]*

1. Department of Biological and Environmental Engineering, Hefei University, Hefei, 230601 ;

2. Department of Chemistry and Materials Engineering, Hefei University, Hefei, 230601, China

Abstract: BiOBr/g-C_3N_4 composite catalyst was prepared by hydrothermal method, and was characterized by XRD and SEM. The photocatalytic degradation rate of rhodamine B catalyzed by BiOBr/g-C_3N_4 is 96% after 60 min visible light irradiation.

Key words: g-C_3N_4; BiOBr; Heterojunction; Catalytic degradation

1 Introduction

BiOBr, with a band gap width of 2.75eV, has a good response to visible light. However, the catalytic degradation activity of a single BiOBr catalyst is not high due to the high photogenerated electron-hole recombination rate [1]. BiOBr, with a two-dimensional lamellar structure, can form heterojunction structure with other semiconductorstobuild an internal electrostatic field along the vertical direction of halogen lamination of crystal growth.This electrostatic field can effectively promote the separation of photogenerated electron-hole pairs [2].g-C_3N_4 holds a band gap width of 2.7 eV, and has good photoelectric chemical characteristics [3].BiOBr nano-plates can grow on the surfaceof g-C_3N_4 nanosheets to form BiOBr/g-C_3N_4 heterojunction [4], in which there are strong interfacial interactions between the (001) crystal faces of BiOBr and the (002) crystal faces of g-C_3N_4, which could improve the photocatalytic activity [5].In this paper, BiOBr/g-C_3N_4 heterojunction was prepared by hydrothermal method, and was used to investigate the degradation performance of rhodamine B (RhB).

*Corresponding author, Email: yangbh@hfuu.edu.cn.

This project was supported by National Natural Science Foundation of China (51403048) and Talent Scientific Research Foundation of Hefei University (16-17RC07).

2 Experimental

2.1 Preparation of g-$C_3N_4$and BiOBr

g-C_3N_4 was prepared by pyrolysis of melamine, and BiOBr was prepared by hydrothermal method.

2.2 Preparation of BiOBr/g-C_3N_4

The 0.375 g KBr and 0.4575g g-C_3N_4 were dissolved in 40 mL of deionized water, ultrasonically shocked for 30 min and recorded as solution A. 1.455 g $Bi(NO_3)_3 \cdot 5H_2O$ was dissolved in 20 mL ethylene glycol and recorded as solution B. Solution B were addeddropwise to solution A. The mixture was stirred at room temperature for 1 h, diluted to 80 mL with water, transferred to 100 mL autoclave, and heatedat 140 ^oC for 8 h. The products were centrifuged, washed, dried for later use.

2.3 Photocatalytic degradation of RhB

A certain amount of photocatalyst and 100 mL of RhB solution (5 mg/L) were mixed together in room temperature and kept in dark for 30 min. Then the light source (xenon lamp, 700 W) was turned on. 5 mL of RhB solution was taken out for light absorbance measurement every 10 min. Concentration of RhB solution was obtained by using standard curve. The catalytic degradation rate was calculated according to the formula $(C_0-C_t)/C_0\times100\%$, Where, C_0 is the concentration of RhB before catalytic degradation, andC_t is concentration of RhB after catalytic degradation for a period of time.

3 Results and discussion

3.1Morphology characterization

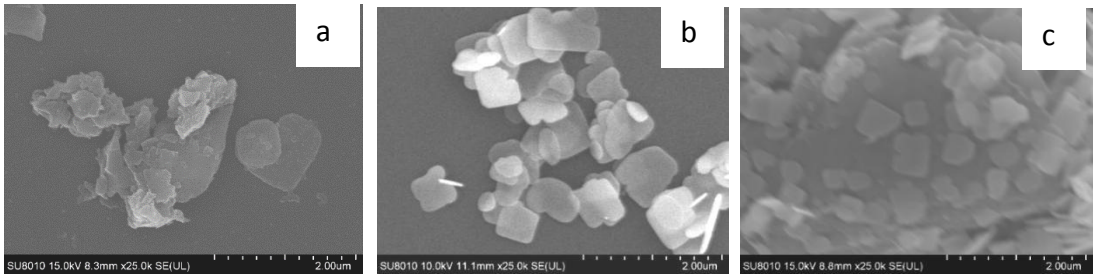

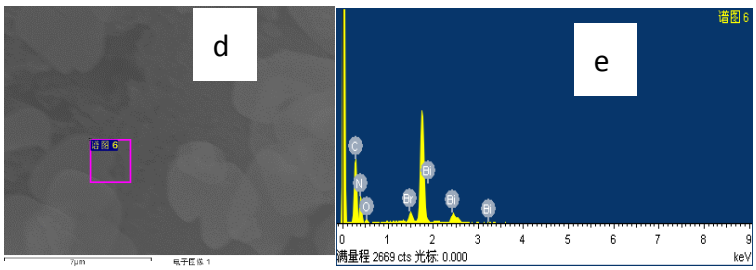

Fig. 1SEM and EDS spectra of g-C_3N_4, BiOBr and BiOBr/g-C_3N_4

Fig.1a is the SEM photo of pure g-C_3N_4. It can be seen in Fig.1a that g-C_3N_4 presents a layered-sheet structure. Fig.1b is SEM photo of pure BiOBr. As shown in Fig.1b, BiOBr is approximately square flake particle. Fig.1c is the SEM photo of BiOBr/g-C_3N_4. It can be seen that the BiOBr flake particles are evenly distributed on the surface of g-C_3N_4, and BiOBrand g-C_3N_4 particles are organically combined together. Elemental analysis was carried out on BiOBr/g-C_3N_4(Fig.1d). Fig.1e shows five target elements C, N, Bi, O and Br appear at the binding site of g-C_3N_4 and BiOBr, indicating the successful preparation of BiOBr/g-C_3N_4.

3.2 XRD characterization

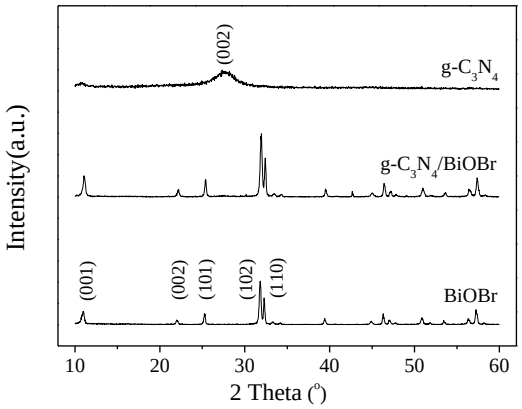

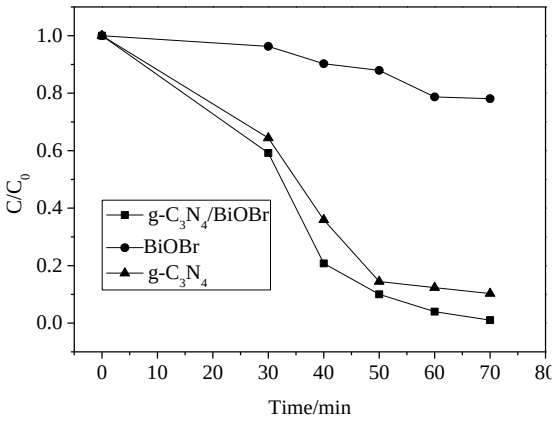

Fig. 2XRD patterns ofpotocatalysts**Fig. 3**PhotodegradationcurvesofRhB

Fig.2 shows the XRD patterns of g-C_3N_4, BiOBr and BiOBr/g-C_3N_4. The diffraction peaks of BiOBr at 2θ=11.0º, 22.2º, 25.3º, 31.8º and 32.5º correspond to the crystal faces (001), (002), (101), (102) and (110) of tetragonal BiOBr standard card (JCPDS 87-1526), respectively. The g-C_3N_4 presents a diffraction peak at 2θ=27.4º, corresponding to the (002) crystal face of layered g-C_3N_4.The XRD pattern of BiOBr/g-C_3N_4 is basically the same as that of BiOBr, and the diffraction peak at 27.4º is not obvious, which may be caused by BiOBr particles entering

the layers of g-C_3N_4 and breaking the structure order of g-C_3N_4.

3.3Photocatalytic degradation

Fig.3 shows the photodegradation curves of RhB catalyzed by g-C_3N_4, BiOBr and BiOBr/g-C_3N_4. As seen in Fig.3, pure BiOBr has a high degradation effect toward RhB, and the degradation rate was about 90% at 60 min, while g-C_3N_4 has a very low degradation efficiency toward RhB, the degradation rate was less than 20% at 60 min. BiOBr/g-C_3N_4 shows even higher degradation effect toward RhB. the degradation rate reached 96% after 60 min of illumination, exhibiting a strong photocatalytic activity. It may be due to the formation of heterojunction between BiOBr and g-C_3N_4 particles, in which the built-in electric field promotes the separation of photogenerated electron-hole pairs.

4 Conclusion

BiOBr/g-C_3N_4 composite photocatalyst was prepared by hydrothermal method. SEM characterization showed that, the lamellar BiOBr particles were evenly distributed on the g-C_3N_4 flakes, and g-C_3N_4 formed a heterojunction with BiOBr in the composite catalyst. It effectively improves the separation rate of electron-hole pairs. The degradation rate of RhB catalyzed by BiOBr/g-C_3N_4 can reach 98%, higherthan either component.

References:

[1] Zhao W, Liu Y, Wei Z B et.al. *Appl. Cata. B：Envi.*2016 **185**242-252.

[2] Thamaraiselvi K, Sivakumar T, Sahaya M K P et.al. *Appl. Surf. Sci.* 2017 **426** 1030-1045.

[3] Bao Y C, Chen K Z. *Appl. Surf. Sce.* 2018 **437** 51-61.

[4] Yang L W, Liang L L, Wang L J et.al. *Appl. Surf. Sce.* 2019 **473** 527-539.

[5] Yu X, Wu P W, Qi C X et.al. *J. Allo. Compo.* 2017 **729** 162–170.

Preparation and Photocatalytic Application of Ag_3PO_4/GO Composites

HU Junjun[1], DING Tongyue[v], CHEN Yihua[1], YANG Benhong[2]*

1. Department of Biological and Environmental Engineering, Hefei University, Hefei, 230601, China ;

2. Department of Chemistry and Materials Engineering, Hefei University, Hefei, 230601, China

Abstract: Ag_3PO_4/GO composite was prepared via loading with Ag_3PO_4 nanoparticles on GO template by in situ precipitation method, and was characterized by SEM and XRD. The photocatalytic degradation of RhB catalyzed by Ag_3PO_4/GO-7.53% composite showed a degradation rate of 95.7% after 60 min visible light irradiation.

Key words: Ag_3PO_4; GO; Photocatalytic activity; Composite materials

2 Introduction

Ag_3PO_4, a new photocatalyst with narrow band gap (2.36eV), can absorb sunlight with wavelength less than 530 nm and has high photocatalytic activity [1]. However, the structure of Ag_3PO_4 is unstable and the separation efficiency of photogenerated electron-hole pairs is not high [2]. The improvement of photocatalytic activity of Ag_3PO_4 by doping, precious metal deposition and material compounding has been explored [3]. Pakpoom et.al. tried to enhance the separation rate of photogenerated electron-hole pairs by doping Mn^{2+} ions to form impurity levels in Ag_3PO_4[4]. Ma et.al. combined Ag_3PO_4 with TiO_2 to achieve the effect of broadening the spectral absorption range [5]. Graphene oxide (GO) has special structure and properties. The combination of Ag_3PO_4 and GO does not affect the transmission and absorption of light. Photogenerated electrons of Ag_3PO_4/GO can be transmitted through GO to improve the separation rate of photogenerated electron-hole pairs, which may effectively enhance the photocatalytic activity. In this paper, Ag_3PO_4 was compounded with GO by in situ precipitation method and used to investigate the degradation performance toward rhodamine B (RhB).

[*]Corresponding author, Email: yangbh@hfuu.edu.cn.

This project was supported by National Natural Science Foundation of China (51403048).

2 Experimental

2.1 Preparation of Ag_3PO_4/GO Composite Photocatalyst

The GO of 40 mg, 60 mg, 80 mg and 100 mg were added into 60 mL Na_2HPO_4 (0.05 mol/L) solution, respectively, then ultrasonic concussion for 1 h to give GO/Na_2HPO_4 dispersions. 1.503 g $AgNO_3$ and 0.4 g PVP were dissolved in 60 mL water. The mixed solution was added dropwise into GO/Na_2HPO_4 dispersions and stirred for 1 h, then centrifuged, washed, dried to give Ag_3PO_4/GO composite photocatalysts with different mass ratios.

2.2 Degradation of RhB

30 mg of catalyst and 100 mL of RhB solution (5 mg/L) were mixed together in room temperature and kept in dark for 30 min to achieve the adsorption equilibrium. Then the light source (xenon lamp, 700 W) was turned on, 5 mL of RhB solution was taken out for light absorbance measurement every 10 min. Concentration of RhB solution was obtained by using standard curve. The catalytic degradation rate was calculated according to the formula (1-C/C_0) *100%, where C_0 is the original concentration of RhB and C is the RhB concentration after catalytic degradation for a period of time.

3 Results and discussion

3.1 Morphology Characterization

Ag_3PO_4 and Ag_3PO_4/GO samples with different mass ratios were characterized by SEM. The results are shown in Fig.1.

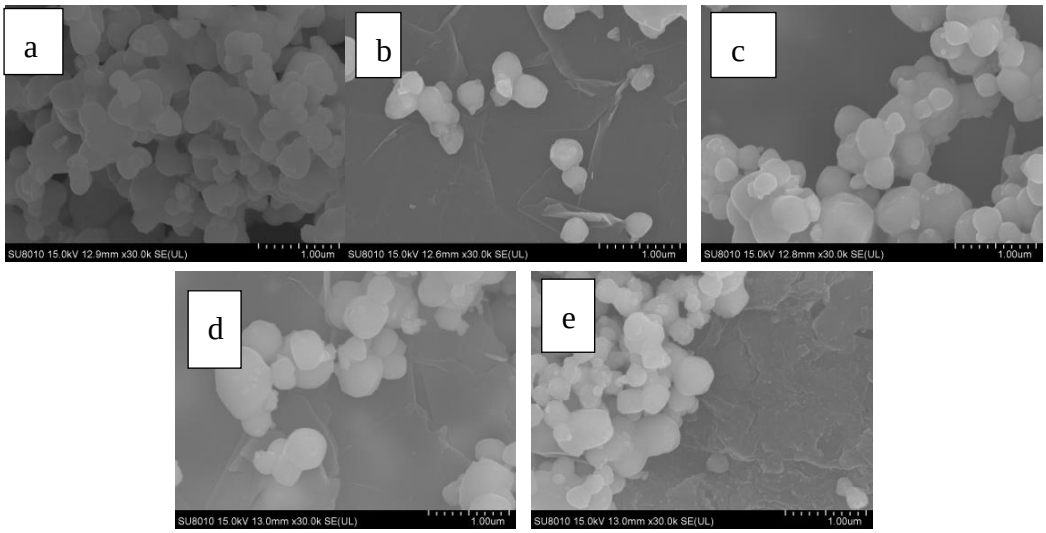

Fig.1 SEM photos of the samples

a: Ag_3PO_4; b: Ag_3PO_4/GO-3.76 wt.%; c: Ag_3PO_4/GO-5.65 wt.%;

d: Ag_3PO_4/GO-7.53 wt.%; e: Ag_3PO_4/GO-9.41 wt.%

Fig.1a shows the SEM image of pure Ag_3PO_4. As can be seen from the Fig.1a, Ag_3PO_4 particles are approximately spherical, with size ranges from 300 to 500 nm. Fig.1b-1e shows the SEM photograph of Ag_3PO_4/GO with different mass ratios. It can be seen, the approximate spherical Ag_3PO_4 nanoparticles adhere to GO sheets, and the two components organically combine together. With the increase of GO content, the morphology of Ag_3PO_4/GO do not change much.

3.2 XRD Characterization

Fig.2 shows the XRD patterns of Ag_3PO_4, GO and Ag_3PO_4/GO with different mass ratios. The diffraction peaksof pure Ag_3PO_4at 2θ=29.69, 33.29, 42.49, 52.69, 55.02 and 57.29correspond respectively to the crystal faces {200}, {210}, {211}, {211}, {222}, {320} and {321} of Ag_3PO_4 standard card (JCPDS06-0505) with tetragonal structure. The diffraction peak of pure GOat 2θ=26.47correspondsto the crystal face of {002} of GO. The diffraction peak of Ag_3PO_4/GO is almost the superposition of the diffraction peaks ofboth $Ag_3PO_4$and GO, indicating that Ag_3PO_4 nanoparticles have been successfully loaded onto the thin films of GO. The diffraction peaks of the samples are sharp and no impurity peaks appear, meaning that the samples prepared by this method have high purity and crystallinity.

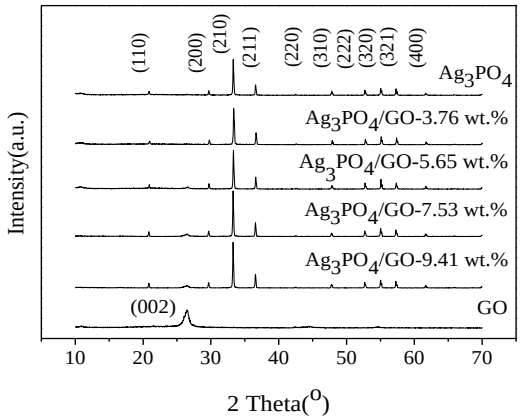

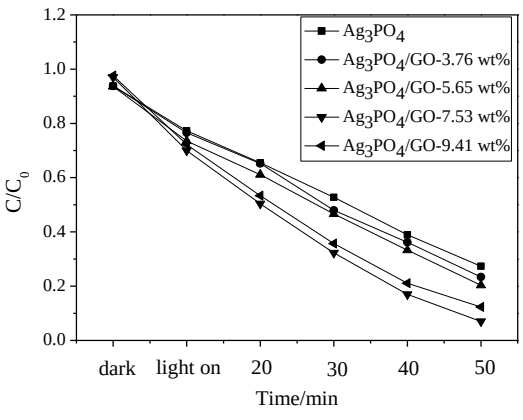

Fig.2 XRD patterns of catalysts Fig. 3 Photocatalytic activities of catalysts

3.3 Photocatalytic Degradation Performance

Fig.3 shows the degradation curves of RhB solutions catalyzed by Ag_3PO_4 and Ag_3PO_4/GO composites with different mass ratios. The results show that the photocatalytic degradations of RhB by Ag_3PO_4/GO composites are significantly higher than that of pure Ag_3PO_4, and the degradation effect of Ag_3PO_4/GO increases with the increase of composite mass ratio.

Among them, the degradation effect of Ag_3PO_4/GO-7.53% is the best, whose degradation rate reaches 95.4%, which may be due to two reasons. Firstly, the proper addition of GO enhances the specific surface area of photocatalyst. Secondly, because of the excellent conductivity of GO, It can export photogenerated electrons fast, restraining the recombination of photogenerated electron-hole pairs, thereby improving the photocatalytic activity of Ag_3PO_4/GO.

4 Conclusion

Ag_3PO_4/GO composite photocatalyst was prepared by in-situ precipitation method. RhB was used as a simulated pollutant to evaluate the photocatalytic performance of the prepared samples. The results show that the photocatalytic degradations of RhB by Ag_3PO_4/GO composites are obviously higher than that of pure Ag_3PO_4. The degradation rate of RhB photocatalyzed by Ag_3PO_4-7.53% reached 95.7% after 60 min visible light irradiation.

References：

[1] Peng Y D, Hou G H. Materials, 2016, **296**: 12-19.

[2] Xu J J, Wang Y K, Niu J F, et.al. Sepa. Puri. Tech., 2019, **225**: 24-32.

[3] Yin J, Zou Z G, Ye J H. J. Phys. Chem. B, 2004, **108**:8888-8893.

[4] Pakpoom R, Naoto U. J. Phys. Chem. C, 2015, **119**: 2284-2289.

[5] Ma X L, Li H H, Wang Y H, et.al . Appl. Cata. B Envi, 2014, **44:** 314－320.

Preparation and properties of fly ash supported MoS_2 lubricants

Hu Kunhong*[vi], Chen min, Shi yongjie, Lu Ziyan

School of Energy, Materials and Chemical Engineering, , Hefei University, Hefei, 230601, China

Abstract

As industrial solid waste, fly ash (FA) can cause a series of pollution, but it also has some special functional characteristics. The current leading objective of comprehensive utilization of FA is to investigate new research directions and develop a utilization approach of higher value according to these characteristics. Previous studies have found that the application of FA in base oil after simple treatment cannot fully utilize its good effect. Transition metal bisulfide is highly important due to its excellent lubrication performance, but its application is limited due to its production cost. A comprehensive analysis of the two materials finds that the concept of composite materials provides us with the idea of designing a new type of green lubricant. The preparation of composites using FA load transition metal bisulfide as lubricant additive is expected to provide a new approach for the use of FA. Moreover, composite materials can greatly reduce the cost of lubricants due to the low cost of FA and even as solid waste. This study mainly considers FA as the object, and the composites were successfully prepared by loading transition metal sulfide on its surface. Then, the lubrication property of the composites in base oil was investigated.

The FA obtained from the power plant is treated with physical and chemical processes, including calcining, ball grinding, and chemical reagents, such as acid, alkali, and oleic acid, and various approaches of modifying FA were obtained. X-ray diffraction (XRD), scanning electron microscope (SEM), elemental analyzer (EA), and X-ray fluorescence (XRF) were used to characterize the FA before and after modification, and relevant data on FA were obtained. Second, considering that the simple modification of FA cannot satisfy the requirements of lubricant, MoS_2/FA composites were prepared by liquid phase synthesis, and their lubrication properties in PAO were investigated. The prepared MoS_2/FA composite

*Corresponding author, Email: hukunhong@163.com

showed good tribological properties in the PAO compared with the pure PAO, and adding an amount of 1.5 wt% time performance is relatively good.

Key words: Fly ash; Transition metal sulfide; Composites; Lubrication performance

Acknowledgments: This project was supported by Anhui Province Universities and Colleges Natural Science Foundations (Grant Nos. KJ2018ZD053) and National Natural Science Foundation of China (Grant No. 51375139).

References：

[6] Lu Z, Cao Z, Hu E, Hu K, Hu X. Preparation and tribological properties of WS_2 and WS_2/TiO_2 nanoparticles. Tribology International, 2019, 130:308-316.

[7] Yan H, Li J, Liu D, Jing X. Controlled preparation of high quality WS_2 nanostructures by a microwave-assisted solvothermal method. Crystengcomm, 2018, 20:2324-2330.

[8] Ye Y, Wang Y, Wang C, Li J, Yao Y. An analysis on tribological performance of CrCN coatings with different carbon contents in seawater. Tribology International, 2015, 91:131-139.

A facile process to fabricate metal coating on PET sheet: Preparation of highly active polymer brush/Ag particle and Its application in electroless copper plating

Junjun Huang*, Ya Gao, Jinsong Xie, Chengliang Han, Difang Zhao

Department of Chemistry and Materials Engineering, Hefei University, Hefei, 230601

Abstract：

Electroless plating on polymer surface is a low-cost process for surface metallization, but it exhibits low adhesive force and complex production process, which makes it difficult to practical use. We employ a facile method combined with novel catalyst solution printing and electroless plating to fabricate high-adhesion copper coating on (polyethylene terephthalate (PET). The catalyst solution is a mixture of $AgNO_3$, PVA, KH550, alcohol and deionized water. On the one hand, hydrophilic PVA and hydrophobic KH550 condense to helical conformaticatalyst solutionon, which could synergistically absorb Ag. On the other hand, the two phase separation structure facilitate the formation of roughness surface. As a result, the catalyst solution can form highly active polymer brush/Ag particle structure on the PET surface, and realize to modify and activate PET simultaneously. Region-selective copper coating could plate on PET surface, the maximum effective thickness is 3.6 μm, rupture work is 4.5 J/m^2, adhesion is 5B, electrical resistivity is 2.3×10^{-6} Ω cm. Our results provide the underlying insights needed to guide the design of the fabrication of metal polymer.

Keywords: Facile method; electroless plating; Ag electron structure; polymer brush; copper

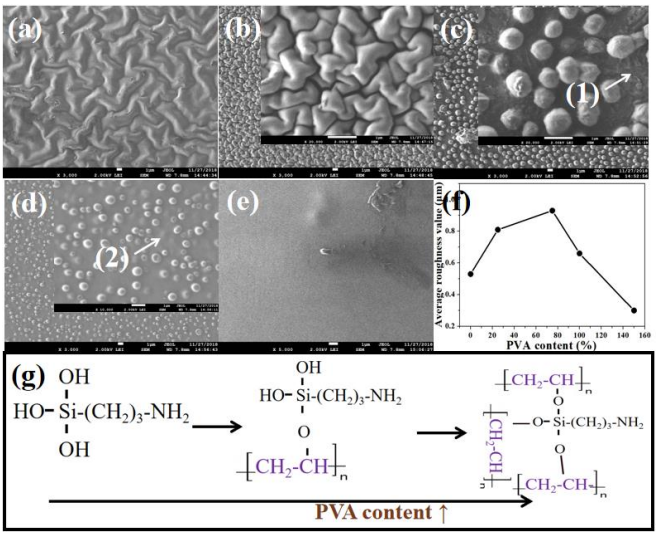

Fig.1 SEM images (a) (b) (c) (d) (e), Sr (f) and reaction mechanism (g) of ASP PET with different PVA content

References

[1] Y. Wang, Y. Wang, J.J. Chen, et al. A facile process combined with inkjet printing, surface modification and electroless deposition to fabricate adhesion-enhanced copper patterns on flexible polymer substrates for functional flexible electronics, Electrochim Acta 218 (2016) 24-31.

[2] S.J. Park, T.J. Ko, J. Yoon, et al. Highly adhesive and high fatigue-resistant copper/PET flexible electronic substrates. Appl. Surf. Sci. 427 (2018) 1-9.

Facile Controllable Synthesis and Photocatalytic Properties of Assembled Hierarchical AgBr/Fe_3O_4 Microspheres

Jinsong Xie*, Dehan Li, Junjun Huang, Chengliang Han, Difang Zhao

Department of Chemistry and Materials Engineering, Hefei University, Hefei, 230601

Abstract：

In the paper, the magnetic Fe_3O_4 microspheres with its average diameter in 200-300 nm assembled from hierarchical structure of 10 nm particles, have been prepared through hydrothermal method by sodium acetate and $FeCl_3 \cdot 6H_2O$ as raw materials, using glycol as solvent. Then, the AgBr/Fe_3O_4 composite powder was been obtained by ultrasonic precipitation method, by adding hexadecyltrimethyl ammonium bromide (CTAB) and silver nitrate solution into the above formed Fe_3O_4solution under ultrasonic treatment. Finally, the structures and morphologies of AgBr/Fe_3O_4 composite catalysts were characterized by X-ray diffraction (XRD), field emission scanning electron microscopy (FE-SEM) analysis. The photocatalytic experimental results show that the composite catalyst has good catalytic degradation ability of methyl orange under visible-light irradiation.

Key words: AgBr/Fe_3O_4 microspheres；Composite catalyst；Hydrothermal synthesis.

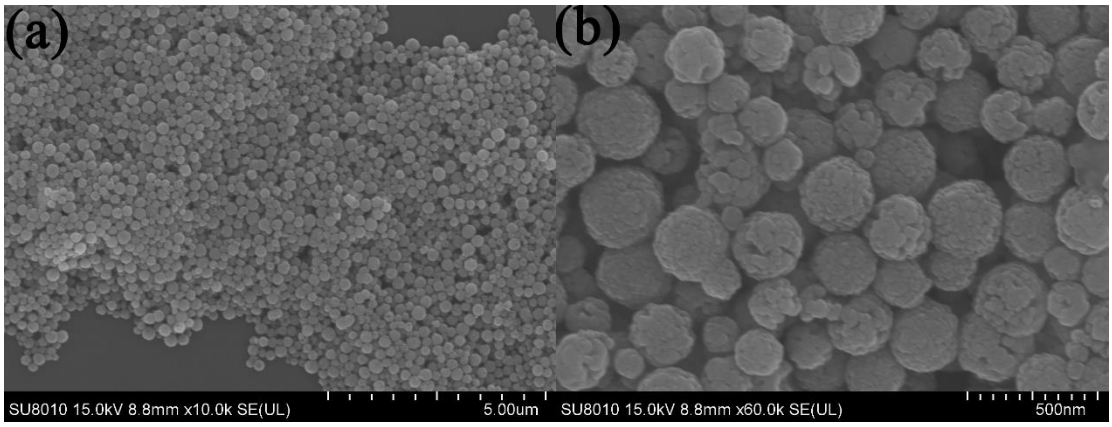

Fig.1 Representative FE-SEM images ofAgBr/Fe_3O_4

References

[1] H. Zhao, L. Zhang, X. Gu, S. Li, B.Li, H. Wang. Fe_2O_3-AgBr nonwoven cloth with hierarchicalnanostructures as efficient and easily recyclable macroscale photocatalysts. RSC Adv. 2015, 5, 10951–10959.

[2] W. Szeto, J. Li, H. Huang, J. Xuan, D.Y.C. Leung. Novel urchin-like Fe_2O_3@SiO_2@TiO_2microparticles withmagnetically separable and photocatalytic properties. RSC Adv. 2015, 5, 55363–55371.

[3] S.G. Maryam, H.Y. Aziz. Novel magnetically separable ZnO/AgBr/Fe_3O_4/Ag_3VO_4 nanocomposites with tandem n–nheterojunctions as highly efficient visible-lightdrivenphotocatalysts
RSC Adv., 2016, 6, 2402–2413.

[4] W. Wu, S. Zhang, X. Xiao, J. Zhou, F. Ren, L. Sun, C. Jiang. Controllable synthesis, magnetic properties, and enhanced photocatalytic activity of spindle-like mesoporous α-Fe_2O_3/ZnO core-shell heterostructures.ACS Appl. Mater. Interfaces 2012, 4, 3602–3609.

Development of the ZnO: Ga microrods - epoxy composite as a scintillation screen for ultrafast X-ray detection

QianliLi[a], Shutong Hao [b], RuiYuan [a], Yunling Yang [a], Xuechun Yang [a],
Xiaolin Liu [b], Mu Gu [b], Zhijun Zhang [a, *] and Jingtai Zhao [a, *]

[a] *School of Materials Science and Engineering, Shanghai University, Shanghai 200444, China*

[b]*School of Physics Science and Engineering, Tongji University, Shanghai 200092, China*

**CorrespondingAuthor: *E-mail zhangzhijun@shu.edu.cn and jtzhao@shu.edu.cn*

Abstract:

X-ray imaging detectors have currently widely applications in many fields, such as high energy physics, radiochemistry, medical imaging, security inspection, and so on. The development of X-ray imaging detector has been for a long time mostly focusing on improving the light yield and energy proportionality response in order to improve the energy resolution. However, a new tendency has recently emerged for ultrafast time performance of the X-ray imaging detector. This new requirement is mainly driven by the existing and upcoming high energy physics experimental facilities [1], e.g. the matter-radiation interaction in extreme (MaRIE) facility, the new generation for the time of flight positron emission tomography (TOF-PET) scanners and X-ray free electron lasers (XFELs) et al. In order to satisfy the requirements of ultrafast X-ray imaging in the existing and upcoming high energy physics experiments, the ZnO: Ga microrods – epoxy (ZnO: Ga-EP) composite with subnanosecond decay time were successfully synthesized by the simple hydrothermal reaction method and polymerization method. The result indicates ZnO: Ga-EP composite has an intense ultraviolet emission under X-ray excitation. Simultaneously, the decay time measurements indicate the ultraviolet and visible emissions of the samples are subnanosecond and nanosecond, respectively, which is extremely important for ultrafast X-ray imaging. The present work shows the ZnO: Ga-EP composite can be used as potential ultrafast scintillation screen for applications in ultrafast X-ray imaging detectors.

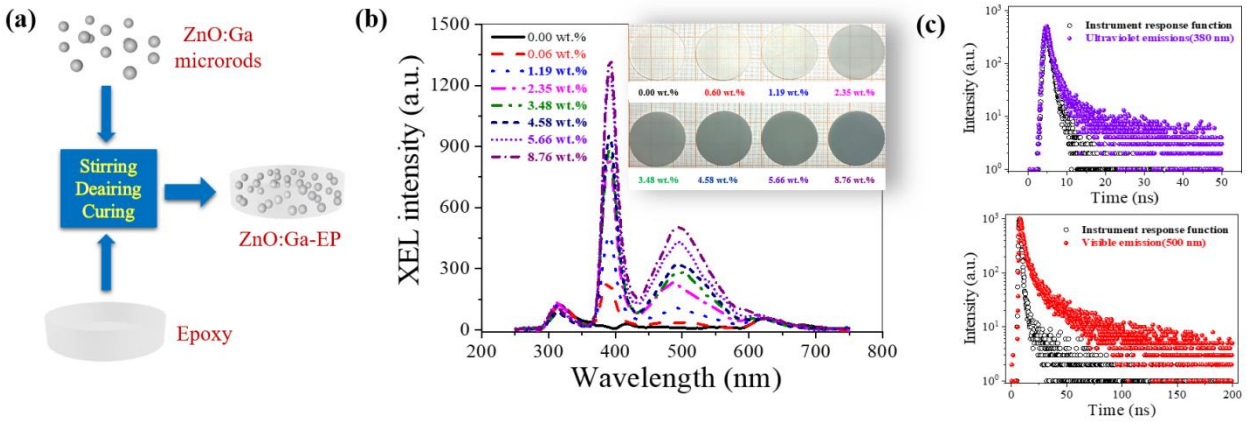

Fig.1. (a) Schematic illustration of the fabrication process, (b) X-ray excited luminescence and (c) the decay time of ultraviolet and visible emissions for the ZnO: Ga-EP composite.

References

[1] C. Dujardin, E. Auffray, E. Bourret-Courchesne, et al, *IEEE Trans. Nucl. Sci.***2018,** 65, 1977-1997.

Dynamic Adsorption Red X-3B on the Modified Phoenix leaves

CHEN Long[1], HUANG Song[1], ZHANG Qi[vii], JIANG Xvwen[1], MA Run[1], WU YING[1]*

1. Department of Chemistry and Materials Engineering，Hefei University，Hefei，230601，China

Abstract:

Phoenix tree leaves are one of the common agricultural and forestry wastes. Reactive brilliant red X-3B is a widely used stain. In this study, Phoenix tree leaves were selected as raw materials, and phosphate acid was used as modifier by means of oxygen restriction. The dynamic adsorption property, law and mechanism of modified on X-3B were studied.

(1) In the adsorption of reactive brilliant red by modified Phoenix tree, the optimum experimental conditions are as follows: the dosage of adsorbents is 2g/100mL, the flow rate is 50mL/min, pH is 6, the initial concentration is 30 mg/L, and the removal rate is 81.46%. And the existence of salt ions is not conducive to adsorption.

(2) The adsorption kinetics process of the experiment is more in accordance with the pseudo-first-order kinetic model, which indicates that the adsorption rate of reactive brilliant red on the modified Phoenix tree is controlled by diffusion steps, and the maximum adsorption capacity Q_m in the adsorption isotherm is 19.923 mg/g, but the fitting degree is poor.

(3) BET characterization showed that the specific surface area of natural Phoenix tree increased from 1.048 m^2/g to 1.955 m^2/g, and the pore capacity increased from 0.0039 cm^3/g to 0.0126 cm^3/g. IR results showed that after phosphate modification, the position of the peaks corresponding to the functional groups in the leaves of Indus did not change, but the intensity of some peaks decreased.

Keywords: Dynamic adsorption; reactive brilliant red X-3B; kinetic model

Acknowledgments:

***Corresponding author. Email:wuying@hfuu.edu.cn.**

This project was supported by Anhui province natural science research fund follow-up project. (No.1800031822), Anhui university student innovation and entrepreneurship training program recommendation project (No. 201811059109)

References:

[1] Zhang W X, Li H G, Kan X W, et al. Adsorption of anionic dyes from aqueous solutions using chemically modified straw[J]. Bioresource Technology, 2012,117.

[2] Jiban S, Yeasin S, Bedabrata S, et al. Malachite nanoparticle: A potent surface for the adsorption of Xanthene dyes[J]. Journal of Environmental Chemical Engineering,2013, 1(4).

[3] Mehmet E A, Dünyamin G, Mustafa K. Adsorption of Reactive Blue 114 dye by using a new adsorbent: Pomelopeel[J]. Journal of Industrial and Engineering Chemistry,2014, 20(3).

[4] Neha G, Atul K K, et al. Adsorption studies of cationic dyes onto Ashoka(Saracaasoca) leaf powder[J]. Journal of the Taiwan Institute of Chemical Engineers,2012, 43(4).

Antioxidant Activity and Total Phenolics Content of ethanolic extracts from *Elateriospermum tapos* Blume: seed and seed skin

Naengnoi Sangsane[*1], Paweena Porrawatkul, Namtip kotcharin[1], Thanawan Srikan[1], Siwaporn Buakaew[1], Nareerat Jommala[1] and Nichapa Rattanakomol[1]

[1]*Nanomaterials Chemistry Research Unit, Department of Chemistry, Faculty of Science and Technology, Nakhon Si Thammarat Rajabhat University, 80280, Thailand.*

[*]*Corresponding author. e-mail :* s.saengsane@gmail.com; *Tel. +66-7537-7443, Fax +66-7537-7443*

Abstract

The local plants in Euphorbiaceae family, *Elateriospermum tapos* Blume (Pra) was traditionally used in local cuisine and herbal medicines in Thailand. In this study, ethanolic extracts prepared from, seed and seed skin of these plants were tested for antioxidant properties using DPPH assay and total phenolic content also were screened. Pra are a domestic of various regions of Thailand including Nakhon Si Thammarat. The part of them; fruit, root and peel stems have an effect of herb. The results were calculated as an inhibitory concentration at 50% (IC_{50} mg/L ± S.D.) using ascorbic acid as a reference compound (IC_{50} = 39.71±2.14 mg/L). As the result, in the seed exhibited the higher antioxidant activity with $IC_{50}$of 43.52±2.06mg/L than seed skinwith IC_{50} = 58.62±1.20 mg/L. Total phenolic content of the ethanolic seed and seed skin extractsshowed the closely total phenolic content (11.06±2.11 and 11.27±1.16 mg GAE/100 g of dry weight, respectively). The results suggest that *Elateriospermum tapos* Blume. is a good source of natural antioxidants and further studies should be undertaken for their pharmacological properties

Introduction

Elateriospermum tapos Blume, locally known in Thai as Pra, Kra, or Perah, is a plant in the family Euphorbiaceae, distributed across the national highland rain forest or the high humidity mountain located in the southern part of Thailand especially in the Bantad Mountain Range in Trang and Nakhon Si Thammarat provinces [1]. *E. tapos*is a large

deciduous tree about 20 to 40 meters in height which grows in the highland rain forest, locally known as Pra. Pra fruits are oval, approximately 5 to 6 centimeters long and grow in strands. Each fruit has brown skin, which wrinkles at ripening. It is filled with pale brown pulp containing 3-5 seeds, which separate readily with each segment containing brown oval seeds. The seeds are used as flavoring agent for curries, sweet and are used in the preparation of snacks. The eatable seeds are cooked. The raw seeds are hazardous because they contain cyanide. The ground seeds are rich in nutrients containing considerable amounts of protein, carbohydrate and fat high in unsaturated fatty acids [2], therefore it has been used in the nutrition area. Inthis study, we aimed to compare the antioxidant activity and total phenolic content from different extracted part of this species in green ethanol solvent. The characteristicsof *Elateriospermum tapos* Blume seed and seed skin shown in Fig 1.

Seed Seed Skin

Fig1. Appearence of *Elateriospermum tapos* Blume seed and seed skin.

Materials and Methods

Phytochemical screening of extract

Quantitative phytochemical tests for the identification of anthraquinones, flavonoids, steroids, terpenoids, saponins, cumarins, cardiac glycoside and tannins were carried out for the extract [3,6].

Samplepreparation

The parts of *Elateriospermum tapos* Blume. were collected from Ban Maireang Amphoe ChawangNakhon Si Thammarat province. Theseed and seed skin of*Elateriospermum tapos*

Blume were cleaned to remove any residual compost. The ethanolic crudes were studied DPPH radical-scavenging activity and total phenolic compound.

DPPH radical-scavenging activity

The antioxidant activity was determined using DPPH radical scavenging model with a slight modification. Various concentrations of test compounds in methanol were mixed with a ethanolic solution having a final DPPH radical concentration of 0.1 mM. The mixture was shaken vigorously and left to stand for 30 min in the dark. Scavenging capacity was measured spectrophotometrically at 515 nm [4].

The percent DPPH inhibition was calculated from the following equation:

$$\%\text{DPPH Inhibition} = \frac{(\text{Abs}_{\text{control}} - \text{Abs}_{\text{sample}}) \times 100}{\text{Abs}_{\text{control}}}$$

Total phenolic compound analysis

The amount of total phenolic in the herb extracts was determined with the Folin-Ciocalteu reagent according to the method of AOAC on using gallic acid as a standard. Samples 0.1 mL were introducing to test cuvettes, and then 0.3 mL of Folin Ciocalteu's reagent and 2 mL of Na_2CO_3 (15 %) were added. The absorbance of all samples was measured at 765 nm using the PerkinElmer UV–VIS Spectrometer lambda12. Results were expressed as milligrams of gallic acid equivalent (GAE) per 100 gram of dry weight.

Results and discussion

Table 1 Chemical composition of *Elateriospermum tapos* Blume seed and seed skin.

Chemical compositions	**Seed skin**	**Seed**
Saponins	A	A
Tannins	P	P
Terpenoids	P	P
Steriods	P	P
Anthraquinones	A	A
Flavonoids	P	P
Alkaloids	P	P

Cardiac glycoside	P	P
Cumarins	P	P

A=Absent P=Present

The quantitative chemical composition analysis of seed and seed skin extracts showed the presence of tannins, terpenoids, steroids, flavonoids, alkaloids, cardiac glycoside and cumarins, but both extracts not present of saponins and anthraquinones that results showed in Table 1.

Table 2 Antioxidant activities on DPPH free radical and concentration of total phenolic compound of *Elateriospermum tapos* Blume seed and seed skin.

samples	IC_{50})mg/L(	Total phenolic content mg GAE/ 100 g of dry weight
Ascrobic acid	39.71±2.14	-
Seed skin	58.62±1.20	11.27±1.16
Seed	43.52±2.06	11.06±2.11

Table 2 showed the antioxidant activities and and concentration of total phenolic compound of*Elateriospermum tapos* Blume seed and seed skin extracts. The result indicated that seed had higher an antioxidant activity with a lowest IC_{50} value = 43.52±2.06 mg/L and had significantly closely antioxidant activity with ascorbic acid (IC_{50} = 39.71±2.14mg/L). Total phenolic content of the ethanolic seed and seed skin extractsshowed the closely total phenolic content (11.06±2.11 and 11.27±1.16 mg GAE/ 100 g of dry weight, respectively).

Conclusions

The antioxidative activity and total phenolic content from the part of*Elateriospermum tapos* Blume seed and seed skin extracts exhibited high antioxidant activity especially *Elateriospermum tapos* Blume seed which had closly IC_{50} value with ascrocic acid. The results suggest that*Elateriospermum tapos* Blumewas a good source of natural antioxidants and further studies should be undertaken for their pharmacological properties [5].

References

[1] Chayamarit K, van Welzen PC (2005). Euphorbiaceae (Genera A-F). Euphorbiaceae (Genera AF). Forest Herbarium, National Part Wildlife and Plant Conservation Department.

[2] Choonhahirun A. (2009). The use of pra seed (*Elateriospermum tapos* Bl.) in combination with maltodextrin as fat substitute in ice cream. Department of Food Science and Technology, School of Science, University of the Thai Chamber of Commerce.

[3] Rangkadilok N, Worasuttayangkurn L, Bennett RN, Satayavivad (2005). Identification and Quantification of Polyphenolic Compounds in Longan (*Euphoria longana Lam.*) fruit. J agric Food Chem. 53(5), 1287 - 92.

[4] Riachi LG, De Maria CAB (2015). Peppermint antioxidants revisited. Food Chemistry 176:72-81.

[5] Tisadondilok S, Senawong T (2017). Antioxidant activities and anticancer screening of ethanolic extracts from *Baccaureamacrophylla* Muell and *Elateriospermum tapos* Blume. Journal of Thai Interdisciplinary Research 12(5),11-18.

[6] Vongsak B, Sithisarn P, Mangmool S, Thongpraditchote S, Wongkrajang Y, Gritsanapan W (2013). Maximizing total phenolics, total flavonoids contents and antioxidant activity of *Moringa oleifera* extract by the appropriate extraction method. Industrial Crops and Products 44, 566-571.

Development and Evaluation of Herbal Anti-Acne Cream from Extract of *Eupatorium odoratum* L. *leave*and *Garcinia mangostana* L. peel

Paweena Porrawatkul[*1], Alisa Pipak[1], Tuangrat Senmard[1], Laddarak Aupakankaew[1] and Montakarn Thongsom[2]

[1]*Nanomaterials Chemistry Research Unit, Department of Chemistry,* [2]*Department of Biology Science,*

Faculty of Science and Technology, Nakhon Si Thammarat Rajabhat University, 80280, Thailand.

[*]*Corresponding author. e-mail: paweena.n@gmail.com; Tel. +66-7537-7443, Fax +66-7537-7443*

Abstract

Everyone needs natural and beautiful skin so that the natural skin care products are growing day by day in the present market. The main objective of these natural products is to avoid skin problems and to protect the skin from harmful chemicals and also to give healthy skin. Accordingly, the main objective of this study was the antibacterial potency of herbal cream formulated with ethanolic extract of *Eupatorium odoratum* L. leaveand *Garcinia mangostana* L. peel were evaluated by extracting the *Eupatorium odoratum* L. leaveand *Garcinia mangostana* L. peel with coconut oil. The prepared 2 formulations were evaluated for physical evaluation tests like color, odor, homogeneity and pH. Antibacterial activity was determined by disc diffusion method against strains of *Staphylococcus epidermidis* (*S. epidermidis*)and *Propionibacterium acnes* (*P. acne*). Activity of extracts was compared against standard antibiotic chloramphenicol and clindamycin. The formulation 2 demonstrated good antibacterial activity for *Staphylococcus epidermidis* and *Propionibacterium acnes* with inhibition zone was 22.00 ± 1.43 mm and 23.50 ± 1.60 mm, respectively. The prepared herbal cream of *Eupatorium odoratum* L. Leaveand *Garcinia mangostana L.* Peel was found to be natural and could be used topically in order to treat skin infection further.

Keywords: Anti-acne, *Eupatorium odoratum* L, *Garcinia mangostana L*, Herbal cream,

Introduction

Cosmetic products are used to protect skin against exogenous and endogenous harmful agents and improve the beauty and attractiveness of skin, but in cosmetic have a various synthetic compounds, chemicals, dye and their derivative proved to cause various skin diseases having numerous side effects[1-3]. The value of herbs in the cosmeceutical making has been extensively improved in personal care system and there is a great demand for the herbal cosmetics. Therefore, we are using herbal cosmetics as much as possible. In this work, ethanolic extract of *Eupatorium odoratum* L. leaveand *Garcinia mangostana* L. peel were evaluated herbal cream. Many reports have shown that some *Eupatorium odoratum* L. leaveand *Garcinia mangostana* L. peelspecies contain antimicrobial substances. Recent studies revealed that *Eupatorium odoratum* L. leaveand *Garcinia mangostana* L. peel have been proven to be effective against bacteria and fungi species[4-5]. The objective of his present work was carried out to evaluate the antioxidant, antibacterial (*Staphylococcus epidermidis* and *Propionibacteriu acnes*) activities of the ethanolic extract of *Eupatorium odoratum* L. leaveand *Garcinia mangostana* L. peel in formulated cream.

Materials and methods

The *Eupatorium odoratum* L. leaveand *Garcinia mangostana* L. peel was corrected from surrounding area of Nakhon Si Thammarat Rajabhat university Tambon Tha-Ngio, Amphoe Mueang, Nakhon Si Thammarat Province, Thailand. All analytical reagents used in the study were of analytical grade and were purchased from Merck. Nutrient agar for bacterial culture and Mueller–Hinton broth and agar for antimicrobial activity were purchased from Hi-Media, Mumbai, India.

Preparation of extract and herbal cream formulation

Eupatorium odoratum L. leaveand *Garcinia mangostana* L. peel 50 g were weighed, cut into fine pieces, each sample crushed with 100 mL of ethanol for 24 h at 60 °C, and filtered through Whatman No.1 filter paper. The solvent was removed using rotary evaporator to get brown semisolid extract for blend in herbal cream. Oil in water (O/W) emulsion-based cream (semisolid formulation) was formulated. The emulsifier (stearic acid) and other oil soluble components were dissolved in the oil phase (Phase B) and heated to 50° C. The preservatives

and other water soluble components was dissolved in the aqueous phase (Phase A) and heated to 50° C. After heating, the aqueous phase was added in portions to the oil phase with continuous stirring until cooling of emulsifier took place and Phase C was added[6]. The formula for the cream is given in table 1.

Table 1 Composition of herbal cream

Ingredients	**Amount (g)**	
	Formulation 1	**Formulation 2**
Phase A		
DI water	Up to 100 mL	Up to 100 mL
EDTA	0.50	0.50
Glycerin	2.00	2.00
Carbomer (Carbopol 940)	1.00	1.00
Phase B		
Cetearyl alcohol	4.00	4.00
Stearic Acid	6.00	6.00
Squalane	3.00	3.00
Coconut oil	3.00	3.00
Eumulgin B1	3.00	3.00
Vitamin E di-alpha tocopherol	1.00	1.00
Phase C		
Triethanolamine	1.00	1.00
Phenoxyethanol	2.00	2.00
Fragrance	1.00	1.00
Extract *Garcinia : Eupatorium*	1:1	2:1
Total	100	100

Phytochemical screening of extract

Quantitative phytochemical tests for the identification of anthraquinones, flavonoids, steroids, terpenoids, saponins, alkaloids and tannins were carried out for the leave extract.

Antibacterial study

Eupatorium odoratum L. leaveand *Garcinia mangostana* L. peel extract and herbal cream were tested for their antibacterial activity against *P. acne* and*S. epidermidis* by using the Agar-well diffusion method. The bacteria culture was spread evenly on the nutrient agar plate using sterile cotton swab. Wells were prepared on agar plates. To these wells standard antibiotic disc (chloramphenicol and clindamycin) were added. After incubation at 37 °C for 24 h, the diameter of inhibition zones around herbal cream were measured and compared with that around the commercial standard antibiotic chloramphenicol, clindamycin and ethanoic extract.

Physical evaluation of formulated herbal cream

Physical assessments were carried out on the ointments and cream over a period of 30 days using the following parameters: Appearance, odour test by smelling, color test by naked eye and homogeneity test by physical touch with hands. The pH of various formulationswas determined by using Digital pH meter. 0.5 g of the weighed formulation was dispersed in 50 mL of distilled water and the pH was measured[7].

Results and discussion

(a) (b) (c)

Fig. 1 (a) *Eupatorium odoratum* L. leaveand *Garcinia mangostana* L. peel (b) Formulation1 of herbal cream (c) Formulation2 of herbal cream.

Result and discussion

The percentage yield and nature of *Eupatorium odoratum* L. leaveand *Garcinia mangostana* L. peelextract was 18.7%. The quantitative phytochemical analysis of extracts showed the presence of flavonoids, steroids, saponins, alkaloids and tannins. The prepared polyherbal cream using different concentration of extracts of *Eupatorium odoratum* L. leaveand *Garcinia mangostana* L. peel were tested for appearance, pH, viscosity, homogeneity content and antibacterial activity for *P. acne* and*S. epidermidis*. The prepared formulations (Table 2) show a smooth and homogeneous appearance. The pH values of all the prepared formulations ranged from 7.1 to 7.5, which are measured acceptable to avoid the risk of irritation upon application to the skin. The pH values of the formulations are within the normal pH range of the human skin (6.8 ± 1). From the study, the cream showed no changes in pH. Appearance of formula 1 and formula 2 creams shown in fig.1(b) and fig1(c).

Table 2 Evaluation parameters of the formulations

Formulation	color	odour	pH	homogeneity
1	yellow	coconut oil	7.2±1	homogenous
2	yellow-green	coconut oil	7.4±1	homogenous

Antibacterial activity

The *Eupatorium odoratum* L. leaveand *Garcinia mangostana* L. peel based herbal cream formulation 2 demonstrated excellent antibacterial activity for *P. acne* and *S. epidermidis*. The order of antibacterial activity of *Eupatorium odoratum* L. leaveand *Garcinia mangostana* L. peel in the topical bases was as follows: formulation 2 > formulation 1 > crude extract. The results also revealed that the extracts incorporated into the cream bases showed better activity than that of the crude extract of *Eupatorium odoratum* L. leaveand *Garcinia mangostana* L. peel. The activity against *P. acne* and *S. epidermidis* are significant interest because it is commonly found on the hands, face and in deep layers of the skin and is perhaps the most widely encountered and very undesirable. *S. epidermidis* is not easily eliminated especially in the deeper skin layers, sweat gland, sebaceous gland, and the hair-follicles by routine washing and scrubbing even with some antiseptic soap[8]. *Eupatorium*

odoratum L. leaveand *Garcinia mangostana* L. peel herbal cream shows good activity against *P. Acne S. epidermidis* the standard drug clindamycin and chloramphenicol showed relatively high activity against *S. epidermidis* and *P. acne* that result show in Table 3.

Table 3 Preliminary *in vitro* antibacterial activity of ethanolic extract of *Eupatorium odoratum* L. leaveand *Garcinia mangostana* L. peel (Zone of inhibition in mm)

sample	Zone of Inhibition (mm)	
	S. epidermidis	***P. acnes***
Formulation 1	19.50 ± 1.50	24.75 ± 3.56
Formulation 2	22.00 ±1.43	23.50 ±1.60
Eupatorium odoratum L. leave extract	16.25 ± 2.38	22.00 ± 1.22
Garcinia mangostana L. peel extract	16.50 ± 3.20	18.50 ± 5.55
Chloramphenicol	31.88 ± 1.30	-
Clindamycin	-	31.38 ± 0.50

Conclusion

Eupatorium odoratum L. leaveand *Garcinia mangostana* L. peel have been reported in the literature as a good antibacterial agent and anti-inflammatory agent. The developed formulations 2 with more *Garcinia mangostana* L. peel extract than formulations 1 was evaluated for them *in vitro* anti-bacterial activity excellence against *P. acne*. The Zones of inhibitions for the antibacterial activity were compared with the standard chloramphenicol. Moreover, the formulated *Eupatorium odoratum* L. leaveand *Garcinia mangostana* L. peel creams were homogenous appearance, good smell and good pH. The prepared herbal creams of *Eupatorium odoratum* L. leaveand *Garcinia mangostana* L. peel were found to be natural and could be used topically in order to treat skin infection further.

Acknowledgements

This work was supported by Research and Development Institute, Nakhon Si Thammarat Rajabhat University and Nanomaterials Chemistry Research Unit, Department of Chemistry,

Faculty of Science and Technology, Nakhon Si Thammarat Rajabhat University**.**

References

[1] Nirmala kumari, D., Satyanarayana, T., Sai kumar, CH., Moulabi, SK., Pullarao, B., Gavamma, A., Nagamani, K. **(2016)**. Formulation and evaluation of herbal vanishing cream containing Punica Granatum. *Indo American J. Pharm. Res***.,** 6: 4938-4944.

[2]. Ibrahim, D., Osman, H. **(1995)**. Antimicrobial activity of Cassia alata from Malaysia. *J. Ethnopharmacol*. 45(3): 151-156.

[3]. Agarkar, S.V., Jadge, D. R. **(1999)**. Phytochemical and pharmacological investigations of genus Cassia: a Review. *Asian J. Chem*.11: 295-299.

[4]. Amao, S.Y., Ajani, R.S., Oladapo, O. **(2010).** *Cassia alata* alters Liver Structure in Rat Afr. *J. Biomed. Res*. 13: 231 – 233.

[5]. Villasenor, I. M., Canlas, A. P., Pascua, M. P. I., Sabando, M. N., Soliven, L. A. **(2002)** Bioactivity studies on studies on *Cassia alata* Linn. leaf extract. *Phytother Res.* 16: 93-96.

[6] Abubacker, M. N., Ramanathan, R., Senthil, K. T. **(2008)**. In vitroantifungal activities of *Cassia alata* Linn. Flower extract. *Natural product Radiance*. 7(1): 6-9.

[7]. Panigrahi, L., Jhon, T., Shariff, A., Shobanirani, R. S. **(1997)**. Formulation and evaluation of lincomycin HCL gels. *Ind. J. Pharm. Sci*. 59: 330-332.

[8] Kumar, R., Bhagat, S. K., Kumar, V., Nirmala, A. **(2013)**. AntioxidentActivtiy & Cytotoxic Analysis of Seed Extract of *Punica Granatum*. *Asian J. Biochem. and Pharm*. 3(1): 225-236.

Inhibition of Citrus Green Mold by Chitosan Obtained from Shells of Mantis Shrimp (*Oratosquilla nepa*)

Arnannit Kuyyogsuy[*1], Thanawan Srikan[1], Siwaporn Buakaew[1], Nareerat Jommala[1] and Naruemon Meeboon[2]

[1]Nanomaterials Chemistry Research Unit, Department of Chemistry, [2] Department of Agriculture

Faculty of Science and Technology, Nakhon Si Thammarat Rajabhat University, 80280, Thailand.

[*]Corresponding author. e-mail: arnannit.k@gmail.com; Tel. +66-7537-7443, Fax +66-7537-7443

Abstract

Chitosan is aminoglucopyranans consisted of β-(1,4)-linked glucosamine units together with *N*-acetylglucosamine units. It is present in the cell walls or fungi, green algae and in the exoskeleton of crustaceans. A novel procedure for preparing chitosan from the shells of mantis shrimp (*Oratosquilla nepa*) was developed. The procedure involves three steps composing demineralization, deproteinzation and deacetylation (immersed in 40% NaOH) processes. The obtained chitosan was characterized using Fourier transform infrared spectroscopy (FTIR). Samples of white chitosan with degrees of deacetylation (DD) as 96.20% were obtained, which analyzed by FTIR. *In-vitro* assay, the effect of 0.10% (w/v) of chitosan on *Penicillium digitatum* growth that cause postharvest disease in citrus fruit. The results indicated that it can against this fungus, the values of inhibition were significant complete as 99%$\pm$0.40.

Keywords: chitosan, *Oratosquilla nepa*, degrees of deacetylation, *Penicillium digitatum*

Introduction

Chitosan is a natural, biodegradable, non-toxicity. The structure of chitosan is a linear polysaccharide which consisted of β-(1,4)-linked glucosamine units together with *N*-acetylglucosamine units. It is soluble in dilute solutions of various organic and inorganic

acids (pH<6), due to the protonation of its amino groups [1]. The OH and NH_2 functionalities in chitosan's structure allow the preparation of diverse derivatives with improved properties for specific applications. Chitosan is used in a wide range such as the food industry, waste water treatment, cosmetics, medicine, pharmacy and agriculture [2,3,4]. For the agriculture, chitosan has been exhibited to be useful as well as increasing crop yields. Moreover, chitosan is associated with its fungicidal properties inhibit postharvest fungi such as *Alternaria alternata*, *Colletotrichum gloeosporioides*, *Fusarium oxysporum* and *Penicillium digitatum* [5]. Green mold, caused by *P. digitatum* is important postharvest fungi causing severe diseases through injuries during harvesting, transportation and storage of citrus fruits resulting in economic losses [6]. The aim of this study was to synthesize chitosan from the shells of mantis shrimp (*Oratosquilla nepa*) and determine the effect of chitosan on mycelial growth of *P. digitatum*.

Material and Methods

Chemicals

The organic solvents were used in the experiments for analytical grade and purchased from Merck, Thailand.

Samples preparation

Mantis shrimp (*O. nepa*) shells were obtained from a byproduct of the fishing industry, southern of Thailand. Firstly, the shells were washed by tap water several times and dried in a hot-air oven. After that they were homogenized in a blender into small sized pieces and kept frozen until used.

Chitosan production

Chitosan was synthesized by three steps which composing demineralization, deproteinzation and deacetylation. Firstly, Demineralization was carried out by adding 1 L of 2 M HCl to 50 g of mantis shrimp shells. The reaction proceeded at room temperature for 2 h under agitation at 250 rpm. After that, they were filtrated and washed with distilled water until neutral pH. They were bleached by immersing in ethanol for 2 h and dried in an oven at 80 °C. For Deproteinization, deprotein was carried out by adding 2 M NaOH. The reaction was performed at 55 °C for 2 h then it was filtrated and washed with distilled water until

neutral pH. After that, it was immersed in ethanol for 2 h for bleaching, and the resulting chitin was dried in an oven at 100 °C for 1 h. Finally, deacetylation of chitin was carried out by reacting chitin with 40%(w/v) NaOH. The temperature of the mixture was increased to 100 °C for 2 h with agitation at 250 rpm. The resulting chitosan was filtrated and washed with distilled water until neutral pH and then dried in an oven at 60 °C for 4 h.

Measuring the degree of deacetylation (DD)

The degree of deacetylation of chitosan was determined by Fourier Transform Infrared Spectroscopy (FTIR). FTIR spectra were recorded at room temperature using a 400 Perkin Elmer spectrometer (Perkin-Dlmer, Norwalk, CA, USA) from 4000 cm^{-1} to 400 cm^{-1}. Sample was dried and ground with KBr. DD was calculated from the spectra using formula [7].

$$DD\% = 100 - \frac{A1655}{A3450}\ x\ 115$$

Penicillium digitatum and chitosan preparation

P. digitatum was isolated from citrus fruit rot, kindly provided by the Prince of Songkhla University, Thailand, and grown in potato dextrose agar (PDA) plate at room temperature for 7 days. For chitosan, a stock solution of chitosan was prepared in 1% (v/v) acetic acid with pH5.6, stirring at 150 rpm for 24 h at room temperature, then it was autoclaved at 121 °C for 15 min. After that, the chitosan solution was mixed with the PDA medium until the final concentration at 0.1, 0.05 and 0.01% (v/v). Sterile distilled water of pH5.6 was used as a control.

Antifungal activity testing

The effect of chitosan on *P. digitatum* growth was determined. The mycelial disc of *P. digitatum* was put on the center PDA medium amended with each chitosan (final concentration 0.1, 0.05 and 0.01% (v/v)). Plates were incubated at room temperature for 7 days. After that, the diameters of the fungal colonies were assayed by an equation of Gamlielandcoworker [8], which presented as %inhibition. Each treatment was replicated using three plates, and experiment was performed three times.

$$\%\text{inhibition} = 100\text{-}[(R^2/r^2)100]($$

(when R is radial of the fungal colonies for control, r is radial of the fungal colonies for treatment)

Statistical analysis

The data were performed by one-way analysis of variance (ANOVA) at $p<0.05$ Significant means were compared by Duncan's multiple range test using SPSS Statistics 17.0 softwere.

Results and Discussion

Chitosan production

Chitosan samples from shell of mantis shrimp were shown in Figure 1. They were obtained as a white powder after the demineralization and deproteinization steps that the results were similar with Antonino andcoworker [9].

Figure 1. Chitosan from shell of mantis shrimp were synthesized by 40% (w/v) NaOH

Degree of Deacetylation

The FTIR spectra of chitosan from the shells of mantis shrimp was shown in Figure 2. The results showed characteristic absorption bands similar during commercial chitosan and chitosan samples (Figure 2A and 2B) at 3450 cm^{-1} which refers to O-H stretching, Aliphatic C-H stretching at 2925 cm^{-1}, N-H stretching (Amide I) at 1655 cm^{-1}, 1580 cm^{-1} ($-NH_2$ bending), and 1320 cm^{-1} (Amide III) [10]. The degree of deacetylation of chitosan samples from FTIR spectra was shown as 96.20% (Figure 2B). When DD was calculated from the spectra using formula [7].

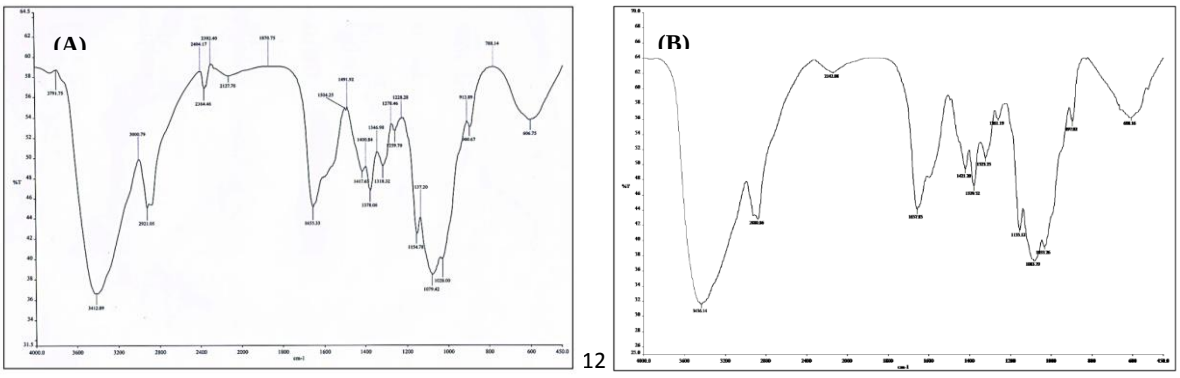

Figure 2. FTIR spectra of chitosan; (A) commercial chitosan, (B) chitosan samples

Determination of chitosan antifungal activity

The effect of 0.01%, 0.05% and 0.10% (w/v) chitosan on *P. digitatum* growth showed in Figure 3 and Table 1. The results exhibited the concentration of 0.10% (w/v) chitosan was more effective against fungi *P. digitatum* (Figure 3D) when compared to the control (Figure 3A), including the concentration of 0.01% (Figure 3B) and 0.05% (w/v) chitosan (Figure 3C). The values of inhibition were significant complete as 99% (Table 1) while the concentration of 0.01% and 0.05% (w/v) chitosan as 62% and 96%, respectively. The inhibitory effect of chitosan was calculated when the control plate was incubated for 7 days. There is strong evidence that the fungal mycelium growth can inhibit by using chitosan. The concentration of 3% (w/v) chitosan can completely inhibit the fungi *F. oxysporum*, *Rhizopus stolonifer*, *C. gloeosporioid*es and *P. digitatum*[11,12].

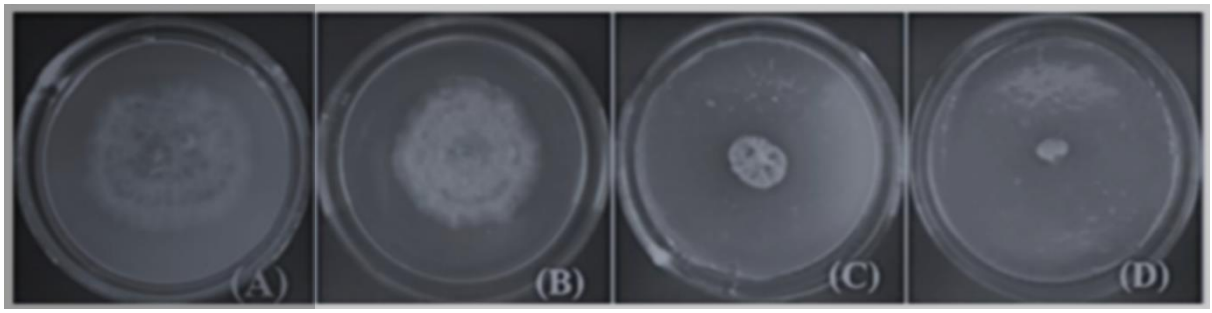

Figure 3. Effect of each chitosan to inhibit *P. digitatum* for 7 days; (A) control, (B) 0.01%(w/v) chitosan, (C) 0.05%(w/v) chitosan and (D) 0.10%(w/v) chitosan

Table 1. Effect of each chitosan for antifungal activity

sample	% inhibition±SD
0.01%(w/v) chitosan	62^{c}±0.98
0.05%(w/v) chitosan	96^{b}±0.79
0.10%(w/v) chitosan	99^{a}±0.40

Conclusions

In the summary, chitosan was synthesized from shells of mantis shrimp (*O. nepa*) as a white powder. The degree of deacetylation (DD) is an important property of chitosan to analyze the way of application of the biopolymer. Chitosan was partially deacetylated and obtained samples were characterized using FTIR. It is noticed that the acetyl group can

contribute to the formation of hydrogen bonds that can stabilize the crystalline structure. In addition, it is found that chitosan sample properties suitable for agricultural applications are obtained.

Acknowledgements

This work was financially supported by Nanomaterials Chemistry Research Unit, Department of Chemistry, Faculty of Science and Technology, Nakhon Si Thammarat Rajabhat University.

References

[1] E. Costa, S. Silva, F. Tavaria, M. Pintado, *Pathogens*, **3**, 908–919 (2014).

[2] R.G. Sharp, *Agronomy*, **3**, 757–793 (2013).

[3] S. Bautista-Banos, G. Romanazzi, and A. Jiménez-Aparicio, *Academic Press, Elsevier: Amsterdam, The Netherlands*, 2016.

[4] L.H.K. No, and S.P. Meyers, *Rev. Environ. Contam. Toxicol*., **1**, 1–27 (2000).

[5] A.L. Snowdon, *CRCR Press. London, UK*, **1**, 302 (1990)

[6] J. Liu, Y. Sui, M. Wisniewski, S. Droby, and Y. Liu, *Intl. J. Food Microbiol*., **167**, 153–160 (2013).

[7] D. Baskar, and T.S. Sampath Kumar, *Carbohydr. Polym*., **78**, 767–772 (2009).

[8] A. Gamliel, J. Kantan, and E. Cohon, *Phytoparasitica*., **17**, 101–106 (1989).

[9] R.S.C.M. de Q. Antonino, B. R. P.L. Fook, V.A. de O. Lim, R.I. de F. Rached, E.P.N. Lima, R.J. da S. Lima, C.A.P. Covas, and M.V.L. Fook, *Mar. Drugs*, **15**, 141 (2017).

[10] M.B. Povea, W.A. Monal, J.V. Cauich-Rodríguez, A.M. Pat, N.B. Rivero, and C.P Covas, *Mater. Sci. Appl*., **2**, 509–520 (2011).

[11] S. Bautista-Baños, M. Hernández-López, E. Bosquez-Molina, and C.L. Wilson, *Crop Protection*., **22**, 1087–1092 (2003).

[12] S. Bautista-Baños, M. Hernández-López, and E. Bosquez-Molina, *Mexican J. Phytopathol*., **22**, 178–186 (2004).

Method Development for Determination of Pb(II) Ions in Thai Herbs Using Flame Atomic Absorption Spectrometry

Prawit Nuengmatcha[1*], Tuangrat Senmard[1], Alisa Pipak[1], Laddarak Aupakankaew[1], Nichapa Rattanakomon[1] and Piyawan Nuengmatcha[2]

[1]Nanomaterials Chemistry Research Unit, Department of Chemistry,[2]Department of Environmental Science, Faculty of Science and Technology, Nakhon Si Thammarat Rajabhat University, Nakhon Si Thammarat 80280, Thailand.

Corresponding author: E-mail:pnuengmatcha@gmail.com

Abstract

An accurate and precise quantitation method for the determination of Pb(II) ions in Thai herbs has been developed by using wet digestion method followed by atomic absorption spectrometry (AAS). The developed method has been fully validated in various parameters including linearity range, accuracy, precision, limit of detection (LOD), and limit of quantitation (LOQ). The results exhibited that the calibration graph was linear in the range of 1.0-10.0 mg/L, with a detection limit (LOD) and limit of quantitation (LOQ) of 0.03 mg/L and 1.2 mg/L, respectively. The relative standard deviation (%RSD) for 6 replicate measurements of 1.0 mg/L Pb(II) was ±2.5%. The method was applied to the analysis of 5 types of Thai herb samples. Percentage recoveries were in the range 90.4-110.6%. It was found that Pb(II) concentrations in all Thai herb samples were less than the maximum residue level.

Keywords: Lead; Thai herbs; Atomic Absorption Spectrometry

Introduction

Herbal products are traditionally used in developing countries. Nowadays, interest in natural therapies has also become popular, resulting in the rapidly increasing worldwide consumption of these herbal. Therefore, a critical evaluation of their safety and quality is important. The World Health Organization[1] has established standards for the quality control of medicinal plants including the classification, botanical identification, determination of active principles, and identification of contaminants. One of the most frequent contaminants likely to be found in herbal products is Pb(II) ions[2]. Pb(II)is known to be not only high toxic elements to

human beings but also may cause critical environment problems[3].The World Health Organization sets the maximum permissible levels of Pb(II) in medicinal herbs[4] at 10 mg/kg. And also, in Thailand, the Ministry of Public Health sets the maximum permissible levels of Pb(II) in medicinal plant materials and herbal products[5] at 10 mg/kg. In this work, an accurate and precise quantitation method for the determination of Pb(II) ions in Thai herbs has been developed by using wet digestion method followed by atomic absorption spectrometry (AAS). The developed method has been fully validated in various parameters including linearity range, accuracy, precision, limit of detection (LOD), and limit of quantitation (LOQ).

Experimental

Sample collection

Five samples of herbal medicines in the form of powder were selected and bought directly from herbal drug stores in Nakhon Si Thammarat Provinces, Thailand between April 2019 and June 2019. All samples were from domestic cultivated plants and produced in Thailand. After delivery to the laboratory, coarse particles like powders were ground to fine particles using mortar and pestle. The fine powdered form samples were dried in an oven at 60 °C for 4 hours and stored in a desiccator at room temperature for about 10 days until it reached a constant mass. The dried samples were then individually packaged in clean poly-ethylene bags and stored in a desiccator. Each sample was analyzed in triplicate.

Sample preparation

Approximately 0.25 g of all herbal samples were accurately weighed into glass test tubes with a cap (50 mL), and 2.0 mL of 2:1 acid-oxidant mixture (conc. HNO_3:H_2O_2) was added. The glass tube cap was tightly closed. All tubes were allowed to stand for 10 minutes at room temperature. And then, the tubes were immersed in the ultrasonic water bath for 10 minutes. After 10 minutes of the first digestion step, 10 mL of 2:1 acid-oxidant mixture was added and the tubes were digested under the same condition for a further 10 minutes. After sonication, the sample digestion was made up to 10 mL in volumetric flasks with deionized water and then was filtered through filter paper. The final volume was stored in polyethylene bottles at 4 °C for analysis. Blanks were also treated in the same manner without samples for each experiment.

Results and Discussion

Analytical features of the proposed system

The analytical characteristics of the proposed method were investigated. Using the optimum conditions, the standard calibration in the range of 1-10 mg/L was constructed by plotting the absorbance against concentrations. The limit of detection (LOD) (3σ/s) and limit of quantification (LOQ) (10σ/s) [where σ is SD of digestion blank (n = 11) and s is the slope of calibration curve] were obtained at LOD 0.03 mg/L and LOQ 1.20 mg/L, respectively. The relative SDs for 6 replicate determinations of 1 mg/L Pb(II) was ±2.5%. The reproducibility for six determinations of 1 mg/L Pb(II) was 3.2%.

Analysis of herbal medicine samples

The proposed procedure was used for flame atomic absorption spectrometry (FAAS) determination of Pb(II) in herb samples. The analysis results of Pb(II) in all samples are presented in Table 1. To perform the recovery study, all samples were spiked with Pb(II) at 1 mg/L and 10 mg/L, respectively. Satisfactory results for the concentration levels studied were obtained for Pb(II), with percentage recoveries of 90.4-110.6%. As presented in Table 1, most of all studied samples were not contaminated with Pb(II). The maximum permitted level (MPL) of Pb(II) in medicinal plant materials and finished herbal products[6] is 10 mg/kg. Therefore, It was found that Pb(II) concentrations in all Thai herb samples were less than the maximum permitted level.

Table 1 Analytical features of merit for Pb(II) using wet digestion-FAAS method

Linear equation	Y = 0.0275X + 0.0015
Linear range (mg/L)	1.0 - 10.0
Correlation coefficient (R^2)	0.997
Precision (%RSD) Intra-day (n = 6)	2.5
	3.2
Inter-day (n = 6)	
Limit of detection (mg/L)	0.03
Limit of quantitation (mg/L)	1.20

Table 2. Analysis of Pb(II) in herbal samples by wet digestion-FAAS method

Common name	Scientific name	Amount of Pb(II)(mg/kg)	Recovery (%)
Soap pod (leaf)	*Acacia concinna* (Wild.) DC	ND	98.7
Mangosteen (peel)	*Garcinia mangostana* Linn.	ND	90.4
Sappan wood	*Caesalpinia sappan* Linn.	ND	105.4
Horseradish tree (leaf)	*Moringa oleifera* Lam.	ND	110.6
Turmeric	*Curcuma longa* Linn.	ND	103.9

Conclusion

High efficiency sample preparation procedure based on wet digestion was successfully applied for the acid digestion of the herbal samples. Determination of Pb(II) was performed by FAAS with sensitive, precise, and accurate results. The recommended method offered fast, convenient, and high sample throughput for herbal samples. The amount of Pb(II) contaminants in the herbal plants were not found for all samples. And also, all herbal samples were less than the maximum permitted level. This study provides significant data on the safety and quality of herbal medicine consumed in Thailand. In addition, the proposed method has potential as a good alternative for analysis of Pb(II) contaminants in various biological samples.

Acknowledgements

This work was supported by Research and Development Institute, Nakhon Si Thammarat Rajabhat University and Nanomaterials Chemistry Research Unit, Department of Chemistry, Faculty of Science and Technology, Nakhon Si Thammarat Rajabhat University.

References

1. World Health Organization. WHO Quality control methods for medicinal plant materials. Geneva: WHO; 1998.

2. J. Zhang, B. Wider, H, Shang, X. Li, E. Ernst, Quality of herbal medicines: challenges and solutions. *Complement Ther Med.* 2012, 20, 100-6.

3. V. Tripathy, B.B. Basak, T.S. Varghese, A. Saha, Residues and contaminants in medicinal herbs a review. Phytochem Lett. 2015, 14, 67-78.

4. M.C.V. Mamani, L.M. Aleixo, M.F. De Abreu, S. Rath, Simultaneous determination of cadmium and lead in medicinal plants by anodic striping voltammetry. *J. Pharmaceut. Biomed.* 2005, 37, 709-13.

5. S. Nookabkaew, N. Rangkadilok, J. Satayavivad, Determinationof trace elements in herbal tea products and their infusions consumed in Thailand. *J. Agr. Food. Chem.* 2006, 54, 39-44.

6. World Health Organization. WHO guidelines for assessing quality of herbal medicines with reference to contaminants and residues. Geneva: WHO; 2007.

Antibacterial Activity of *Borrasus Flabellifer* Vinegar-Graphene Quantum Dots Against Gram-Positive and Gram-Negative Bacteria

Amnuay Noypha[1], Prawit Nuengmatcha[1,2*]

[1]Creative Innovation in Science and Technology, [2]Nanomaterials Chemistry Research Unit, Department of Chemistry, Faculty of Science and Technology, Nakhon Si Thammarat Rajabhat University, 80280, Thailand.

[*]Corresponding author:pnuengmatcha@gmail.com; Tel. +66-7537-7443, Fax +66-7537-7443

Abstract

The *Borrasus flabellifer* vinegar-graphene quantum dots (BFV-GQDs) was successfully synthesized by pyrolysis method. All samples were characterized by using ultraviolet visible spectrophotometer (UV-vis), scanning electron microscopy (SEM) and energy-dispersive X-ray spectroscopy (EDX). Antibacterial activity of BFV-GQDs was determined by disc diffusion method against strains of Gram-negative bacteria (*Escherchia coli*) and Gram-positive bacteria (*Staphylococcus aureus*). Their inhibition zones were compared with citric acid-graphene quantum dots (CA-GQDs). From the results, it was found that the synthesized BFV-GQDs demonstrated excellent antibacterial activity for *Escherchia coli* bacteria at 95.8% which accepted significance at level of 0.05. While *Staphylococcus aureus*bacteriashowed inhibition zone at 89.0% which rejected significance at level of 0.05.

Keywords: *Borrasus flabellifer* vinegar; Graphene quantum dots; Antibacterial activity

Preparation and characterization of highly efficient upconversion photoluminescence particles of ternary metal molybdates for biomedical applications

Won-Chun Oh, Ji Soon Park, Eung Gyun Kim, Hak Su Kim, Chang Sung Lim*
Department of Advanced Materials Science & Engineering, Hanseo University, Seosan 356-706, Republic of Korea
**E-mail: cslim@hanseo.ac.kr*

Rare earth-doped upconversion (UC) particles have attracted great interest in recent years due to the luminescent properties and potential applications in products such as lasers, three-dimensional displays, light-emitting devices, and biological detectors[1]. The ternary molybdate compounds with general composition of $NaMR_2(MoO_4)_4$ (M: bivalent alkaline earth metal ion, R: trivalent rare earth ion) belong to a group of double alkaline earth lanthanide molybdates. It is possible that the trivalent rare earth ions in the disordered tetragonal phase could be partially substituted by Er^{3+}/Yb^{3+}, $Ho^{3+}/Yb^{3+}$and $Ho^{3+}/Yb^{3+}/Tm^{3+}$ions, and the ions are effectively doped into the crystal lattice of the tetragonalphase due to the similar radii of trivalent rare earth ions of R^{3+}, resulted in the excellent UC photoluminescence properties[2-4].In this study, microwave sol-gel derived $NaMR_{2-x}(MoO_4)_4$ ($M = Ca^{2+}$, Sr^{2+}, Ba^{2+}; $R = La^{3+}$, Gd^{3+}, Y^{3+}) phosphors with suitable doping concentrations of Er^{3+}/Yb^{3+}, $Ho^{3+}/Yb^{3+}$and $Ho^{3+}/Yb^{3+}/Tm^{3+}$ions were successfully synthesized, and upconversion photoluminescence properties were investigated in detail. The synthesized particles were characterized by X-ray diffraction (XRD) and scanning electron microscopy (SEM). Pump power dependence and Commission International de L'Eclairage (CIE) chromaticity of the UC emission intensity were evaluated in detail. The spectropic properties were examined comparatively using photoluminescence (PL) emission and Raman spectroscopy. These results led to high emitting efficiency and the involved materials can be considered potentially active components in new optoelectronic devices and in the field of luminescent imaging for biomedical applications.

References

1. M.V. DaCosta, S. Doughan, U.J. Krull, Analyca Chimica Acta, **832**, 1-33 (2014).
2. Chang Sung Lim, Aleksandr Aleksandrovsky, Maxim Molokeev, Aleksandr Oreshonkov, Victor Atuchin, Physical Chemistry Chemical Physics, **17**, 19278-19287 (2015).
3. Chang Sung Lim, Aleksandr Aleksandrovsky, Maxim Molokeev, Aleksandr Oreshonkov, Victor Atuchin, J. Solid State Chemistry,**228**, 160-166 (2015).
4. Chang Sung Lim, Materials Research Bulletin, **75**, 211-216 (2016).

Rapid preparation of YAG: Ce phosphor and transparent ceramic

Rui Yuan, [a] Qian-Li Li, [a] Jian-Feng Hu, [a] Zhi-Jun Zhang, [a, *] and Jing-Tai Zhao[a, *]

[a] *School of Materials Science and Engineering, Shanghai University, Shanghai 200444, China*

**E-mail Address: zhangzhijun@shu.edu.cn (Zhi-Jun Zhang)and*

jtzhao@shu.edu.cn (Jing-Tai Zhao)

Rare-earth doped yttrium aluminum garnet ($Y_3Al_5O_{12}$, YAG) phosphor and transparent ceramic are widely used in white light-emitting diodes (WLEDs) and laser-driven white lighting due to its stable chemical property and high luminous efficiency [1-3]. In order to improve the disadvantages of low efficiency and high energy consumption existed in traditional phosphor and transparent ceramic preparation methods, Cerium doped YAG (YAG: Ce) phosphors and transparent ceramics have successfully and rapidly been prepared by laser sintering method and spark plasma sintering (SPS) method, respectively. Spherical YAG: Ce phosphors with an average particle size of 50 μm and luminous efficiency (LE) of 80 lm/W and color rendering index (CRI) of 76.4 can be obtained in a few minutes through selecting appropriate parameters. YAG: Ce transparent ceramics with high transmittance (78.4 % @ 800 nm, thickness = 0.25 mm) and high quantum yield (85.73 %) can be prepared in one hour.

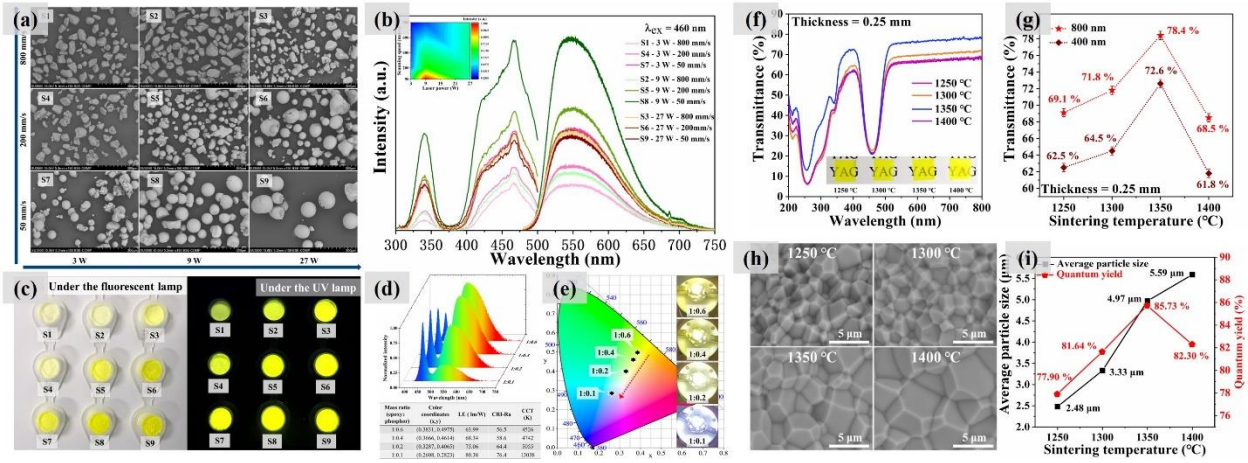

Figure 1. SEM images (a), PLE/PL spectra (b) and photographs (c) of prepared YAG: Ce phosphors under different laser scanning speed and laser power; EL spectra and correlated test results (d) and the CIE chromaticity diagram (e) of different mass ratio of epoxy resin to phosphor; Transmittance (a-b), SEM images (c), and quantum yield (d) of YAG: Ce transparent ceramics sintered under different temperature.

References

[1] Zheng, P.; Li, S.; Wang, L.; Zhou, T. L.; You, S.; Takeda, T.; Hirosaki, N.; Xie, R. J. Unique Color Converter Architecture Enabling Phosphor-in-Glass (PiG) Films Suitable for High-Power and High-Luminance Laser-Driven White Lighting. *ACS applied materials & interfaces* **2018,***10* (17), 14930-14940.

[2] Pimputkar, S.; Speck, J. S.; DenBaars, S. P.; Nakamura, S. Prospects for LED lighting. *Nature Photonics* **2009** *3*,180-182.

[3] Song, Y. H.; Ji, E. K.; Jeong, B. W.; Jung, M. K.; Kim, E. Y.; Yoon, D. H. High power laser-driven ceramic phosphor plate for outstanding efficient white light conversion in application of automotive lighting. *Scientific reports* **2016,***6*, 31206.

The effect of rheological properties of aluminosilicate melts on the mechanical properties of spun fibers

Hyunseok Ko, Myounguk Kim, Sun-Min Park†, Hyung Mi Lim*

Fibrous Ceramics & Aerospace Materials Center, Korea Institute of Ceramic Engineering and Technology, Jinju 52851, Republic of Korea

† and * are co-corresponding authors:

†Corresponding Author; Tel: +82-55-792-2624; Fax: +82-55-792-2447; E-mail: psm@kicet.re.kr

** Corresponding Author; Tel: +82-55-792-2450; Fax: +82-55-792-2447; E-mail: lim@kicet.re.kr*

Introduction

Aluminosilicate glasses have been developed to make use in the industry, for instance as fillers, filters, coatings, or insulation materials [1,2]. One of the effort to reuse the aluminosilicate industrial wastes, such as blast furnace slags and fly ashes, is to transform them into a ceramic fiber through melting. For instance, aluminosilicate based mineral wool (short fiber) insulation board panels are manufactured from slags via commercialized process [3,4] In general, the fiberization is processed via the melt-spinning process [5], and the rheological properties of the melts, such as their viscoelasticity, helps to understand the process conditions.

Methods

A high temperature rheometer FRS1600 (Anton Paar, Austraila) was used for the rheological analysis presented in this study. To assess the viscoelasticity, both rotational and oscillatory mode was employed. The fibers are fabricated using 10-hole bushing fiberization apparatus and properties of spun fibers are analyzed with following equipments; the diameter is measured with opticalspectroscopy (DM2700 M, Leica, Germany) and the tensile strength of the fiber is measured 30 specimens for each sample according to ASTM D 3379-75, using ultimate testing machine (Instron 5544, 2712-013, USA) with a 10 N load cell at 0.5 mm/mintensile rate.

Results and Discussions

We analyzed the correlation between chemical compositions vs. high temperature rheological properties vs. fiber properties, and assessed their connection. The results show that the viscosities of melts significantly depends on the acidic and basicity, and less on amphoteric. In

terms of fiber properties, no strong correlation was observed with the chemical composition. The fiber diameter was primarily determined by the winding rate. However, the high temperature rheological properties indeed had an influence on the fiber property. We found that the elastic moduli of fibers are inversely proportional to shear modulus of the melts at the transient temperature. A further investigation of tensile strength at elevated temperature, Fig. 1, showed that the fiber expected to have a higher degree of pseudo-strain hardening had a more rapid decrease in elastic modulus. It demonstrates the shear modulus value of the melt influence the recovery of quenching melt while spun, and sequentially pseudo-strain hardening takes place in melt spun fibers.

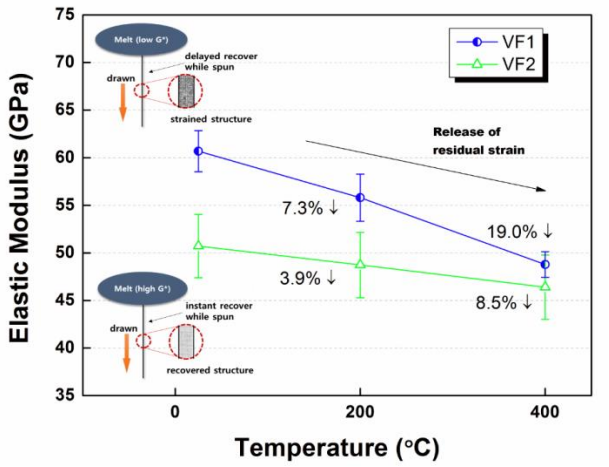

Fig 1. The elastic moduli at elevated temperatures for fibers with different melt shear moduli.

References

1Yi, H. *et al.* An Overview of Utilization of Steel Slag. *Procedia Environmental Sciences***16**, 791-801, doi:https://doi.org/10.1016/j.proenv.2012.10.108 (2012).

2Pati, P. R. & Satapathy, A. Development of wear resistant coatings using LD slag premixed with Al2O3. *J. Mater. Cycles Waste Manage.***17**, 135-143, doi:10.1007/s10163-014-0234-1 (2015).

3Balcerowiak, W., Gryta, M. & Kalędkowski, B. Thermal stability of binder for mineral wool insulations. *J. Therm. Anal.***43**, 299-303, doi:https://doi.org/10.1007/BF02635997 (1995).

4ÖHberg, I. Technological development of the mineral wool industry in Europe. *The Annals of Occupational Hygiene***31**, 529-545, doi:https://doi.org/10.1093/annhyg/31.4B.529 (1987).

5Ziabicki, A. *Fundamentals of fibre formation: the science of fibre spinning and drawing*. (Wiley, 1976).

Activated Biochar-based Hydrogel Composited for Slow Release Urea Fertilizer

Rungnapa Pimsen*, Alisa Pipak, Tuangrat Senmard and Laddarak Aupakankaew

Nanomaterials Chemistry Research Unit, Department of Chemistry,

Nakhon Si Thammarat Rajabhat University, 80280, Thailand.

**Corresponding author. e-mail: rpimsen@gmail.com; Tel. +66-7537-7443, Fax +66-7537-7443*

Abstract

This study aimed to develop and optimize a novel activated biochar (ABC)-based hydrogel fertilizer composed of ABC, sago starch (SSt), acrylamide (AM) and urea utilizing MBA as crosslinking reagent and ceric ammonium nitrate as initiator at 65 °C for 60 min, which can simultaneously slowly release urea nitrogen. The structure and properties of the resulting ABC-AM/SSt/Urea samples were characterized using the scanning electron microscope (SEM) and Energy Dispersive X-ray Spectrometer (EDX). SEM image of ABC showed a highly porous structure which facilitated the permeation of water into the polymeric network. Results suggest that ABC-AM/SSt/Urea could significantly improve the water-holding. ABC-AM/SSt/Urea effectively reduced the nitrogen-release rate which 40 % of urea nitrogen was released after 30 days.

Keywords: Activated Biochar, Hydrogel, Slow Release Fertilizer, Urea

Introduction

Global crop production, fertilizers were used for enhance crop yield. However, the loss of nutrient elements is one of considerable problems causes the inadequate of plant nutrients, increases route cost and contaminates the environment. Slow release fertilizers may be one such method as they can use to solve this problem [1]. Several researches were used nanotechnology to promote the ability of slow release fertilizers. Biochar (BC) is a porous material that is produced from the pyrolysis of various biomass. BC deliver numerous conspicuous agricultural and environmental such as providing a long-term carbon descend,

increasing soil nutrient availability and porosity, enhancing soil fertility and crop productivity, increasing cation-exchange capacity and water-holding capacity, reducing the greenhouse effect [2], [3]. Hence, using BC to sorb nutrients from water was an eco-friendly. Although these biochar-based slow release fertilizer are able to effectively increase nutrient-use efficiency, most of them do not possess water retention capacity.

Polymer hydrogels are 3D networks that can maintain water within their structures, and swell without dissolving in water. The biopolymer hydrogel is increased considerable for agricultural as slow release fertilizer (i.e. chitosan [4], [5] starches [4], [6] and cellulose [7][8]) as a result of low cost, non-polluting characteristics and the ability to reduce fertilizer release. Polyacrylamide and sago starch were designated to use as hydrogel part for slow release fertilizer.

In this study, the slow release fertilizer hydrogels were prepared from ABC, AM and sago starch, using MBA as a crosslinking agent. Swelling rate on the ABC-AM/SSt/Urea and urea release behavior of such the ABC-AM/SSt/Urea hydrogels in water were investigated.

Materials and methods

All chemicals used in the study are of analytical grade. Acrylamide (C_3H_5NO), N, N'-methylenebisacrylamide, and ceric ammonium nitrate ($H_8N_8CeO_{18}$) were taken from Merck, Germany. Sodium hydroxide (NaOH) and urea (CH_4N_2O) were supplied by Sigma-Aldrich. Sago starch was supplied by Faculty of Science and Technology, Nakhon Si Thammarat Rajabhat University, Thailand.

Preparation of activated biochar

Activated biochar (ABC) was prepared through pyrolysis of coconut shells at 300◦C for 2 hours. The biochar was crushed and passed through 100-mesh standard metal sieves. The biochar powder soaked in 25% NaCl solution for 24 hours and heated at 750 °C for 30 min in a box furnace. The prepared activated biochar particles was analyzed by the scanning electron microscope (SEM) and Energy Dispersive X-ray Spectrometer (EDX).

Preparation of activated biochar hydrogel composite

The ABC- hydrogelwas composited using prepared ABC, SSt, AM, urea utilizing MBA as crosslinking reagent and ceric ammonium nitrate as initiator at 65 °C for 60 min. A mixed solution containing 15 g of AM, 10 g of SSt, 20 g of urea, 0.07 g of MBA (N, N′-methylene bis acrylamide), and 0.5 g of ceric ammonium nitrate was introduced to a 250 mL round-bottom flask under under constant stirring 65 °C for 50 min until the mixture was uniform. Adding 9 g of sodium hydroxide, the mixture heated at 65 °C for 10 min. The hydrogel was soaked in water for 2 days. The resulting gel products were washed with water and dried to constant weight in an oven at 60 °C, milled, sifted, and stored for future use.

Swelling ratio (SR) of the ABC-AM/SSt/Urea

0.5 g of ABC-AM/SSt with various ABC, AM and MBA amount were immersed in distilled water 200 mL and allowed to swell for 360 min under ambient conditions of temperature and pressure. The contents were filtered and SR was calculated using Eqs. (1).

$$SR\% = (W_2 - W_1)/ W_1 \quad (1)$$

where $W_1$and W_2 referred to the weight of dry NZ-CS/ST and swollen biopolymer composite, respectively.

Effect of AM to swelling ratio (SR) of the ABC-AM/SSt/Urea

0.5 g of ABC-AM/SSt with various AM amount was immersed in distilled water 200 mL and allowed to swell for 360 min under ambient conditions of temperature and pressure. The contents were filtered and SR was calculated using Eqs. (1).

Effect of MBA to swelling ratio (SR) of the ABC-AM/SSt/Urea

0.5 g of ABC-AM/SSt with various MBA amount was immersed in distilled water 200 mL and allowed to swell for 360 min under ambient conditions of temperature and pressure. The contents were filtered and SR was calculated using Eqs. (1).

Slow release behavior of urea

30 days' slow release performance of N-urea within ABC-AM/SSt/Urea in water was determined by using 1.0 g of ABC-AM/SSt/Urea immersed in deionized water 200 mL. For the period of 30 days, water was collected daily at 24 h time interval to determine the leakage of urea. The release behaviors of urea from the ABC-AM/SSt/Urea in deionized water was investigated by UV-visible spectrophotometry.

Results and discussion

ABC characterization

The obtained ABC was characterized by SEM and EDX are shown in Fig.1a. The SEM image of ABC showed full of cavities and in a honeycomb-like structure on surface of ABC [9]. Fig. 1b shows the elemental percentage composition of C and O in the synthesized ABC where C contain was found to be 89.3% and that of O is found to be10.7% [10].

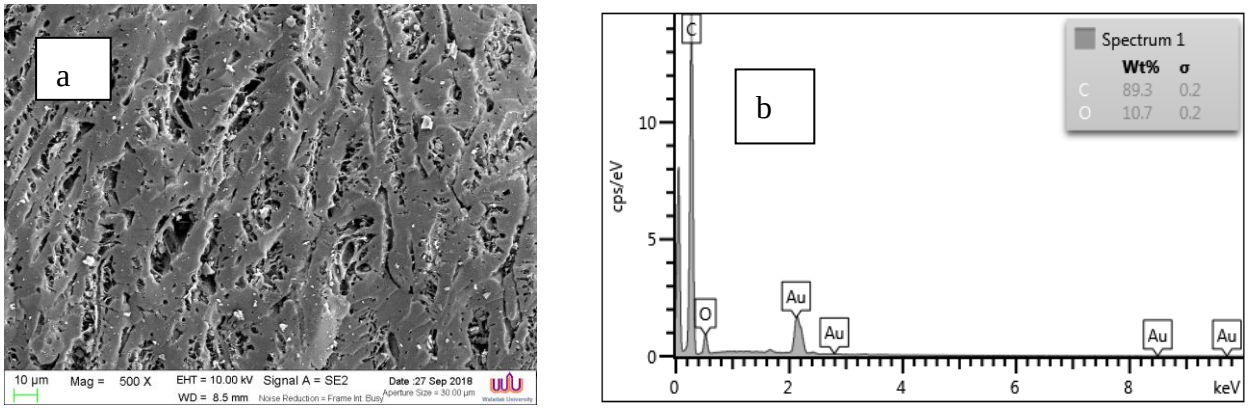

Fig. 1 (a) SEM image of activated coconut shell charcoal showing the area used in measuring elemental composition and (b) corresponding EDX spectrum.

Effect of ABC to swelling ratio (SR) of the ABC-AM/SSt/Urea

Water swelling of theABC-AM/SSt/Urea polymeric network has a key role in influential fertilizer release, as a result of the correlation between the swelling and the structure of the material. The swelling ratio of the ABC-AM/SSt/Urea increased when theABC amount increased up to 0.5 g and decreased after addition ABC amount more than 0.7% which displayed in Fig. 2 due to effect of carboxylic group in the present of ABC can interact with other functional group of AM and SSt via hydrogen bonding interaction [2], [3].

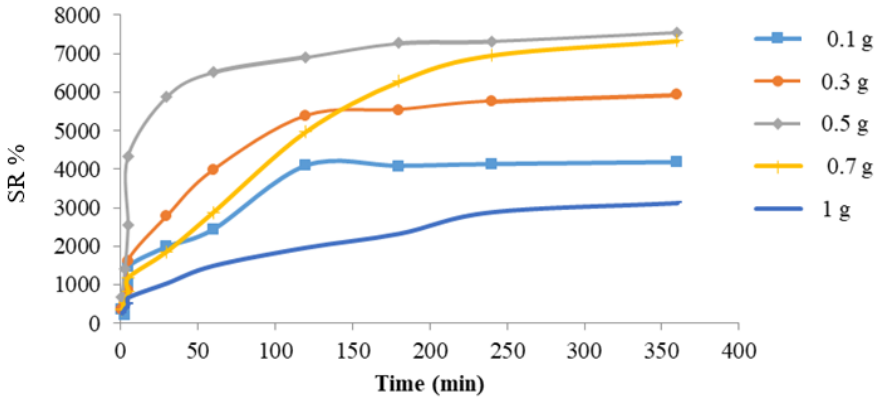

Fig. 2 Swelling ratio of ABC-AM/SSt/Urea with various amount of ABC; 0.1, 0.3, 0.5,0.7 and 1 g.

Effect of MBA to swelling ratio (SR) of the ABC-AM/SSt/Urea

From the Fig. 3, the swelling ratios increased when MBA amount increased. This behavior can be indicated to the increase in reactive functional groups present in MBA causes high efficiency the hydrogel crosslinking. In this study, 0.5 g of MBA at 0.5 g was used to produce the ABC based hydrogel due to swelling affecting the release.

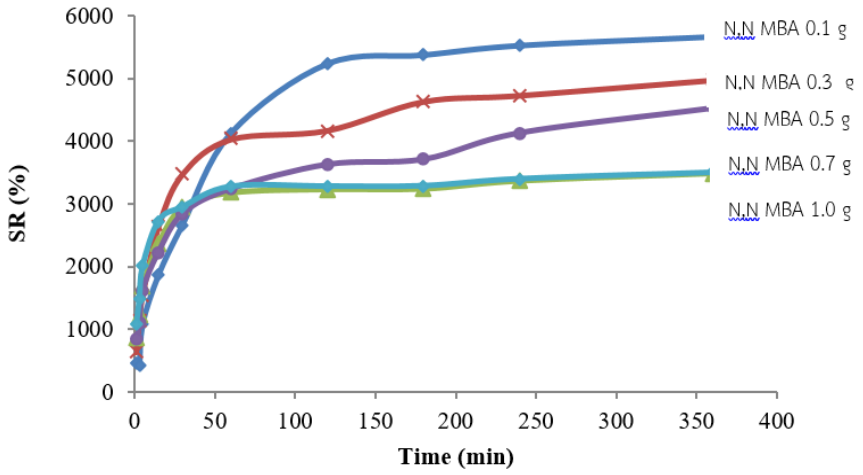

Fig. 3 Swelling ratio of ABC-AM/SSt/Urea with various amount of MBA; 0.1, 0.3, 0.5, 0.7 and 1 g.

Effect of AM to swelling ratio (SR) of the ABC-AM/SSt/Urea

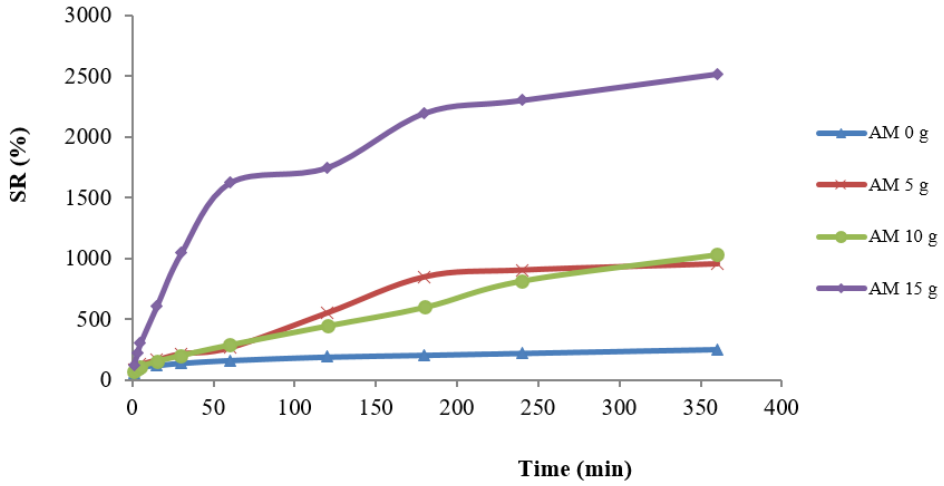

Fig. 4 Swelling ratio of ABC-AM/SSt/Urea with various amount of AM; 0, 5, 10 and 15 g.

Fig. 4 showed the effect of AM to swelling ratio of ABC-AM/SSt/Urea. It was found that an increase of AM in the range of 0-15 g led to swelling of the hydrogel increase. Due to polyacrylamide contain water solubility groups -$CONH_2$ those imbibe large quantity of water without dissolving themselves. In this study, 15 g of AM was used for synthesized the hydrogel fertilizer which needs to water retention purpose.

Urea release behaviors of the ABC-AM/SSt/Urea

The urea release behaviors of the ABC-AM/SSt/Urea within 30 days in the deionized water at the room temperature are shown in Fig. 5. The ABC-AM/SSt/Urea showed percent amount release of urea at day 30^{th} of 40%. Obtained ABC based hydrogel composite showed the higher efficiency of slow release urea than numerous reports e.g. a poly (vinyl alcohol)/chitosan hydrogel that released up to 70% of the same fertilizer only four days [4].

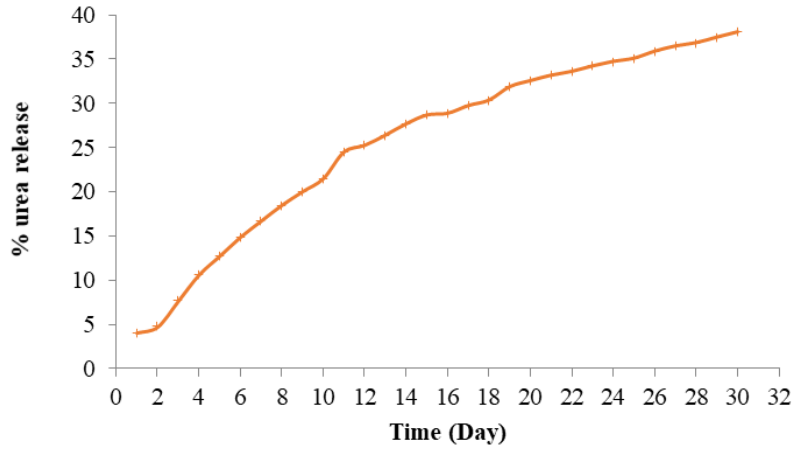

Fig. 5 Urea release behavior of ABC-AM/SSt/Urea within 30 days.

Conclusion

We successfully prepared the ABC-AM/SSt/Urea hydrogel composite used for slow release of urea fertilizer. The ABC-AM/SSt/Urea hydrogel composite can be easily prepared from an ionic interaction between ABC-AM/SSt/Urea hydrogel composite using MBA ascrosslinking agent. The crosslinking agent, AM and ABC amount effected to the release of urea fertilizer. The urea release behavior of the ABC-AM/SSt/Urea composite provided the slow release urea, it is clear that the developed materials would be potentially useful as slow release fertilizers.

Acknowledgements

This work was supported by Research and Development Institute, Nakhon Si Thammarat Rajabhat University and Nanomaterials Chemistry Research Unit, Department of Chemistry, Faculty of Science and Technology, Nakhon Si Thammarat Rajabhat University.

References

[1] J. Liu, Y. Yang, B. Gao, Y. C. Li, and J. Xie, “Bio-based elastic polyurethane for controlled-release urea fertilizer: Fabrication, properties, swelling and nitrogen release characteristics,” *J. Clean. Prod.*, vol. 209, pp. 528–537, 2019.

[2] L. Chen, Q. Chen, P. Rao, L. Yan, A. Shakib, and G. Shen, “Formulating and optimizing a novel biochar-based fertilizer for simultaneous slow-release of nitrogen and

immobilization of cadmium," *Sustain.*, vol. 10, no. 8, 2018.

[3] P. Wen, Z. Wu, Y. Han, G. Cravotto, J. Wang, and B. C. Ye, "Microwave-Assisted Synthesis of a Novel Biochar-Based Slow-Release Nitrogen Fertilizer with Enhanced Water-Retention Capacity," *ACS Sustain. Chem. Eng.*, vol. 5, no. 8, pp. 7374–7382, 2017.

[4] J. J. Perez and N. J. Francois, "Chitosan-starch beads prepared by ionotropic gelation as potential matrices for controlled release of fertilizers," *Carbohydr. Polym.*, vol. 148, pp. 134–142, 2016.

[5] B. R. Araújo, L. P. C. Romão, M. E. Doumer, and A. S. Mangrich, "Evaluation of the interactions between chitosan and humics in media for the controlled release of nitrogen fertilizer," *J. Environ. Manage.*, vol. 190, pp. 122–131, 2017.

[6] X. Han, S. Chen, and X. Hu, "Controlled-release fertilizer encapsulated by starch / polyvinyl alcohol coating," *DES*, vol. 240, no. 1–3, pp. 21–26, 2009.

[7] H. Geng, "A one-step approach to make cellulose-based hydrogels of various transparency and swelling degrees," *Carbohydr. Polym.*, vol. 186, no. October 2017, pp. 208–216, 2018.

[8] T. a. Tari and R. S. Singhal, "Starch-based spherical aggregates: Stability of a model flavouring compound, vanillin entrapped therein," *Carbohydr. Polym.*, vol. 50, no. 4, pp. 417–421, 2002.

[9] V. V. T. S.M. Anisuzzaman , Collin G. Joseph, Y.H. Taufiq-Yap, Duduku Krishnaiah, "Modification of commercial activated carbon for the removal of 2,4-dichlorophenol from simulated wastewater.pdf," *J. King Saud Univ. – Sci.*, vol. 27, pp. 318–330, 2015.

[10] C. Pongener, D. Kibami, and K. S. Rao, "Synthesis and Characterization of Activated Carbon from the Biowaste of the Plant Manihot Esculenta," *Chem. Sci. Trans.*, vol. 4, no. 1, pp. 59–68, 2015.

Preparation of few-layered graphene using Graphite Intercalation Compounds (GICs)

○Yoshihisa Nanri[1], Hiroshi Yoshitani[2], Hiroji Fukui[2], Akira Nakasuga[2], Tomoki Tsumura[1], Masahiro Toyoda[1]

[1]*Department of Applied Chemistry, Graduate School of Engineering, Oita University, 700 Dannoharu, Oita 870-1124, Japan*

[2]*Sekisui Chemical Co, LTD. 2-1 Hyakuyama, Shimamoto-cho, Mishima-gun, Osaka 530-8565, Japan*

1. Introduction

Preparation of the non-oxidized graphene have been required. So far, non-oxidized few-layered graphene have been prepared by adding water to the K- Tetrahydrofuran-Graphite Intercalation Compounds (K-THF-GICs), which ternary GICs. However, prepared graphene cannot achieve the large area required for practical applications, with the addition of an electron–withdrawing aldehyde may result in the fabrication of forming thin and large-area graphene sheets by nucleophilic substitution reaction on the carbon-based hexagonal networks.Furthermore, an aldehyde solvent containing long alkyl chains is preferable for the preparation of large-area few-layered graphene when compared with an aldehyde solvent containing short alkyl chains [1]. Therefore, we considered that few-layered graphene can be prepared from alcohol containing long alkyl chains. In this study, the non-oxidized few-layered graphene with a large area were prepared by the addition of a long alkyl chains aldehyde or alcohol solution to the host K-THF-GICs

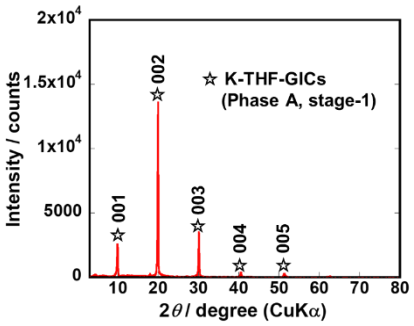

Fig.1 XRD patterns of K-THF-GICs.

2. Materials and methods

A K-THF solution was prepared by dissolving naphthalene in THF and adding potassium and by stirring for 30 min. Subsequently, K-THF-GICs were prepared by soaking the as-obtained graphite (grain size = 100 μm) in the prepared solution. Few-layered graphene was further prepared by the addition of decanal and decanol (having long alkyl chains) to the K-THF-GICs and stirring. After stirring, supernatant and

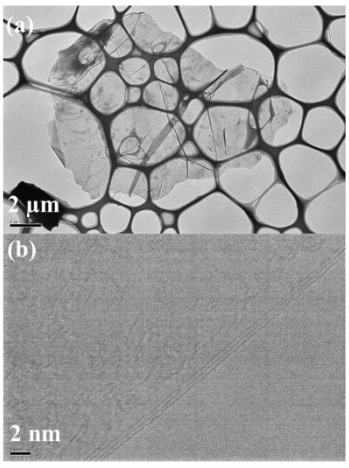

Fig.2TEM micrographs of few-layered graphene obtained by the exfoliation of K-THF-GICs in decanal

sediment were separated and the supernatant was centrifuged for obtaining few-layered graphene. The synthesized K-THF-GICs were characterized using XRD and the obtained graphene was characterized using TEM imaging respectively.

3. Result and discussion

Figs. 1 depicts the XRD patterns of the synthesized K-THF-GICs. The sequence peaks are contributed by stage-1 of K-THF-GICs. Few-layered graphene was prepared by the addition of decanal to the K-THF-GICs. Figs. 2(a) and (b) represent the TEM micrographs of few-layered graphene obtained by the addition of decanal to the K-THF-GICs. As revealed in micrograph of (a) and (b), prepared three-layered graphene had an area of dozens of square micrometers. The area of few-layered graphene prepared by addition of the decanal to K-THF-GICs (74 μm^2 on an average) was larger than the area prepared by the addition of the water to the K-THF-GICs (6.2 μm^2 on an average).

Reference

[1] Yoshihisa Nanri, Hiroshi Yoshitani, Hiroji Fukui, Akira Nakasuga, Taro Kinumoto, Tomoki Tsumura, Masahiro Toyoda, 「Preparation of few-layered graphene using Graphite Intercalation Compounds (GICs)」, The 56th FNTG Society 3P-10, 2019

Biotemplating synthesis of N-doped two-dimensional CeO_2-TiO_2 nanosheets with enhanced visible lightphotocatalytic desulfurization performance

Xiaowang Lu[a, b], Meng Fu[b]

a. School of Material Science and Engineering, Yancheng Institute of Technology, Yancheng 224051, China

b. Jiangsu Key Laboratory of Materials Surface Science and Technology, Changzhou University, Changzhou, 213164, Jiangsu, China

Nowadays, the combustion commercial fuels (gasoline and diesel oil) releasing sulfur oxides (SO_X) is one of the important sources of air pollution, which can cause haze, acid rain, acid fog and many other environmental issues [1]. Hence, many countries have formulated relevant laws in order to reduce the sulfur content in the gasoline and diesel fuel, thus deep desulfurization of fuel has been urged needed. Photocatalyticoxidative desulfurization technology recognized as a new desulfurization method, which can be conducted at ambienttemperature, atmospheric pressure and high efficiency [2,3].

We established a novel method by using inexpensive, efficient and environment-friendly Chinese rose petal as biotemplate to biomimetically synthesize N-dope two-dimensional CeO_2-TiO_2nanosheets. The detailed characterization exhibited that the CeO_2-TiO_2 composite exactly duplicated the microstructure of Chinese rose petal and the self-ownednitrogen was successfully doped into the CeO_2-TiO_2 composite, which could enhance the visible light absorption efficiency. The CeO_2 and TiO_2 formed well-defined heterojunctions promoting the effective separation of photogenerated electrons and holes. The photocatalytic activity of the samples was evaluated by photocatalytic degradationof dibenzothiphene (DBT) in model oil. The results showed that the N-dopedCeO_2-TiO_2 nanosheets showed thatthe removal rate of DBT could reach 93.7 % under visible light irritation for 3 hours, when the moral rate of Ce and Ti was 1:1.

This work was supportedthe Jiangsu Province Key Laboratory of Materials Surface Science and Technology.

Reference

[1] S. A. AL-Hammadi, A. M. Al-Amer, T. A. Saleh, Chem. Eng. J.345 (2018) 242-251.

[2] X.W. Lu, X.Z. Li, J.C. Qian, N.M. Miao, C. Yao, Z.G. Chen, J. Alloys Compd.661(2016) 363-371.

[3] X.Z. Li, W. Zhu, X.W. Lu, S.X. Zuo, C. Yao, C.Y. Ni, Chem. Eng. J. 326(2017) 87-98.

High-performance gas phase synthesized palladium nanoparticles for H_2O_2 sensingand methanol electro-oxidation

Jue Wang[1]

[1]*Key Laboratory for Advanced Technology in Environmental Protection of Jiangsu Province, Yancheng Institute of Technology, Yancheng 224051, China*

wangjue@ycit.edu.cn

Abstract:

In recent years, Pd nanoparticles (NPs) have attracted much research interests in H_2O_2 sensing and methanol electro-oxidation applications. Pd NPs used for electro-catalytic applications was commonly synthesized by chemical routes such as chemical reduction and electrodeposition. In each case, it is inevitable that the chemical solution would affect the catalytic activity. Recently, we used the gas phase cluster beam deposition process to fabricate Pd NP-deposited-glassy carbon electrode (GCE), which enabled highly selective amperometric detection of H_2O_2 at a sufficiently low applied potential (∼−0.12 V) [1]. In order to improve the response time and the linear response range, Pd NPs were deposited on chemical vapor deposition synthesized bilayer graphene films (BGFs) supported with GCEs in the gas phase. With the introduction of BGFs, the catalytic activity of Pd NP-modified electrodes toward H_2O_2 reduction was largely enhanced [2]. Because of outstanding catalytic activity of the Pd NPs, we fabricated Pd NPs supported on carbon supports and used them as the electro-catalysts for methanol oxidation reactions. The resulting Pd NPs/multi-walled carbon nanotubes/few-layer graphene sheets combination exhibits an ultrahigh electrocatalytic activity and unusual long-term durability for methanol oxidation [3]. These results indicate that the Pd NP catalysts produced by gas phase cluster beam deposition are promising applications in H_2O_2 sensing and methanol electro-oxidation.

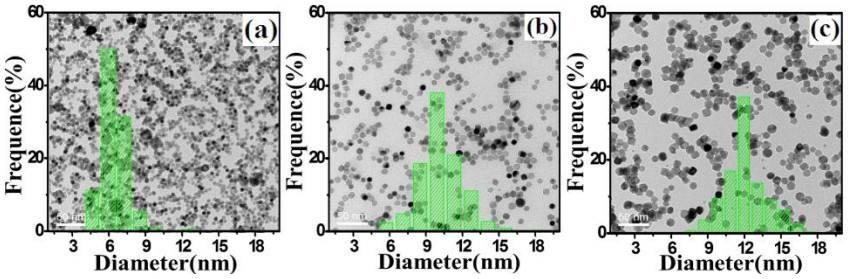

Figure 1: *TEM images of Pd NPs produced with argon gas pressure of (a) 90 Pa, (b) 110 Pa, and (c) 130 Pa and the corresponding size distributions.*

References:

[1] J. Wang, et al., Nanoscale Res. Lett. (2015) 10:311

[2] J. Wang, et al., Sensor. Actuat. B-Chem. 230 (2016) 690–696

[3] J. Wang, et al., Electrochim. Acta 251 (2017) 631–637

Defect engineering and hole doping for tuning photocatalytic H_2O reduction in $Sc_2Cu_2O_5$: DFT study

Lawal Mohammed [a, b]*, Qinfang Zhang [a]*, Anjli Sharma [a, c]

[a]*School of Material Science and Engineering, Yancheng Institute of Technology, Yancheng, 224051, PR China*

[b]*Physics Department Ahmadu Bello University, Zaria, 833201, Nigeria*

[c]*Department of Information Display, Sun Moon University, South Korea*

Abstract:

Transition metals based oxide semiconductors are known to be active photocatalytic materials for both half and overall water splitting reactions. For the first time a systematic investigation of the electronic, optical and thermoelectric properties of isostructural oxide is presented. More explicitly, this paper reports, the computational analysis of the photocatalytic properties of the crystalline $Sc_2Cu_2O_5$. The analyses are based on the optical absorption, band edge potential, energy band gap, and electrons and holes effective masses. The hole-doped $Sc_2Cu_2O_5$ compound with Ca@Cusite @25 percent,show high optical absorption in the visible range and small effective masses efficient to suppress backward oxidation reaction. The computed band edge potentials for both valence and conduction band of the Ni@Cu site are deep enough for these compounds to be use as cocatalyst for either of redox reactions. Hgh absorption under visible light irradiation in oxygen vacancy configurations for which the nearest bond length of Cu-O contract after geometry relaxation, which might be due to high magnetic moments at the twovacancy sites.

Keywords: Water splitting; Oxygen vacancies; Oxide semiconductors; Thermoelectric

References

Denisova, L. T., Kargin Yu F., Chumilina, L. G., Denisova, V. M., and Kirik, S. D. High Temperature Heat Capacity of $Sc_2Cu_2O_5$*Inorganic Materials*, **50**(5) (2014)

Maeda, K. Z-Scheme Water Splitting Using Two Different Semiconductor Photocatalysts.*ACS Catalysis*, **3**(7) 1486-1503 (2013)

Kong, D., et al. Recent advances in visible light-driven water oxidation and reduction in suspension systems*Materials Today*, https://doi.org/10.1016/j.mattod.2018.04.009, (2018)

First principles study of electronic and magnetic properties of graphene-ferromagnet interface

Kumneger Tadele, Qinfang Zhang

School of Materials Science and Engineering, Yancheng Institute of Technology, Yancheng, PR China

Abstract: The single layer carbon material, Graphene, which is characterized by unique electrical and chemical properties, features the long distance diffusion length, high carrier mobility and chemical and electrical tunability, which marked its potential for wide technological applications including spintronics, sensors and other graphene-based electronic devices. The nearly ideal transport properties and the tunability of the charge carrier concentration in graphene led to a wide range of applications for graphene-based electronics [1,2]. A ferromagnetic material supported graphene layer also shows a promising potential for technological applications in spintronics. The graphene-metal interfaces evidently change the electronic and magnetic properties of the interface [3]. This phenomenon can be investigated for different graphene-based electronic devices and/or any other technological applications.

The interfacial interaction between graphene and ferromagnetic substance is known to bring additional controls to the intrinsic properties of graphene, in addition to, probably, inducing some novel properties to the system which may have potential application in spintronics and computing. However, there is a lack of fundamental understanding on the interaction of graphene with metallic surfaces. And hence, in this work the spin-polarized electronic structures across the graphene-ferromagnet interface has been investigated using first principles density functional theory calculation as it is implemented on Vienna ab-initio simulation package (*VASP*). The electronic and magnetic properties of the interface have also been investigated while the ferromagnetic substrate was represented by *Ni (111)* and *Co(111)* surfaces due to their structural resemblance to graphene. The study reveals that the ferromagnetic layers adjacent to the interface show a transition of spin orientation from in plane to out of plane. Strong hybridization between different orbitals of graphene and ferromagnet was observed. The hybridization significantly affects the electronic and magnetic properties of the interface. Reduction on the local magnetic moments of the ferromagnet layers

adjacent to the interface and induced spin polarization on the graphene layer were also observed which should be understood as the impacts of the hybridization. This work provides important information which can be used for efficient design of interfaces for graphene-based spintronics.

1. A. K. Geim and K. S. Novoselov, Nat. Mater 6, 183 (2007)
2. F. Schwierz, Nat. Nanotechnol 5, 487 (2010)
3. Y. Matsumoto, S. Entani, A. Koide, M. Ohtomo, P. V. Avramov, H. Naramoto, K. Amemiya, T. Fujikawa, andS. Sakai, J. Mater. Chem. C 1, 5533 (2013).

Graphene wraped $AgInS_2$ flower nanocompositewithexcellent visible light photocatalytic properties

Lei Zhu[1], Lele Fan[1], and Qinfang Zhang[2,1*]

[1]*Key Laboratory for Advanced Technology in Environmental Protection of Jiangsu Province, Yancheng Institute of Technology, Yancheng, 224051, P.R. China*

[2]*School of Materials Science and Engineering, Yancheng Institute of Technology, Yancheng 2 24051, P.R. China*

A microwave assisted hydrothermal method [1] was introduced for the synthesis of hybrid graphene-$AgInS_2$nanocomposite (GA). The graphene wraped $AgInS_2$nanocomposites were obtained, $AgInS_2$ flower was consist of large size nanosheets. From the photocatalytic results, the excellent activity of graphene-$AgInS_2$nanocompositefor degradation of methylene blue (MB)and Texbrite BA-L (TBA) undervisible irradiation could be attributed to both the effects of $AgInS_2$ and charge transfer of the graphene nanosheet, and the introduction of $AgInS_2$ to enhance the photogenerated electrons.

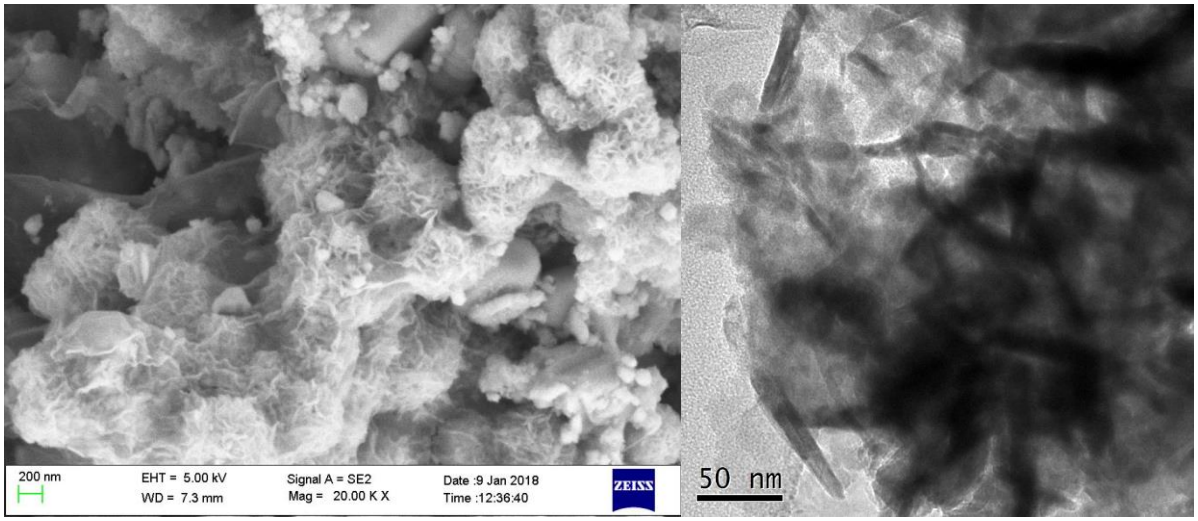

Figure 1:FE-SEM(a) and TEM (b) micrographs of as-prepared graphene wraped $AgInS_2$ nanocomposite.

[1] Refe Wenjuan Zhang, Danzhen Li, Zhixin Chen, Meng Sun, Wenjuan Li, Qiang Lin, Xianzhi Fu, Materials Research Bulletin 46 (2011) 975–982

Synthesis of Li-dopingTetragonal-Bi_2O_3 nanomaterial with high efficient visible light photocatalysis

Lele Fan[a], Lei Zhu[a*]Qinfang Zhang[b*]

[a] *Key Laboratory for Advanced Technology in Environmental Protection of Jiangsu Province, Yancheng Institute of Technology, Yancheng 224051, P. R. China*

[b] *School of Materials Science and Engineering, Yancheng Institute of Technology, Yancheng 224051, P. R. China*

** Corresponding authorsE-mail addresses: qfangzhang@gmail.com (Q. Zhang), dream909@126.com (L. Zhu).*

Nowadays, photocatalysis has attracted wide attention due to its special advantage in sewage disposal. To enhance photocatalyticactivity, the poor visible light absorption and recombination between electron and hole should be avoided. Therefore, many methods such as morphology tailor, elements doping or heterojunction have been proposed in order to address the aforementioned problems. However, it's still high desirable to design new photocatalytic materials with environmental friendly and low-cost.

As a typical binary metal oxide material, Bismuth oxide (Bi_2O_3) shows polymorphic phase including α, β, γ and δ phases, which are corresponding to the monoclinic, tetragonal, body-centered cubic and face-centered cubic phase, respectively. The α-Bi_2O_3 phase can be stable at as high as 729°C with a bandgap of 2.8eV, while metastable β-Bi_2O_3 has a bandgap of 2.3eV and outperforms high efficient photocatalytic property. Nevertheless, the unstable property of β-Bi_2O_3conventionally makes it impossible to fulfill its practical application. One possible route to eliminate the mutability is to construct heterostructure. However, for heterostructure constructing, the lattice matching should be considered since the poor interface can extremely impede the charge transfer, consequently decreasing the photocatalystic activity. The structure aligning also must be taken into account, since the Z-type heterojunction conventional exhibits high photocatalytic efficient. Compared with heterostructure, element doping is more flexible, and the bandgap or even crystal structure can be easily controlled.

In this work, Li_xBiO_y compounds were synthesized via a facile calcination method. It was

surprising that the as-prepared Li_7BiO_6 compounds transformed into Li-doping tetragonal Bi_2O_3 phase after undergoing water washing process, which was well verified by combining with XRD and HR-TEM. In addition, the energy bandgap of prepared compound was derived based on UV–Visdiff use reflectance spectrumand results indicate a lower band gap formation when increasing Li dopant concentration. Moreover, the Li-doping tetragonal Bi_2O_3 exhibited high visible-light-driven photocatalytic activity and the methylene blue can be well degraded in 10min. The enhanced photocatalytic activity was illustrated according tothe the improvement of charge transfer. Our current work will boost the development of photocatalysis and bring insight into other Li_xMO_6 (e.g. Li_6WO_6, Li_7TabO_6, Li_7NbO_6, Li_8ZrO_6) compounds to extend their photocatalytic application.

Chemical dissolution of glass fiber in NaOH alkaline solution using different condition

Su-Yeon Lee[a, b], Jin-Uk Hwang[b], Woo-Seong Tak[b], Woo-Sik Kim[b]*

[a] *Polymer Science and Engineering, Pusan National University, 2 Busandaehak-ro 63beon-gil, Geumjeong-gu, Busan, 46241, Korea*

[b] *Fibrous Ceramics & Aerospace Materials Center, Korea Institute of Ceramic Engineering and Technology, 101 Soho-ro, Jinju-si, Gyengsangnam-do, 52851, Korea*

E-mail: wskim@kicet.re.kr

Introduction

Recently, recycling technology for waste of wind power blades is arising issue for reasons of low manageability and high cost of wastes. Though glass fiber is perfectly dissolved in hydrofluoric acid, Low cost for recycling and harmless to human is important for recycling of blades. Chemically melted glass fiber will be used as different purpose like accelerator of hardening for shotcrete. In this study, dissolution process of glass fiber is tested in NaOH solution at low temperature. In addition, difference in diameter reduction of glass fiber is observed by various alkali concentration and reaction time, treatment temperature.

Experimental procedure

Because a wind power blade is made of GFRP (Glass fiber reinforced plastics), dis solution of glass fiber should be tested before proceeding of GFRP dissolution. Dissolution process is tested by various parameters such as alkaline concentration (3, 6, 9 mol of NaOH solution) and reaction time (1, 2, 3 and 5h), treatment temperature (75, 85, 95℃). Also, Heating mantle is used for uniform dissolution at 100rpm.

Results and discussion

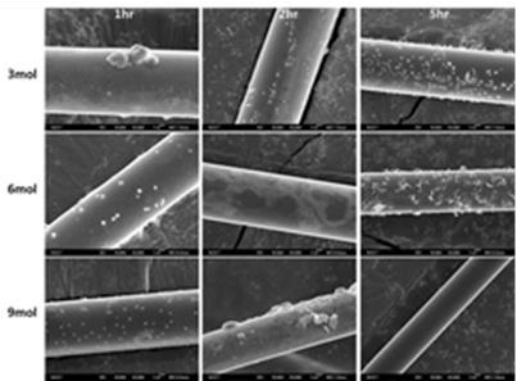

Fig. 1 FE-SEM images of glass fiber in alkali solution using different NaOH concentration and reaction time

The diameter change of glass fiber was observed with the use of FE-SEM. In results of FE-SEM images, the differences of diameter reduction between alkali concentration and reaction times take place and increase in the fiber diameter reduction with higher alkali concentration and longer reaction time.

Keywords: Glass fiber, Alkali solution, Chemical dissolution, Recycling

References:

1. Bashir, S. T., Yang, L., Liggat, J. J., & Thomason, J. L. (2018). Kinetics of dissolution of glass fiber in hot alkaline solution. Journal of materials science, 53(3), 1710-1722

The potential to improve the oxidation resistance of BN coated on SiC fibers

Woo-Seong Tak[a, b], Jin-Uk Hwang[a], Su-Yean Lee[a], Woo-Sik Kim[a]*

[a] *Fibrous ceramics & aerospace materials center, Korea Institute of Ceramic Engineering and Technology, 101, Soho-ro, Jinju-si, Gyeongsangnam-do, 52851, Korea*

[b] *School of Cenvergence Science, Pusan National Univ., 2, Busandaehak-ro 63bean-gil, Busan-si, 46241 Korea*

E-mail: wskim@kicet.re.kr

Introduction

The strength of SiC fiber began to decrease from about 1400℃ because oxide layer that has lower strength than SiC helped crack progress to the SiC layer. Boron nitride, which has high thermal conductivity and thermal stability, has been used as a solid lubricant in SiC/SiC composites. In this study, we want to see the possibility that BN can improve the high-temperature oxidation resistance of SiC fiber as well as lubricant.

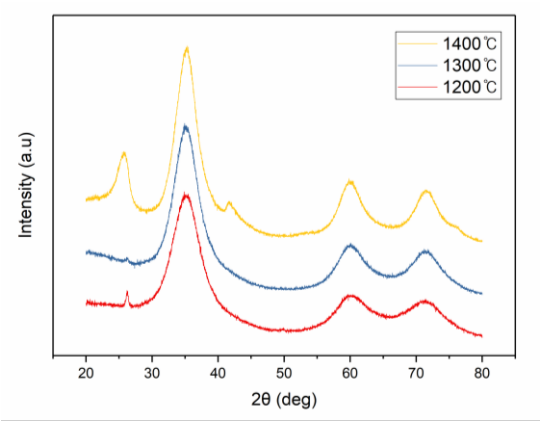

Experimental procedure

For surface modification of SiC fibers, ultrasonic treatment was performed for 3hours in 9M KOH solution after heat treatment at 800℃ for 1hour. After (3-aminopropyl) triethoxysilane was added to 50% ethanol solution and treated for 10hours at 80℃. The fiber surface was coated with graphene oxide (GO) by reacting the fiber modified with amine in GO solution at 80℃. The GO-coated fibers and SiC fibers were placed with boric acid in a furnace and treated for 2hours 1200-1400℃ with flowing N_2 and NH_3 gas.

Results and discussion

The hydroxyl surface is present on the GO surface coated with the fibers. Above a certain temperature, the carbon atoms bonded to the hydroxyl group are substituted with nitrogen atoms. Then, the carbon atoms that binding with N are replaced with boron atoms, and the process is repeated, which leads from GO to BN. X-ray diffraction analysis was performed to determine the crystallinity of this change, and the crystal pattern of hexagonal-BN was shown at 1400℃.

Fig 1. X-ray diffraction graph of SiC-BN fiber by atomic substitution

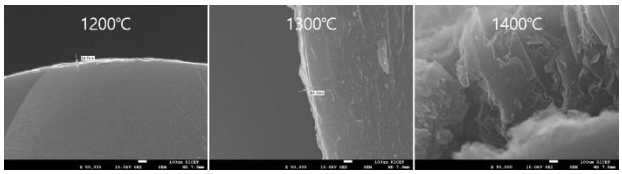

Fig 2. Cross-section morphology of the fiber by reaction temperature

Keywords: SiC fiber, Boron Nitride, Thermal resistance, Tensile strength

References:

1. K. Morishita, T. Matsumoto, S. Ochiai, et al., Mater. Trans. 48[2] (2007) 111-116

2. Y. Gong, G. Shi, Z. Zhang, et al., Nat. Commun. 5 (2014) 3193

Synthesis and Thermal Conductivity of N-doped Graphene Coated Aluminum Composites

Jin-Uk Hwang[a, b], Woo-Seong Tak[a], Soo-Yeon Lee[a], Sang-Yong Nam[b], Woo-Sik Kim[a, *]

[a] *Fibrous ceramics & aerospace materials center, Korea Institute of Ceramic Engineering and Technology, 101, Soho-ro, Jinju-si, Gyeongsangnam-do, 52851, Korea*

[b]*Functional nano laboratary, Gyeongsang National Univ., 501, Jinju-daero, Jinju-si, Gyeongsangnam-do, 52828 Korea*

E-mail: wskim@kicet.re.kr

Introduction

Aluminum is a metal with Competitive price, low density and good mechanical properties, as well as excellent thermal and electrical properties. Due to these characteristics, the heat dissipation substrate made of aluminum has high economic efficiency and good heat dissipation performance but the limits are clear.

Lots of attempts have been made to improve its thermal properties, and graphene has attracted much attention as an additive to improve conductivity by its extra ordinary characteristic such as electron mobility, thermal conductivity (~5,000 W/mK) [1] and mechanical properties (modulus: ~1 TPa, intrinsic strength: 130 GPa) [2]. Despite these superior properties, the mechanical strength of Al / GO composites was improved, but the thermal conductivity was rather reduced. Because uniform dispersion of graphene in aluminum matrix is difficult and the low interfacial properties between graphene and oxide layer on the surfaces of aluminum particles. In addition, rGO produced from graphene oxide has many defects and thus has overall lower characteristics than graphene.

We added aluminum particles to the pH-adjusted graphene oxide dispersion solution and coated heterogeneous materials through self-assemble reaction to produce composite particles in which graphene oxide was uniformly dispersed. Thermal conductivity can be improved by producing N-doped graphene through oxygen reduction reaction (ORR) of the manufactured composite surface.

Experimental procedure

Graphene oxide was added to 200 ml of distilled water and dispersed for 30 minutes using an ultrasonic generator. Nitric acid (HNO_3) was added to the solution to adjust the pH to 2, and then 10 g of aluminum particles were added and stirred until the solution was completely transparent. Al/GO particles are transferred to a solution in which melamine and urea are dissolved, stirred for 30 minutes, and then the remaining solution is removed using a vacuum filter and dried overnight in vacuum oven. The composite material containing the N source was doped by heat treatment, and then sintered through SPS.

Results and discussions

Composite materials were prepared by different graphene oxide addition amounts. The coating of graphene oxide using the self-assemble process on the aluminum surface was smooth. This resulted in the production of a composite material uniformly dispersed in the matrix and improved thermal conductivity than conventional aluminum. Nitrogen doping was confirmed that nitrogen atoms were doped in the form of Graphitic-N, pyrollic-N, pyridinic-N through hydrothermal and pyrolysis methods.

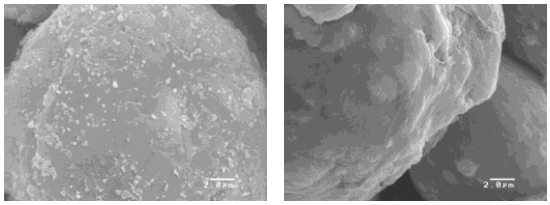

Fig. Micro morphology of (left) pristine aluminum particle (right) graphene oxide coated aluminum composites

Keywords: Heat dissipation material, Aluminum matrix composite, Graphene oxide, self-assemble, Thermal conductivity

References

1. Alexander A. Balandin, Suchismita Ghosh, Wenzhong Bao, Irene Calizo, Desalegne Teweldebrhan, Feng Miao, and Chun Ning Lau, Nano Latters Vol.8 (2008) 902-907

2. Ji Won Suk, Richard D. Piner, Jinho an, and Rodney S. Ruoff, ACS Nano Vol.4 (2010) 6557-6564

Effect of Pyrolysis Temperature on Heat-generating Behavior and Morphology of SiC Fiber Mats

Young-Jun Joo[ab], Dong-Gun Shin[a], Wook-Sik Kim[a], Kwang-Youn Cho[a]*

[a]*Fiber and Composite Center, Korea Institute of Ceramic Engineering and Technology, 101, Soho-ro, Jinju-si, Gyeongsangnam-do, 660-031 Korea*

[b]*Div. of Nano & Advanced Materials Engineering, Gyeongsang National Univ., 501, Ji nju-daero, Jinju-si, Gyeongsangnam-do, 52828 Korea*

E-mail: kycho@kicet.re.kr

Introduction

The development of polymer-derived SiC fibers have been focused on improving the heat-resistant characteristics because SiC fibers are generally used as a reinforcing material of the composite materials. In a previous study by Korea Institute of Ceramic Engineering and Technology (KICET), SiC fibers were fabricated in the form of multi-layered mats, which showed heat-generating behavior up to 1100°C under microwave. This fiber mats also reached a maximum temperature in about 30 sec. Therefore, a heat treatment system with SiC fiber mats under microwave can significantly reduce the time and cost of the thermal production process.

Experimental procedure

Polycarbosilane (PCS) as a ceramic precursor was melt-spun using spinning machine at 240°C into the fiber with a 20–25 μm diameter. The PCS green fibers were put into graphite crucible, and then heat-treated under the low pressure for the CVC process. The cured PCS fibers were lastly converted to SiC fibers through the pyrolysis in an argon atmosphere. In this experiments, the pyrolysis temperature was controlled to 1300–1450°C for 2 h, respectively.

Results and discussion

Silicon carbide fiber mats, which can generate heat under microwave, were fabricated at different pyrolysis temperatures. As the pyrolysis temperature increased, the strength of the fibers decreased relatively, and the maximum heat-generating temperature under microwave

increased due to the growth of delocalized π-electron in the SiC fibers. Also, SiC fiber mats with low oxygen content maintained its color and shape despite heat-generating up to 1560 °C under microwave for 2 h. In other words, the heat-generating temperature and life-time of SiC fiber mats were increased by controlling the pyrolysis temperature.

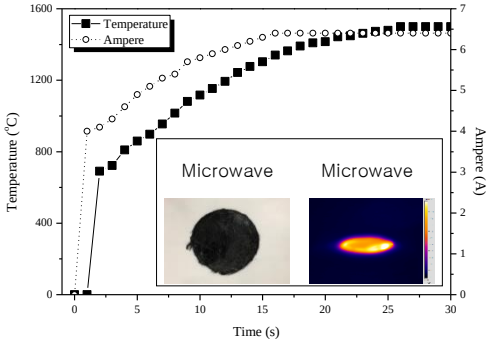

Fig. Time-temperature graph of polymer-derived SiC fibers mats under microwave

Keywords: SiC fiber, Microwave, Heat-generating, Morphology, Degradation

References:

1. K. E. Khishingbayar, Y. J. Joo, and K. Y. Cho, J. Korean Ceram. Soc. 54[6] (2017) 499-505

Mechanical and thermal properties of polymer-derived amorphous SiC block

Young-Jun Joo[ab], Kwang-Youn Cho[a]*

[a]*Fiber and Composite Center, Korea Institute of Ceramic Engineering and Technology, 101, Soho-ro, Jinju-si, Gyeongsangnam-do, 660-031 Korea*

[b]*Div. of Nano & Advanced Materials Engineering, Gyeongsang National Univ., 501, Ji nju-daero, Jinju-si, Gyeongsangnam-do, 52828 Korea*

E-mail: kycho@kicet.re.kr

Introduction

Silicon carbide (SiC), which has excellent mechanical and thermal properties, is generally synthesized by solid state sintering using α-SiC and β-SiC powder at high temperature (> 2000°C) under high pressure or by reaction sintering using silicon and carbon above 1500°C. In this study, amorphous SiC block was easily prepared using polycarbosilane (PCS), a ceramic precursor mainly used for SiC fibers or SiC coating. Also, the synthesis conditions were optimized for densification of amorphous SiC block. Amorphous SiC blocks derived from ceramic precursor can be fabricated easily and inexpensively compared to SiC sintered bodies, and therefore, it is expected to be applied to industrial fields as a structural material in a vicinity of 1300°C.

Experimental procedure

Bulk polycarbosilane (PCS) as a ceramic precursor was pulverized into a powder. PCS powder was placed in graphite mold with iodine metal and heat-treated at 180°C for 2 h. The ceramic yield-controlled PCS powder was pressed in a cuboid form using a uniaxial press. PCS blocks were pyrolyzed at temperature ranging from 1000 to 1300°C for 2 h under inert atmosphere.

Results and discussion

Amorphous SiC blocks have been successfully prepared using polycarbosilane. The XRD results showed that the SiC block had only broad β-SiC peak. The microstructure of SiC block became slightly porous as the heat treatment temperature increased. In addition,

the SiC blocks were finely ground via a ball-milling after controlling the ceramic yield of PCS for densification. As a result, densified SiC blocks were prepared and mechanical strength was measured via universal testing machine (UTM).

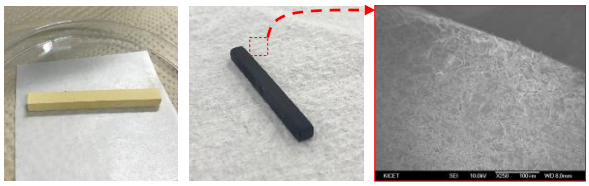

Fig. Photographs and SEM image of PCS block and polymer-derived SiC block.

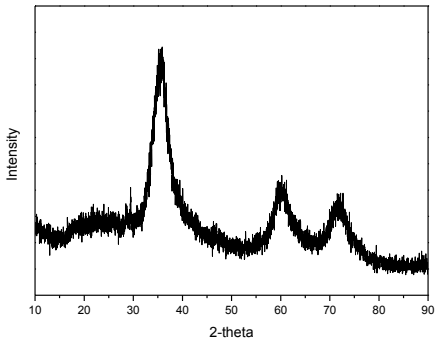

Fig. X-ray diffraction pattern of amorphous SiC block fabricated using ceramic precursor

Keywords: SiC block, Densification, Morphology,

References:

1. Y. J. Joo, K. Y. Cho, and C. J. Kim, J. Ceram. Process. Res. 20 (2019) 1-7

Fabrication and Characterization of Porous SiC Fiber Mats as Burner media for gas combustion system

Seong GunBae[ab], Dong Geun Shin[a]*, KwangYoun Cho[a], Yeong Keun Jeong[b]

[a]*Fibrous ceramics & Aerospace materials center, Korea Institute of Ceramic Engineering and Technology, 101, Soho-ro, Jinju-si, Gyeongsangnam-do, 52851, Korea*

[b]*Department of Convergence, Pusan National Univ., 63, 2busandaehak-ro, Geumjeong-gu, Busan,46241, Korea*

E-mail: Dgshin73@kicet.re.kr

Introduction

As global issues on energy and environment have been steadily raised last decades, interests on energy-efficient ceramics is also growing. Recently, research on ceramic porous bodies for gas combustion system with low NOx generation rate and high energy efficiency has been actively conducted. Among them, porous SiC fibers mat shows high temperature stability up to 1200^{o}C and excellent infrared heating efficiency.

In this study, we have investigated a low cost and efficient process to make porous SiC fiber mat and application to gas combustion burner media

Experimental procedure

SiC fibers were prepared by melt-spinning of polycarbosilane, a pre-ceramic polymer, into green fibers, followed by thermal oxidation at around 200^{o}C and spontaneously pyrolysis at inert atmosphere. Continuous SiC fibers were chopped into 10 to 50mm length and then dispersed uniformly to make porous mat before inter-connection coating by chemical vapor deposition. Porous mat was conducted gas-firing test.

Results and discussion

Silicon carbide deposition using the CVD process showed a linear increase in thickness with time, and 5-10um was considered to be the most suitable for the characteristics of the porous fiber mat. Non-destructive analysis of the fiber mat confirmed that the fibers were randomly arranged in general and that beta-silicon carbide was formed. It was found that the silicon carbide coating layer between the fibers induces physical contact and maintains its

shape.

As a result of gas combustion analysis, it showed a homogeneous exothermic tendency and no significant temperature deviation. Unlike commercially available fiber mats, there is no carbon present between the fiber and the CVD coating layer.

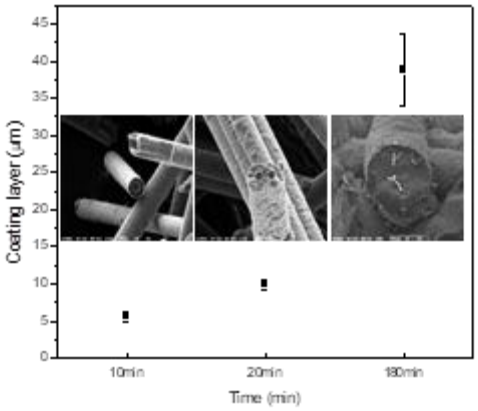

Fig. Silicon carbide-CVD coating layer versus coating times and its microstructure.

Keywords: SiC fiber, chemical vapor deposition, burner media, heating elements

References:

1. D. G. Shin, K. Y. Cho and D. H. Riu, Asian Journal of Chemistry; Vol. 24, No. 9(2012), 4225-4231

2. R.-U. Hasse and M. Kahlke, US Patent 5,800,157 (1998)

Morphological technique for age estimation from sacrum bone

Tatiya PhuphaleeandRachadaporn Benchawattananon

Integrated Science Faculty of Science Khon Kaen University Khon Kaen Thailand 40000

E-mail*: *tatiya.phu@gmail.com

Abstract

Age-at-death estimation of unknown human skeletal remains it is important to personal identification from crime scene investigation or a mass disaster. It necessary to develop reliable age estimation techniques for a different human bone. The aim of this study is to determine of the sacral vertebrae bodies fusion correlates with age in Northeast Thai skeleton sample. A four-stage range of fusion of the sacral vertebrae, from absence)degree 0(, fusion less than 50%)degree 1(, fusion more than 50%)degree 2(to complete fusion)degree 3(was used for scoring of individual sacra. And after that the sacral vertebral body fusion patternsconsisting of type a, b, c and d were determined. The sacrum bone sample was use in this study 513 sacra, 300 in male and 213 in female skeletons from the Khon Kaen Universitydocumented collection, ranging from 20 to 100 years in age and this study have 3 range age consist of young adult, middle adult and old adult. Thesacral vertebral body fusion pattern was significantly associated withage range)p = 0.000(. Incomplete fusion)degree 0 and 1(were prevalent in young adults)20-34 years(. Complete fusion)degree 3(is most frequent in old adults)over 50 years(, however, itdid not distinguish among young, middle)35-49 years(and old adults. And result of this study, young adult found sacral vertebral body fusion patterns type a= 90.48%, type c = 4.76% and type d = 4.76% , middle adult found sacral vertebral body fusion patterns type a= 96.30%, type b = 2.47% and type d = 1.23%, old adult found sacral vertebral body fusion patterns type a= 98.54%, type b = 1.46% . Anassociation of sacral fusion with age was observed. This study suggests that the scoring method of the degree of fusion of the anterior aspect of the sacral vertebrae can be a simple and informative tool for differentiating young adults from older adults in the Thai population.

Keywords: sacrum bone, age estimation, sacral vertebral body fusion

Role of Palladium Catalyst to the Addition Polymerization of Norbornenes

Dong Jin Lee, Ik Mo Lee, and Chan Kyung Kim*

Department of Chemistry and Chemical Engineering, Center for Design and Applications of Molecular Catalysts, Inha University, Incheon 22212, Korea

Polynorbornenes (PNBEs) synthesized by addition polymerization (AP) showing restricted rotation about the main chain have been predicted to have a number of attractive properties such as low moisture uptake, optical birefringence, and dielectric loss for optical and opto-electric applications. It was also known to have high chemical and thermal stability due to saturated structure of main chain, high glass transition temperature, and optical transparency. PNBEs typically suffer from brittleness, low solubility and adhesion, and poor processability in the molten state due to decomposition. From experimental work, novel Pd complexes containing NHC and β-diketonate ligands ([(NHC)Pd(β-diketonate) Cl]) were successfully synthesized by a simple substitution reaction between NHC salts and Pd(β-diketonate)$_2$. Catalytic activity of the complexes towards addition polymerization of various functional norbornenes exhibited high activity towards polymerization of polar functional norbornenes with the yields increased by the increased exo: endo ratio as expected. To understand the reaction mechanism, we have performed semi-empirical calculations using Gaussian 09 package. All the reactants, reactant complexes, transition states, product complexes, and products were fully optimized without geometrical constraint. The reaction proceeds through different channels depending on the solvent property. The stability of the stationary points is also affected by the solvent polarity.

Acknowledgements This work was supported by the Brain Korea 21 Plus and Inha University.

DFT Studies on third row element doping to TiO_2 Polymorphs

Jun Ren and Chan Kyung Kim*

Department of Chemistry and Chemical Engineering, Center for Design and Applications of Molecular Catalysts, Inha University, Incheon 22212, Korea

Photocatalytic degradation of environmental pollutants by semiconductor has aroused academic and industrial interests for more than decades. As one of the photocatalytic all-star semiconductor materials, titanium dioxide (TiO_2) remains the widely researched and promising photocatalyst owing to its relatively low cost, high optical absorption, and excellent chemical and optical reaction stability over a wide range of pH values and voltages for water splitting. The doing of third row elements is one of the methods to improve the properties of TiO2 crystals related to wavelength and electron-hole recombination. In this work, four polymorphs of TiO_2 lattice, such as rutile, anatase, brookite, and TiO_2(B), were considered to modify the bandgap using doping of small atoms. To understand the role of doping, we performed DFT+U calculations on the modified polymorphs by using the appropriate U(U-J) values. From the modified polymorphs, we have studied two cases: (1) third row atom (T) doping systems by substituting one Ti atom with one third row atom, (2) system with oxygen vacancy and third row atom (T) substitution. Our calculations show that introducing third row elements into Ti sites in the TiO_2 lattice lowers the formation energy and facilitates the formation of lattice defects in all the crystal structures. Additionally, introduction of doping atoms changed the Ti 3*d* gap states and thus, be conducive to the photocatalytic process.

Acknowledgements This work was supported by the Brain Korea 21 Plus and Inha University.

Synthesis and Characterization of Some Biological Relevant Lanthanide(III) Complexes of Thiosemicarbazone and Picoline

Ram K. Agarwal

Lajpat Rai Postgraduate College, (C C S University)

SAHIBABAD(GHAZIABAD)-201005, INDIA.

Coordination compounds are a class of substances with chemical structures in which central metal is surrounded by non-metal atoms or groups of atoms joined to it by chemical bonds. Coordination compounds include such substances in vitamin B12, hemoglobin, chlorophyll, dyes and pigments, and catalysts used in preparing organic compounds. Perhaps the earliest known coordination compound is the bright red alizarin dye first used in India and known to the ancient Persians and Egyptians, the first synthesis of a complex is available in literature by German physicist and alchemist Andres Libravius (1549-1615). Around the year 1600 he obtained blue [Cu(NH3)4]2+ from NH4Cl, Ca(OH)2 and brass in water. The modern theory of coordination chemistry is based on the work of Alfred Werner (1866-1919, Nobel prize in Chemistry in 1913). The application of coordination compounds is of great importance and play important functions in the area of analytical chemistry, metallurgy, biological function system, industries and medicines. Medicinal inorganic chemistry is a discipline of growing significance in both therapeutic and diagnostic medicine. The discovery and development of the antitumour compound cisplatin cis[Pt(NH3)2Cl2] played a profound role in establishing in the field of medicinal inorganic chemistry.

Thiosemicarbazones and their metal complexes are a broad class of biologically active compounds. Mixed ligand complexes of transition metal containing ligands with N, S and N, S, O donors are known to exhibit interesting stereochemical, electrochemical and electronic properties. The real impetus towards developing their coordination chemistry was due to their physic-chemical properties and significant biological activities. Heterocyclic compounds are widely distributed in nature and are essential to life. They play a vital role in the metabolism of all living cells. The chemistry of heterocycles will continue to grow for the creation of new drugs, agrochemicals, novel materials etc. Pyridine and derivatives possess significant importance. In present studies some mixed ligand

complexes of lanthanides (III) derived from 4[N(2',4'-dichlorobenzalidene) amino] antipyrine thiosemicarbazone (DCBAAPTS) and -picoline (-Pic) with the general composition $LnX_3.n$(DCBAAPTS). Pic (Ln = La, Pr, Nd, Sm, Gd, Tb, Dy or Ho; X = NO_3^-. n = 1; X = NCS^- or ClO_4^-, n = 2 are reported. All the synthesized complexes were characterized through various physico-chemical studies. The coordinated DCBAAPTS behaves as neutral tridentate (N, N, S-donor) while -picoline acts as unidentate N-donor. The ligand and the corresponding Ln(III) complexes were simultaneously screened for their antibacterial and antifungal activities.

A Study on the Design and Fabrication of Wafer Scale Microlens Modules

Young Bok Lee, Hyung Woo Kim, Yongjin Yoo, Geonwoo Lee,

Dae-Wook Kim, Seungjoon Ahn, Ho Seob Kim

Department of Physics and Nanoscience and Center for Next-Generation Semiconductor Technology, Sun Moon University, Asan-si Chungnam Korea, 31460

Abstract:

Since the creation of the first microcolumn in the 1990s, research and improvement on microcolumn have been made in various ways. [viii][ix] One of the most important aspects of microcolumn characteristics is very small and simple structure. The total length is 10mm and has a electrostatic lens structure consisting of only a few electrodes. Among the various applications of microcolumn, it is the multi electron beam system that makes the best use of these features. [x][xi]The multiple electron beam system composes a number of electron beam equipment in a given area in the proposed manner to improve the low throughput of the electron beam equipment, thereby increasing the throughput. Microcolumn is small in size and simple in structure, and has a relatively simple advantage of being able to install more numbers in the same area. Microcolumn is made very elaborate through the MEMS process. In multi electron beam systems, increasing the number of microcolumn deployments creates several difficulties, including the time and cost of producing individual microcolumns and the difference in the equivalence between microcolumns. Wafer scale microcolumn was proposed to solve the problem of multi electron beam system using existing single column. Wafer scale microcalum is designed to overlap Si wafers on multiple layers, so that pattered electrodes and wiring on them function as microwave or microcolumn.[xii] The arrangement of wafer scale microcolumns studied in the past is usually a difficult structure to actually produce when the maximum number is determined in theory. In this study, the efficient layout structure and manufacturing process of wafer scale microcolumn were conducted.

[viii] T. H. P. Chang, D. P. Kern and L. P. Muray, J. 1990, Vac. Sci. Technol. B8 (6): 1698-1705

[ix] E. Kratschmer, H. S. Kim, M. G. R. Thomson, K. Y. Lee, S. A. Rishton, M. L. Yu, S. Zolgharnain, B. W. Hussey, and T. H. P. Chang, 1996, J. Vac. Sci. Technol. B 14, 3792-3796

[x] T. H. P. Chang, M. G. R. Thomson, E. Kratschmer, H. S. Kim, M. L. Yu, K. Y. Lee, S. A. Rishton, B. W. Hussey, and S. Zolgharnain, 1996, J. Vac. Sci. Technol. B 14, 3774

[xi] L. P. Muray, K. Y. Lee, J. P. Spallas, M. Mankos, Y. Hsu, M. R. Gmur, H. S. Gross, C. B. Stebler, and T. H. P. Chang, 2000, Microelectron. Eng. 53, 271

[xii] H. Kim, C. Han, J. Kim, H. S. Kim, and K. Chun, 2004, J. Vac. Sci. Technol. B 22, 2912

Kinetic analysis on the curing kinetics of epoxy/Ni-PS composites

Yi Hao, Pian-pian Zhao, Shuang Liang, Meng Wu, Qiao Shi, Ji-nian Yang*

School of Material Science and Engineering, Anhui University of Science and Technology, Anhui, Huainan, 232001, China

Corresponding to Jinian Yang (yangjinian@163.com)

ABSTRACT: Nickel phyllosilicate (Ni-PS) was synthesized by hydrothermal method, and then introduced into epoxy resin to generate the composites via solution method, with 4,4′-diamino diphenyl methane as the hardener. XRD, SEM, FT-IR, and TGA were utilized to investigate the phase structure, morphology, thermal stability, etc. The effect of Ni-PS on the curing behavior of epoxy was studied by DSC. Results showed that Ni-PS was successfully obtained with lamellar structure and excellent thermal stability. It is noted that the addition of Ni-PS shows scare influence on the curing behavior of epoxy. Based on the mathematic models of Starink and Málek methods, the kinetic analysis of curing properties of epoxy and the composites have been performed and some characteristic parameters have been calculated with the aid of least square regression (LSR) procedure. The resulted conclusion has verified the experimental observation, indicating the autocatalytic process for both the control sample and the composites.

Keywords: epoxy; nickel phyllosilicate; curing; kinetic analysis

Preparation of Novel Carbon Materials and Their applications in Electrode materials

Youyang Chen, Jing Wang*, Zhihao Hu, Xiachun Zhu, Qin Chen

** School of Materials & Science Engineering, Anhui University of Science& Technology, Anhui, 232001, CHINA*

*jingwang@aust.edu.cn

Abstract: Now the polyaniline electrode of Supercapacitorshas the problems of poor circulation stability, low actual capacitance and low conductivity. As a new type of carbon material, both carbon quantum dots and graphene have large specific surface area, which can provide more space for electronic transmission and storage. In this paper, a new type of carbon material with plane-point structure was prepared based on the preparation of carbon dots and the combination of graphene and carbon dots. Carbon quantum dots were prepared by microwave and electrochemical process. Then carbon dots were doped into the polyaniline system by in-situ polymerization, and the composite electrode was improved in the aspects of conductivity, specific capacitance and cycling stability. Compared with pure polyaniline at 0.5 A/g current density, the specific capacitance of PANI@25minCQDs composite electrode was improved by 25.72%, and the specific capacity was maintained at 78% after 1000 cycles under 5 A/g current density. By using graphene matrix and hydrothermal composite of carbon dots and graphene oxide, a carbon material with a plane-point structure was successfully prepared. Using the size advantage of carbon dots and abundant functional groups, the graphene was modified effectively and the graphene stacking phenomenon was greatly improved. The GO@CQDs composite material prepared has a flatter structure, larger actual specific surface area and better mechanical strength. The electrochemical properties of the composite electrode PANI@GO@CQDs were greatly improved after the GO@CQDs was compounded into the polyaniline system.

Keywords: Carbon quantum dots; Graphene; Polyaniline; Specific capacitance; Electrochemical

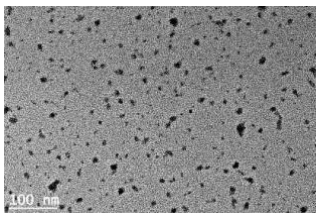

A

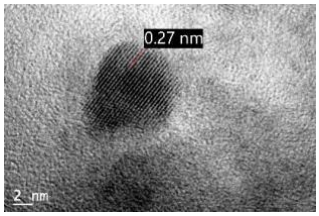

C

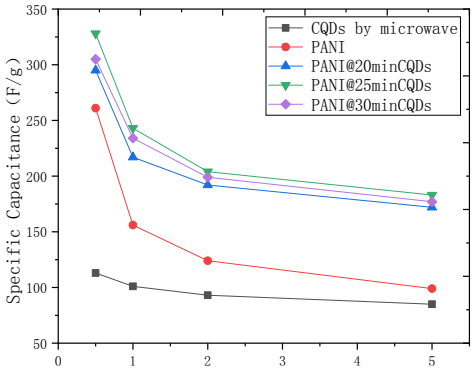

B

Figure 1 (A)TEM of CQDs (B)HR-TEM of CQDs. (C) GCD curves of CQDs/PANI composites

Experimental investigation and thermodynamic modeling of the Cu-Cr-Ni、Cu-Cr-Ag and Cu-Ag-Si systems

Chengliang Qiu, Biao Hu*, Jiaqiang Zhou, Yin Liu, Yu Zhang, Jin Zhang

School of Materials Science and Engineering, Anhui University of Science and Technology, Huainan, Anhui 232001, PR China

Abstract

The phase equilibria of the Cu-Cr-Ni, Cu-Cr-Ag and Cu-Ag-Si systems were investigated combining thermodynamic modeling with key experiments. Thirty-sixternary alloys of the Cu-Cr-Ni, Cu-Cr-Ag and Cu-Ag-Si systems were prepared to determine the isothermal sections by means of X-ray diffraction (XRD) and scanning electron microscopy with energy dispersive X-ray spectroscopy (SEM/EDX). The three- and two-phase equilibria were accurately determined. The solubility of the third elements in the phases of the binary systemswas measured. Based on the experimental equilibria data from the literature and the present work, a thermodynamic modeling of the Cu-Cr-Ni, Cu-Cr-Ag and Cu-Ag-Si systems was performed by using the CALPHAD (CALculation of PHAse Diagrams) method. The substitutional solution model was used to describe the solution phases. A set of self-consistent thermodynamic parameters of the Cu-Cr-Ni, Cu-Cr-Ag and Cu-Ag-Si systems was obtained. Most of the experimental data can be well reproduced by the present thermodynamic modeling.

Keywords: Cu alloys; Phase equilibria; Thermodynamic modeling; Experimental investigation

Acknowledgments

The financial support from Natural Science Research Projects of Colleges and Universities in Anhui Province (Grant No. KJ2019A0113) and Anhui Province Postdoctoral Science Foundation (Grant No. 2017B210) are greatly acknowledged.

***E-mail address: hubiao05047071@163.com (B. Hu); Tel.: +86 554 6601194**

Thermodynamic modeling of the Ag-X (X=B, Fe, Sm, Pu) binary Systems

Jiaqiang Zhou, Biao Hu*, Chengliang Qiu, Yin Liu, Jin Zhang, Yu Zhang

School of MaterialsScience and Engineering, Anhui University of Science and Technology, Huainan, Anhui 232001, PR China

Abstract

Based on the phase equilibria and thermodynamic properties data available in the literature, the Ag-X (X = B, Fe, Sm, Pu) binary systems were assessed by means of the CALPHAD (CALculation of PHAse Diagram) approach. In the Ag-Sm system, six intermetallic compounds, i.e. α-Ag_2Sm (the low-temperature form of the Ag_2Sm), β-Ag_2Sm (the high-temperature form of the Ag_2Sm), AgSm, $Ag_{51}Sm_{14}$, $Ag_{51}Pu_{14}$ and Ag_2Pu, were treated as stoichiometric phases. The solution phases including liquid, (Ag), (βB), (αFe), (γFe), (δFe), (αSm), (βSm), (αPu), (βPu), (γPu), (δPu) and (δ'Pu) were described by the substitutional solution model with the Redlich-Kister polynomial equation. A set of self-consistent thermodynamic parameters was finally obtained in the present work. Comparisons between the calculated and measured phase diagrams and thermodynamic properties indicate that almostall of the reliable experimental information is satisfactorily accounted for by the present modeling.

Keywords: Ag-X (B, Fe, Sm, Pu); CALPHAD; Phase diagram; thermodynamic modeling

Acknowledgements

The financial support from the Natural Science Research Projects of Colleges and Universities in Anhui Province (Grant No. KJ2019A0113) and Anhui Province Postdoctoral Science Foundation (Grant No. 2017B210) are greatlyacknowledged.

***E-mail address: hubiao05047071@163.com (B. Hu); Tel.: +86 554 6601194**

The Preparation of Ceramic Tiles of $CaO-B_2O_3-SiO_2-ZnO-BaO$ Glass/$CaO-B_2O_3-SiO_2$Glass System

Guotao Dong, Jing Wang*[a], [b]EnxiangGuan

*[a] *School of Materials & Science Engineering, Anhui University of Science& Technology, Anhui, 232001, CHINA*

[b]*Chemical & Material College, Huainan Normal University, Anhui, 232001, CHINA*

**jingwang@aust.edu.cn*

Abstract: Nowadays, the whole electronic machine is developing in the direction of miniaturization, portable, digital, multi-function, high performance and high reliability, which requires that electronic components increasingly tend to miniaturization, lightweight, high integration and high performance.The low temperature co-fired ceramic technology makes the circuits interconnect vertically, breaks through the limitation of designing circuits in a single plane, puts forward an ideal solution for designing circuits in three-dimensional space, and greatly promotes the miniaturization and lightweight of electronic components.In this paper,$CaCO_3$, H_3BO_3 and SiO_2 were mixed in 7:1:2 proportion and placed in corundum crucible to prepare CBS glass by high temperature melting method. $CaCO_3$, H_3BO_3, SiO_2, ZnO, $BaCO_3$ and other raw materials were mixed in 10:4:3:3:5 proportion and placed in corundum crucible to obtain CBSZB glass by high temperature melting method. According to the ratio of CBSZB: CBS=6:4, CBSZB, CBS glass and proper amount of water were milled, dried and screened, and the composite powder of CBS/CBSZB was obtained. Then the raw porcelain sheet was prepared by casting, and then the sintering properties of the raw ceramic sheet and its co-firing matching with electronic slurry were studied.

Keywords: Glass, LTCC, Green Tape

Study on Modification of Concrete Foaming Agent

Ye Ge, Jing Wang*

** School of Materials & Science Engineering, Anhui University of Science& Technology, Anhui, 232001, CHINA*

*jingwang@aust.edu.cn

Abstract: Foam concrete is a kind of light and excellent environmental protection material. There are many factors affecting the properties of foam concrete, among which the influence of foaming agent is most significant. By observing and measuring the foaming amount, half-life, 1-hour bleeding amount and 1-hour settlement distance of different kinds of foaming agents, the stability of foam and the size of bubble hole were compared, and the comprehensive properties of foam were measured by adding it to a certain proportion of concrete, so that the stability and distribution of foam hole in concrete can be observed more intuitively and realistically. The excellent foaming agent type formula was achieved and the foam concrete with excellent performance was fabricated.

In this experiment, sodium lauryl sulfate (3g/L) lauryl alcohol (0.6g/L) was used as the basic foaming mix, in which silica fume, nano-silica or cellulose ether were added to explore the effect of silica fume, nano-silica or cellulose ether on foaming, and the foaming agent was modified. On the other hand, animal protein foaming agent and plant protein foaming agent have high foaming capacity and good foam stability. In this paper, we want to explore the best mixing ratio of animal and plant protein and water, and test their foam stability. The comprehensive properties of concrete were tested and the similarities and differences between them and surfactants foaming agents were compared.

By configuring different kinds of foaming agents and adding silica fume and cellulose ether to the foaming agents of surfactants, it is found that the consistency and foam stability of foam can be improved by adding 4g/L silica fume on the basis of basic foaming combination. When silica fume is mixed with hydrophilic nano-silica, the effect is better. The viscosity of foam increased obviously by adding cellulose ether, but the defoaming and foaming in concrete was obvious. The foam performance of animal protein foaming agent is better than that of plant protein blowing agent. The foam performance of plant protein blowing agent is the worst. The optimum ratio of animal protein to water is 1: 20.and the optimum ratio of plant protein to water was 1:40.

Keywords: foam; modification; stability; foam concrete

Controllable Preparation of Transition Metal Double Oxides for Nano-scale Hollow Polyhedral Structures for Supercapacitors

Zhihao Hu, Jing Wang*, Youyang Chen

** School of Materials & Science Engineering, Anhui University of Science& Technology, Anhui, 232001, CHINA*

*jingwang@aust.edu.cn

Abstract: Nowadays, the world is facing an increasingly severe energy crisis and the resulting environmental problems. Researchers are committed to developing new energy materials and energy storage devices, and supercapacitors are one of the hottest energy storage devices. Similar to ordinary batteries, supercapacitors are also composed of two electrodes and a kind of electrolyte. The electrode materials mainly include carbon-based materials, metal oxides, and conductive polymers. In this paper, a bimetallic oxide powder with a specified morphology was prepared by a controlled hydrothermal synthesis method to prepare a bipolar material for a water-based supercapacitor. A predetermined ratio of the cobalt salt and the manganese salt are mixed by a chemical solution coprecipitation method, and a dimethylimidazole aqueous solution is added dropwise as a ligand, stirred at room temperature, washed and dried to obtain a ZIF-67 precursor, and then the precursor is obtained. A Mn-Co layered double hydroxide with a hollow n-dodecahedral structure was obtained by a hydrothermal method, then heated in a muffle furnace, and the powder was obtained. The electrode was prepared by grinding the powder with a conductive agent, binder, dispersant, and its electrochemical performance was tested in alkaline electrolyte conditions. It is then assembled into an asymmetric supercapacitor and tested for its performance.

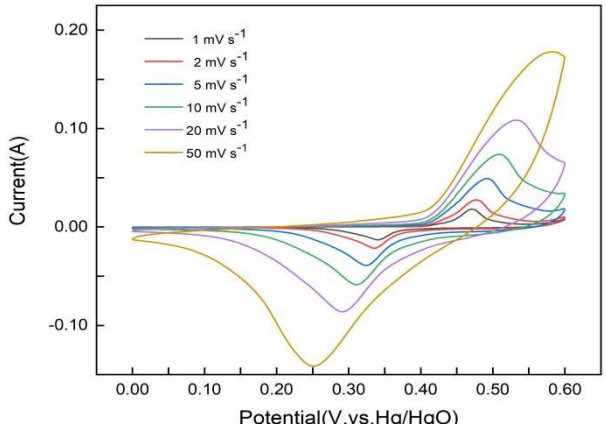

Keywords: Bimetallic oxide; Hydrothermal method; Hollow n-dodecahedral structure; Electrochemical performance

Synthesis of Low-temperature Belite- CalciumSulphoaluminate-Ternesite Cement and their Hydration

Qin Chen, Jing Wang*[a], Wei Guo*[b], Xiao Wang, Youyang Chen, Zhihao Hu

*[a] *School of Materials & Science Engineering, Anhui University of Science& Technology, Anhui, 232001, CHINA*

*[b] *School of Materials Science & Engineering, Yancheng Institute of Technology, Yancheng, 224001, CHINA*

**jingwang@aust.edu.cn,*guowei68550@163.com*

Abstract: In this work, Belite-Calcium sulphoaluminate-Ternesite (BCT) cement clinkers were prepared by using industrial by-products such as slag, steel slag and kaolin as raw materials. Based on C_2S: $C_4A_3\$$ of 55: 45, four groups of the $C_5S_2\$$ percentages were designed and prepared. The $C_5S_2\$$ percentage (wt.%) increased from 5 wt.% in increments of 5 wt.%. The cement clinker with the main minerals of belite (C_2S), calcium sulphoaluminate ($C_4A_3\$$) and ternesite($C_5S_2\$$) was prepared by hydrothermal synthesis-low temperature calcination. The influences of calcination temperature on the mineralogical compositions of cement clinker was studied, and the compressive strength development of the hydrated BCT cement paste was tested. The phase evolution and microstructure of the hydrated paste was analyzed using the X-ray powder diffraction (XRD) and scanning electron microscopy (SEM) techniques. And the compressive strength was tested to determine the effects of the different ratio in the C_2S-$C_4A_3\$$- $C_5S_2\$$ hydration system on the mechanical properties, hydration process, and hydration mechanism. Meanwhile, the hydration properties of the hardened cement paste, including hydration rate, hydration heat release and microstructures of hydration products, were characterized.

The results show that when the precursor is hydrothermally synthesized at 95 °C, the BCT cement clinkers can be fabricated under a low temperature of 1200 °C. It can be seen from the XRD pattern that the BCT cement clinkers fired with slag as the main raw material has the best synthetic effect compared with steel slag and kaolin. In the CN-1~ CN-4 samples, the BCT cement clinkers of CN-2 (C_2S: $C_4A_3\$$= 55: 45, $C_5S_2\$$ = 10 wt%) have the highest compressive strength after hydration, up to 103.7MPa. It can be seen from the hydration XRD pattern and the SEM image that the hydrated samples contain a large amount of AFt and a small amount of

AFm. It proves that $C_4A_3\$$ and $C_5S_2\$$ in the cement have been basically hydrated at 21d, and C_2S has also been partially hydrated to form C-S-H gel and $Ca(OH)_2$. Through mathematical modeling, it can be seen that the compressive strength of cement can still grow.

Keywords: belite-calcium sulphoaluminate-ternesite cement; hydrothermal synthesis; low temperature calcination; hydration

Table 1 Hydration performance of BCT cement

	3d	7d	14d	28d
CN-1	22.07	34.975	39.69	70.22
CN-2	44.8	38.73	75.21	103.73
CN-3	47.64	26.97	49.23	81.74
CN-4	54.93	36.18	70.6	90.87

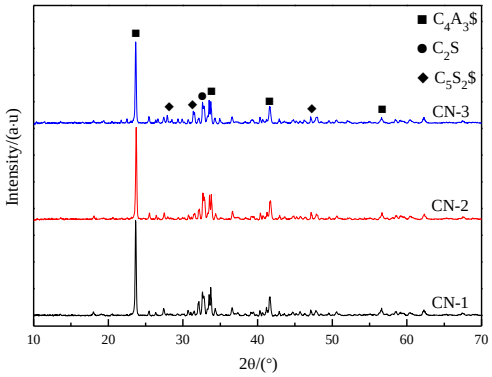

Figure 1 XRD of different formulations of BCT cement clinker

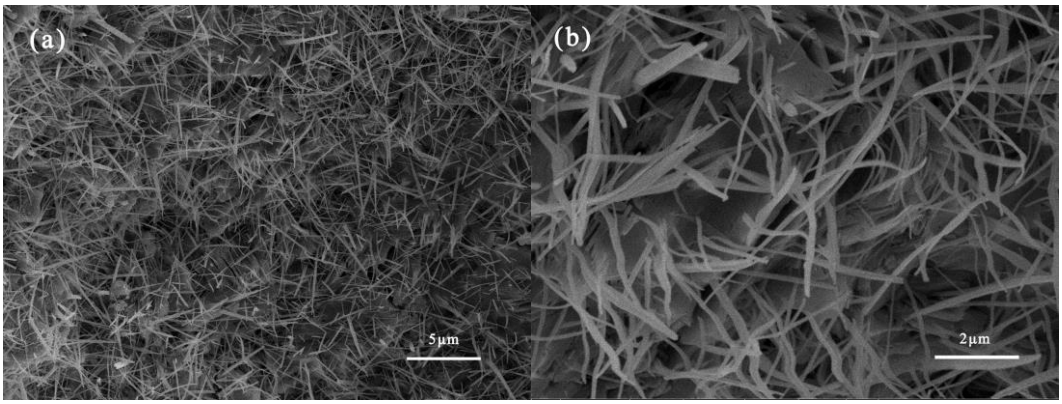

Figure 2 SEM morphology of BCT cement hydration product

Study on the Rapid Preparation Technology of Carbon Quantum dots

Jing Wang*，Tianhao Hu

** School of Materials & Science Engineering, Anhui University of Science& Technology, Anhui, 232001, CHINA*

*jingwang@aust.edu.cn

Abstract: Carbon quantum dots (CQD), often referred to as carbon dots, have become an important member of nanomaterials since their appearance in people's field of vision. Carbon quantum dots (CQD) are still the research focus of nanomaterials. There are many ways to prepare carbon quantum dots, including microwave, hydrothermal and electrochemical methods. Microwave method is to obtain carbon quantum dots by heating carbon precursors. Usually, propylene glycol is mainly used as raw material for preparation (common carbon sources can also be used in egg white, fruit juice and glucose, etc). The electrochemical method is mainly used to prepare carbon quantum dots from graphite electrodes by oxidizing water molecules. In the experiment, the working electrode was carbon rods and graphene, etc, the current or voltage was adjusted, and with anodic oxidation process, electrolyte got into graphite layer and with other treatments to peel large carbon materials into small carbon nanoparticles. The pure carbon quantum dot solution was obtained by centrifugation and purification. In addition, we also analyzed the ultraviolet and infrared spectra of the products, and the effects of PEG dosage, microwave heating time, microwave power and other factors in the test, so as to explore the performance characteristics of carbon quantum dots, and further study the unique application. Based on this point, this paper will explore carbon quantum dots in depth from the perspective of experiments, and conduct detailed research and analysis of its rapid preparation scheme through various control experiments.

Keywords: Carbon quantum dots, fluorescence carbon dots, microwave method , Electrochemical method

In-situ synthesis of carbon@Ni and high microwave absorption performance

Hengdong Ren, Yin Liu*

School of Materials Sciernce and Engineering, Anhui University of Science and Technology, Huainan 232001, China

***Corresponding authors:** yinliu@aust.edu.cn (Yin Liu)*

Abstract: Due to the rapid development of electronic communication equipment, the resulting microwave pollution can damage human health and cause electronic equipment to fail to operate normally. In order to solve this problem, a layered carbon composite Ni was prepared. In this work, the prepared pure carbon shows an optimum reflection loss of -31.84 dB at 9.52 GHz with a coating thickness is 2.29mm. At the same temperature, Carbon@Ni synthesized by coal in a ratio of 1:1 than nickel chloride hexahydrate achieved a reflection loss of -56.64 dB and a thickness of 2.31 mm at 10.40 GHz. It is proved that the Carbon composite nickel has excellent microwave absorption properties. Besides, we explored the effect of temperature and nickel doping ratio on microwave absorption performance. By adding magnetic metal, the magnetic loss of the carbon material can be improved, and a better impedance matching is obtained, so that the microwaves pass through the material with less reflection and more absorption. In addition, carbon is an ideal microwave absorbing material because of its light weight, high stability and low cost.

Key words: Microwave absorption; Carbon; Magnetic metal; Electrical conductivity

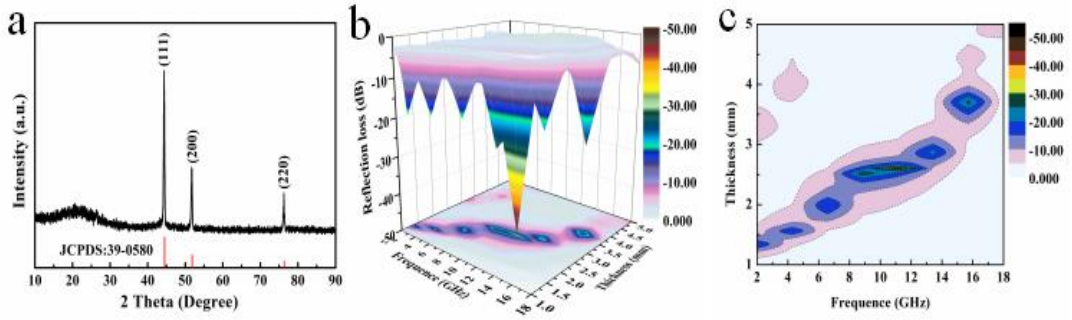

Fig.1. (a) XRD patterns, (b) three-dimensional representation of reflection loss and (c) contour maps of the carbon@Ni.

Enhanced Microwave Absorption Properties of (1-x) $CoFe_2O_4$/xCoFe Composites at Multiple Frequency Bands

Jun Zhou, Yin Liu*

School of Materials Science and Engineering, Anhui University of Science and Technology, Huainan 232001, Anhui, China

Abstract: (1-x) $CoFe_2O_4$/xCoFe composites with x=0.3, 0.4, 0.5, 0.6 were synthesized by using a hydrothermal method. The effects of compositions of the $CoFe_2O_4$/CoFe composites on their microwave absorption properties were studied. The sample with a composition of $0.4CoFe_2O_4/0.6Co_4Fe_6$ showed optimal reflection loss (RL) -58.22 dB at 12.96 GHz, and the matching thickness was 1.45 mm. Meanwhile, it had an effective absorption frequency range of 11.12-15.28 GHz (RL<-10 dB), with a bandwidth of 4.16 GHz, covering the X-band and Ku-band. The enhanced microwave absorption properties of the composites, as compared with the two components, are attributed to the strengthened natural resonance and the increased impedance matching. Most importantly, by adjusting their composition, the $CoFe_2O_4$/CoFe composites can be used as microwave absorbers at C, X or Ku bands. Consequently, these $CoFe_2O_4$/CoFe composites are promising candidates that can be used to design effective microwave absorbers over wide frequency bands.

Keywords: $CoFe_2O_4$; CoFe; impedance matching; microwave absorption

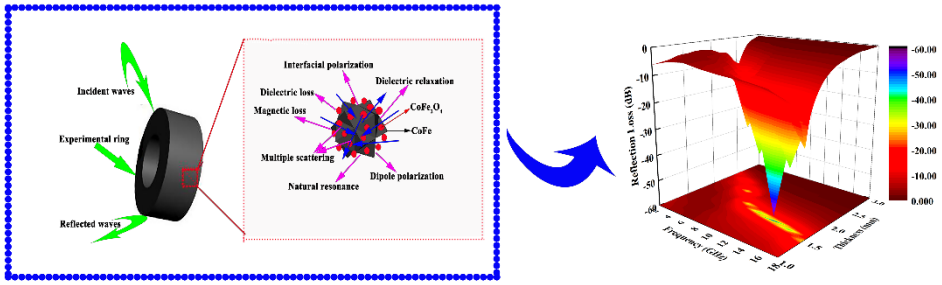

Schematic of microwave absorption mechanisms of the $CoFe_2O_4$/CoFe composites.

*Corresponding authors: yinliu@aust.edu.cn (Yin Liu)

Resource Utilization of Polygorskite

Sheng Wang, Yin Liu*

School of Materials Science and Engineering, Anhui University of Science and Technology, Huainan 232001, Anhui, China

**Corresponding authors:yinliu@aust.edu.cn*

Abstract: Attapulgite is a natural nonmetallic clay mineral, withexcellent properties, owing to its special crystal structure. The ideal chemical formula is $Mg_5Si_8O_{20}(OH)_2(OH_2)_4 \cdot 4H_2O$. Fig. 1 shows crystal structure of palygorskite. Natural attapulgite is non-toxic and cost-effective, making it potential for a wide range of applicationsHowever, there are often impurities in natural attapulgite clay, such as jellyfish cloud, dolomite, quartz and montmorillonite. The presence of these impuritieswould weaken the gelatinization, decolorization and adsorption capabilities of attapulgite. As a result, in order to make full use of attapulgite, it is necessary to purify the original ores. The applications will be focused on pollution treatment, soil remediation and photocatalysts.

Keywords: Attapulgite clay, Impurity, Purification, Application, Adsorption

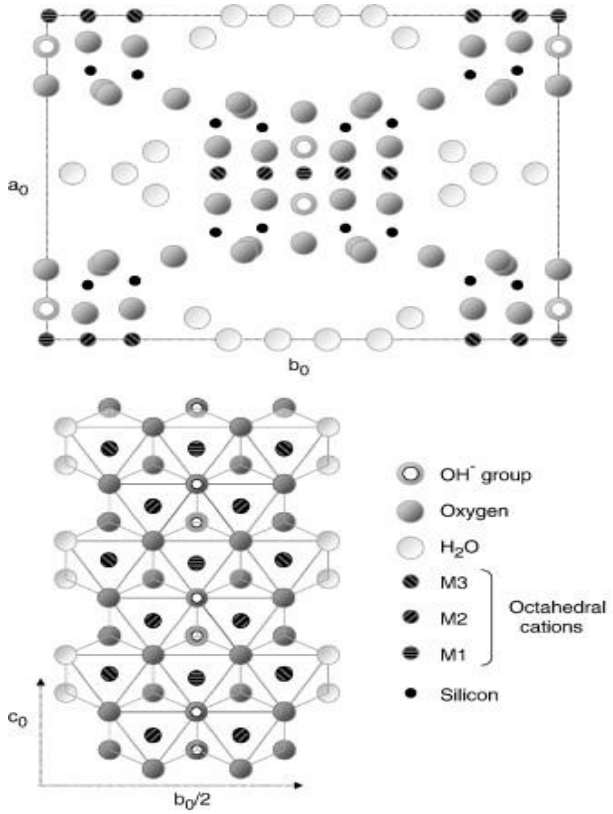

Fig. 1. Crystalline structure of attapulgite.

Preparation and Photocatalytic Degradation of Single-Layer TiO_2 Photocatalyst

Wei Lian[1], Qian Zhai[1], Yueqin Wang[2], Yin Liu[1†]

1. *School of Materials Science and Engineering, Anhui University of Science and Technology, Huainan 232001, Anhui, China*
2. *School of Mechanics and Photoelectric Physics, Anhui University of Science and Technology, Huainan 232001, Anhui, China*

Abstract: An amorphous silica/TiO_2 material was prepared by hydrolyzing an ester titanium source, using amorphous silica extracted from coal gangue as a carrier. XRD analysis shows that the characteristic peaks of TiO_2 shift to a large angle and the spacing between crystal planes decreases. The separation efficiency of photogenerated carriers will also be improved. The smallest molar ratio of silicon to titanium is 6:4(ST6). SEM shows that the surface of ST6 sample is smooth and uniform. BET shows that it has abundant mesoporous and microporous materials with a specific surface area of 78.81 m^2/g, a pore volume of 0.027 cm^3/g and an average pore size of 29.16nm.It was observed from FT-IR that there was Si-O-Ti bond in ST6, but there was no Ti-O-Ti bond, which indicated that the distribution of titanium dioxide on the surface of amorphous silica was monolayer.Ultraviolet-visible diffuse reflectance results show that the energy band of ST6 (3.04) is close to that of titanium dioxide (3.0). At the same time, the degradation rate of RhB reached 89% after 60 minutes. This experiment provides a method to prevent the recombination of electrons and holes by reducing the spacing between crystal planes, and to increase the photocatalytic rate of photocatalytic materials.

Keywords: Photocatalysis; load; Titanium dioxide; Amorphous silica; RhB

†Corresponding author: Tel:86-554-6668643; E-mail: yinliu@aust.edu.cn (Liu Yin)

Enhanced electromagnetic absorption performance of silane coupling agent KH550@Fe_3O_4 hollow nanospheres/graphene composites

Xiangfeng Shu, Yin Liu*

School of Science and Engineering, Anhui University of Science & Technology, Huainan 232001, China

**Corresponding authors: yinliu@aust.edu.cn (Yin Liu)*

Tel: 86-554-6668643

Abstract: In this experiment, the monodisperse Fe_3O_4 particles were controlled to obtain the precursor nanospheres with the best morphology and performance. Then the surface was modified with silane coupling agent KH550 and combined with rGO to obtain the composite (KF1-2) for the best absorbing property. The main challenge in the preparation of Fe_3O_4/rGO composites is the dispersion of magnetic nanoparticles and their adhesion to the rGO flexible substrate. Therefore, the surfactant coupling agent KH550 was selected as the surface treatment agent for Fe_3O_4 to increase the hydrophobicity, thereby improving dispersibility and adhesion. The composition, microstructure and electromagnetic properties of thecomposites were systematically studied by using various analytical techniques. The KF1-2 composite prepared by the mass ratio of modified KH550@Fe_3O_4 to GO was 1:1 which could achieve a maximum reflection loss (R_L) of -57.87 dB at 14.96 GHz, from 13.1 GHz to 17.6 GHz with the broadband of 4.5 GHz and particularly the thickness was only 1.48 mm, demonstrating the ultra-thin and high-intensity electromagnetic wave absorption capability of this composite material.

Keywords: Hollow Fe_3O_4nanospheres, KH550, Graphene, Solvothermal method, Electromagnetic absorption

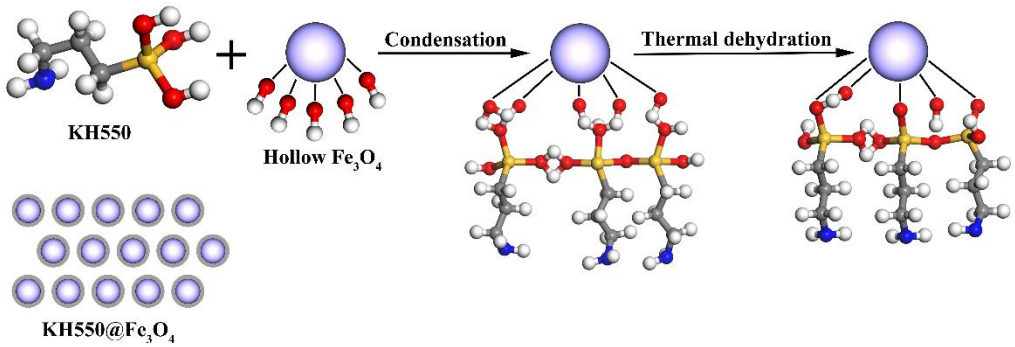
KH550
Hollow Fe_3O_4
Condensation
Thermal dehydration
KH550@Fe_3O_4
EG / 200 °C / 16~24h
Formation of Hollow Fe_3O_4 sub-nanoparticles
Aggregation

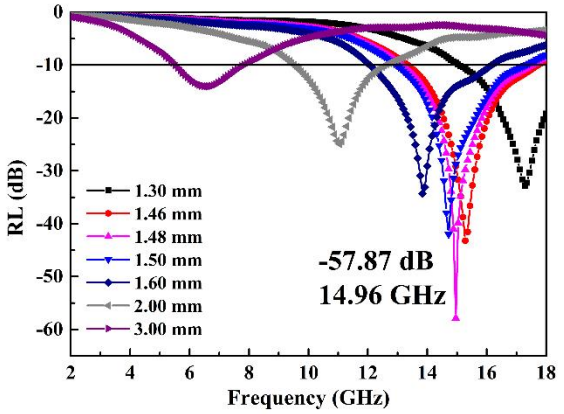
RL (dB)
Frequency (GHz)
1.30 mm
1.46 mm
1.48 mm
1.50 mm
1.60 mm
2.00 mm
3.00 mm
-57.87 dB
14.96 GHz

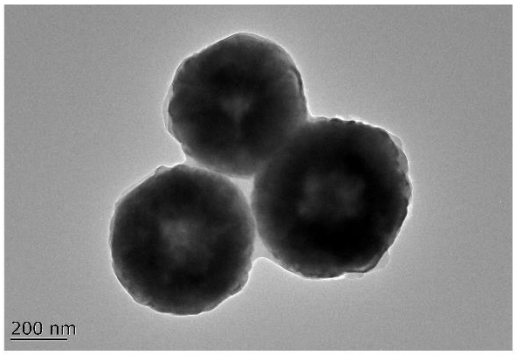
200 nm

MicrocantileverSensors Coated with Doped Polyaniline for the Detection of Humidity

Yongsong Mei, ShiqinLi, Dongyang Yu, ZhaofaYang, Changguo Xue*

School of Material science and Engineering, Anhui University of Science and Technology, Anhui, Huainan 232001, China

chgxue@foxmail.com

Abstract: This paper describes the use of PANI (polyaniline) acid doped as a sensitivelayer on a silicon cantilever sensor. Andthe mechanical response (deflection) of the bimaterial (coated microcantilever) was investigated under theinfluence of relativehumidity. In this paper, several kinds of polyaniline were synthesized by chemical oxidation polymerization. The doped polyaniline was prepared by using 1mol/L hydrochloric acid, sulfuric acid andphosphoric acid. The variations in the deflection of the coated (doped andundoped PANI) and uncoated microcantilever were evaluated when exposed different humidities atroom pressure and temperature. The relative humidity(RH) in the chamber was varied from 20% to 70% usingdry nitrogen as the carrier gas, which flows rate was controlled when passed through water to generate humidity. The results indicateda linear sensitivity in ranges, where the high value was obtained for a polypyrrole-sensitive layer between 20 and 45% of moisture. Furthermore, the sensor shows excellent performance along withrapid response and recovery times, relatively low hysteresis, and excellent stability. The sensors developed are potentiallyunique materials for sensing low humidity for a long time.

Keywords: Microcantileversensor; dopedpolyaniline; relativehumidity; sensitivity

Hydrothermal synthesis of silver nanoparticles and their application in SERS

Yu Tang, Shiqin Li, Saipeng Huang, Xingyu Qi, Zhaofa Yang, Changguo Xue*

School of Material science and Engineering, Anhui University of Science and Technology, Anhui, Huainan 232001, China

chgxue@foxmail.com

Abstract: Silver nanoparticles were synthesized using sodium alginate as reduction and water as reaction medium by hydrothermal method. And the structure and apparent morphology of silver nanoparticles were analyzed by UV-Vis and TEM. In addition, three dyes (methylene blue, rhodamine B and methyl blue) were configured into solutions with different concentration gradients and then mixed with prepared silver gel for surface-enhanced Raman detection. The results indicate that silver nanoparticles have good Raman enhancement effect on the three dyes. And with the increase of the dye concentration, the Raman enhancement effect of Ag/dye solution significantly improve.

Keywords: Sodium alginate; Silver nanoparticles; Dye; Surface-enhanced Raman.

*Email: chgxue@foxmail.com

Effect of interface thickness and products on residual stress distributionof SiCp/Al6061 composites

Zhiqiang Zhu, Qingping Wang, Tingting Xue, Chunyang Lu

School of Materials Science and Engineering, Anhui University of Science and Technology, Huainan 232001, China

Abstract: In this study, the influence of different interface products and thickness on the residual stress distribution of SiCp/Al6061 composites was simulated by using finite element (FE) software (ABAQUS). It was found that the SiC/MgO/Al interfacial layer has the most obvious residual stress concentration. This is mainly due to the large difference between the thermal expansion coefficient of the MgO formed by interfacial reaction and that of the matrix and the reinforcement, resulting in the brittle interfacial layer of the newly formed SiC/MgO/Al.

In addition, the residual stress concentration of SiC/Si/Al interfacial layer is the lowest, because, Si element generated by interfacial reactions were enriched in the interfacial layer, inhibiting the occurrence of other adverse interfacial reactions, thus making the whole interface smoother. Meanwhile, during the preparation of SiCp/Al6061 composites, the residual stress near the interface layer increases with the decrease of the interface layer thickness. Therefore, the FE simulation results from the above two aspects can provide some reliable ideas for researchers to prepare particle reinforced metal matrix composites with excellent properties.

Key words: FE simulation; interface product; interface layer thickness; SiCp/Al6061 composite; interface reaction

Investigation ofCarbon and Oxygen Occurrence Characteristics in Different Densities Coking Coal Surface by XPS

Li Yang, GE Tao,

（Department of Material Science & Engineering, Anhui University of Science and Technology, Huainan 232001, China）

Abstract: Apply XPS toanalyze the carbon and oxygen spectrum, grasp the occurrence characteristics of there and reveal the relationship betweenthe structuresof the main elements in coal surface and densities. It is of great significance to improve the level of comprehensive utilization of coking coal. Coal sample is divided into fourdensities, and they are -1.3,1.3-1.4,1.4-1.6 and +1.6. Resultsshowed thatthe C-C, C-H and C-O groups are the major forms of the carbon in the coal, C-C and C-H accounts for 90%. As a result, it has high content of alkyl side chain in the coking coal. Also, there are C-O, C=O and O=C-O three forms of oxygenin the surface texture of the coking coal, with C-O accounting for more than 60%. As densities increases, C-O tends to increase in content, and the relative content of C=O, O=C-O tends to decrease.

Key Words: Coking Coal, XPS, OccurrenceCharacteristics, Density

Absorption properties of molybdenum disulfide matrixcomposites

Jialin Ma, Yin Liu*

School of Materials Science and Engineering, Anhui University of Science and Technology, Huainan, 232001, China

Abstrcat: The layered flower-like 2H-MoS_2 was synthesized by hydrothermal method at a temperature of 200℃for 16h. On the basis of this, MoS_2-PANI was synthesized by in-situ polymerization under ice bath conditions. The effects of the composition of different ratios of MoS_2-PANI on its microwave absorption properties were investigated. The experimental results show that the optimal reflection loss (RL) of MoS_2-PANI composite reaches a minimum of -47.45dB and a matching thickness of 2.4mm at a mass ratio of 1:2, and its effective absorption frequency ranges from 8.88-12.4GHz (RL< -10dB), bandwidth is 3.52GHz, covering X-band and Ku-band. Consequently, these MoS_2-PANI composites are promising candidates that can be used to design effective microwave absorbers over wide frequency bands. The microwave absorption properties of MoS_2–PANI composites could be tuned by changing the PANI content to reach the best impedance match.

Keywords: molybdenum disulfide; electromagnetic absorption; in-situ polymerization

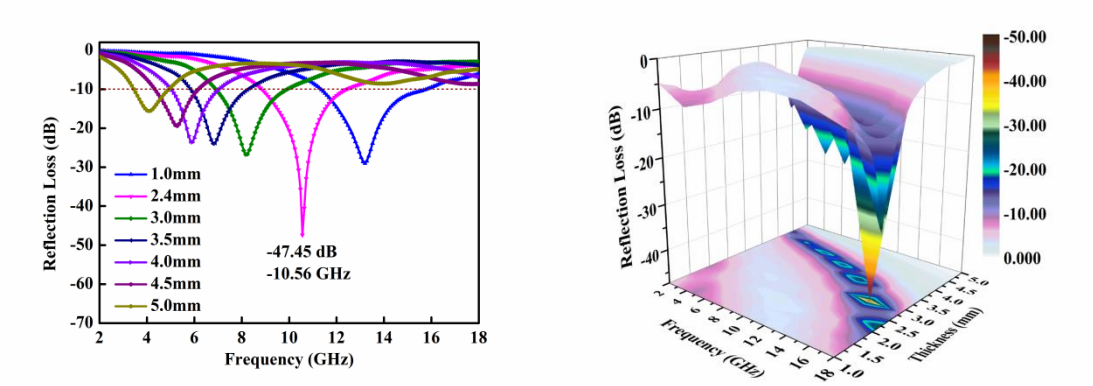

Microwave reflection loss of molybdenum disulfide matrix composites.

*Corresponding authors: yinliu@aust.edu.cn (Yin Liu)

Synthesis and dye adsorption of Coal-fly-ash based green magnetic adsorbent

Li Meng, Orphe B Tshinkobo, Peng Xujie, Song Linlin, Rong Xin, Li Jianjun*

（Department of Materials Science and Engineering,Anhui University of Science and Technology,Huainan，Anhui 232001，China）

Abstract：

Owing to the wide using of synthetic organic dyes in the printing and dyeing industry, dye pollution posed heavy threaten to natural environment and human health. Even a small amount of dyes in water could increase the cancer risk. Removing dyes from water has been one of the most urgent tasks for all the human beings. Many techniques were employed to treat the dye waste water, such as flocculating, coagulating, biodegradable, catalytic oxidation, ion exchange, and adsorption. Adsorption method is one of the most promising methods widely used in recent years. Adsorbent is the key effector in dye adsorption, therefore, the preparation of a low cost and good absorption attracted lot of attentions of the researchers. Various organic and inorganic adsorbents have been fabricated. One of the main obstacles in this field is how to separate the adsorbent from the water effectively. Thanks for the previous hard work, several techniques were developed to deal with this problem, including magnetic separation, which was ardently studied recently. However, this technique needs magnetic adsorbents, which are chemically synthesized. In addition, magnetic nano-particles (eg. nano-Fe_3O_4) are used as magnetic core in most reported magnetic adsorbents. Because the synthesis process of nano-Fe_3O_4 is chemical, complex, high-price and easy to cause secondary pollution, the widely use of magnetic separation technique was limited.

It is necessary to develop green and effective magnetic adsorbents using clean and cheap materials as magnetic core. The coal-fly-ash magnetic spheres (CMS) is derived from industrial coal fly ash, which has low price, tremendous output, and widespread distribution. CMS often has high porosity and magnetic magnetism, thus, it could be a promising candidate for the magnetic core. Polyaniline (PANI) , as an widely used polymer, has been intensively studied as selective adsorption materials. Its molecular chain contains a large number of amino and imino group functional groups, which can absorb dye molecules by

electrostatic action, hydrogen bonding and chemical interaction. The combination of CMS and PANI may has both good dye adsorption performance and high magnetism.

In this work, the CMS@ SiO_2@PANI magnetic adsorbents were synthesized by a simple chemical precipitation method, using CMS as magnetic core. CMS particles were carefully separated from the coal fly ash obtained fromLuohe Power Plant in Huainan, P. R. China. The CMS particles were cover by SiO_2 to prevent the acid reaction in the follow-up process. The CMS@SiO_2@PANI was fabricated by adding the CMS@SiO_2 magnetic particles into the reaction solution, during the polymerization process of PANI. The whole reaction condition was mild, and the operation was simple and easy.

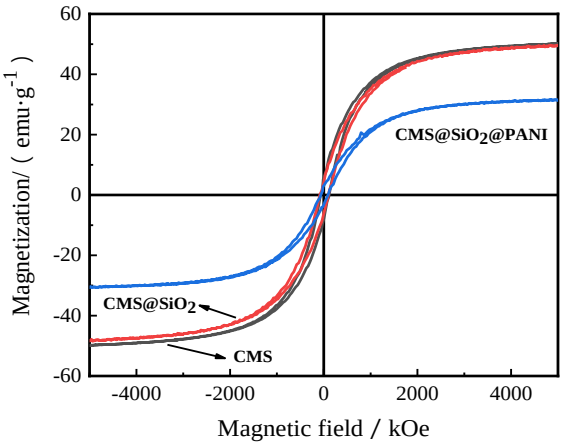

Fig.1 Magnetic hysteresis loops of CMS、CMS@$SiO_2$and CMS@SiO_2@PANI

Systemic characterization shows the obtain samples are the expected core-shell CMS@SiO_2@PANI with multi-hole structure. The diameter ranges from 8.1 to 16.5 μm. Figure 1 shows the magnetic hysteresis loop of the magnetic products before and after polyaniline modification. According to the graph, the saturation magnetization of the CMS, CMS@SiO_2, and CMS@SiO_2@PANI are detected as 50.17, 49.66, and 31.73 emu·g^{-1}, respectively. Although the magnetism of CMS@SiO_2@PANI decreased compared with the original CMS, it still has relative high ferromagnetism, which is strong enough for effective magnetic separation. The reduction of the magnetism could be due to the mass percentage decrease of the magnetic content after the polyaniline load.

Adsorption experimental results show that the CMS@SiO_2@PANI composites have strong adsorption for various dyes. As shown in Figure 2, the adsorption of Methyl Orange

(MO), Congo Red (CR), Rhodamine B (RhB), and Methylene Blue (MB) are 173.11, 62.5, 36.57, and 46.62 $mg \cdot L^{-1}$, respectively. The dye adsorptions for anion dyes are much higher than those for cationic dyes. Detailed analysis indicates these dye adsorption differences could be owing to the electrostatic property of acid-doped PANI, which is positive charged. MO and CR are anionic dyes, thus they are electrically attracted by the PANI molecular, the adsorption is strong. While RhB and MB are cationic dyes, thus the adsorption is weak. It was found that the dye adsorption is very fast in the beginning stage. Taking MO as an example, the dye adsorption reached 138.49 $mg \cdot L^{-1}$ within 16 min and reached equilibrium at 30 min, under the condition: dye concentration of 350$mg \cdot L^{-1}$, magnetic adsorbent dose of 0.4$g \cdot L^{-1}$. As shown in the figure 2, the adsorption of all dyes reached equilibrium at 30 min, beyond which there is little increase of adsorption.

Adsorption experiments indicates that the dye adsorption performance of the CMS@SiO_2@PANI changes with the dye concentration. The best dye concentrations of MO, CR, MB, and RhB are tested to be 350, 100, 70, and 50$mg \cdot L^{-1}$, respectively. That's probably because the increase in dye concentration eases the resistance and makes more contact between dye and solvent. Availability of dye molecules in the vicinity of adsorbent also increased while increasing the concentration, which results high uptake of dye at higher concentration. The initial pH value of the solution also has important effect on dye adsorption. Under low pH, the surface of PANI is positively charged, thus could attract the negative charged dye molecules effectively. Polyaniline may also be protonized by hydrogen ions in solution, which will enhance the adsorption of anion dyes. With the increase of pH value, the amount of negative charge in the solution increases, which hinders the contact and adsorption between the anion dye and the adsorbent.

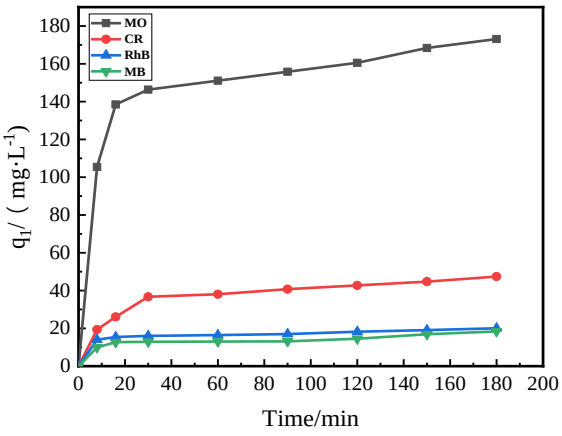

Fig.2 The effect of adsorption time on the dye adsorption capacity of CMS@SiO_2@PANI

In conclusion, we synthesized an acid-doped polyanliline magnetic adsorbents, using CMS as magnetic core. The obtained samples are environmentally friendly, cheap, and have an effective dye adsorption, especially for anion dyes like MO. Since the adsorbents are ferromagnetic, they could be effectively separated by the external magnetic. CMS@SiO_2@PANI combines the advantages of magnetic material and adsorption material, making coal-fly-ash magnetic spheres functional, which is a new type of environmental adsorption material.

Keywords： magnetic adsorbent; coal fly ash; magnetic sphere; dye adsorption; polyaniline

Preparation and application of guanidine sulfonate ammonium salt

Ziyue Xuan, Guojun Cheng*, Shen Tian, Feixiang Sha

School of Materials Science and Engineering, Anhui University of Science and Technology, Taifeng Street, Huainan 232001, Anhui, china

Corresponding author: Guojun Cheng

E-mail：chengguojun0436@126.com

Abstract: In this paper, a novel flame retardant, guanidine sulfonate ammonium salt, was synthesized from guanidine sulfamate (GAS) and 2,3-epoxypropyltrimethylammonium chloride (GTA). The chemical structures were confirmed by Fourier transform infrared spectroscopy (FTIR) and ^{1}H nuclear magnetic resonance spectroscopy (^{1}H NMR). The results of infrared spectroscopy indicated that the products exhibited deformation vibration peaks and stretching of quaternary ammonium groups at 1490 cm^{-1} and 3014 cm^{-1}, respectively. The nuclear magnetic resonance spectrum showed δ = 3.100 ppm was the hydrogen on the methyl group of quaternary ammonium group, and the above results indicated that the quaternary ammonium group in the GTA has been successfully grafted into the GAS. The thermo-gravimetric analysis shows, under nitrogen atmosphere, the temperature loss of product about 60% is 276 ℃. The initial temperature is higher than the processing temperature of most polymer materials and lower than the decomposition of polymer materials. When burning, it can be decomposed before the polymer material to play a flame retardant role. The various factors affecting the reaction parameters were optimized, when the reaction temperature kept at 75 ℃ with molar ratio of GAS and GTA of 1:31, and pH=5 was determined as the solvent, and the yield was the highest.

Since the guanidine sulfonate ammonium salt contained quaternary ammonium salt cation, the subject used the prepared cerium sulfonate ammonium salt and sodium montmorillonite layer to carry out cation exchange reaction to prepare organic montmorillonite. The modification effect was characterized by FTIR, X-ray diffraction (XRD), TGA, contact angle and other test methods. In the infrared spectrum, the strong absorption peak at 2925cm^{-1} and 2853cm^{-1} is the symmetry and antisymmetric stretching vibration peak of C-H. The results showed that the guanidine sulfonate ammonium salt was

successfully grafted onto montmorillonite, the interlayer spacing of organic montmorillonite did not change significantly, but when the mass ratio of guanidine sulfonate ammonium salt to sodium montmorillonite was 30%, The contact angle of organic montmorillonite is increased by about 30° compared to the original montmorillonite, and the hydrophobicity of the surface of the montmorillonite is greatly improved. In summary, the guanidine sulfonate ammonium salt has a weaker stripping effect on the montmorillonite layer, and most of them adsord on the surface of Na-MMT. The thermal properties of organic montmorillonite were analyzed by thermogravimetry (TGA). After modification, the decrease of residual rate indicates that the guanidine sulfonate ammonium salt was successfully grafted onto montmorillonite. The weight loss at 250-380 °C is due to the decomposition of the organic intercalation agent grafted onto the montmorillonite, this also corresponds to the decomposition range of the guanidine sulfonate ammonium salt.

Keyword: guanidine sulfonate，montmorillonite，flame retardant，intercalation agent，quaternary ammonium salt

Acknowledgments

This research was supported by the University outstanding young talents support program (NO. gxyq2017006), Anhui university natural science research project (NO. KJ2019A0118), Innovation and entrepreneurship training program for college students (NO. 201810361071），(NO. 201810361294）and （NO. 201810361278）.

Synthesis of MXenes and the Effects of Solvent Types on MXenes Morphology and Modification of MXenes

Shen Tian, Guojun Cheng*, Ziyue Xuan, Feixiang Sha

(School of Materials Science and Engineering, Anhui University of Science and Technology, Taifeng Street, Huainan 232001, Anhui, china)

Corresponding author: Guojun Cheng

E-mail：chengguojun0436@126.com

Abstract

MXenes is a new carbon/nitride two-dimensional nano-layered material with unique properties. It has a structure similar to that of graphene. The chemical formula can be expressed as $M_{n+1}X_nT_z$, n=1, 2, 3, where M representing an early transition metal, X represents carbon or nitrogen, and T_z represents a reactive functional group such as -OH, -F and =O linked on the surface during etching. In this paper, MAX phase (Ti_3AlC_2) was used as the master material, and the method of Ti_3AlC_2 and LiF mixed ball grinding and liquid phase etching was adopted. During the process of ball grinding, the particle size of the mixed raw material became smaller and smaller, the surface energy increased, and the reaction activation energy decreased, making it easier to prepare MXenes ($Ti_3C_2T_z$). Ethanol and deionized water are used as washing liquid to treat the etched products, and the effects of ethanol and deionized water on the morphology of the product are studied. The effects of ethanol and deionized water on the morphology of the product were studied by using ethanol and deionized water as the washing solution. The microstructure of the product was analyzed by X-ray diffraction (XRD) and scanning electron microscopy (SEM). The results show that the ethanol treated product has a good layered structure.; after deionized water treatment, the product structure was worse than the former. The silane coupling agent was used as a surface treatment agent. It has been widely used in industry. The MXenes treated with ethanol was modified with γ-Methacryloxypropyl trimethoxy silane (KH-570) to study the performance changes of MXenes before and after modification. According to the contact angle test results, the contact angle of MXenes before modification is 29.8°, which has strong hydrophilicity. This also proves that there are surface hydrophilic groups in MXene; the modified

M-MXenes contact angle increases to 114.5°, the surface can be reduced, and the hydrophilic group is successfully grafted with the silane coupling agent KH-570, and the substance is converted from a hydrophilic surface to a hydrophobic surface.

Keywords: MXenes phase；preparation；morphology；modification

Acknowledgments

This research was supported by the University outstanding young talents support program (NO. gxyq2017006), Anhui university natural science research project (NO. KJ2019A0118), Innovation and entrepreneurship training program for college students (NO. 201810361071），（NO. 201810361294）and （NO. 201810361278）.

Preparation and Property of La, Nd, Bi Co-doped TiO_2 Electrochromic Film

JIANG Yujie, XU Zi-Fang, GUI Chan, MA Jun,

School of Materials Science and Engineering, Anhui University of Science & Technology, Huainan 232001, Anhui Province, P.R. China

**Corresponding author: Fax: +86 554 6668643; Tel: +86 554 6668649; E-mail: zhfxu@aust.edu.cn*

Abstract: To improve optical property and coloration effect, La, Nd and Bi co-doped TiO_2 films were synthesized via a Sol-Gel method, by using butyl titanate as precursor on the surface of ITO glass substrate. Structural surface morphologies and electrochromic properties of the as-prepared films were examined with TG-DTA、XRD、UV-vis and Electrochemical workstation. The results showed that anatase TiO_2 formed from TiO_2 dry gels after heat treatment at 400℃, 500℃, 600℃, and showing tendency of the higher the temperature heat treatment, the more complete the crystal development. La, Nd and Bi doped TiO_2 increased the disorder of the TiO_2 octahedron, resulting in increase of the amorphized degree. TiO_2 films prepared with acurate 12% tetrabutyl titanate exhibited the best electrochemic properties. TiO_2 films heat-treated at 500℃ showed excellent electrochemical properties. TiO_2 films separately doped with molar amount fraction of 8%La, 18%Nd, 6%Bi, possess excellent electrochemic properties, and single doping effect is in the order of 6% Bi < 8 %La<18% Nd. La-Nd-Bi co-doped TiO_2 is anatase with a very high amorphized degree, with the best cyclic valtammentry and highest amorphized degree when the molar amount ratio of La: Nd: Bi=4:10:2.

Key words: electrochromism; Sol-Gel; La-Nd -Bi co-doped TiO_2 film; cyclic voltammetry; coloration efficiency

Effect of carbon black/ white carbon black dual phase filler on properties of solution-polymerized styrene-butadiene rubber

QIU Liu，DING Guo-xin

School of MaterialsScience and Engineering, Anhui University of Science and Technology, HuaiNan, 232001, China

Abstract:

In order to reduce the interaction between filler and filler, carbon black /white carbon black dual phase filler was prepared by sol-gel. This paper focuses on the effect of the number of additions of this new type of reinforcing filler on the properties of solution-polymerized styrene-butadiene rubber. The results show that with the increase of the number of reinforcing fillers, the thermal stability of rubber composites has little effect. However, during the vulcanization process, the maximum torque is gradually increased, the scorch time (t_{10}) is gradually shortened, and the vulcanization time (t_{90}) is first lengthened and then shortened. When the filler reaches 70 parts, the vulcanization time is up to 204 s. Its mechanical properties increase as the number of reinforcing fillers increases. When the reinforcing filler reaches 80 parts, the tensile strength is increased by 88.45%, hardness increased by 48.89%, the tear strength increased by 28.90%.

Keywords: Rubber composite; Carbon black /white carbon black dual phase filler; Solution-polymerized styrene-butadiene rubber; Mechanical properties

Effect of Hydrothermal Reaction Time on Structure and Electromagnetic Shielding Propertiesof $CuFe_2O_4$ Ferrite

Chen Chuan-xin, Ding Guo-xin

School of materials Science and Engineering，Anhui University of Science and Technology, Huainan 232000, China

Abstract: In this paper, $CuFe_2O_4$ ferrite materials were synthesized by hydrothermal method at different reaction times, and the hydrothermal reaction time was 8, 10, 12, 18, 24h. The microstructure and electromagnetic shielding properties of $CuFe_2O_4$ ferrite materials were characterized by X-ray diffraction (XRD), Fourier transform infrared spectroscopy (FTIR), scanning electron microscopy (SEM) and vector network analysis (VNA). XRD and FTIR spectra show that the $CuFe_2O_4$ ferrite materials synthesized in each reaction time are single spinel phases, and the growth of reaction time promotes the growth of crystallites. The electromagnetic shielding performance study shows that the reaction time is 10h. The sample has a reflection loss of -25.8 dB at a thickness of 4.5 mm and a frequency of 2-18 GHz.

Keywords: Ferrite, hydrothermal method, electromagnetic shielding

Comparative Study on Gas Sensing bySchottky Diode Electrode Prepared with Graphene-Semiconductor-Polymer Nanocomposites

Md Rokon Ud Dowla Biswas & Won-Chun Oh

Department of Advanced Materials Science & Engineering, Hanseo University, Seosan-si, Chungnam, Korea, 356-706

Abstract:

This paper studies the performance of a gas sensor based on an organic/ inorganic diode for ammonia (NH_3), nitrogen (N_2) & oxygen (O_2) sensing under atmospheric conditions at room temperature and different humidity levels. The diode structure consists of a layer of different kinds of polymer (PTFE, PVDF, PANI) deposited on top of $BiVO_4$. The polymer layer, which is filled with different ratios of graphene oxide (GO), is prepared from the solution phase. We show that the current–voltage (I–V) response of the diode and the sensing performance are improved significantly by adding GO to the polymer layer. The sensing response is highest for a diode with 0.04 wt.% of GO. At room temperature, the Poly-GO (0.04 wt.%) /$BiVO_4$ Schottky diode shows a sensitivity of 194 upon exposure to 20 ppm of NH_3 in ambient air with rapid response and recovery times between 95 and 101 s, respectively. The sensor based on the polymer: GO diode is cost-effective, environmentally friendly, and easy to fabricate using low-cost solution-processing methods.

Application of Anti-Skid Particle Based on modified Flyash

FeiZeng, Yanfeng Qian, Xianglong Wan*

School of Materials Science and Engineering, Anhui University of Science and Technology, Huainan 232001, Anhui, China

**Corresponding authors:xlwan@aust.edu.cn*

Abstract:

Anti-skid particle is a kind of functional and expensive filler for non-slip coating. We report a new type of Anti-skid particle based on modified flyash which is a solid waste with high hardness. The properties of surface of flyash particle were observed in this paper for its modification design. By using a two-step method for modification, the performance of hard flyash with different surface agents can be controlled to integrate with different polymers. The results of FT-IR spectrum and thermo gravimetric analysis (TGA) showed that the modification was successful and can be designed to fit the requirement in different applications. Moreover, the modified flyash was applied to a polyacrylate emulsion with silica sol to get a non-slip coating. The non-slip properties were investigated with the changes of the pigment volume concentration (PVC). The results showed when the pigment volume concentration closed to the critical pigment volume concentration (CPVC), the maximumcoefficient offriction on wet film reached to 0.885. Meanwhile, the hydrophilicity of the coating was enhanced by added silica sol. The maximum coefficient of friction on wet film could riseup to 1. 054.The pencil hardness of the film was about 3H. After rubbing on the surface (100 times) with sandpaper, the coefficient of friction can still keep to 0.821. This non-slip coatingalso passed the test of water resistance in 72 h at room temperature. From above, the modified flyash can be acted as a cheap anti-skid particle in a non-slip coating successfully. At the same time, the integrated utilization of solid waste can bring good environmental benefits.

Keywords: modification；fly ash；anti-skid particle；PVC；silica sol；coefficient of friction

Preparation and Characterization of ZnO Coated Flyash Composite Powders

Kaiqiang Hu, Zhibo Chen, Shi Jin, Xianglong Wan*

School of Materials Science and Engineering, Anhui University of Science and Technology, Huainan 232001, Anhui, China

**Corresponding authors:xlwan@aust.edu.cn*

Abstract:

Flyash is a solid waste of power plants that has the reactants, high temperature resistant, light weight, good liquidity characteristics. It is widely applied in the production of building materials, road engineering, agriculture, sewage treatment, and other fields. But its serious defects such as color led to cause a combined interface craze when it applied to polymer engineering. In order to solve the problem of low whiteness of fly ash, a zinc oxide-coated composite of modified flyash was designed by using modified flyash as raw material and $Ba(OH)_2$ and $ZnSO_4$ as coating agents. The ratioof coated layer and flyash, the reaction rates, concentrations of agents, and reaction temperatures were observed in this paper. The composite powders were characterized by albedo, particle size analyzer, BET, XRD, and SEM.From SEM image, the Zinc oxide grew outside on flyash particles with heterogeneous nucleation. And the whiteness of flyash was depended on the ration of coated layer. The results showed thatthe ratio of coated layer was 80 wt% when the reaction rates at 3 mL/min$ZnSO_4$ solution and $Ba(OH)_2$ solution with concentration 0.3 mol/L and 0.1 mol/L respectively. The reaction happened at 75±5℃ for 30 min, and the pH of solution was 9 with solid-liquid ratio at 1:6. The whiteness of flyash rise from34.7%up to74.4%. This white flyash could be applied to different industries.

Keywords: modified fly ash；Zinc oxide；heterogeneous nucleation；growth；whiteness

Preparation and properties of non-slip coatingbased on compositeof flyash/ polyurethane

Shengfa Lai, Meiling Gao, Xianglong Wan*

School of Materials Science and Engineering, Anhui University of Science and Technology, Huainan 232001, Anhui, China

**Corresponding authors:xlwan@aust.edu.cn*

Abstract:

Both waste cross-linked polyurethane (CPU) and flyash are solid wastes. In this paper, we tried to combine CPU (organic) with flyash(inorganic) to designa new type ofnon-slip coating. By modifying the CPU and flyash, the compatibility of the two solid wastes was improved. The critical pigment volume concentration (CPVC) of waste polyurethane, flyash, and PU latexwas calculated. Then the composite ratio of CPU and flyashwas designed based on the calculation to obtain different non-slip coatings. Theresults showed that the coefficient offriction reached to 0.87when the ratio of CPU to fly ash was 5:1. After the non-slip film was rubbed 100 times with sandpaper, the coefficient offriction still kept to 0.82. The composite filmhadgood wear resistance and mechanical stability. From the FT-IR spectrum, the modification of agents on CPU and flyash was successful. The hardness of the coating mainly depended on flyash, so the hardness of the filmwasdecided by the amount of flyash in non-slip coating. The Shore Hardness for optimalnon-slip coating was 56.8HA. At the same time, the film passed the test of water resistance in 60 h at room temperature. The contact angle was maintained at about 76.5° which did not change after the test of water resistance. The method gives new insight that CPU and flyash can be applied to coating industry.

Key words: flyash, cross-linked polyurethane (CPU), modification, CPVC, friction coefficient, non-slip coating

Study on the absorbing properties of graphene composites prepared from lignin

Zhao Yan*, Wen Minyue
School of Materials Science and Engineering, Anhui University of Science and Technology, Huainan 232001, Anhui, China
*Corresponding authors:yanzhao@aust.edu.cn

Abstract: Lignin is rich in reserves, low in cost, and high in carbon, and can be used as a carbon source for the preparation of graphene. Lignin contains many active functional groups that play an important role in the preparation of graphene composites. This paper briefly introduces the excellent properties of lignin and graphene as well as the absorption prospects of graphene complexes. It is mainly described that the mixture of lignin and iron nitrate and tetrahydrofuran is kept warm at 110 ℃ for 12 hours under water bath conditions, the temperature is set at 110 ℃ for thermal hydrolysis for 12 hours in a high-pressure reactor, and the temperature is set in a drying box after magnetic stirring is evenly. 110 ℃ 12 hours, the preparation method of graphene complexes prepared by calcination after three pretreatment lignins was tested. The properties of graphene complexes prepared were better than that of pure graphene, and their future development was forecasted

Keywords: lignin; Graphene; Composite materials; Absorption.

Hydrothermal synthesis of GO@Ni-PS for enhanced tribological, thermal and flame retardant properties of epoxy resins

Yue Liu, Ji-nian Yang
Anhui University of Science and Technology, Huainan 232001, Anhui, China

Abstract: A novel mesoporous SiO_2−graphene nanohybrid was successfully synthesized by sol-gel method firstly, and then nickel silicate nanosheets grown on graphene oxide(GO@Ni-PS) are synthesized by a mild hydrothermal method, aiming to improve wear and fire retardancy of epoxy resin (EP). The nano-dispersion of GO@Ni-PS in EP was certified via TEM and XRD. With the incorporation of 3 wt% GO@Ni-PS, the LOI value of the EP/ GO@Ni-PS nanocomposites were decreased by 8.4% when compared to pure EP. The frictional coefficient of epoxy/GO@Ni-PS composite coatings reduced from 0.4167 of pure EP to a minimum 0.3482 for the epoxy composites with 3% GO@Ni-PS. Moreover, the EP/GO@Ni-PS nanocomposites exhibited excellent impact and tensile strength performances due to the formation of a strong three-dimensional network structure in the EP matrix.

Keywords: Graphene oxide (GO), layered nickel silicates(Ni-PS), fire retardancy, tribological properties

Inhibition effect of THEIC/APP intumescent flame retardant on the spontaneous combustion of coal

Shi-chao Xing, Shi-bin Nie

School of Energy Resources and Safety, Anhui University of Science and Technology, Huainan, 232001, Anhui China

Corresponding to 2961583480@qq.com

Abstract: In order to prevent coal spontaneous combustion effectively, an intumescent flame retardant (IFR) combined with tri (2-hydroxyethyl) isocyanurate (THEIC) and ammonium polyphosphate (APP) was employed. The effect of IFRs on the thermal stability and combustions of coal was investigated carefully. The results showed that the flame retardant THEIC: APP=1:2 has the best synergistic flame retardant effect on coal. Coal with THEIC/APP IFR had better carbonization performance and thermal stability at high temperature, and the residual weight was 44.1% than that of raw coal (6.6%). The activation energy of the treated coal was increased up to 283.1 kJ/mol, indicating it more difficult to be oxidized than that of control sample (168.4 kJ/mol). An expanded carbonized layer was formed during the combustion for the sample with IFR, generating the transferring barriers of combustible gases, heat and free radicals and preventing further oxidation and decomposition of coal. Here, we hope to provide an effective method for the further understanding of the flame retardant mechanism of coal.

Keywords: coal spontaneous combustion, thermal analysis, intumescent flame retardant, combustion

Study on the Fabrication and Friction-wear Properties of Fly Ash/Graphite/Aluminum Matrix Composites

Qingping Wang, Tingting Xue, Zhiqiang Zhu, Chunyang Lu, Pakeeza Maryum

School of Materials Science and Engineering, Anhui University of Science and Technology, Huainan 232001, China

Abstract: This study investigated the friction and wear properties of fly ash/graphite/aluminum matrix composites under dry sliding conditions. Powder metallurgy was used for the fabrication of composite materials. The chosen enhanced content was 2, 4, 6 and 8wt.% graphite and 10wt.% fly ash hybrid reinforced aluminum matrix composite. The samples of fly ash/graphite/aluminum matrix composites were tested for their hardness and wear behavior. Test results confirm that the hardness of the fly ash/graphite/aluminum composite material increased compared with the base alloy due to the presence of hard and brittle granular fly ash, wherein the hardness of 10FA/4Gr/Al6061 was 55.8HV. The wear resistance of the composite increased as the graphite content also increased. The lubricating film formed on the surface served as an effective insulating layer for preventing metal from contacting the metal. As the load increased, the amount of wear increased and the wear mechanism changed from abrasive wear and adhesive wear to peeling wear.

Keyword: Fly ash; Graphite; Powder metallurgy; Friction and wear

Electrical Properties of Polyvinyl Alcohol DopedPolyaniline/Graphene Composites

Shuai Zhao, ShunYao, Yulun Tao*

(School of Materials Science and Engineering, Anhui University of Science and Technology, Anhui Huainan 232001 China)

***Corresponding authors:** **Yulun Tao**,williamtao795322@163.com*

Abstract

Polyaniline/graphene composites were prepared by in-situ polymerization, the molar ratio of Graphene to polyaniline was 1:3, 1:6 and 1:10. It is found that 1:6 have the best ratio and its specific capacitance can reach 513 F/g. The optimum proportion of polyaniline/graphene doped with trace polyvinyl alcohol, the results show that the maximum specific capacitance of the composites can reach 1044 F/g. After 2000 cycles of charge and discharge, the specific capacitance of the composites is still 916 F/g, which proves that the stability of the composites is much greater than that of polyaniline. Characterization by XRD, FT-IR, SEM, TEM and UV-Vis spectrophotometer.

Key words: In-situ Polymerization, Polyaniline, Graphene, Polyvinyl Alcohol, Supercapacitor, Specific Capacit

Applications of Radiopharmaceuticals in Human Health Care System: Current Scenario and Future Prospects

Praveen Kumar[1, *] and Laxmi Tripathi[2]

[1]*Department of Pharmaceutical Chemistry, Faculty of Pharmacy, Uttar Pradesh University of Medical Sciences, Saifai, Etawah-206301, India*

**Corresponding author: E-mail: praveensha77@gmail.com;*

Tel.: +91 9897112288, Fax: +91-5688-276599

[2]*Department of Pharmaceutical Chemistry, Moradabad Educational Trust, Group of Institutions Faculty of Pharmacy, Moradabad-244001, India*

Abstract

Radiopharmaceuticals are unique medicinal formulations containing radioisotopes which are used in major clinical areas for diagnosis and/or therapy. The facilities and procedures for the production, use, and storage of radiopharmaceuticals are subject to licensing by national and/or regional authorities including compliance both with regulations governing pharmaceutical preparations and with those governing radioactive materials. There is a significant increase in the global demand of radiopharmaceuticals, with the increasing incidences of cardiac, neurological and cancer disease. The global radiopharmaceutical applications market is expected to grow from $ 4.9 billion in 2010 and to $ 7.9 billion in 2011, at a CAGR of 9.25% from 2010 to 2015. The nuclear medicine (NM) growth has gone through both evolutionary and revolutionary changes over decades, mostly attributable to the dynamic and responsive trends in the global development and deployment of radiopharmaceuticals, as well as the advent of superior technology imaging systems *viz*. computed tomography, positron emission tomography, PET/magnetic resonance with quantification capability [1]. Diagnostic radiopharmaceuticals are radioisotopes bound to biological molecules able to target specific organs, tissues or cells within the human body. The most widely used radioisotope in diagnostic nuclear medicine is technetium-99m. For instance, technetium-99m-MDP (methylene diphosphonate) is widely used to detect bone metastasis associated with cancer. Therapeutic radiopharmaceuticals are mostly labelled with a radionuclide that decays with the emission of β-particles, thereby delivering all their energy

in a small area and kill hyper-functioning or malignant cells [2]. This study is an attempt to explore the diagnostic and therapeutic potential of radiopharmaceuticals in human health and their future prospects.

References

1. B. Gutfilen and G. Valentini, Pharmaceuticals in Nuclear Medicine: Recent Developments for SPECT and PET Studies, *Biomed Res. Int*., **2014**, 426892 (2014).
2. Iverson, Cheryl, et al. (eds) (2007), "15.9.2 Radiopharmaceuticals", AMA Manual of Style (10th ed.), Oxford, Oxfordshire: Oxford University Press, ISBN 978-0-19-517633-9.

Photocatalytic simultaneous removal of nitrite and ammonia via zinc ferrite-activated carbon hybrid catalyst

Shou-Qing Liu, *Li Luo, Ze-Da Meng, Xin Zhang, Yiwen Zhou, Jing Zhou, Dongwen Li

†*Jiangsu Key Laboratory of Environmental Functional Materials; School of Chemistry, Biology and Material Engineering, Suzhou University of Science and Technology, Suzhou 215009, China*

ABSTRACT: Nitrite and ammonia often coexist in waters. Thus, it is very significant to develop a photocatalytic process for the simultaneous removal of nitrite and ammonia. Herein, zinc ferrite-activated carbon ($ZnFe_2O_4$/AC) was synthesized and characterized by X-ray diffraction spectroscopy, transmission electron microscopy, Raman spectroscopy and ultraviolet-visible diffuse reflectance spectroscopy. The valence band level of $ZnFe_2O_4$ was measured by XPS valence band spectroscopy and the first-principle calculation was performed to confirm the band structure of $ZnFe_2O_4$. The as-synthesized $ZnFe_2O_4$/AC species functioned as a photocatalyst to remove simultaneously nitrite and ammonia under anaerobic conditions upon white light irradiation at the first stage. The results indicated that a removal ratio of 92.7 % for nitrite was achieved in 50.0 mg/L nitrite plus 100.0 mg/L ammonia solution with pH 9.5 under anaerobic conditions for 3 h at this stage, simultaneously, the removal ratio of 64.0 % for ammonia was also achieved. At the second stage, oxygen gas was bubbled in the reactor to photocatalytically eliminate residual ammonia under aerobic conditions upon continuous irradiation. The results demonstrated that the removal ratios for nitrite, ammonia and total nitrogen reached to 92.0, 90.0 and 90.2% at 12^{th} h, respectively, the product released during phptpcatalysis is N_2 gas detected by gas chromatography, fulfilling the simultaneous removal of nitrite and ammonia. The reaction mechanism was exploited.

Effects of Plasma Gas Flow Rate and Input Current on Characteristics of Nano Composite Particles Synthesized by Transferred DC Thermal Plasma

Seung Kyu Park and Heon Chang Kim†

Department of Chemical Engineering, Hoseo University, Asan 31499, Korea

Tel: +82 41 5405752, email: heonchan@hoseo.edu†

Abstract: Nano composite powder of the ZrVFe alloy were synthesized, as a candidate for gettering material, by a transferred DC plasma. The effects of the flow rate of the plasma gas and the input current were investigated on the characteristics of the produced powder such as particle size and size distribution, particle crystallinity, surface area, *etc*.

As the flow rate of the plasma gas increased with the fixed input current, the particles were found to be spherical, from the SEM images, although severely agglomerated and the particle size was found to decrease. Although the shape of the particle obtained from the PSA was almost unaffected as the flow rate increased, the size of most abundant particles was found to decrease, the average particles size decreased almost linearly, and the surface area measured by the BET correspondingly increased.

As the input current increased with the fixed flow rate of the plasma gas, the particle size was found to decrease since the higher plasma input current not only had the maximum plasma temperature higher, generating more abundant nuclei, but also made the temperature gradient stiffer, limiting the particle growth. The PSA measurement also confirmed that the average particle size decreased as the input current increased. Furthermore, the particle size distribution became narrower, the surface area increased.

In all cases, oxide particles were formed because the reaction chamber was not perfectly sealed from surroundings. Increasing either the flow rate of the plasma gas or the input current caused the peak for Zr_3V_3O sharply increased.

Key words: Nano Composite Powder, Transferred Thermal Plasma, Plasma Gas Flow Rate, Plasma Input Current

Raman Spectroscopy Study of the Electrostatic Microcolumn Lenses

Dong-Huyun Baek, Young Bok Lee, Geon Woo Lee, YongJin Yoo,

Dae-Wook Kim, Seungjoon Ahn, and Ho Seob Kim*

Department of Physics and Nanoscience, and Center for Next-Generation Semiconductor Technology, Sun Moon University, Asan-si Chungnam Korea, 31460

**hskim3@sunmoon.ac.kr*

Abstract:

Miniaturized electron beam (e-beam) columns consist of emitter, electrostatic lenses and deflectors which are fabricated by using microelectromechanical system (MEMS) process. Although every process step variable was made identical, the lifetime of the electrostatic lens was different. So, we have studied to find various lifetime parameters of electrostatic lens caused by electron bombardments. The electrostatic lens surface was evaluated by Raman spectroscopy to study the characteristics of various defects caused by the electron impact on the lens surface. Two results were obtained from this study. First, the emitted electrons are physically damaged by the physical collision with 20 μm of thickness electrostatic lens. Second, the conductivity change caused by the surface defect of the electron lens by the emitted electrons. The results present that the change in the physical properties of the silicon surface caused by electron impacts and the possibility of changing the conductivity of silicon property.

Evaluation of the microalgae growth using Raman Spectroscopy

Dong-Huyun Baek[1, 3], Geon Woo Lee[1, 3], YongJin Yoo1[1, 4],

Jin woo Kim[2, 3], and Ho Seob Kim[1, 4, *]

[1]*Department of Physics and Nanoscience, Sun Moon University, Asan-si Chungnam Korea, 31460*

[2]*Department of Food Science, Sun Moon University, Asan-si Chungnam Korea, 31460*

[3]*Center for Next-Generation Semiconductor Technology, Sun Moon University, Asan-si Chungnam Korea, 31460*

[4]*CEBT Co., Asan-si Chungnam Korea, 31460*

**hskim3@sunmoon.ac.kr*

Abstract:

Scenedesmus sp. has been used species for biomass production due to its relatively fast growth compared with other microalgae species, advantageous to outdoor culture and largescale cultivation. This study was conducted to evaluate the growth effect of Scenedesmus sp. with Raman spectroscopy. Microalgae were cultured for 60 days in the same medium, temperature and CO_2 concentration. The experiment was conducted using the LED light source as a control group. The results from Raman spectroscopy of Scenedesmus sp. indicated that the irradiated LED light source revealed a significant cell volume change (~80%) and an increase in the number of microalgae (~10 times). Consequently, Light source has a great influence on factor for growth of microalgae. Further study will be conducted on the effects of the light quantity of the LED light source and light wavelength.

This research was financially supported by the Ministry of SMEs and Startups(MSS), Korea, under the "Regional Specialized Industry Development Program (R&D P0004891)" supervised by the Korea Institute for Advancement of Technology (KIAT).

3D materials with the property of 2D materials ; a case study of magnetized TiO2 DSSC

Soon Wook Kwon[1], Hyun Sik Kang[1], Dae Hyun Kim[1], Woo Seoung Kim[1], Sung Jun On[1], Hyun Min Jung[1], Soo Min Lee[1], Jae Eun Gwon[1]and Hak Soo Kim[1,*] , Tae Ho Kim[2,*]

[1]Department of Environmental & Bio-Chemical Engineering, Sun Moon University, Asan, Republic of Korea

[2]Research Center for Eco Multi-Functional Nano Materials, Sun Moon University, Asan, Republic of Korea

** Corresponding author*

Abstract:

Currently, various technologies are being developed to improve the electron mo bility performance of semiconductor materials. We studied magnetization semiconducto rs to increase the total amount of current by controlling the direction of electronic flo w. Thissuggests a new material in which a ferromagnetic material is impregnated or d oped into an existing semiconductor and then magnetized. And we propose a novel w ay of enhancing the efficiency of the TiO_2 based dye sensitized solar cell (DSSC).

We impregnated Fe_2O_3 and Fe_3O_4 into TiO_2 and the studied the effect of magnetizati on on improving of efficiency of the TiO_2 DSSC. The result shows that it is possible to control the direction of charge flow in the bulk TiO_2. And, in the case of DSSC i n which polarization is induced using the Hall Effect, it has a higher electron density and efficiency. This was confirmed by a comparative experiment of the efficiency of the ferromagnetic DSSC with magnetized direction.

Such magnetized semiconductors can be used to develop solar cells with high efficie cy when used as a substitute for TiO_2 used in thin film solar cells, which are the ne xt generation solar cells, and can be applied in various other fields.

Reliability and reproducibility characterization of CNT emitter for microcolumn

Hyo Eun Yoon[1], Yongjin Yoo[1], Geonwoo Lee[1], Dea-Wook Kim[1],
Yoon Ho Song[2], June Tae Kang[2], and Ho Seob Kim[1], Seungjoon Ahn[1*]

[1]*Dept. of Physics and Nanoscience and Center for Next Generation Semiconductor Technology, Sun Moon University, Korea*

[2]*Electronics and Telecommunications Research Institute, Korea*

[*]sjoonahn@naver.com

One of the most important factors when fabricating a CNT-emitter for a micro columnis uniform dispersion of CNT. If the CNT are not sufficiently dispersed, the fi eld emission will not occur effectively when used in a microcolumn, and the reprodu cibility will be greatly reduced. The next most important factor is the stickiness of th e CNT paste. When the stickiness of CNT paste is lowered, blurring may occur when pattern is formed on the kovar-rod by the point-contact-method, and it becomes very difficult to form a desired pattern. In addition, since the CNT is not properly adhere d to the kovar-rod, a significant portion of the CNT is lost during the physical surfac e treatment after firing, which is also an important factor that deteriorates the reprodu cibility of the field emission test. Similarly, CNT should not be separated from the k ovar-rod when used as an electron source in a microcolumn. Therefore, a ball-milling-process using a ceramic-ball was introduced for effective dispersion. SiC, an inorganic filler of nano size, and ethyl cellulose, an organic binder, were used to improve the adhesion of CNT cathod-rod electrodes, and CNT paste was prepared by mixing tepin eol. The contact process was confirmed by using optical glass. The CNT are then sin tered at 350° C in air to facilitate the field emission. This surface treatment method was carried out by using a cylindrical adhesive roller having a strong adhesive proper ty to produce a CNT emission source. The CNT-emitter-tip for microcolumn was firstl y visualized as an optical image and its growth state was confirmed by electron micr oscope (SEM) image. Finally, the reproducibility and stability of the applied electric fi eld were confirmed through the evaluation of the field emission characteristics and the repetitive characteristics experiments.

Electrospinning preparation of PAN/TiO_2/PANI hybrid fiber membranes with high adsorption and visible light photocatalysis properties

Bao Xu, Xianbiao Wang *, Yuanyuan Huang, Jiali Liu, Yangyang Zhao, Wen Ji, Renwu Zhu

Anhui Key Laboratory of Advanced Building Materials, School of Materials Science and Chemical Engineering, Anhui Jianzhu University, Hefei 230601, PR China

Corresponding Author：

**E-mail: xbwang@ahjzu.edu.cn*

Abstract:

APAN/TiO_2/PANI hybridmembraneswere successively prepared. Firstly, PAN/TiO_2 fibers membranes were obtained by electrospinning PAN solution with TiO_2 particles. Then, PANI was decorated by in-situ oxidative polymerization of aniline on PAN/TiO_2 membranes. SEM results show that the fibers have ~200 nm in width. PANI and TiO_2 particles were dispersed uniformly. Importantly, such hybrid membranes have excellent adsorption performance. The as-obtained sample can adsorb Congo red from water effectivelywith the removal rate of92%. Detailed investigation reveals thatthe adsorption behavior fits Langmuir model well. In addition, the membranes could be regenerated byphotocatalytic degradation under visible light. After 4 times photocatalysis regenerations the removal rate remained upon 50%. Also, the performance extends to heavy metals [such as Cr (VI)]. After equilibrium adsorption, the adsorbed Cr(VI) on membranes could be reduced by visible light photocatalytic process, leading to effectively regeneration.

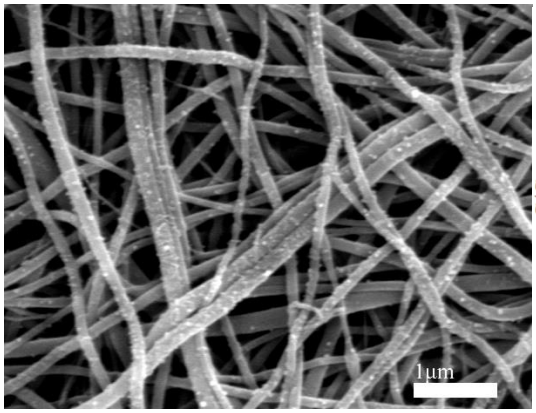

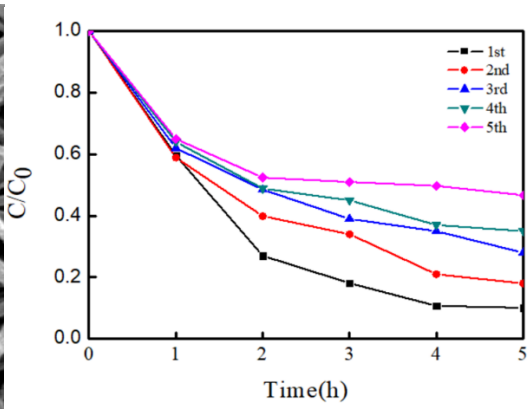

Synthesis and Modification of MOF-808

Jiong Xu[1]; Jin Liu[*1,2]; Xian-biao Wang[1,2]; Zhen Li [1, 2]; Zhou Wang[1]

1: Anhui Key Laboratory of Advanced Building Materials, Anhui JianzhuUniversity, Hefei 230601, P. R. China; 2: School of Materials Science and Chemical Engineering, Anhui Jianzhu University, Hefei 230601, P. R. China

**Corresponding author: E-mail address: liujin@ahjzu.edu.cn*

The core-shell structure and penetrated structure of Pd modified metal organic frameworks MOF-808 series materials (named as Pd@MOF-808), are successfully synthesized using Zr(Ⅳ) as centron ion, trimesic acid as ligand, and Pd as modifier by simple solution method, as Fig.1 showed. The structure control and properties of Pd@MOF-808 are characterized by XRD, FT-IR, TEM, XPS, UV-vis, specific surface area measurement, thermogravimetric analysis, photocatalytic hydrogen production and hydrogen storage testing. The results show that the synthesized Pd nanoparticles have been successfully introduced into the cavity and channel of MOF-808, and the structure of Pd@MOF-808 series materials could remain stable at 350°C. Photocatalytic hydrogen production experiments exhibit the highest hydrogen production of Pd@MOF-808-b (236 μmol g-1 h-1). More importantly, the results of the adsorption experiment show that the hydrogen storage capacities of the as-prepared 10 wt.% Pd@MOF-808-b could reach 2.61 wt.%, 5.04 wt.% and 8.20 wt.% under 4 MPa at 300 K, 195 K and 77 K, respectively. Furthermore, thermodynamic analysis shows that the maximum hydrogen adsorption enthalpy of Pd@MOF-808-b up to -1.378 kJ mol^{-1}, and indicates excellent potential for hydrogen storage and application [1, 2].

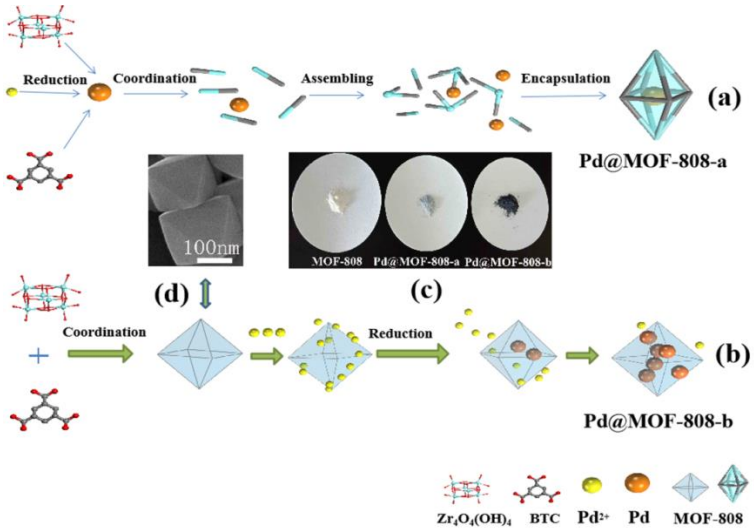

Fig. 1 The schematic illustration for synthesizing MOF-808-a (a) and MOF-808-b (b). The inset images are the color of Pd@MOF-808 series materials (c) and SEM (d) of MOF-808

Acknowledgements

This work was financially supported by the Natural Science Foundation of China (Nos. 21171004), the Science and Technology Project of Anhui Province (Nos. 1604a0802113), Anhui Province Academic Technology Leader Training Funded Projects, Natural Science Foundation of Anhui (Nos 1708085QE120) and Major Projects of Natural Science Research in Colleges and Universities of Anhui (Nos KJ20171495).

References

[1] Jiong Xu, Jin Liu*, Zhen Li, Xianbiao Wang, Zhuo Wang. Synthesis, structure and properties of Pd@MOF-808. Journal of Material Science. 2019, 54:12911–12924.

[2] Jiong Xu, Jin Liu*, Zhen Li, Xianbiao Wang, Yongfei Xu, Saisai Chen, Zhuo Wang. Optimized synthesis of Zr(IV) metal organic frameworks (MOFs-808) for efficient hydrogen storage. New Journal of Chemistry. 2019,43:4092-4099.

Preparation and properties of novel ternary flocculant for underground continuous wall waste mud

Cui Kong[1], Feng-Jun Zhang[1,2*], Xian-YangSun[1],Zi-LuZhang[1], Wen- Jie Xie[2]

[1]*Key Laboratory of Functional Molecule Design and Interface Process, Anhui Jianzhu University, Hefei Anhui, P. R. China, 230601*

[2]*Anhui Key Laboratory of Advanced Building Materials, Anhui Jianzhu University, Hefei Anhui, P. R. China, 230022*

Abstract: A novel ternary flocculant was prepared by simple compounding method. The experimental studies are conduct to explore the effects of different types of flocculants on the separation of waste mud water and the degradation of flocculant in the supernatant. The flocculating component, mixing ratio of flocification accelerator and flocculant and addition amount of novel ternary flocculant was optimized. The experimental results show that the composition of the novel ternary flocculant are cationic polyacrylamide (CP-02), grafted starch (GS-501) and floc sedimentation accelerator (FSA), which has the best effect with the mass ratio of 1:0.5:0.75. And the novel ternary flocculant has been pre-configured into a solution with a concentration of 3 kg/m^3, according to 0.25:1 (volume ratio), to achieve efficient and rapid mud-water separation. The novel ternary flocculant is used for the separation of mud and water in the underground continuous wall waste mud, to realize zero discharge of waste mud and improve the civilized construction level. The possible mud-water separation mechanism was explored.

Key words: novel ternary flocculant; rapid separation; underground continuous wall waste mud; pre-configured

Acknowledgments

This work was financially supported by the Major Projects of Natural Science Research in Anhui Colleges and Universities (KJ2018ZD050), Outstanding Young Talents Support Program in Colleges and Universities (gxyqZD2018056) and the College Students' Science and Technology Innovation Foundation (2019-152).

∗Corresponding author:Feng-Jun Zhang, E-mail: fjzhang@ahjzu.edu.cn
Tel: +86-0551-63828262 Fax: +86-0551-63828106

Pesticide-derived bright chlorine-doped carbon dots for selective determination and intracellular imaging of Fe(III)

Wen-Sheng Zou*

School of Materials and Chemical Engineering, Anhui Jianzhu University, 292Ziyun Road, Hefei, Anhui 230022, China

Abstract:

Inspired by the conversion from organics or biomass to fluorescent carbon dots (C-dots), the use of pesticide 4-chlorophenol (4-CP) as a precursor to prepare C-dots has been reported. The as-prepared chlorine-doped C-dots display a brightly blue emission at ~445 nm with ~22.8% quantum yield. Also, the surface of C-dots enriches functional groups, such as phenolic hydroxyl and carboxylic acid, etc., which can capture ferric ion (Fe(III)), resulting in the quenching of blue fluorescence of C-dots through an inner filter effect. The quantitative assay for Fe(III) was therefore realized by this probe with a 0.36 μM detection limitin the 0.6 to 25 μM concentration range. Most significantly, the cytotoxicity on Hela cells indicates the 4-CP-derived C-dots have a negligible cytotoxicity. The C-dots were applied in detection in environmental samples and imaging in Hela cells of Fe(III), demonstratingtheir goodapplicability, low toxicity andgood biocompatibility, and providing an alterative approachto totally eliminate the harm of chlorophenols (CPs).

Key words: 4-Chlorophenol (4-CP)**,** Carbon dots (C-dots)**,** Fe(III) determination**,** Cellular toxicity**,** Intracellular imaging.

Effect and mechanism of ionic liquid on the interface properties and phase structure of PLA/EMA-GMA/MWCNTs nanocomposites

Ping Wang[1*], Tian Cao[1], Dongxing Wu[1], Yiyang Zhou[2], Jinping Hu[2], Qiancheng Zhang[2], Gang Ruan[2],

1. School of Materials and Chemical Engineering, Anhui Jianzhu University, Hefei, China, 23060, 2. School of Chemistry and Chemical Engineering, Hefei University of Technology, Hefei, China, 230009

Abstract

High-tough dielectric Poly (lactic acid)/ Ethylene–methyl acrylate–glycidyl methacrylate random terpolymer (PLA/EMA-GMA) based nanocomposites containing multi-walled carbon nanotubes (MWCNTs) and ionic liquid (ILs) were prepared by melting blend. The effect and mechanism of phase structure and interfacial enhanced compatibilization behavior of PLA/EMA-GMA/MWCNTs nanocomposites system regulated by ILs were studied by SEM, DSC, rheometer and LRC. The analysis of torque data and SEM results suggested that the addition of ILs could catalysis the reaction between PLA and EMA-GMA and improve the dispersion performance of MWCNTs in matrix. The crystallization ability of PLA/EMA-GMA/MWCNTs nanocomposites was also improved while ILs was introduced. The rheological tests revealed that the G' of the samples was significantly increased and G" was decreased owing to the introduction of ILs into the nanocomposites system, which indicated that a crosslink structure at interface and a solid network structure inside the nanocomposites were formed with the incorporation of ILs. Due to the formation of interfacial crosslink structure and MWCNTs network structure, the toughness and dielectric properties of the materials was significantly improved. When the content of ILs was 2wt% and MWCNTs content reached 4wt%, the dielectric constant and dielectric loss were decreased by 2 and 20 times compared with samples without ILs, respectively, and the material had a certain toughness.

Keywords: Poly (lactic acid); multi-walled carbon nanotubes; ionic liquid; nanocomposties; crosslink structure

*Ping Wang
E-mail:anjzwp@anjzu.edu.cn
Tel: 13866725500

Synthesis and characterization of waterborne polyurethane with covalently linked disperse blue 60

Xian-Hai Hu*, Ming-Jun Li, Peng-Wei Hu,Wang-Yang Ma, Cheng-Bing Gong

School of Materials Science and Chemical Engineering, Anhui Jianzhu University, Hefei 230601, P. R. China

Abstract

A series of sulfonated waterborne polyurethane-based dyes (DB60-SWPUs) with covalently bonded to different proportions of Disperse Blue 60 (DB60) was prepared by a modified acetone process. The basic structure, fluorescent performances, thermal properties and mechanical propertiesDB60-SWPUs were characterized. All of waterborne polyurethane (WPU)withcovalently bonded to Disperse Blue 60, DB60-SWPUs, shows better color fastness, thermal migration resistance and mechanical properties than those with DB60 mixed physically. FTIR (fouriertransform infrared) spectra indicate that DB60 has covalently bonded to polyurethane chains. Compared with DB60 mixed waterborne polyurethane (WPU), the UV-vis spectra of DB60-WPUs have obvious hypochromic shift, and the fluorescence intensities are obviously enhanced in the fluorescence spectra. DB60-SWPUs are polymeric dyes with water as a solvent, which is especially suitable for environmental protection.

Keywords: waterborne polyurethane; Fluorescence; Disperse Blue 60; UV-Vis absorption spectra

*Corresponding author
E-mail: hxyh@ahjzu.edu.cn
Tel: +86-0551-63513136, Fax+86-0551-63513136

Preparation of amino-modified porous PDVB for enhanced fluoride removal

Yuanyuan Huang, Xianbiao Wang *, Bao Xu, Jiali Liu, Yangyang Zhao, Wen Ji, Renwu Zhu

Anhui Key Laboratory of Advanced Building Materials, School of Materials Science and Chemical Engineering, Anhui Jianzhu University, Hefei 230601, PR China

*Corresponding Author：*E-mail: xbwang@ahjzu.edu.cn*

As we all known, fluoride ions are harmful to dental health and excessive exposure to fluoride may result in serious diseases. Therefore, it is urgent to fabricate an effective material for removal of fluoride with fast and high adsorption properties. In this article, amino-modified porous PDVB (polydivinylbenzene)was prepared with a low-cost and simple solvothermal method. The obtained nanostructuredproducts have high surface area of 483m^2g^{-1}. Their adsorption capacity towards fluoride could reach 165.2 mg/g which is ~1.2 times higher than that of PDVB. It was found that the enhanced and fast adsorption performance of amino-modified PDVB was due to amino groups with better binding effect towards fluoride.

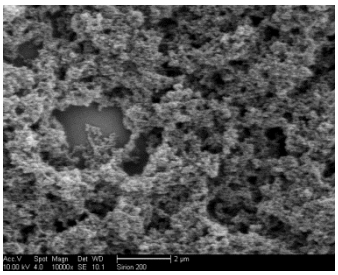

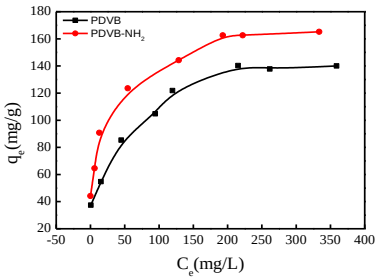

Performance and mechanism of D418 chelating resin for efficient removal of copper (II): Site energy distribution theory consideration

Hai-binLI [1,2], Fa-zhi XIE[1,2], Ke-huaZHANG [1], Wweiwei DONG, Qing-dianCHEN[1], Zhan LIU[1], Daode ZHANG[1], Yuting YANG[1]

1.School of Materials and Chemical Engineering, Anhui Jianzhu University, Hefei 230601, China, 2. Anhui Key Laboratory of Water Pollution Control and Wastewater Resource, Hefei 230601, China

Abstract：In order to elucidate the adsorption mechanism of D418 resin with high efficiency for removal of Cu(Ⅱ) from wastewater, the influence of pH, ionic strength, contact time and temperature were fully investigated through kinetics, isotherm models, thermodynamics and site energy distribution theory.The results demonstrated that the optimal removal effciency reached to 97.20% at initial pH of 9.00, and the zeta potential to the influence of adsorption capacity was more compatible with Boltzmann model. Meanwhile, the adsoption of Cu(Ⅱ) increased with ionic strength increased. According to comparisons of linear correlation coefficient values, the adsorption kinetic and isotherm models data fitted well to the intraparticle diffusion and Sips model, respectively. Presenting the Langmuir model, isotherm parameters and adsorption site energy distributions were reckond. Moreover, Thermodynamic studies showed that sorption of Cu(Ⅱ) were spontaneous and endothermic. With higher site energies, the D418 resin demonstrated a much stronger adsorption affinity for 308K than 298K. Based on XPS and FTIR analysis, the sorption mechanism was mainly attributed to the electrostatic interaction, chemical precipitation and the inner-sphere complaxation.

Keywords Copper(II); D418 resin; adsorption; kinetics; thermodynamics; site energy distribution

High sensitive ethylene sensors based on ultrafine Pd nanoparticles decorated porous ZnO nanosheets

Zhen Jin, Huang Zhang, Min-He Liao, Min-Da Xu, Yi Ding,

School of Materials and Chemical Engineering, Anhui JianZhu University, Hefei Anhui 230601, PR China.

**Correspondence should be addressed to Zhen Jin*

E-mail: ftbjin@hotmail.com Tel.: +86-551-63828103

Abstract

Through a facile solvent reduction method, the ultrafine Pd nanoparticles decorated porous ZnO nanosheets (UPNP ZnO nanosheets) can be conveniently obtained. The as-prepared samples were characterized by scanning electron microscopy (SEM), transmission electron microscopy (TEM), energy dispersive spectrum (EDS), X-ray diffraction (XRD) and X-ray photoelectron spectroscopy (XPS). It can be found that the ZnO nanosheets were uniformly coated with Pd nanoparticles. The size of the Pd nanoparticle is very small, and the diameter is about 2 nm. Due to the unique structure of the porous ZnO nanosheets and the excellent catalytic property of the ultrafine Pd nanoparticles, the as-prepared samples present a dramatically high sensing performance in ethylene detection. The lowest detection concentration is 10 ppb, which is the lowest detection limit to our knowledge. It has been proved that the decoration of ultrafine Pd nanoparticles can largely increase the relative percentage of chemisorbed oxygen and deficient oxygen, which are benefit for the ethylene oxidation, and actually accelerating the process of the sensing reaction. Furthermore, the UPNP ZnO nanosheets even can be applied in fruit maturity detection. Using mangos as an example, our experiment revealed that, to the mangos at different maturity stages, the response of UPNP ZnO nanosheets is quite different. This result suggest that our product have broad application prospects in fruit ripen stage monitor.

Electrospun antibacterialnanofibrousmembrane anchored with silvernanoparticles for air filtration application

Yaying You[1], Qianyu Yan[2], Wenyu Wang[2], Feng Chen[2], Zhigang Chen[1,2*]

[1]*School of Material Science and Engineering, Jiangsu University, Zhenjiang 212013, China*

[2]*Jiangsu Key Laboratory for Environment Functional Materials, School of Chemistry, Biology and Materials Engineering, Suzhou University of Science and technology, Suzhou 215009, China*

Abstract: Respiratorydisease induced by bacterial spread in atmosphere seriously threaten human health. Air pollution like haze with harmful suspendedparticles, as an appropriate condition of bacterial spread and breeding, need to be prevent from respiratorytract. Herein, filtration membranes possessing superior antibacterial activity are considered as effectivemeans to protect us from atmosphericcontamination with bacteria. Here, we synthesize an antibacterial nanofibrous membrane that silver nanoparticles (Ag NPs) are anchored in nanofibers composed of gelatin(GT) and silk fibroin(SF) via electrostatic spinning. Ag NPs as a available kind of inorganic antibacterial agent are imported by $AgNO_3$ and exposed to the radiation of UV light. The existence of SF which has unique mechanical properties like good flexibility and tensile strength, high elasticity and resilience, enhance the toughness of filtration membranes. In addition, both GT and SF can degrade in natural environment, which avoid the secondarypollution to atmosphere. Meanwhile, Maillard reaction cross-linking the materials in high temperature heighten the water resistence of nanofibrous membranes. Several characterizationand testing indicate that GT/SF/Ag NPs nanofibrous membranes exhibit feasible antibacterial efficiency against both Gram-positive and Gram-negative bacteria. Moreover, water vapor transmission rate test reflects the excellent filtration performance of materials. Thus, this environmentallyfriendly, biodegradable and multifunctional GT/SF/Ag NPs nanofibrous membranes can be regarded as an underlying candidate for air filtration applications.

Keywords：Electrospun；Air Filtration；Silver Nanoparticles；Antibacterial Activity

* Corresponding author
E-mail: czg@ujs.edu.cn
Tel: +86-0512-67374120, Fax:+86-0512-67374120

Efficient Photocatalytic Hydrogen Evolution from water on Ag-loaded biostructural carbon/cadmium sulfide nano-catalysis

Qianyu Yan, Yaying You, Wenyu Wang, Feng Chen*

Jiangsu Key Laboratory for Environment Functional Materials, School of Chemistry, Biology and Materials Engineering, Suzhou University of Science and technology, Suzhou 215009, China

Abstract: Photocatalytic hydrogen production from water hasbeen considered to be an effective strategy for solving energy crises. In this work, Ag-loaded biostructural carbon/cadmium sulfide composite photocatalyst was synthesized by simple hydrothermal method and photodeposition method. The structure and morphology of the nanocomposite was characterized by X-ray diffraction (XRD), scanning electron microscopy (SEM), high-resolution transmission electron microscopy (HRTEM), UV-Vis diffuse reflectance spectroscopy (DRS) and X-ray photoelectron spectrum (XPS). By studying the photocatalytic properties of materials, it was found that the deposition of Agsignificantly improved the hydrogen absorption performance of biostructure carbon/CdS. The enhanced catalytic performance can be ascribed to the combination of carbon which can expand the range of absorbed sunlight, and the loading of silver reduces the composite of photogenerated electrons - hole pairs and their photooxidative corrosion.

Keywords：cadmium sulfide; biostructural carbon; photocatalysis

Acknowledge: Natural Science Foundation of Jiangsu Province (BK20180103); Collegiate Natural Science Fund of Jiangsu Province (16KJA430008); Jiangsu Collaborative Innovation Center of Technology and Material for Water Treatment

* Corresponding author
E-mail: chenfeng@mail.usts.edu.cn
Tel: +86-0512-67374120, Fax:+86-0512-67374120

SIMULATION FOR THE OPTIMUM HEAT SINK DESIGN IN THE HIGH POWER LED PCB SYSTEMS

JU YONG CHO,[1] AND WON KWEON JANG[1,*]

[1]*Department of Aeronautic Electricity, University of Hanseo, Hanseo 1-ro 46, Seosan-si 31962, South Korea*

**jwk@hanseo.ac.kr*

1. Introduction

LED has replaced the conventional artificial illumination and broadened the applications in fields of display, farm factory, the indoor and outdoor lighting. Long life and environment friendly property are the key factors for the future smart industry.

The power of single LED chip has already exceeded W level, but the thermal treatment for the dissipative heat generation remains as a hard homework to the researchers. In normal, LED converts 1530% of input power into light emission and 70~85% into heat. Therefore, high power LEDs are usually operated at high temperature conditions, which lower the power conversion efficiency and chip lifetime. Moreover, the high temperature operating environment can make troubles of quantum efficiency and wavelength shift [1-5]. In order to avoid these problems, many researchs have been reported to reduce the disadvantages and to get the general method how to manage the heat dissumption. However, the passive cooling solution considering convection and conduction to get the optimal thermal treatment still remains as a complicated matter. In this paper, we investigated the effects of convection and conduction for the optimal heatsink design. Thermal resistance of the heatsink attached to the PCB was theoretically studied to investigate the dependence of the geometrical figure of heat sink. The thermal profiles for the given LEDs on the PCB could be acquired by Computational Fluid Dynamics(CFD) analysis and compared to theoretical study.

2. Heat transfer

We assume that the heat dissipation of LED and PCB are mainly affected by convection and conduction effects. Heat dissipation by convection is caused by exchanging thermal energy between surface and fluid and it can be expressed by eq.1.

$$Q_{\text{convection}}=h(T_s-T_{ambient}) \quad [1]$$

Where Q is heat flux, h is convection coefficient, T_s is surface temperature of material, and $T_{ambient}$ is ambient temperature. Heat dissipation by conduction strongly depends on

conduction between the highest and the lowest temperature regions and it can be written as eq.2.

$$Q_{\text{conduction}}=k\frac{(T_{high}-T_{low})}{L} \quad [2]$$

Where Q is heat flux, k is thermal conductivity, T_{high} is higher temperature, T_{low} is lower temperature, and L is length of material. Thermal resistance for convection and conduction can be expressed by eq.3 and eq.4, respectively.

$$R_{\text{conduction}}=\frac{(T_{high}-T_{low})}{q_{\text{conduction}}}=\frac{(T_{high}-T_{low})}{kA_{conduction}\frac{(T_{high}-T_{low})}{L}}=\frac{L}{kA_{conduction}} \quad [3]$$

$$R_{\text{convection}}=1/hA_{convection} \quad [4]$$

Where $R_{\text{conduction}}$ is thermal resistance for conduction, $q_{\text{conduction}}$ is $Q_{\text{conduction}}A_{conduction}$, $A_{conduction}$ is surface area for conduction, $R_{\text{conduction}}$ is thermal resistance for convention and $A_{convection}$ is surface area for convection.Fig. 1 shows that LED light system that contacts fluid. The system consists of Metal-Core PCB(MCPCB) and Aluminium based Heat sink. Total thermal resistance for this system can be expressed by eq.5.

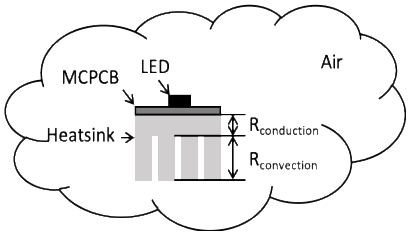

Figure 1. LED lighting system surrounded by the air

$$R_{Convection+conduction}=\frac{1}{h(A_{bottom}+N_{fin}\eta_{fin}A_{fin})}+\frac{H-H_{fin}}{k\ w\ L}+N_{fin}\frac{H_{fin}}{k\ t_{fin}\ L} \quad [5]$$

Where A_{base} is the exposed surface area, N_{fin} is the number of fins, A_{fin} is the side surface area of fins, η_{fin} is fin efficiency, h is convection coefficient, k is thermal conductivity of heatsink, h is height of heatsink, and m is non-dimensional parameter.

3. Experiment

Fig. 2 shows that temperature change of the surface of the PCB with thickness of heat sink. The data points indicate the temperature at the center of PCB. The highest temperature of a 18mm thickness of heat sink was 58.82℃ and the lowest temperature of 45.85℃ could be found in 0mm thickness of heat sink.

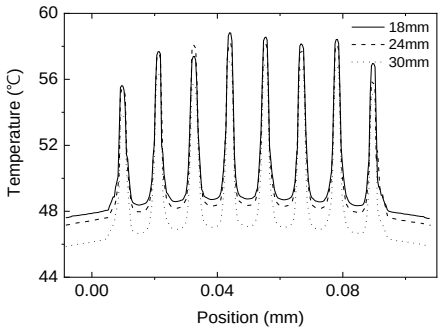

Figure 2. temperature at the center of PCB.

4. Conclusion

Thermal resistance of heast sink was theoretically investigated. Temperature change for various heat sink configuration could be acquired by means of computational fluid dynamics. This calculation of thermal resistance can be applied to find the optimal selection of heat sink for various LED configuration for effective thermal dissipation.

References

1. T. Cheng, X. Luo, S. Huang, S. Liu, “Thermal analysis and optimization of mulatiple LED packaging based on a general analytical solution”. Int. J. Therm. Sci., Vol. 49, 196-201(2010)
2. H.H. Cheng, D. Huang, and M. Lin, “Heat dissipation design and analysis of high power LED array using the finite element method, Microelectron”, Vol52, No. 5, 905-911(2012)
3. K.C. Yung, H. Liem, H.S. Choy,” Heat transfer analysis of a high-brightness LED array on PCB under different placement configurations”, Internaltional Communications in Heat and Mass Transfer, Vol.53, 79-86(2014)
4. J. Petroski, spacing of high-brightness LEDs on metal substrate PCB’s for proper thermal performance, in: Proceedings of the IEEE Inter Society Con- ference on Thermal Phenomena, Las Vegas, Nevada, 2004, 507e514.
5. J. Petroski, understanding longitudinal fin heat sink orientation sensitivity for Light Emitting Diode (LED) lighting applications, in: Proceedings of the In- ternational Electronic Packaging Technical Conference and Exhibition, Maui, Hawaii, 2003, 111e117.

Vibisility degradation and spectral distortion in a spatially modulated Fourier transform spectrometer base on a birefringent prosm

JU YONG CHO,[1] AND WON KWEON JANG[1,*]

[1]*Department of Aeronautic Electricity, University of Hanseo, Hanseo 1-ro 46, Seosan-si 31962, South Korea*

**jwk@hanseo.ac.kr*

1. Introduction

Fourier transform spectrometer has many advantages compared to other types of spectrometers. It is possible to get the faster measurement in broader spectral range and the higher throughput than other dispersive type of spectrometers. Though these multiplex advantage, it has been limited by a strict operation requirement that has hindered its field application.

The Fourier transform spectrometers are based on an interferometer, which produces an interferogram with spectral information. Most of it typically produce an interferogram by a moving optics inside the interferometers. During this procedure, the optical alignment can be badly affected even due to a small vibration. The misinterpreted spectral information can come from a slight optical misalignment or a minor vibration [1-2].

In order to overcome this disadvantage many structural researches have been reported. The most important consideration was to ensure that the interferogram should be produced without any moving optical element inside the interferometer. It is called the spatially modulated interferometer and split into two categories. One consists of one beam splitter and two mirrors and the other is consists of birefringent crystal and two polarizers.

In this paper, we investigated the visibility of interferometer with a birefringent crtstal, and also the mechanism of generating interferogram.

2. Wollaston prism interferometer

The interferometer using the birefringent effect consists of one birefringent crystal, a polarizer and an analyzer. The incident light is linearly polarized after it passes through the polarizer. When the linearly polarized light passes through the birefringent prism, it is split into two individual lights at the wedge of the birefringent prism. The two split beams are polarized orthogonally. During two beams pass through the prism, they interfere each other, and produce an interferogram as described in the fig. 1.

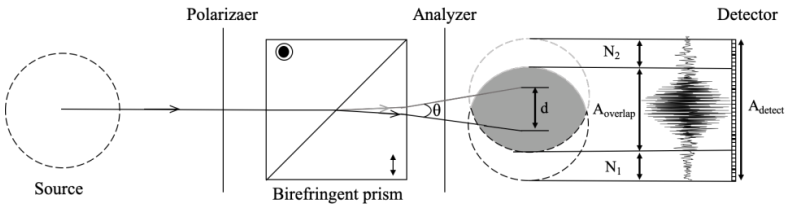

Figure 3. Schematic diagram of the interferometer composed of a birefringent prism and a polarizer and an analyzer

An interferogram generated by a birefringent crystal shows the spatial distribution of intensity in the overlapped sector of two orthogonally polarized beams. The overlapped sector can be caculated as follows.

$$A_{overlap}=2(r-d)=2(r-[x \cdot \tan(\frac{\theta}{2})]) \quad [1]$$

Where $A_{overlap}$ is overlapped sector, θ is the separation angle between two orthogonally polarized beams, x is the distance from the wedge the prism to the detector, and y is the lateral distance, d is the displacement of the center of one of polarized beam from the optical axis.

The separation angle θ is given by eq.2.

$$\theta \approx 4(n_e - n_o)\tan\alpha \quad [2]$$

Where n_e is refractive index for extra-ordinary light, n_o is refractive index for ordinary light, and α is angle of the wedge interface of the birefringent prism.

3. Visibility

In the birefringent prism, the overlap sector is depending on the detector position from the wedge of prism. Because the incident light normally has gaussian distribution, the visibility degrades harder as the detector position moves far from the wedge. The visibility V can be calculated by eq.3.

$$V=\frac{I_{max}-I_{min}}{I_{max}+I_{min}} \quad [3]$$

Where I_{max} is the maximum intensity in the interferogram and I_{min} is the minimum intensity in the interferogram.

4. Experiment

The detector was placed at 25mm, 50mm, 75mm and 100mm from the wedge in order to investigate the change of visibility of interferogram. The measured visibility change is

shown in the fig.2. The beam profile was gaussian and the distance between two orthogonally polarized beams increased when the detector position moves far from the wedge. The visibility was 0.41 at 25mm and decreased to 0.22 at 100mm.

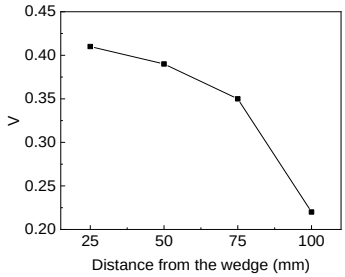

Figure 4. Visibility change in terms of measurement point.

5. Conclusion

The mechanism of producing interferogram base on a birefringent crystal is discussed and the visibility change was inverstigated. In condition of low visibility, the signal to noise ratio was so low that Fourier transformed spectrum from the acquired interferogram can easily be distorted. In order to increase the signal to noise ratio, the apodization should be applied to the acquired interferogram with considering the gain ranging in spatial domain.

References

6. Haiwu Yu, and Shaoxian Meng, “Wollaston prism design and working parameters in the Normarski polarized light interferometer”, Opt. Eng., Vol. 35, No. 8, 2310-2312(1996)
7. Yixuan Xu, Jianxin Li, Caixun Bai, Heng Yuan, and Jie Lie, “Ultra-compact Fourier transform imaging spectrometer using a focal plane birefringent interferometer”, Vol. 43, No. 17, 4081-4084(2018)
8. Maria C. Simon, “Wollaston prism with large split angle”, Applied optics, Vol.25, No. 3, 369-376(1986)

Near-infrared-driven selective photocatalytic removal of ammonia based on valence band recognition of α-MnO_2/N-doped graphene hybrid catalyst

Shou-Qing Liu, * Li Luo, Ze-Da Meng, Xin Zhang, Yiwen Zhou, Jing Zhou, Dongwen Li

†*Jiangsu Key Laboratory of Environmental Functional Materials; School of Chemistry, Biology and Material Engineering, Suzhou University of Science and Technology, Suzhou 215009, China*

Abstract: Near-infrared (NIR) response photocatalysts are desired to make use of 44% NIR solar irradiation. A flower-like α-MnO_2/N-doped graphene (NG) hybrid catalyst were synthesized and characterized by X-ray diffraction spectroscopy, transmission electron microscopy, Raman spectroscopy, UV-Vis-NIR diffuse reflectance spectroscopy and X-ray photoelectron spectroscopy. The flower-like material of α-MnO_2/NG was oval-shaped with the semi major axis of 140 nm and semi minor axis of 95 nm and the petal thickness of 3.5 to 8.0 nm. The indirect band gap was measured to be 1.16 eV, which is very close to 0.909 eV estimated by the First-principles calculation. The band gap can harvest NIR irradiation to 1069 nm. The coupling α-MnO_2 with NG sheets to form α-MnO_2/NG can significantly extend the spectrum response up to 1722 nm, improving dramatically photocatalytic activity. The experimental results displayed that the α-MnO_2/NG hybrid catalyst can recognize ammonia in methyl orange-ammonia, rhodamine B-ammonia and humic acid-ammonia mixed solutions and selectively degrade ammonia. The degradation ratio of ammonia reached over 93.0% upon NIR light irradiation in the mixed solutions, while the ones of MO, RHB and humic acid were only 9.7%, 9.4% and 15.7%, respectively. The products formed during the photocatalytic process were followed with ion chromatography, gas chromatography and electrochemistry. The formed nitrogen gas has been identified during the photocatalytic process. A valence band recognition model was suggested based on the selective degradation of ammonia via α-MnO_2/NG.

Study on Electron Mobility Control through Magnetization of Ferromagnetic Semiconductor

Hyun Sik Kang[1], Soon Wook Kwon[1], Woo Seoung Kim[1], Sung Jun On[1], Hyun Min Jung[1], Soo Min Lee[1], Jae Eun Gwon[1] and Hak Soo Kim[1,*] , Tae Ho Kim[2,*]

[1]*Department of Environmental & Bio-Chemical Engineering, Sun Moon University, Asan, Republic of Korea*

[2]*Research Center for Eco Multi-Functional Nano Materials, Sun Moon University, Asan, Republic of Korea*

[*] *Corresponding author*

Abstract

The magnetic field is used to control the electron movement of three-dimensional material and to confirm the same behavior as the two-dimensional material by using semiconductor. $BiFeO_3$ semiconductor were prepared by mixing TiO_2 of dye-sensitized solar cells with ferromagnetic Perovskite $BiFeO_3$ at a ratio of wt% 1, 3, 5 and then analyzing the results through a solar simulator and an electrical and electronic property measuring device. The overall efficiency decreases with increasing $BiFeO_3$ content, which may be attributed to the uneven dispersion of the produced TiO_2-$BiFeO_3$ Paste and the decreased TiO_2 content. However, the results showed different results according to the four directions. Among them, the semiconductor which induced the Hall effect vertically in the direction of the magnetic field and the electric current showed high efficiency and V_{OC} values. This is due to the polarization of the material, which reduces the degree of freedom of electrons and induces the movement of electrons in a certain direction.

Enhancement of Photocatalytic Activity for Chemically Etched ZnO Thin Films Prepared by Pulsed Spray Pyrolysis

Qin-fang Zhang[1], M. Obaida[1,2], I. Moussa[2,3], S. A. Hassan[2] and H. H. Afify[2]

[1]School of Materials Science and Engineering, Yancheng Institute of Technology, Yancheng 224051, P. R. China.

[2]Solid State Physics Department, Physics Division, National Research Centre (NRC), Dokki, Cairo, 12622, Egypt.

[3]School of Energy and Engineering, Huazhong University of Science and Technology (HUST), 1037 Luoyu Road, Wuhan, Hubei, China; P.C: 430074.

Simple pulsed spray pyrsolysis (PSP) technique is used to prepare pure nanostructured zinc oxide (ZnO) thin films at different deposition temperatures and spraying times on glass substrates. XRD measurements show polycrystalline ZnO hexagonal wurtzite phase preferably oriented perpendicular through c- axis along (002) plane. SEM images demonstrate the formation of highly ordered hexagonal nanorods with a crystallite sizes ranged from 40 to 500 nm depending on the film thickness. Optical measurements show transmittance of nearly 90% at low thicknesses and about 60% for higher thickness with a calculated energy band gap values spanning from 2.85 to 3.20 eV, respectively. Photocatalytic activity is performed on selected ZnO samples have highly oriented nanorods with large hexagonal cross-section area. Photocatalytic activity takes place on etched and as prepared ZnO film samples by monitoring photodegradation process of methylene blue MB using double beam spectrophotometer. Etched samples show higher photo activity than non- etched ones.

Molecular Ordering Coating Method to improve the performance of polymer OLED by Solution Process

Seok Je Lee[1,2], Fangnan Yao[1], Xudong Dai[1], Seung il Lee[2],

Woo Young Kim[2], Cao Jin[1], Chul Gyu Jhun[2†]

[1]*Key Laboratory of Advanced Display and System Applications, Shanghai University,*

Ministry of Education, Shanghai, 200072, China

[2]*Division of Electronics and Display Engineering, Hoseo University, Asan 31499, Korea*

Tel: +82 41 540 5899, Fax: + 82 41 540 5618, email: cgjhun@hoseo.edu

Abstract:

We improved the performance of OLED device with MEH-PPV, Poly[2-methoxy-5-(2-ethylhexyloxy)-1,4-phenylenevinylene]. First, the solvents and the concentrations were optimized for the solution process. MEH-PPV was mixed into the three different solvents of toluene, chloroform, chlorobenzene with various concentration of 0.1 wt%, 0.5 wt%, and 1 wt%. The coated devices were put in the anti-chamber of the glove box, and the solvent was dried in a vacuum state for 12 hours. We compared the electro-optical performance by measuring I-V-L characteristics. Optimum conditions were obtained with the solvent of toluene and concentration of 0.5 wt%.

We also proposed a novel solution process, which is the molecular ordering coating method. In this method, organic polymers were coated by using bar coater (OSP- 30, S60 of Japanese genuine) at a constant speed in one direction. With this coating method, the polymer molecules aligned. By comparing the measured J-V characteristics of the fabricated devices by the spin coating and the bar coating method, it is confirmed that the device efficiency fabricated by the molecular ordering coating method was improved. As a result, the turn-on voltage and the luminescence of OLED fabricated by spin coating were 4.5 V and 34.74 cd/m^2, respectively. Those by polymer crystal were 4 V and 35.95 cd/m^2. This reason is due to the orientation of the molecules, which improved the conductivity.

Key words: J-V characteristic, solution process, space charge limited current

[1] A. Köohler, H. Bäassler, WILEY-VCH Verlag GmbH & Co. KGaA: Weinheim, Germany, (2015)

[2] ID Parker, J. Appl. Phys. 75, 1656 (1998)

[3] W. Y. Kim, Y.-H. Kim, C.-G. Jhun, R. Wood, P. Mascher, and C.-B. Moon, J. Appl. Phys. 111, 014507 (2012)

Enhanced Power Conversion Efficiency of Organic Photovoltaic Device by Energy Conversion Layer

Zhou Zhou, Seok Je Lee, Seung il Lee, Woo Young Kim, Chul Gyu Jhun†

Division of Electronics and Display Engineering, Hoseo University, Asan 31499, Korea

Tel: +82 41 540 5899, Fax: + 82 41 540 5618, email: cgjhun@hoseo.edu

Abstract:

The organic photovoltaic (OPV) devices have many advantages, such as easy large-area processibility, low produce cost, lightweight, and possibility of portable application [1-7]. However, the power conversion efficiency (PCE) is limited due to the narrow absorption spectrum of the organic active layer [8-10]. In this paper, to improve the PCE, we propose an OPV device with an energy conversion layer (ECL). The spectral down-conversion layer was fabricated the outer side of the OPV device. The energy conversion layer was fabricated with energy conversion materials. It absorbs the ultraviolet light and re-emits visible light, wavelengths of which coincide with the optical absorption spectrum range of the photoactive layer of the solar cell. We investigated the effects of the ECL layer on the PCE of the proposed OPV device [11].

Key words: organic photovoltaic, energy conversion, power conversion efficiency

[1]. G. Yu, J. Gao, J. C. Hummelen, F. Wudl, and A. J. Heeger, Science vol. 270, pp. 1789, 1995.

[2]. S. Gunes, H. Neugebauer, and N. S. Sariciftci, Chem. Rev., vol. 107, pp. 1324, 2007.

[3]. G. Li, V. Shrotriya, J. S. Huang, Y. Yao, T. Moriarty, K. Emery, and Y. Yang, Nat. Mater., vol. 4, pp. 864, 2005.

[4]. G. Li, R. Zhu, and Y. Yang, Nat. Photonics, vol. 6, pp. 153, 2012.

[5]. A. Facchetti, Chem. Mater., vol. 23(3), pp. 733, 2011.

[6]. D. Gendron and M. Leclerc, Energy Environ. Sci., vol. 4(4), pp. 1225, 2011.

[7]. G. Dinnler, M. C. Scharber, and C. J. Brabec, Adv. Mater., vol. 21(4), pp. 1323, 2009.

[8]. L.-M. Chen, Z. Xu, Z. Hong, and Y. Yang, J. Mater. Chem., vol. 20, pp. 2575 (2010).

[9]. M. C. Scharber, D. Muhlacher, M. Koppe, P. Denk, C. Waldauf, A. J. Heeger, and C. J. Brabec, Adv. Mater., vol. 18, pp. 789, 2006.

[10]. J. Peet, J. Y. Kim, N. E. Coates, W. L. Ma, D. Moses, A. J. Heeger, and G. C. Bazan, Nat. Mater., vol. 6, pp. 497, 2007.

[11]. D. B. Yeo, K. C. Heo, G. Bae, S. H. Chae, C.-B. Moon, W. Y. Kim, C. G. lhun, Photovoltaic Specialist Conference (PVSC), 2015 IEEE 42nd, 2015.

High sensitive ethylene sensors based on ultrafine Pd nanoparticles decorated porous ZnO nanosheets

Zhen Jin, Huang Zhang, Min-He Liao, Min-Da Xu, Yi Ding,

School of Materials and Chemical Engineering, Anhui JianZhu University, Hefei Anhui 230601, PR China.

**Correspondence should be addressed to Zhen Jin*

E-mail: ftbjin@hotmail.com Tel.: +86-551-63828103

Abstract

Through a facile solvent reduction method, the ultrafine Pd nanoparticles decorated porous ZnO nanosheets (UPNP ZnO nanosheets) can be conveniently obtained. The as-prepared samples were characterized by scanning electron microscopy (SEM), transmission electron microscopy (TEM), energy dispersive spectrum (EDS), X-ray diffraction (XRD) and X-ray photoelectron spectroscopy (XPS). It can be found that the ZnO nanosheets were uniformly coated with Pd nanoparticles. The size of the Pd nanoparticle is very small, and the diameter is about 2 nm. Due to the unique structure of the porous ZnO nanosheets and the excellent catalytic property of the ultrafine Pd nanoparticles, the as-prepared samples present a dramatically high sensing performance in ethylene detection. The lowest detection concentration is 10 ppb, which is the lowest detection limit to our knowledge. It has been proved that the decoration of ultrafine Pd nanoparticles can largely increase the relative percentage of chemisorbed oxygen and deficient oxygen, which are benefit for the ethylene oxidation, and actually accelerating the process of the sensing reaction. Furthermore, the UPNP ZnO nanosheets even can be applied in fruit maturity detection. Using mangos as an example, our experiment revealed that, to the mangos at different maturity stages, the response of UPNP ZnO nanosheets is quite different. This result suggest that our product have broad application prospects in fruit ripen stage monitor.

Water-dispersible graphene based photocatalysts and their high-performance in water treatment

Liyuan Zhang [*,1,2], Xiaoying Hu [2], Linlin Zhu [1]

[1] *School of Material and Chemical Engineering, Bengbu University, Bengbu, Anhui 233000, People's Republic of China*

[2] *Anhui Shengyun Machinery Co. Ltd., TongCheng, Anhui 231400, People's Republic of China*

Abstract: The water-dispersible graphene based photocatalysts were fabricated via a facile and efficient approach: magnetic nanoparticles and photocatalysts (TiO_2 or ZnO) were attached on the surface of sulfonated graphene by hydrothermal method. This novel water-dispersible graphene based nanocomposites could be used as high effective photocatalysts and displayed high photocatalytic activity and convenient magnetic separation property for removal of dye pollutants. Moreover, these novel photocatalysts could be recycled more than 10 consecutive trials without noticeable decrease in its effectiveness and have a great potential application in water treatment.

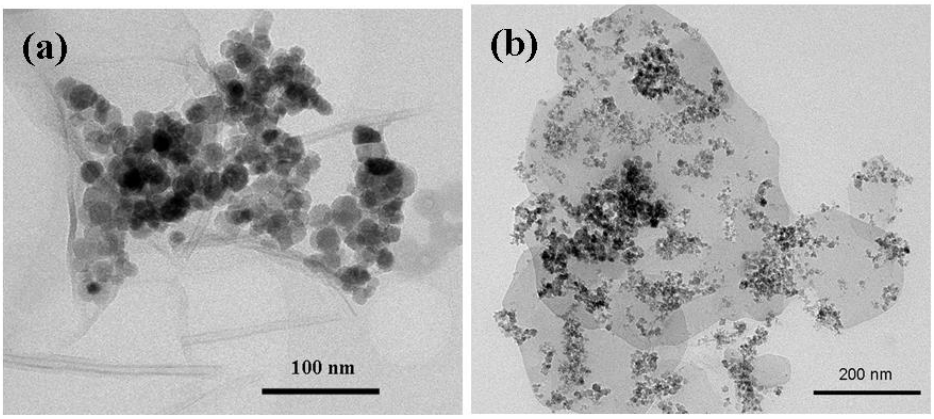

Figure (a): The TEM images of water-dispersible magnetic TiO_2/graphene nanocomposites. FROM: Water-dispersible and recyclable magnetic TiO_2/graphene nanocomposites in wastewater treatment. *Materials Letters*, **2018**, *231:*80-83.

Figure (b): The TEM images of water-dispersible magnetic ZnO/graphene nanocomposites. FROM: Water-dispersible ZnO/$C_OFe_2O_4$/graphene photocatalyst and their high-performance in water treatment. *Fullerenes, Nanotubes and Carbon Nanostructures*, **2019**, *27(11):*873-877.

Research Support Fund: the Natural Science Foundation of Anhui Province's Higher Education of China (No. KJ2019A0847), Scientific Research Foundation for Postdoctoral Research Projects of Anhui Province (2017B203) and Engineering Research Centers Program of Bengbu University (BBXYGC2016B01).

*** Corresponding Author:**

Liyuan Zhang, School of Material and Chemical Engineering, Bengbu University, Bengbu, Anhui 233000, People's Republic of China

Email: liyuanzhang522@163.com

Preparation and Performance of $DyBaCo_2O_{5+\delta}$ as Cathode Material of Intermediate Temperature Solid Oxide Fuel Cells

Xiaoyu Ma, Mingwen Xiong

School of Materials and Chemical Engineering, Bengbu University, Bengbu 233000, China.

E-mail: pineapplehhh@163.com

One of the major goals in solid oxide fuel cell research is the reduction of the operating temperature to intermediate temperature range (500-700℃) in order to improve the compatibility of the constituent materials, prolong the cell lifetime and decrease the operation costs. However, the lowing of working temperature will lead to the increase of the cathode polarization resistance and the drastic decrease in the performance of the whole cell. Development of cathode materials with high catalytic activity for oxygen reduction and low polarization resistance, therefore, is critical for intermediate-temperature solid oxide fuel cells.

The $DyBaCo_2O_{5+\delta}$ cathode materials with perovskite structure are synthesized by EDTA-citric acid sol-gel method and evaluated as potential cathodes for intermediate-temperature solid oxide fuel cells. The experimental results show that the electrical conductivity of $DyBaCo_2O_{5+\delta}$ exhibits maximum value of 254 S cm^{-1} at 325℃ and the peak power density of the cell with $DyBaCo_2O_{5+\delta}$ cathode reaches 436 mW cm^{-2} at 650℃. which are suitable for intermediate-temperature solid oxide fuel cells.

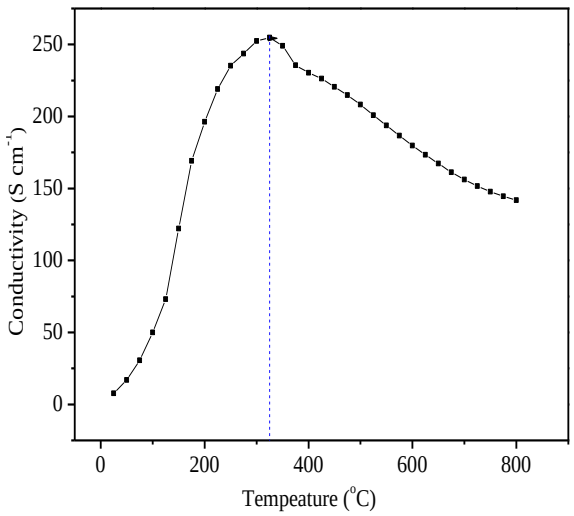

Fig. 1 Electrical conductivity of $DyBaCo_2O_{5+\delta}$ as function of temperature

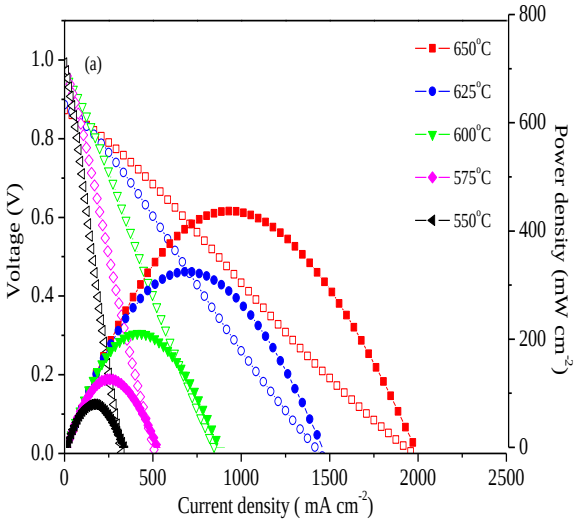

Fig. 2 *I-V* and *I-W* curves for single cell with the $DyBaCo_2O_{5+\delta}$ cathode

References:

[1] Xianshuang Xin, Leimin Liu, Yan Liu, Qingshan Zhu. Novel perovskite-spinel composite conductive ceramics for SOFC cathode contact layer[J]. *International Journal of Hydrogen Energy*, **2018**, 43 (51): 23036-23040.

[2] Jialun Mao, Shuting Peng, Chao Zhang, Siming Qi, Qingjun Zhou . Electrode properties of $(Pr_{0.9}La_{0.1})_{2-x}(Ni_{0.74}Cu_{0.21}Al_{0.05})O_{4+\delta}$ (with x=0, 0.05, and 0.1) as cathodes in IT-SOFCs[J]. *Journal of Alloys and Compounds*, **2019,** 793 (01): 519-525.

Graphene oxide assisted synthesis of heteroatom-doping mesoporous carbon nanosheets with improved capacitive performances in redox-active electrolyte

Zhong Wu*

Abstract: Significant enhancement of energy density of electrical double layered capacitors is a major challenge for electrochemical capacitors to conquer the emerging field of large scale renewable energy storage. The enhancement of specific capacitance is an effective strategy to obtain higher energy density. Addition of redox mediator in the electrolyte as pseudocapacitive sources could enhance the specifc capacitance, but well-coupled electrode materials should be developed as well. Herein, as a proof-of-concept experiment, N, O-codoped porous carbon nanosheets have been fabricated, wherein graphene oxide is employed as both oxygen source as well as structure directing agent. Unexpectedly, the obtained electrode materials endow electrical double layered capacitors with excellent capacitive performances, including the ultra-high specific capacitance (5073.5 F g^{-1}) and excellent cycling stability, which could be attributed To the synergy of morphology and surface chemistry of N, O-codoped porous carbon nanosheets. These results would form the basis for an unprecedented perspective in the development of next generation electrode materials for electrical double layered capacitors.

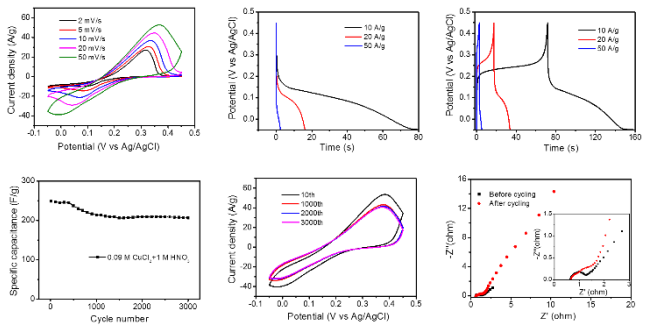

Figure 1. Electrochemistry properties of the as-prepared samples in 1 M CuCl2-HNO3. (a) Cyclic voltammetry curves at various scan rates. (b) Galvanostatic discharging curves and (c) galvanostatic charging and discharging curves at various current densities. (d) cycling stability (10^{th}, 1000^{th}, 2000^{th}, 3000^{th}). (f) EIS before and after cycling.

References:

1.Esouni M, Schopf D. Modified nanocarbon surfaces for high performance supercapacitor and electrocatalysis applications. Chem Commun,2015,51:13650–13653.

2.Hasegawa G, Deguchi T, Kanamori K, et al. High-level doping of nitrogen, phosphorus, and sulfur into activated carbon monoliths and their electrochemical capacitances. ChemMater, 2015, 27:4703–4712.

3.Wu ZS, Parvez K, Winter A, et al. Layer-by-layer assembled heteroatom-doped graphene films with ultrahigh volumetric capacitance and rate capability for micro-supercapacitors. Adv Mater, 2014, 26: 4552–4558.

4.Li B, Dai F, Xiao Q, et al. Nitrogen-doped activated carbon for a high energy hybrid supercapacitor. Energy Environ Sci, 2016, 9: 102–106.

5. Hao GP, Li WC, Qian D, et al. Structurally designed synthesis of mechanically stable poly(benzoxazine-co-resol)-based porous carbon monoliths and their application as high-performance CO2 capturesorbents. J Am Chem Soc, 2011, 133:11378–11388.

Acknowledgments: This work was supported by the Bengbu university doctoral research fuding project （BBXY2018KYQD16）, Anhui university natural science research project(KJ2019A0848).

Compatibility study of poly (vinyl chloride)/epoxidated cardanol acetate blends by molecular dynamic simulations

Xi Li [1,2], Ran Ran He [1], Bo-liang Wang [2]

1, School of chemical and materials engineering, Bengbu University

2, School of chemical engineering, Nanjing University of Science and Technology

Abstract: Poly (vinyl chloride) (PVC) is commonly used in commercial applications. Due to its high glass-transition temperature, plasticizers are often used. The most widely applicated commercial plasticizers are phthalate compounds, however, these compounds are easily migrating to external media and harmful to medical plastics, toys and children. Possible alternative natural-based plasticizers have drawn much attention. Cardanol (CD) and its derivatives, commonly used renewable raw materials, have major applications as a plasticizer in the polymer and rubber industries. There are a number of experimental investigations concerning on plasticizing effect of cardanol (CD) and its derivatives on PVC. While related theoretical explorations are still limited. In order to explore the compatibility and interaction between poly (vinyl chloride) and epoxidated cardanol acetate (ECA), five different mass ratios (100/0, 70/30, 50/50, 30/70 and 0/100) were constructed by molecular dynamic simulations. Solubility parameters, blending ability, glass-transition temperatures and radical distribution function. Calculations results of solubility parameters and blending ability indicated that PVC and ECA are compatible. ECA has effective effects on decreasing glass-transition temperatures of PVC. Hydrogen bonds can be formed between the oxygen of ECA and hydrogen of PVC from the analysis of radical distribution function.

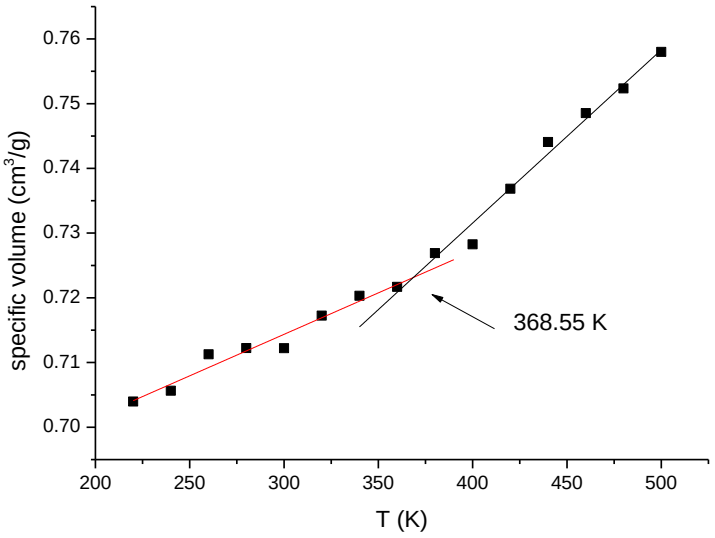

(a) PVC

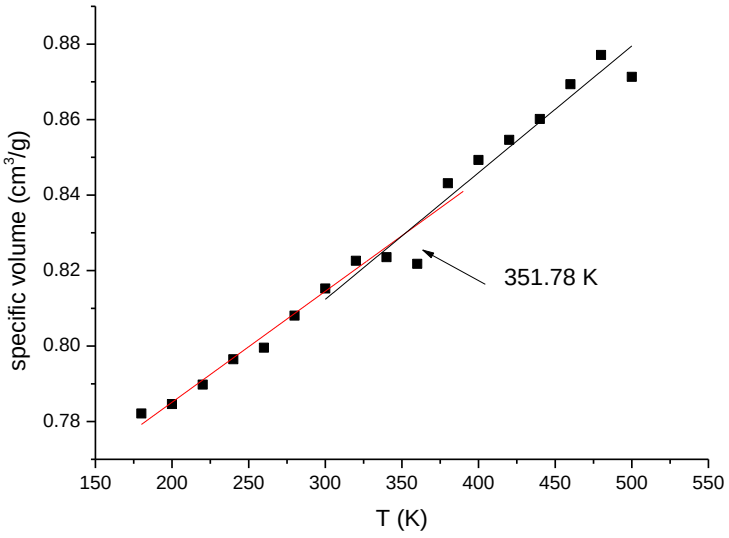

(b) 70PVC/30ECA

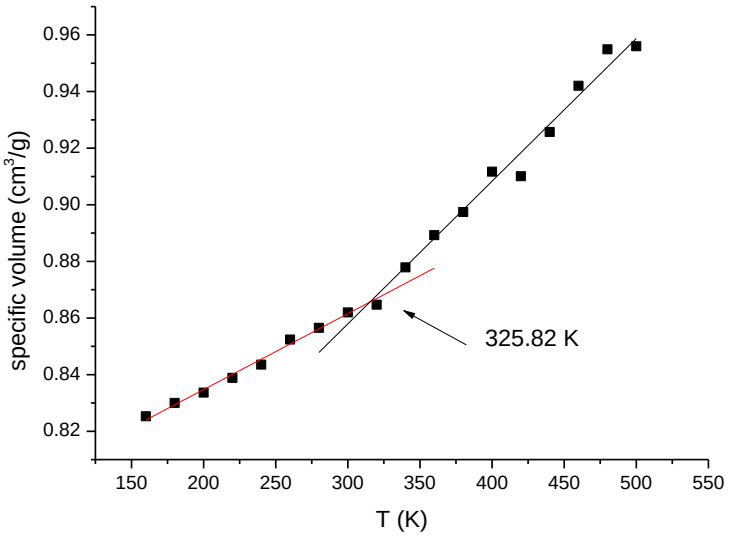

（c）50PVC/50ECA

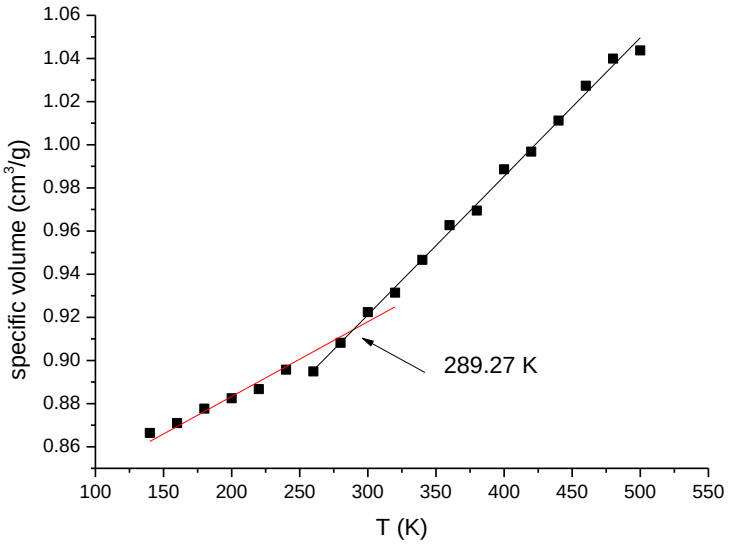

(d) 30PVC/70ECA

Fig.1 Glass-transition temperatures of different PVC/ECA composites

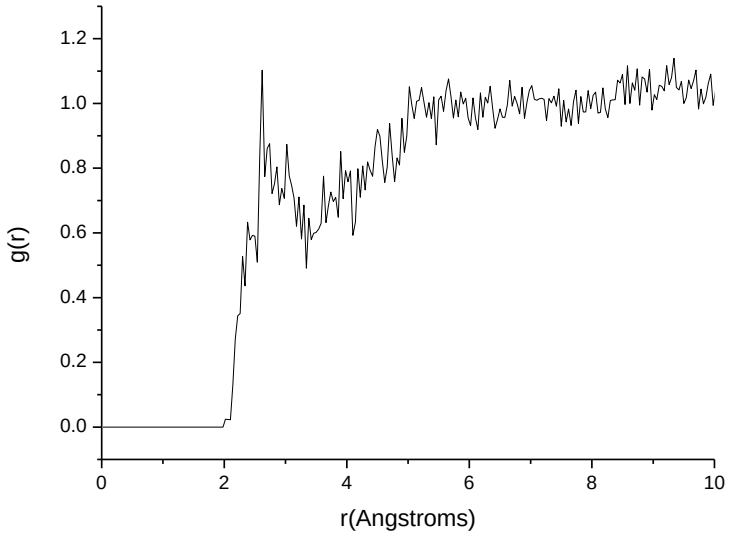

Fig.2 g(r) of PVC/ECA（30/70）

Acknowledgments

This article is funded by the project of Natural Science Research Projects in Colleges and Universities of Anhui Province, (No. KJ2019A0859).

Preparation and application of a gas sensitive material for detecting ammonia

Xianfeng Zhang*, Jingbo Lu, Xuyan Wang, Zhong Wu, Changpeng Lv, Zongqun Li

Anhui Provincial Engineering Laboratory of Silicon-based Materials, School of Material and Chemical Engineering, Bengbu University, Bengbu, 233030, PR China

Abstract

Two-dimensional (2D) nanostructures have great appeal for the preparation of nanodevices due to their high specific surface area and good compatibility with device design. [1] In recent years, two-dimensional nanostructures of various materials including metal oxides, graphene, metallocenes, phosphenes, boron nitrides, and nitrides have shown great potential in gas sensors, including two-dimensional molybdenum sulfide (MoS_2) is a promising gas sensing material for low temperature detection. [2] In this paper, MoS_2 and g-C_3N_4 materials were prepared separately, and g-C_3N_4/MoS_2 nanocomposites were prepared by sol method as gas sensing materials to detect ammonia gas; gas-sensitive components coated with g-C_3N_4/MoS_2 nanocomposites were aged and resistors were used. The wire passes through the inside of the wire, and then the six filaments on the ceramic tube are welded with the six pillars of the gas sensor base with tin to obtain the desired gas sensor for detecting ammonia gas. The experimental results show that the TEM image of g-C_3N_4/MoS_2 confirms that the sample has a sheet structure (Fig. 1), and the sensitivity of g-C_3N_4/MoS_2 with mass ratio of 1.84% is 22.1, which is 6.94 times of the sensitivity of the single MoS_2 sensor. Preferably, it has good sensitivity and selectivity to ammonia. The response recovery curve of g-C_3N_4/MoS_2 sensor to 50 ppm ammonia gas can be seen that its response/recovery time is 19.4 s and 28.5 s (Fig. 2), indicating that the prepared gas sensor has better response to ammonia gas. The obtained gas sensor has the advantages of high sensitivity and high selectivity for the detection of ammonia gas, and can be used for detecting ammonia gas in an industrial environment.

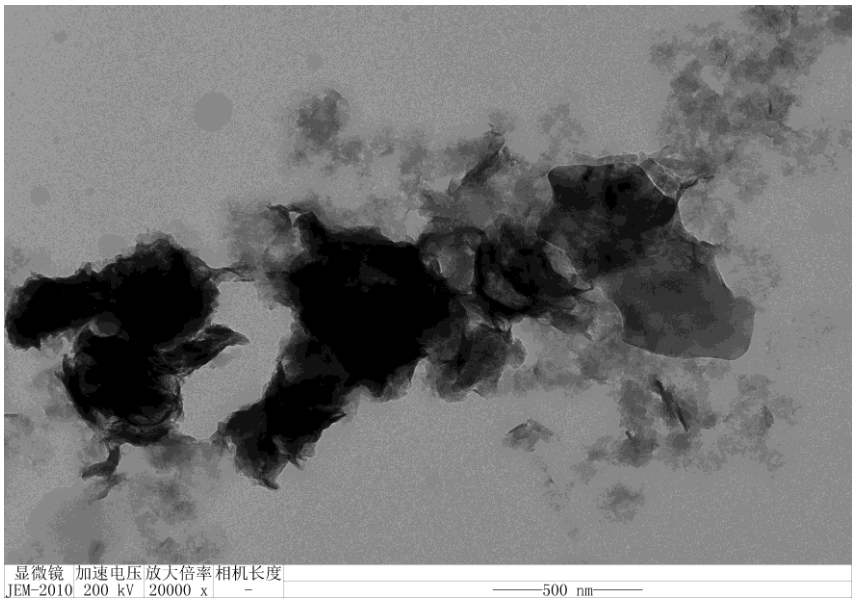

Fig.1 Transmission electron microscopy of C_3N_4/MoS_2 nanocomposites.

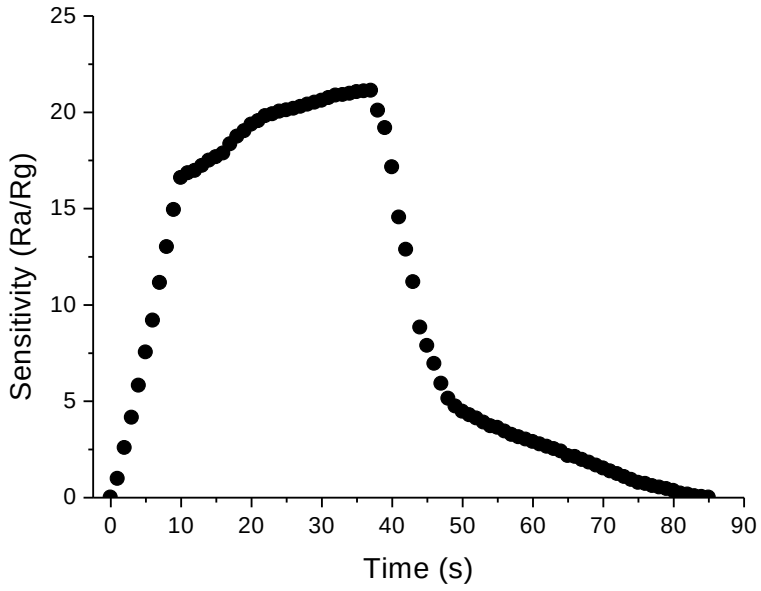

Fig.2 Response recovery curve of sensor to 50 ppm ammonia at 120 ^{O}C.

References

[1] Liu X, Ma T, Pinna N, et al. Two-dimensional nanostructured materials for gas sensing. Advanced Functional Materials, 2017, 27(37):1702168.

[2] Ko K Y, Song J G, Kim Y, et al. Improvement of gas-sensing performance of large-area tungsten disulfide nanosheets by surface functionalization. ACS Nano, 2016, 10(10): 9287-9296.

Acknowledgments

The work was supported by the National Natural Science Foundation of China (No. 21503004) and Key Natural Science Research Projects in Universities of Anhui Province (No. KJ2019A0851).

*** Corresponding author**
E-mail: zxf@bbc.edu.cn
Tel: +86-552-317-9368

Preparation of glutathione molecularly imprinted polymer microspheres by iniferter miniemulsion polymerization

Renyuan Song*

School of Material and Chemical Engineering, Bengbu College, Bengbu 233030, P. R. China

Abstraction: The glutathione (GSH) imprinted polymers (ILs-MIPs) microspheres with large specific surface area and high selectivity were controllably synthesized *via* surface iniferter miniemulsion polymerization using the long-chain alkyl ionic liquids (1-dodecyl-3-methyl imidazole bromide) as solubilizer of template and co-stabilizer of continuous phase. The effects of the ionic liquids on the stability of the template-functional monomer complex were investigated by UV-vis spectroscopy, ^{1}H-NMR spectroscopy and fluorescence spectroscopy, suggesting that the template-functional monomer complex has a good stability in the miniemulsion polymerization systems. In addition, the effects of the ionic liquids on the apparent morphology and recognition property of ILs-MIPs were investigated in detail. The N_2 adsorption tests manifested that the ILs-MIPs have larger specific surface area of 34.58 $m^2 \cdot g^{-1}$, well-distributed pore size and good hydrophilicity for improving the surface biocompatibility of ILs-MIPs.

Keywords: ionic liquid; molecularly imprinted polymer; iniferter miniemulsion polymerization

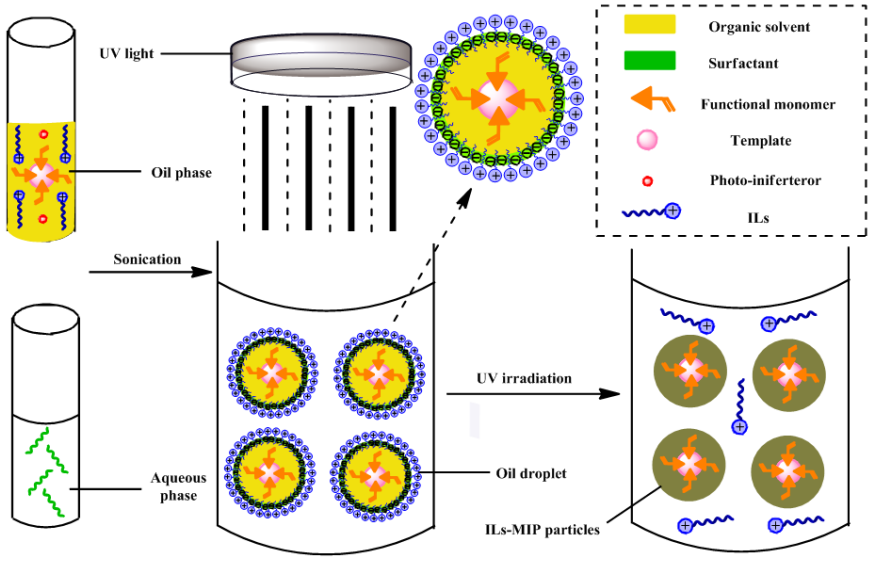

* **Corresponding author. E-mail address: sry0726@163.com.**

Fig.1 Schematic illustration for the preparation of GSH imprinted polymer microspheres in the presence of ILs via iniferter miniemulsion polymerization.

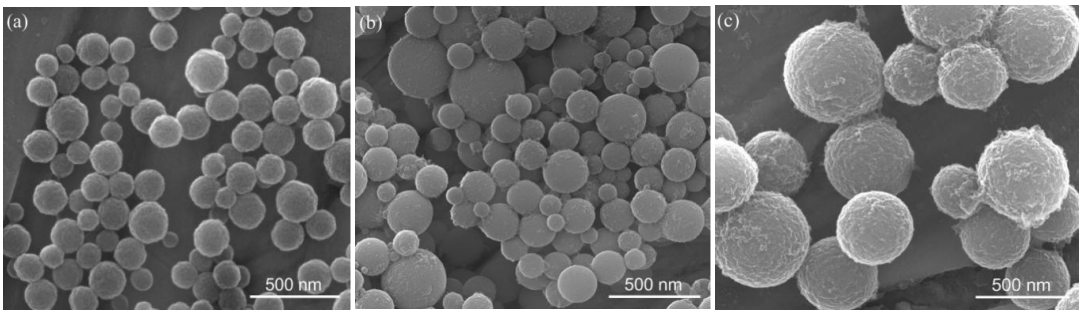

Fig.2 The effects of the amount of ILs on the morphologies of ILs-MIPs particles. (a) 0-ILs-MIPs, (b) 0.4 g-ILs-MIPs, (c) 0.8 g-ILs-MIPs

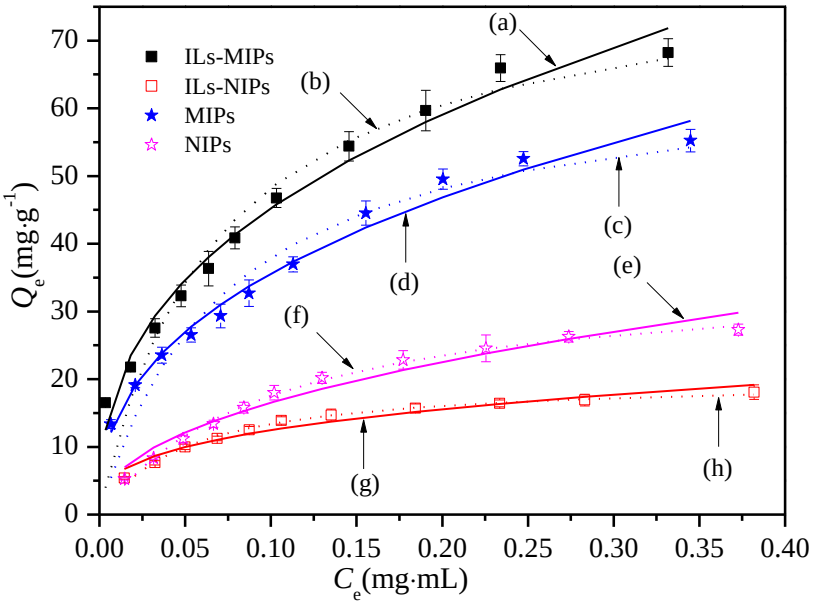

Fig.3 Comparision of Langmuir and Freundlich isotherm models for GSH adsorption onto the ILs-MIPs/NIPs and MIPs/NIPs via non-linear regression. (a) Freundlich isotherms of ILs-MIPs; (b) Langmuir isotherms of ILs-MIPs; (c) Freundlich isotherms of MIPs; (d) Langmuir isotherms of MIPs; (e) Freundlich isotherms of NIPs; (f) Langmuir isotherms of NIPs; (g) Freundlich isotherms of ILs-NIPs; (h) Langmuir isotherms of ILs-NIPs.

Acknowledgments

This work was supported by education commission of Anhui Province of China (KJ2017 A 573).

References

[1] Zhang R, Zhang T, Lv Y, et al. Selective binding of heparin oligosaccharides in a magnetic

thermoresponsive molecularly imprinted polymer [J]. *Talanta*, 2019, 201:441-449.

[2] Ma Y, Gao J, Zheng C, et al. Well-defined biological sample-compatible molecularly imprinted polymer microspheres by combining RAFT polymerization and thiol–epoxy coupling chemistry [J]. *Journal of Materials Chemistry B*, 2019, 7(15) :2474-2483.

[3] Zhu G, Li W, Wang L, et al. Using ionic liquid monomer to improve the selective recognition performance of surface imprinted polymer for sulfamonomethoxine in strong polar medium [J]. *Journal of Chromatography A*, 2019, 1592: 38-46.

Synthesis and Characterization of Alkali and Rare-Earth Metal Complexes Supported by Amidinate Ligand with Neutral Pyrrolyl Moiety

Min Zhou, Huihong Guo, Wenxi Xu, Erdong Bao and Liping Guo*

School of Material and Chemical Engineering, Bengbu University, Bengbu 233030, P. R. China

Abstraction: The reactivity of novel amidinate ligand **HL** bearing neutral pyrrolyl moiety in the side chain was investigated. The acid-base reaction between **HL** and alkali amide $MN(SiMe_3)_2$ (M = K or Na) giving coresponding alkali metal complexes M**L**$(THF)_2$ [M = K (**1**); M = Na (**2**)] in good yields. Rare-earth metal dichloride complexes **L**$RECl_2(THF)_3$ [RE = Y (**3a**), Er (**3b**), Dy (**3c**), Yb (**3d**)] supported by this ligand were obtained by the reaction of **1** and rare-earth metal trichloride. X-ray diffraction indicated that the pendant pyrrolyl moiety in **3a**-**3d** has no interaction with the central metal. Treatment of rear-earth metal dichloride complexes **3a**-**3d** with 2 equivalents of $LiCH_2SiMe_3$ at room temperature gave rare-earth metal dialkyl complexes **L**$RE(CH_2SiMe_3)_2$ [RE = Y (**4a**), Er (**4b**), Dy (**4c**), Yb (**4d**)] in good yields. X-ray diffraction revealed that complexes **4a**-**4d** are solvent-free and the neutral pyrrolyl moiety coordinated to metal centers in the η^5 mode.

Keywords: rare earth metal, amidinate, pyrrole

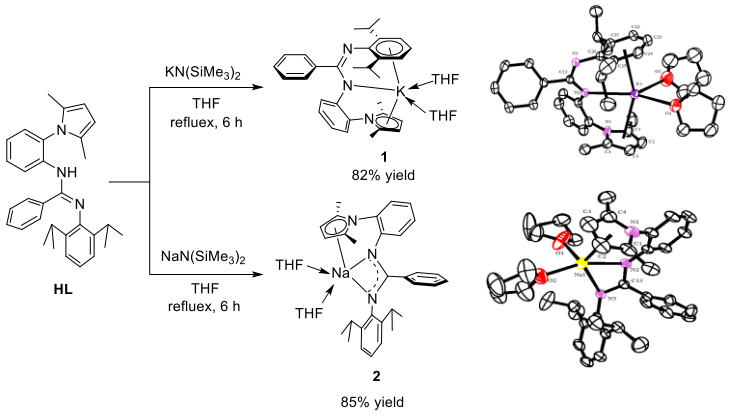

Scheme 1 Preparation of complexes **1** and **2**

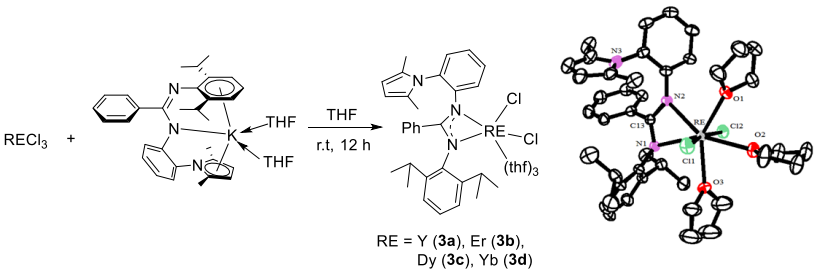

Scheme 2 Preparation of complexes **3a**-**3d**

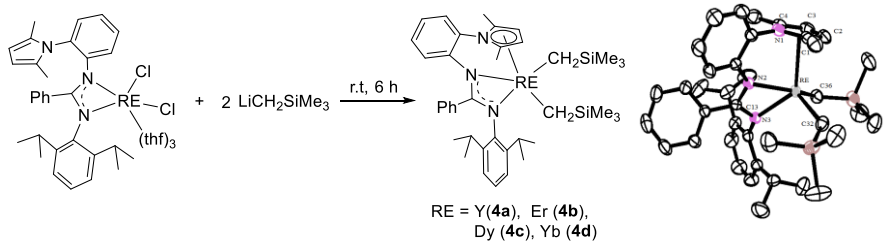

Scheme 3 Preparation of complexes **4a**-**4d**

Acknowledgments

This work was supported by the fund of Bengbu University (2017GJPY07).

Reference

1 (a) F. T. Edelmann, *Adv. Organomet. Chem.* **2008**, *57*, 183. (b) F. T. Edelmann, *Chem. Soc. Rev.* 2012, 41, 7657.

2 (a) V. Yu. Rad′kov, G. G. Skvortsov, D. M. Lyubov, A. V. Cherkasov, G. K. Fukin, A. S. Shavyrin, D. Cui, A. A. Trifonov, *Eur. J. Inorg. Chem.* **2012**, 2289. (b) A. O. Tolpygin, T. A. Glukhova, A. V. Cherkasov, G. K. Fukin, D. V. Aleksanyan, D. Cui, A. A. Trifonov, *Dalton Trans.* **2015**, *44*, 16465.

3 (a) F. H. Wang, S. W. Wang, X. C. Zhu, S. L. Zhou, H. Miao, X. X. Gu, Y. Wei, Q. B. Yan, *Organometallics* **2013**, *32*, 3920. (b) F. H. Wang, Y. Wei, S. W. Wang, X. C. Zhu, S. L. Zhou, G. S. Yang, X. X. Gu, G. C. Zhang, X. L. Mu, Organometallics 2015, 34, 86. (c) M. Li, C. P. Wang, H. Z. Xie, Z. H. Mou, Y. J. Luo, *Dalton Trans.* **2018**, *47*, 9709.

Battery-type Graphene/BiOBr Composite for High-Performance Asymmetrical Supercapacitor

Lingjuan Deng*, Zhanying Ma, Guang Fan

College of Chemistry and Chemical Engineering, Xianyang Normal University, Xianyang 712000, P. R. China

** E-mail: denglingjuan@163.com*

Abstract

In order to acquire high performance supercapacitors, a preferred choice is to prepare battery-type electrode materials. In this work, graphene/BiOBr (GR/BiOBr) composite was prepared by one-step solvothermal method using CTAB, graphite oxide and $Bi(NO_3)_3 \cdot 5H_2O$ as precursor. The GR/BiOBr composite was firstly used as electrode material for supercapacitors. Dynamic calculation suggests that a key feature of battery-like performance for GR/BiOBr composite [1]. When used as electrode in three-electrode system using 2 M NaOH as electrolyte, GR/BiOBr composite can supply an excellent specific capacity of 491 C g^{-1} at 1 A g^{-1} in a wide potential window of -1.1~0.2 V vs. SCE. Furthermore, an asymmetrical supercapacitor cell with a cell voltage of 1.4 V for the aid of GR/BiOBr (negative electrode) and Ni-Co-Al LDH (positive electrode) has been assembled. The symmetrical supercapacitor (LDH// GR/BiOBr) achieves a high energy density of 29.2 Wh kg^{-1} corresponding to a power density of 700 W kg^{-1}.

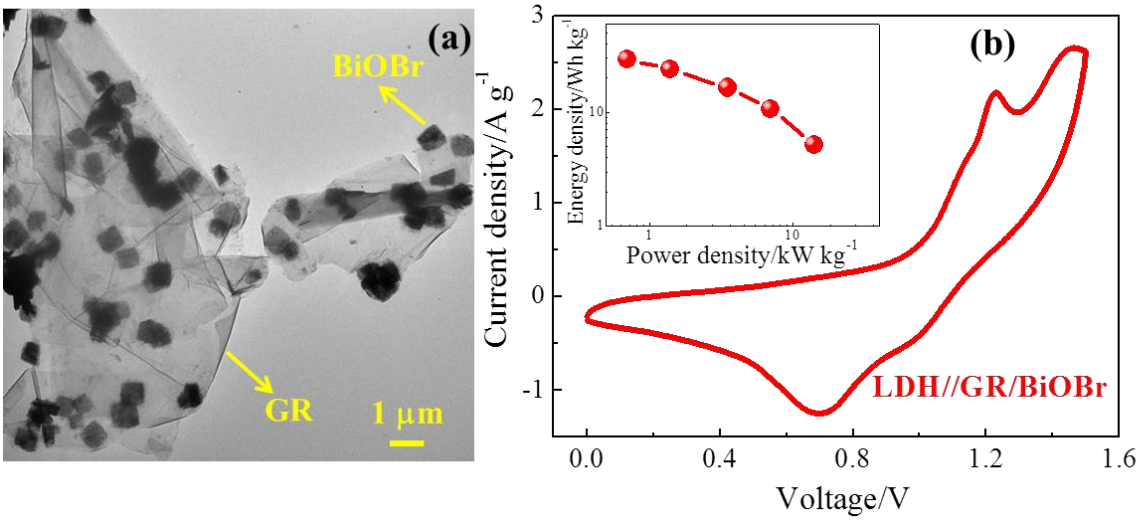

This study promotes that GR/BiOBr composite has great potential for high performance supercapacitors.

Fig1. (a) TEM image of GR/BiOBr composite. (b) CV and Ragon plot of LDH//GR/BiOBr asymmetrical supercapactor

Keyword: GR/BiOBr composite, asymmetrical supercapacitor, energy density, power density

References:

[1]. P. Simon, Yury Gogotsi. Materials for electrochemical capacitors. Nature Mater. 2008; 7: 845-854.

Facile fabricating mesoporous UiO-66 metal-organic frameworks via H_2SO_4 modulator

Zhang Ling, Zongqun Li*, Ruirui Zhang, and Chunyan Guo

Anhui Provincial Engineering Laboratory of Silicon-based Materials, Bengbu University, Bengbu 233030, P. R. China

Mesoporous UiO-66 was prepared through a facile defect engineering strategy in the presence of H_2SO_4 modulator. The obtained meso-UiO-66 were characterized by X-ray diffraction, transmission electron microscopy, and nitrogen adsorption-desorption isotherms. The surface area and pore size of UiO-66 dramatically increased as the concentration of H_2SO_4 was increased. Mesoporous UiO-66 exhibited remarkably adsorption kinetics and capacity for MB adsorption compared with the pristine UiO-66.

Keywords: Metal-organic framework (MOF) | UiO-66 | mesopore

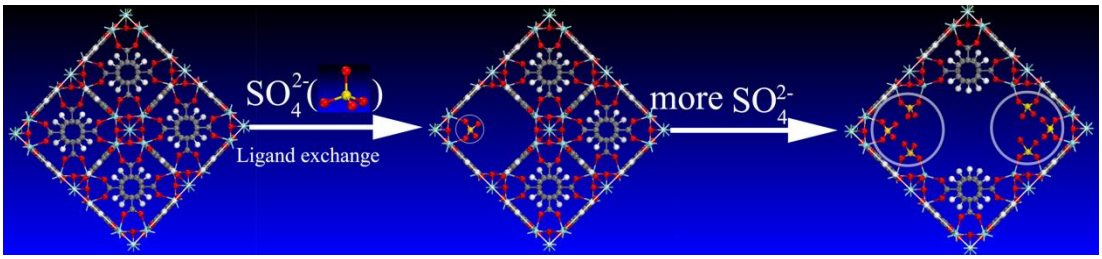

1Q. Yang, Q. Xu, H. L. Jiang, *Chem Soc Rev* **2017**, *46*, 4774-4808.

2T. Islamoglu, S. Goswami, Z. Li, A. J. Howarth, O. K. Farha, J. T. Hupp, *Acc Chem Res* **2017**, *50*, 805-813.

3D. Bradshaw, S. El-Hankari, L. Lupica-Spagnolo, *Chem Soc Rev* **2014**, *43*, 5431-43.

4A. A. Bezrukov, P. D. C. Dietzel, *Inorg Chem* **2017**, *56*, 12830-12838.

5G. Cai, H. L. Jiang, *Angew Chem Int Ed Engl* **2017**, *56*, 563-567.

6C. Liu, C. Zeng, T. Y. Luo, A. D. Merg, R. Jin, N. L. Rosi, *J Am Chem Soc* **2016**, *138*, 12045-8.